Universidad de Alcalá

Programa de Doctorado en Biología Funcional y Biotecnología

Caracterización ultraestructural y bioquímica de la pared celular de microalgas liquénicas sometidas a condiciones de desecación/rehidratación

Tesis Doctoral presentada por

Dª María González Hourcade

Director/a:

Dr. Leonardo Mario Casano Mazza
Dra. Eva María del Campo López

Alcalá de Henares, julio de 2020

Agradecimientos

No podría haber hecho esta Tesis ni estar escribiendo estas palabras sin la ayuda y apoyo de mucha gente, a lo largo de estos tres años. Desde luego ha sido un reto profesional pero también, personal. Si pudiese contarle a la María del 2012, recién terminada el bachillerato y llevando pocos meses en la carrera, que a día de hoy estaría terminando una Tesis Doctoral, seguramente se reiría de mí, asegurando que eso nunca pasaría. Son tantas las cosas que agradeceros que estas palabras siempre se quedarán cortas.

En primer lugar, a mis Directores de Tesis. A Leonardo por guiarme en este mundo desde el 2015, siempre brindándome una oportunidad para crecer, enseñarme a ser ambiciosa pero realista y también mostrarme lo maravillosa, aunque a veces frustrante, que es la investigación. A Eva, por ser también un apoyo fundamental, que finalmente si que pudo dar un enfoque increíble a esta Tesis, que me enseño a sacar todo el jugo a los datos, ver la misma situación desde diferentes perspectivas. Con vosotros siempre estaré en deuda porque es incalculable lo que me habéis aportado como profesionales y, como personas,

A Paco, por estar ahí siempre para ayudarme y aconsejarme, por hacerme sentir una más del equipo desde el primer día hace ya casi 5 años. A Fernando, obviamente ser tan paciente conmigo y acudir cada vez que tengo un problema, que muchas veces eran mucho más sencillas de lo que parecían.

También me gustaría agradecer a Manolo del Departamento de Biomedicina y Biotecnología, por estar siempre disponible a ayudarme, por dejarme usar infinitas veces su laboratorio y enseñarme como mantener un liofilizador, y que, gracias a ello, no he tenido ningún problema con otros equipos y he sabido responder rápido.

A Antonio Salgado del Servicio de Resonancia Magnética de la Universidad de Alcalá por su infinita paciencia para explicarme toda la teoría relacionada con el NMR, y por todas sus horas invertidas y por no dar ninguna muestra, por pequeña que fuese por perdida.

A Marcia Braga del Instituto de Botánica de São Paulo y a Carmen Ascaso del CSIC por ayudarme y enseñarme esas cosas que solo la experiencia te puede enseñar.

Finalmente, ese apoyo diario, y que, sin él, los momentos más duros habrían sido mucho peores. A mis amigas Andrea, Anais, Sara, Lucía, Bea y Fabiola, gracias por vuestra ayuda y básicamente por existir y, estar ahí cada vez que una piedra se interponía en mi camino.

Y a los más importantes, a mis padres, Rosa y Carlos, es incalculable todo el esfuerzo y el sacrificio que han tenido que hacer para que yo esté donde estoy. Que, aunque sabían que esta carrera iba a ser difícil, han seguido apoyándome por el simple hecho que yo nací para dedicarme a la ciencia.

A todos vosotros, las gracias siempre se quedarán cortas.

A mis padres, Rosa y Carlos

A mis mentores, Leonardo y Eva

Índice

Introducción

1. Líquenes

El término "liquen" deriva de la palabra griega *leikhēn*, cuyo significado es "Quién se alimenta de su alrededor". En 1867, a partir de los trabajos de Simon Schwendener, se descubrió su naturaleza dual. Desde ese momento, se describe un liquen como una criptógama talofita, producto de la asociación simbiótica entre dos organismos, un hongo (micobionte) y un socio fotosintético (fotobionte). Este último, puede ser un alga verde unicelular (ficobionte o clorobionte) o una cianobacteria (cianobionte), considerada como un "alga azul-verde", pero únicamente el 10% de los líquenes existentes son considerados como cianolíquenes, el resto se denominan clorolíquenes. Más recientemente se ha demostrado que un mismo hongo puede estar asociado con dos o más especies de ficobiontes (Casano *et al.,* 2011; del Campo *et al.,* 2010; Friedl, 1987). Macroscópicamente, los líquenes forman talos prácticamente homogéneos, en los que a veces resulta complicado diferenciar los diferentes organismos participantes. Por otra parte, en un gran número de líquenes, se ha encontrado una variada microflora bacteriana como tercer componente de la simbiosis, cuyas funciones podrían estar relacionados con una adaptación a determinadas condiciones ambientales (Aschenbrenner *et al.,* 2014; Molins *et al.,* 2013; Printzen *et al.,* 2012).

Existe cierta controversia sobre a qué tipo de simbiosis corresponden los líquenes, aunque la opinión más extendida es que se trata de un sistema mutualista, puesto que todas las partes implicadas obtienen beneficios de esta asociación. Por un lado, los organismos fotosintéticos proporcionan compuestos orgánicos fotoasimilados a su micobionte asociado (Honegger, 1991). A cambio, el fotobionte obtiene un suministro de nutrientes minerales y un nicho en el que desarrollarse, protegido del entorno donde existen factores estresantes. Sin embargo, los líquenes habitan en sustratos con un contenido nutricional limitado, ésta es una de las razones por la cual los líquenes tienen una tasa de crecimiento tan bajo, y por lo general se expanden unos pocos centímetros al año, o incluso escasos milímetros

(Honegger, 2008). Otras condiciones ambientales como cambios marcados en la temperatura, y la humedad, que generalmente provocan ciclos de desecación/rehidratación, son factores que también comprometen y limitan el crecimiento del liquen (Armstrong, 2017). Por otro lado, existe un libre intercambio de gases debido a que los líquenes no presentan una cutícula (Turetsky, 2003), por lo que en zonas donde existen altos niveles de gases contaminantes como el óxido de nitrógeno, el sulfuro o el ozono, se ha demostrado que afectan al crecimiento del liquen, reduciéndolo o impidiendo su desarrollo por completo, como es el caso de los entornos urbanos/industriales donde existe una alta contaminación del aire (Nash, 2008).

En cuanto a la distribución geográfica de los líquenes, se localizan en prácticamente en todos los hábitats terrestres, desde los trópicos hasta los hábitats polares, constituyendo aproximadamente un 8% de la biomasa vegetal global de la Tierra (Ahmadjian, 1995). Dentro de esta variedad de ambientes, destacan aquellos con condiciones extremas como los desiertos cálidos y fríos, y las tundras. Por esta razón, la mayoría de los líquenes se califican como extremo-tolerantes o extremófilos. La clave de la tolerancia a dichos hábitats parece radicar precisamente en la simbiosis, ya que, si bien cada simbionte individualmente suele poseer mecanismos morfo-fisiológicos de adaptación a condiciones estresantes, estos no le permitirían sobrevivir en vida libre bajo condiciones extremas (Beckett *et al.,* 2008).

1.1 Micobionte

El término micobionte proviene de la unión de las palabras; "*mykes"* y "*bios"*, que significan "hongo" y "vida", respectivamente. La liquenización es una de las formas de vida más estables para los hongos, ya que, al ser organismos heterótrofos, están continuamente buscando una nueva fuente de nutrientes. Por esta razón, una gran proporción de los hongos liquenizados son biotrofos obligados, es decir, dependen de su hospedador para la obtención de nutrientes, a través del haustorio. El proceso de simbiosis no se origina de forma aleatoria entre hongo y alga, sino que existe una especificidad y selectividad entre ambos organismos (del Campo *et al.,* 2013), aunque es el hongo quien determina cuál es el compañero fotosintético

más favorable para asociarse. Existen evidencias que apoyan la idea sobre que el fotobionte puede diferir dependiendo de la localización geográfica, ya que intervienen factores ambientales y ecológicos (Peksa & Skaloud, 2011; Williams *et al.,* 2017) Los líquenes presentan diferentes morfologías, siendo el micobionte quien normalmente determina la forma del liquen, puesto que es el organismo con mayor proporción de biomasa (90-95%) de todas las partes o capas del talo liquénico. Dependiendo de la morfología de los líquenes, pueden clasificarse como *fruticuloso* (con un único punto de contacto con el sustrato y una forma muy característica de pequeño arbusto, por su gran ramificación), *crustáceo* (completamente unido al sustrato, estando normalmente asociados a rocas o cortezas de plantas) o *folioso* (parcialmente despegado del sustrato, la mayoría de estos líquenes presentan lóbulos a lo largo del talo).

Hasta la fecha se han descrito alrededor de 20.000 especies de hongos que pueden establecer esta asociación simbiótica (Kirk *et al.,* 2008), correspondiéndose a un 17- 20% de los hongos existentes totales. En cuanto a las especies de hongos liquenizados, cabe destacar que el alrededor del 98% pertenecen a la División Ascomycota, con un total aproximado de 13.500 especies, siendo el orden de Leconorales el que más especies incluye. Menos del 1% se han descrito como micobiontes pertenecientes a la División Basidiomycota, el resto se ha relacionado con el grupo de los Deuteromycetos (Nash, 2008).

1.2 Fotobionte

El socio fotosintético dentro de esta simbiosis puede ser una microalga verde eucariótica unicelular (ficobionte) o una cianobacteria (cianobionte). Incluso se pueden encontrar líquenes en los que coexisten dos tipos de fotobionte, como son los casos de los líquenes tripartitos (3-4%) (Rai, 2002). Sin embargo, las microalgas terrestres que actúan como ficobiontes representan el 95% de los líquenes existentes. Dentro de este último grupo se encuentran las especies escogidas como objetos de estudio para la presente Tesis. Actualmente se han descrito hasta aproximadamente 40 géneros de algas y cianobacterias (Büdel,1992; Tschermak-Woess, 1988), siendo *Nostoc* el más representativo entre los cianobiontes (DePriest, 2004;

Rikkinen, 2002). La proporción de fotobiontes dentro del liquen puede constituir hasta un 10% de la biomasa total, pero el 40-50% de la biomasa del talo liquénico es resultado casi exclusivo del carbono fijado por la fotosíntesis de los fotobiontes.

1.2.1 Ficobionte

Los líquenes que tienen microalgas verdes como fotobionte pueden colonizar casi cualquier ambiente, ya que, a diferencia de los cianolíquenes, pueden mantenerse hidratados utilizando incluso solo el vapor de agua. La mayoría de las algas verdes pertenecen a la división Chlorophyta con un total de 116 especies descritas hasta la fecha (Saini *et al.,* 2019), incluso existen líquenes que pueden albergar más de una especie de microalga (Casano *et al.,* 2011). Dentro de la División Chlorophyta, el 60% de los fotobiontes descritos pertenecen a la clase Trebouxiophyceae (Ahmadjian, 1982; Honegger, 2009).

1.2.1.1 Género *Trebouxia*

Este género se describió por primera vez por Puymaly en 1924 tras caracterizar el primer holotipo, como *Trebouxia arboricola*, el cual se relaciona con más del 20% de todas las especies de hongos liquenizados (Rambold & Triebel, 1992; Nash, 2008). Trebouxia es el género más común entre los líquenes y hasta la fecha se han descrito formalmente 24 especies (Leavitt *et al.,* 2015). Se puede encontrar asociado a cualquier ambiente, con más o menos factores estresantes. Incluso, se han llegado a encontrar líquenes en los que conviven varias especies de *Trebouxia* (Casano *et al.,* 2011). En cuanto a su forma de vida, no se ha determinado fuera de la simbiosis en la naturaleza (Ahmadjian, 1988, 1993; Mukhtar *et al.,* 1994). Sin embargo, existe una brecha de clasificación, especialmente en las microalgas liquénicas, debido a que los sistemas de identificación taxonómica no se han establecido formalmente (Friel & Büdel, 2008). En la actualidad, se están utilizando marcadores moleculares de la región espaciadora interna transcrita (ITS) del ADN ribosomal como método de reconocimiento y así poder establecer relaciones filogenéticas (Friel & Rokitta, 1997), aunque cabe destacar que algunas especies tienen nombres

provisionales hasta la denominación definitiva. Una de las razones por las que este género es el más extendido, es debido a que consigue adaptarse a condiciones ambientales extremas modificando por ejemplo la cantidad de pigmentos fotosintéticos como clorofilas y carotenoides (Erokhina *et al.,* 2004).

Las especies del género Trebouxia, se caracterizan por tener una morfología en forma cocoide (esférica) (Ahmadjian, 1960), con un cloroplasto central que incluye un único pirenoide en el centro, en el cual se encuentran glóbulos ricos en lípidos conocidos como pirenoglóbulos (McCoy, 1977).

1.2.1.2 Género *Coccomyxa*

El género *Coccomyxa* también pertenece a la clase de algas verdes Trebouxiophyceae, sin embargo, es menos frecuente encontrarlo como ficobionte en simbiosis con hongos, ya que se pueden encontrar en otras múltiples formas de vida, en contraposición al género *Trebouxia*. Por un lado, forma biofilms de algas verdes terrestres, como algas del suelo, siendo de vida libre (Honneger, 1991). Por otro lado, también se encuentra formando distintos tipos de relaciones con otros organismos, de las cuales algunas son positivas, como los líquenes, asociándose con hongos de las Divisiones Ascomycota y Basidiomycota (Lutzoni & Vilgalys, 1995), musgos y/o con plantas superiores. En cuanto a plantas vasculares, un ejemplo sería la relación que una especie de *Coccomyxa* ha establecido con *Ginkgo biloba,* aunque no está definida como beneficiosa para ambos participantes (Tremouillaux-Guiller *et al.,* 2002; Tremouillaux-Guiller & Huss, 2007). Finalmente, se ha descrito especies de *Coccomyxa* que viven siendo parásitos de bivalvos (Gray *et al.,* 1999).

La morfología de este género se caracteriza por ser algas unicelulares con forma globular o elipsoide con un cloroplasto parietal sin pirenoide (Peveling & Galum, 1976) y la ausencia de cualquier etapa flagelada (Darienko *et al.*, 2015). A través de imágenes tomadas por microscopia electrónica de transmisión (MET), se pudo describir que la especie *Coccomyxa* sp. aislada del liquen *Solorina crocea*, presenta un cloroplasto que ocupa dos terceras partes del volumen total de la célula (Malavasi *et al.,* 2016).

1.3 Contexto eco-fisiológico de las especies de microalgas liquénicas escogidas como objeto de estudio.

1.3.1 *Trebouxia* sp. TR9

Denominado de forma provisional*, Trebouxia* sp. TR9, es un ficobionte del género *Trebouxia* aislado del asco-liquen *Ramalina farinacea* cuyo micobionte pertenece a al orden Lecanorales. Esta microalga puede coexistir con otro ficobionte, *Trebouxia jamessi*. *R. farinacea* es liquen epifito de tipo fruticuloso. Su localización puede llegar a ser bastante variada, desde ambientes Mediterráneos-Atlánticos hasta casi zonas boreales. Asimismo, se ha sugerido que tiene su origen en la zona macaronésica-mediterránea. En este tipo de hábitats, el liquen está expuesto a cambios rápidos y drásticos en la humedad relativa del aire y, consecuentemente, experimenta continuos ciclos diarios/estacionales de desecación-rehidratación.

1.3.2 *Coccomyxa simplex*

Coccomyxa simplex (anteriormente denominado como *Coccomyxa solorinae-saccatae*) (Darienko e*t al.,* 2015; Malavasi *et al.,* 2016) es el único ficobionte descrito en *Solorina saccata*. Se trata de un liquen foliáceo que presenta una distribución geográfica desde Europa central hasta el ártico. A diferencia de *R. farinacea*, este liquen normalmente se suele encontrar en zonas protegidas como grietas rocosas de base calcárea donde se crea un ambiente más húmedo, y, por lo tanto, está sometido a ciclos de desecación-rehidratación mucho más lentos.

2. Líquenes y su tolerancia a la desecación.

2.1 Aspectos generales

Como se ha comentado anteriormente, todos los entornos terrestres presentan diferentes tipos y niveles de estrés abiótico, donde la baja disponibilidad de agua, las temperaturas extremas y la radiación intensa, se consideran los factores ambientales más estresantes.

Los líquenes en general y las microalgas en particular, se incluyen dentro del grupo de los organismos poiquilohídricos, que, a diferencia de los homeohídricos, no pueden regular activamente el contenido hídrico interno.

Éstos dependen completamente de la disponibilidad de agua que hay en su entorno, tanto en estado gaseoso como líquido. La mayoría de los organismos poiquilohídricos presentan la capacidad de ser tolerantes a la desecación, que se define como la habilidad de sobrevivir cuando el contenido hídrico intracelular es igual o inferior al 10% (Gasulla *et al.,* 2009). En esas condiciones, estos organismos entran en un estado de latencia, reduciendo al máximo su metabolismo respiratorio y la actividad de la maquinaria fotosintética, con el fin de disminuir posibles daños asociados a la formación de especies reactivas del oxígeno (ROS). El estado de deshidratación puede llegar a durar largos periodos de tiempo hasta que exista de nuevo disponibilidad de agua y, tras pocos minutos de rehidratación, empieza un proceso de recuperación en el cual la maquinaria fotosintética vuelve a estar activa (Beckett *et al.,* 2008). Los clorolíquenes y cianolíquenes pueden llegar a absorber agua hasta 200 y 2000 veces su peso seco, respectivamente, durante el proceso de rehidratación (Kranner *et al.,* 2008).

La deshidratación provoca múltiples alteraciones fisiológicas y morfológicas en las células, por ello la tolerancia a la desecación (DT) implica una gran cantidad de mecanismos tanto moleculares como morfológico/estructurales. Gran parte de las investigaciones sobre DT se han realizado en órganos u organismos modelo como son las semillas, las plantas reviviscentes y los briófitos. Uno de los aspectos más críticos de la disminución del agua intracelular es que puede estimular la formación de ROS, tales como el radical-anión superóxido (O_2), el peróxido de hidrógeno (H_2O_2), el radical hidroxilo ($HO^{\cdot}$) y el oxígeno singlete ($^1O_2$). Si bien a bajas concentraciones tienen un papel fundamental en la traducción de señales celulares y en la regulación del metabolismo (Inupakutika *et al.,* 2016), al ser muy reactivas, pueden provocar daños directos a proteínas, lípidos, carbohidratos y ADN, e incluso iniciar el proceso de muerte celular (Halliwell & Cross, 1994). A nivel subcelular, las mitocondrias y los cloroplastos son los principales orgánulos donde tiene origen la producción de ROS como resultado de la respiración celular y fotosíntesis, respectivamente (Inupakutika *et al.,* 2016).

Para mantener los niveles estacionarios de ROS por debajo de valores citotóxicos las células han desarrollado sistemas de protección antioxidante. Por un lado, se encuentran las enzimas antioxidantes, siendo las principales: superóxido dismutasa (SOD) (Casano *et al.,* 1997), catalasa (CAT) (Mittler, 2002), glutatión reductasa (GR) (Foyer *et al.,* 1991) y ascorbato peroxidasa (AP) (Asada, 1999) apoyadas con enzimas auxiliares. Se ha descrito la presencia de estas enzimas antioxidantes en la matriz extracelular, estando asociadas a la pared celular de algunos líquenes, entre las que se incluyen las lacasas (Laufer *et al.,* 2006). Por otro lado, existen otras proteínas que se incluyen en este sistema de control de daños oxidativos causados por ROS como son las proteínas de choque térmico. Esta familia de chaperonas está relacionada con el mantenimiento del normal plegamiento de las proteínas para su correcta funcionalidad, o con el marcaje para la eliminación de aquellas proteínas desnaturalizadas por acción de las ROS (Duan *et al.,* 2011).

No toda la protección antioxidante tiene una naturaleza proteica, también existen ciertos compuestos que ayudan a hacer frente al estrés oxidativo. Los antioxidantes más ubicuos son el ácido ascórbico, glutatión, carotenoides y tocoferoles. Otros compuestos antioxidantes son los polioles, presentes en semillas (Fait *et al.,* 2006), plantas halófitas (Yancey *et al.,* 1982), xerófitas (Boscaiu *et al.,* 2009) y en el espacio intracelular de las microalgas liquénicas (Centeno *et al.,* 2016). Se sugiere que estos azúcares-alcoholes pueden funcionar como osmolitos para conservar la turgencia de célula en condiciones de desecación, mediante el estado de vitrificación y así poder estabilizar las proteínas de las membranas, y también como potentes secuestrantes de ROS (Buitink & Leprince, 2004). En las especies TR9 y *Csol* se han analizado el posible aumento de estos polioles en condiciones de desecación y ambas especies presentan estrategias totalmente diferentes. Por un lado, *Trebouxia* sp. TR9 acumula altas cantidades de pinitol y galactosilglicerol de forma constitutiva, mientras que, *Csol* presenta el incremento en galactinol inducido por la exposición a la desecación- rehidratación (Centeno *et al.,* 2016).

2.22 La pared celular en la defensa frente a la desecación

Se ha constatado que muchas cianobacterias, líquenes, y algunos musgos son tolerantes a la desecación, lo que se sugiere que la DT podría tener un origen ancestral. En cuanto a plantas vasculares, no presentan DT en sus órganos vegetativos, tanto en el caso de las gimnospermas como de las angiospermas, en las cuales solo el polen y sus semillas poseen esta capacidad, la cual dura hasta que se produce la germinación. La excepción a esta regla la constituye un pequeño grupo de plantas vasculares que sí poseen esta tolerancia en todas sus partes vegetativas y son denominadas como plantas reviviscentes. Hasta la fecha, se han descrito aproximadamente 300 especies de angiospermas como plantas reviviscentes (Alpert, 2006), y al igual que otros organismos poiquilohídricos, no poseen un gran tamaño en comparación con otras plantas vasculares. Una característica esencial de estos organismos son sus mecanismos fisiológicos para afrontar uno de los procesos críticos de la deshidratación, la pérdida de agua intracelular. En plantas no tolerantes a la desecación, cuando la célula se deshidrata, se produce una contracción protoplasto y éste se suele separar de la pared celular, ya que esta se caracteriza por ser rígida y robusta, desencadenando así la muerte celular (Lu & Neumann, 1998; Munns *et al.,* 2000). Sin embargo, las plantas reviviscentes presentan una pared celular con composición bioquímica peculiar, la cual confiere mayor flexibilidad a la pared y evitar la posible ruptura entre esta y el plasmalema. La pared celular de las plantas reviviscentes se compone esencialmente de polisacáridos ramificados de cadena larga entrecruzados, y cuánta más laxa sea ésta, más elasticidad se consigue para hacer frente a los continuos cambios de contenido hídrico intracelular. A nivel macroscópico, un efecto evidente e inmediato de las plantas reviviscentes frente a la desecación es el plegamiento de sus hojas. Aquellas plantas que no curvan sus hojas no consiguen sobrevivir a la desecación (Farrant, 2003). Otra consecuencia que trae aparejada el plegamiento celular y foliar, es evitar la sobrexposición a la radiación ultravioleta.

Un claro ejemplo de flexibilidad de la pared celular es la descrita en la planta reviviscente *Craterostigma wilmsii* (Vicré *et al.,* 1999, 2004). Bajo condiciones de desecación, este organismo es capaz de producir cambios en la composición bioquímica de su pared celular, modificando los xiloglucanos de cadena larga de la misma, generando otros de cadena corta. Además, se ha descrito un incremento significativo de las expansinas (Jones & McQueen-Mason, 2004; Moore *et al.,* 2008), cuya función es interrumpir los enlaces de hidrogeno entre las fibras de celulosa y hemicelulosa. Todos estos ajustes bioquímicos contribuyen a facilitar el plegamiento controlado de la pared, disminuyendo así la tensión mecánica entre dicha pared y el protoplasto que se contrae por efecto de la pérdida de agua intracelular.

2.33 Pared celular en algas verdes y su implicación en la tolerancia a la desecación.

Las algas verdes habitan en lugares donde los principales factores del ambiente abiótico fluctúan constantemente provocando situaciones de estrés, siendo las paredes celulares las primeras barreras celulares contra esta condición. Aunque son organismos tolerantes a la desecación, actualmente el conocimiento sobre las microalgas verdes y sus mecanismos de defensa frente a la deshidratación es escaso. Además, al ser organismos unicelulares no tienen sistemas de protección fisiológico-estructurales como son la cutícula, estomas y raíces que sí están presente en plantas vasculares. Por esta razón, la pared celular de las algas verdes es la barrera que se encuentra expuesta continuamente al ambiente externo, incluyendo aquellos organismos con los que se relaciona.

El conocimiento sobre la composición y arquitectura de la pared celular vegetal proviene fundamentalmente de plantas vasculares modelo (Popper *et al.,* 2011) debido a un claro interés para el uso industrial y agrícola. No obstante, la respuesta fisiológica de la pared celular frente a la desecación y su correspondiente remodelación bioquímica/estructural deriva de estudios con el género *Craterostigma*, pues son los organismos de referencia para estudios en plantas tolerantes a la desecación. Sin embargo, existe un vacío de conocimiento en otros grupos de organismos tolerantes a la desecación.

Por esta razón, en la presente Tesis se tratará la posible implicación de la pared celular de las microalgas liquénicas en la tolerancia a la desecación/rehidratación.

De los pocos estudios realizados hasta la fecha, Honegger *et al.* (1996) reveló cambios ultraestructurales de la pared en algunas especies de líquenes, mediante estudios de microscopia electrónica de transmisión (MET) y microscopia electrónica de barrido (MEB), previamente fijados en frio. Con ello, demostraron que en condiciones de desecación tanto las células fúngicas como las algas unicelulares presentan una contracción celular. Mientras que, los protoplastos de las microalgas seguían en continuo contacto con la pared celular, el hongo creaba burbujas de aire entre las paredes celulares y el resto de la célula, consiguiendo evitar el colapso celular ambos organismos. Estas estrategias diferentes se debían a que las paredes celulares del hongo serían más rígidas que las algales y no poseerían la habilidad de plegarse, mientras que las de las algas sí. Se desconoce actualmente el mecanismo molecular del plegamiento de la pared celular de las microalgas liquénicas. En este sentido, destacan los trabajos de Karsten & Holzinger (2012) y Holzinger & Karsten (2013), donde caracterizaron las paredes celulares en dos algas aeroterrestres formadoras de costras biológicas del género *Klebsormidium* (Charophytae), tolerantes a la desecación. Dichas paredes celulares están principalmente compuestas por un polisacárido similar a la calosa, lo que permite que sean más flexibles y fácilmente plegables.

2.3.1 Antecedentes de las paredes celulares de algas verdes

Gracias al avance de las técnicas bioquímicas y moleculares, la investigación sobre la pared celular de las algas verdes se ha visto incrementado debido a su gran interés biotecnológico, siendo una alternativa en varios sectores de la industria. Las especies de Chlorophyta en las que más se han focalizado este tipo de estudios pertenecen a los géneros *Chlorella, Chlamydomonas, Dunaliella* y *Botrycoccus* (Baudelet *et al.,* 2017), presentando cada una de ellas una organización y composición química diferente. Dentro del filo Chlorophyta, la clase Trebouxiophyceae es uno de

los linajes con una forma de vida muy diversa, pudiendo ser tanto acuática como terrestre, por lo tanto, es esperable que las características de la pared celular de estas algas estén estrechamente relacionadas con su forma de vida y adaptada al medio donde se desarrollen.

2.3.2 Conocimientos previos sobre la pared celular en *Trebouxia*

Este género es el más representativo como ficobionte en líquenes, por lo tanto, es el grupo con más conocimiento existente sobre la pared celular de microalgas liquénicas (Nash, 2008). No obstante, dicho conocimiento ha sido muy escaso hasta hace pocos años. En una revisión sobre la evolución de la pared celular desde las microalgas hasta las plantas vasculares realizada hace menos de diez años, Popper *et al.* (2011). Estas microalgas liquénicas solo presentarían celulosa en pequeñas concentraciones y, en algunos casos estaría totalmente ausente, a diferencia del resto de las macroalgas verdes, cuyas paredes celulares están principalmente compuestas por dicho polímero. Los primeros estudios sobre la caracterización de la pared celular se realizaron por Cordeiro *et al.* (2006, 2007), quienes describieron un β-1,4-galactofuranano como principal polisacárido de las paredes celulares de los ficobiontes aislados de los líquenes *Ramalina gracilis* y *Cladina confusa*, respectivamente. Años más tarde, Casano *et al.* (2011, 2015) estudiaron la ultraestructura y la composición polisacarídica de la pared celular de dos especies de *Trebouxia*: TR9 y *Trebouxia jamesii*, que conviven en el liquen *Ramalina farinacea*. Aun cohabitando en el mismo liquen, ambas microalgas presentan analogías y diferencias en cuanto a su pared celular. Por un lado, al igual que los otros dos ficobiontes trebouxioides estudiados (Cordeiro *et al.,* 2006, 2007), TR9 y *T. jamesii* presentan una gran proporción de galactosa, tanto en los polisacáridos matriciales como en los estructurales. En cuanto a la ultraestructura, la pared de *T. jamesii* está compuesta por cuatro capas bien definidas, mientras que la de TR9 está descrita como tri-laminar (TLS), pero no se ha observado una delimitación clara entre las tres capas. Por último, existe una cuestión que ha estado en debate dentro de la clase Trebouxiophyceae, y es la existencia de los algaenanos en las paredes celulares, ya que parece ser que no hay una presencia uniforme entre las especies. El algaenano, es un biopolímero alifático, con una composición

química altamente compleja. Anteriormente, se denominaba esporopolenina, debido a que este compuesto solo se había descrito en granos de polen de las plantas vasculares. Pero una vez identificado también en las paredes celulares de algunas algas, se lo denominó algaenano en el caso de estos organismos. La presencia de estos biopolímeros como capa intermedia en la pared, puede ser considerado como un mecanismo defensivo frente a la desecación. En primer lugar, Konig & Peveling (1984), describieron su presencia en algunas especies de *Trebouxia*, en concreto *T. erici* (actualmente, *Asterochloris erici*), *T. gelatinosa, T. glomerata* y*, T. pyriformis.* Sin embargo, en los trabajos de Honegger & Brunner (1981) y Brunner & Honneger (1985) no lo hallaron en la pared celular de *Trebouxia* sp. aislada del liquen *Cladonia caespiticia*, aún después de exhaustivos procesos de extracción.

2.3.3 Conocimientos previos sobre la pared celular en *Coccomyxa*

Debido a que este género no pertenece a los principales representantes de microalgas liquénicas, como es el caso de *Trebouxia*, el conocimiento existente sobre sus paredes celulares es aún más escaso. A partir de análisis de composición y ligación glicosídica, Centeno *et al.* (2016) informaron que *Coccomyxa simplex* parece presentar una pared diferente a las algas del género *Trebouxia*, siendo en este caso, la glucosa y la galactosa los monosacáridos principales, seguidos por manosa, con una significativa proporción de polímeros similares a la celulosa. Dentro de la clase Trebouxiophyceae, *Coccomyxa* es un género de algas cuya pared celular se ha descrito con una clara organización en tres capas muy bien definidas, que normalmente se asocia con la de microalgas semejantes, como p.e. *Botrycoccus* (Baudelet *et al.,* 2017). Esta microalga es un claro ejemplo de paredes trilaminares, comúnmente denominadas como TLS, entre las cuales se encuentra la capa del compuesto insoluble algaenano. A diferencia de *Trebouxia*, todas las especies del género Coccomyxa estudiadas, tanto simbiontes como de vida libre o parásita, presentan paredes celulares con algaenanos en su capa intermedia (Honegger & Brunner, 1981; Brunner & Honegger, 1985).

2.4 Matriz extracelular, la barrera desconocida frente a la desecación

Al igual que muchos otros organismos, las microalgas liquénicas también presentan una matriz extracelular, localizándose alrededor de su pared celular. Esta matriz generalmente está compuesta por exopolisacáridos de alto peso molecular, tanto de carga neutra como negativa, proteínas, pequeñas moléculas de ácidos nucleicos, y lípidos (Pérez-Garcia, *et al.,* 2011; Liu *et al.,* 2016). Este revestimiento extracelular está implicado en varias funciones esenciales para el desarrollo de estos organismos, como son la adhesión entre células, morfogénesis, expansión celular, sensibilidad a cambios en el ambiente y defensa contra patógenos (Mann & Wozniak, 2012; Dertli *et al.,* 2015). Generalmente, la proporción de polisacáridos es ligeramente superior al 50% debido a que esta matriz funciona también como un importante reservorio de carbono, sobre todo en situaciones de estrés celular se puede transformar en energía (Xiao & Zheng, 2016). La composición monosacarídica de los polisacáridos extracelulares puede diferir entre géneros, incluso entre especies, posiblemente en relación con el ambiente en el que habiten (Rossi & De Phillipis, 2016). Sin embargo, diversos estudios coinciden en que la gran mayoría de los organismos presentan polisacáridos de cadena larga con repeticiones de cuatro monosacáridos principales, de los cuales la glucosa, arabinosa, galactosa, ramnosa y manosa serían los más representativos (Kumar et al., 2018; Raveendran et al., 2013).

Desde el 2009, se han incrementado los estudios sobre la caracterización de la matriz extracelular especialmente en macro y microalgas, debido a que se han descubierto diversos componentes con un alto interés en la industria biotecnológica y farmacéutica (Liu *et al.,* 2016; Rossi & De Phillipis, 2016). Una de las estrategias que se utilizan para aumentar la producción de los compuestos localizados en la matriz extracelular es someter a los cultivos a situaciones de estrés, ya que se ha descrito que la matriz extracelular está relacionada con la protección celular frente a condiciones estresantes y, en dichas condiciones, aumenta

su concentración. En este sentido, la presencia de la matriz extracelular es esencial y está estrechamente relacionado con la tolerancia a la desecación (Tamaru *et al.,* 2005). Además de los polisacáridos extracelulares neutros, existen, aunque en un porcentaje relativamente bajo, los polisacáridos de carga negativa. Sus grupos funcionales aniónicos pueden ser, por un lado, orgánicos como los ácidos urónicos, siendo los ácidos galacturónico y glucurónico los más representativos. Por otro lado, también se han descrito grupos funcionales aniónicos de naturaleza inorgánica como son los grupos sulfato. Estos últimos, se asocian clásicamente a las matrices extracelulares de macroalgas y microalgas de vida acuática, sobre todo marinas. Esta adaptación surge de la deshidratación provocada por el estrés salino, que se debe a que los sulfo-polisacáridos presentan propiedades hidrofílicas (Wingender *et al.,* 1999), por lo que, pueden establecer enlaces electrostáticos con las moléculas de agua, de esta forma reteniéndolas. Este hecho hace que las macroalgas se caractericen por tener una textura superficial gelatinosa.

La bioquímica de los polisacáridos sulfatados presenta un panorama similar al de los azúcares neutros. La composición monosacarídica, el nivel de sulfatación y el carbono al que se encuentra ligado este grupo funcional es diferente entre géneros y especies. Debido a la alta concentración de polisacáridos sulfatados en las macroalgas marinas, estas se han convertido en los organismos modelo para el estudio de estos compuestos. De acuerdo con sus pigmentos fotosintéticos, estos organismos pluricelulares se agrupan en: algas rojas (Rhodophyceae), verdes (Chlorophyceae) y pardas (Phaeophyceae). Las algas rojas poseen un galactano como cadena principal de polisacáridos y, la denominación de tal polímero depende del tipo de enantiómero que predomine, siendo agares cuando contiene residuos de L-galactosa, o carragenanos si son de tipo D. De este último, se han descrito hasta la fecha un total de 15 estructuras diferentes dependiendo de las sustituciones que presente (Jiao *et al.,* 2011). Por otra parte, las algas verdes que pertenecen al orden de los *Ulvales* presentan como polisacárido sulfatado mayoritario, el denominado ulvano. Este polímero está formado por unidades repetitivas

consistentes en un disacárido de ácido glucurónico y ramnosa llamado ácido ulvanaldobiouronico (Lahaye & Robic, 2007). Las sustituciones por sulfato difieren entre especies, siendo en el C-2 la posición mayoritaria como por ejemplo en *Ulva lactuca* (Lahaye *et al.,* 1996) y *Enteromorpha compressa* (McKinnell & Percival, 1962). Por último, los fucoidanos son los polímeros sulfatados que se encuentran en las algas pardas. Esta denominación se origina a raíz de que la fucosa es el monosacárido principal, aunque también presentan otros componentes en bajas concentraciones como manosa, glucosa, galactosa y xilosa (Cunha & Grenha, 2012; Duarte *et al.,* 2001). Los fucoidanos también se caracterizan por tener grandes ramificaciones. Hasta ahora se ha descrito sulfatación en las posiciones C-2, C-3 y C-4, dependiendo de la especie de alga parda (Cunha & Grenha, 2012).

Las proteínas extracelulares son otra parte importante en la matriz extracelular. La cantidad de exoproteínas pueden variar de cientos a miles dependiendo de los organismos y a las condiciones ambientales a las que están sujetos (Ruiz-May *et al.,* 2018). Las exoproteínas por lo general, presentan un peso molecular bajo (Helm & Potts, 2012). Dentro del exoproteoma, un gran porcentaje corresponde a proteínas con actividad enzimática, y dentro de éstas, la mayoría están relacionadas con la modificación de polisacáridos extracelulares ya que, por ejemplo, como se ha descrito anteriormente, en condiciones estresantes estos exopolisacáridos pueden ser hidrolizados para utilizarse como fuente de energía. Por otro lado, las proteasas son el segundo grupo de enzimas más abundantes en la matriz extracelular, siendo en gran medida responsables del metabolismo de las proteínas presentes en dicho espacio. Desde la perspectiva de las microalgas liquénicas, las proteínas extracelulares podrían jugar un papel particularmente importante en el proceso de simbiosis como, por ejemplo, las lectinas. Hasta el momento se han descrito varias lectinas en líquenes, las cuales se han relacionado con la especificidad entre hongo y ficobionte en el momento de la asociación (Díaz *et al.,* 2016; Singh & Walia, 2014; Sacristan *et al.,* 2006). Sin embargo, estas exoproteínas parecen ser exclusivas de la matriz

extracelular de hongos. (Díaz *et al.,* 2016).

2.4.1 Conocimientos previos de la matriz extracelular en microalgas liquénicas

Las investigaciones sobre las matrices extracelulares en microalgas se han centrado casi exclusivamente en aquellas de vida acuática como son *Chlorella* sp., *Chlorella vulgaris, Chlamydomonas, Botrycoccus braunii* (Xiao & Zheng, 2016). En relación con la composición en monosacáridos, la mayoría de las especies estudiadas tienen una característica común: que contienen mayoritariamente cuatro monosacáridos básicos (Moore & Tischer, 1964). Por ejemplo, la manosa parece ser clave en los exopolisacaridos ya que se ha encontrado en varias especies pertenecientes a Chlorophyceae (Lombardi *et al.,* 2005; Lombardi & Vieira, 1999). La galactosa y la glucosa son los dos principales monosacáridos en *Chlorella vulgaris* (Noda *et al.,* 1996) y *Dictyosphaeaerium chlorelloides* (Cybulska *et al.,* 2016), respectivamente. En cuanto a la proporción de proteínas extracelulares en microalgas acuáticas, como por ejemplo *C.vulgaris* y *Chodatella* sp. están entorno a un tercio y la mitad del total de la matriz extracelular (Chiou *et al.,* 2010), respectivamente.

Actualmente el conocimiento sobre la matriz extracelular y su papel fisiológico en las microalgas aeroterrestres es muy escaso. Un estudio referido a la especie liquénica *Trebouxia* sp. TR9, revela que posee una matriz extracelular compuesta predominantemente por un galactano, siendo la mitad del total de los polisacáridos extracelulares (Casano *et al.,* 2015). Por otro lado, la glucosa sería el segundo monosacárido más abundante (después de la galactosa) con casi un 30% del total de monosacáridos, seguida de porcentajes menores de ramnosa, manosa y arabinosa. Asimismo, la matriz extracelular de *Csol* fue analizada por Centeno et al. (2016), indicando que la galactosa se posicionaría como el monosacárido predominante. Sin embargo, a diferencia de TR9, las proporciones galactosa, manosa, glucosa y ramnosa de *Csol* son bastante similares. La matriz extracelular de ambas

microalgas presentaría polisacáridos de tipo aniónico debido a la presencia de ácidos urónicos. Sin embargo, no se ha demostrado la presencia de polisacáridos sulfatados ni en TR9 y *Csol* ni en otras especies del orden Trebouxiales (Baudelet *et al.,* 2017). En el trabajo antes citado, Centeno *et al.* (2016) exploraron también los exoproteomas de TR9 y *Csol*, observando las primeras diferencias en cuanto a las proteínas extracelulares entre ambas algas. *Trebouxia* sp. TR9 presenta un exoproteoma acídico con un punto isoeléctrico mayoritario entre 3.0 y 4.5, mientras que, el punto isoeléctrico de la mayoría de las exoproteínas de *Csol* estaría en un rango levemente más básico (3.8-4.7 pH). En cuanto al peso molecular, las proteínas extracelulares de TR9 son ligeramente superiores a 50KDa, y que, por el contrario, *Csol* estaría por debajo de ese margen.

Finalmente, los estudios que hacen referencia a la caracterización de la matriz extracelular se concentran prácticamente en microalgas de vida acuática y en condiciones control. Sin embargo, no existen investigaciones hasta la fecha sobre la posible participación de los polisacáridos y proteínas extracelulares en la respuesta frente a condiciones de desecación/rehidratación. Tampoco se sabe de qué manera la exposición a estas condiciones puede modificar la composición bioquímica y las propiedades de los polisacáridos y proteínas extracelulares.

Hipótesis y objetivos

Investigaciones sobre la pared celular y la matriz extracelular en otros organismos relacionados tolerantes a la desecación han evidenciado la existencia de una remodelación estructural y bioquímica de estas dos partes celulares, las cuales son esenciales para la supervivencia y adaptación a hábitats estresantes y, frecuentemente extremos. En el caso de las paredes celulares de las microalgas liquénicas, los pocos datos existentes reflejan que las microalgas de los géneros *Trebouxia*, *Asterochloris* y *Coccomyxa* estudiadas (Cordeiro *et al.,* 2005, 2007, 2008; Casano *et al.,* 2015; Centeno *et al.,* 2016) presentan β-galactofurananos como polisacáridos principales. Sin embargo, no existe ningún estudio que refleje cualquier cambio como consecuencia de la exposición a ciclos de desecación/rehidratación. Por otra parte, existe otro vacío de conocimiento acerca de los exopolímeros en algas liquénicas. Los resultados obtenidos en estudios anteriores indican claras diferencias en la abundancia y composición de los exopolisacáridos de *T. jamesii,* TR9 y *Csol*, los cuales son consistentes con las diferencias en la capacidad de retención extracelular de metales pesados (Álvarez *et al.,* 2012) y con la menor tasa de pérdida de agua de TR9 respecto de *Csol* (Centeno *et al.,* 2016).

En base a las evidencias expuestas anteriormente, se plantea la siguiente hipótesis general en la cual se enmarca la presente Tesis Doctoral:

Hipótesis general: *las microalgas liquénicas* Trebouxia *sp. TR9 y Coccomyxa simplex presentarían dos estrategias diferentes de tolerancia a la desecación, las cuales están relacionadas con una adaptación al medio en el que crece el liquen del que forma parte cada microalga. En este contexto, la ultraestructura y propiedades bioquímicas del conjunto formado por la pared celular y la matriz extracelular de Csol serían las que mejor responden a condiciones hídricas relativamente estables, mientras que, en TR9 estarían a adaptadas a ciclos relativamente más rápidos y drásticos de deshidratación/rehidratación. Asimismo, es posible que la exposición a condiciones de estrés hídrico similares a las de sus respectivos hábitats*

provoque cambios bioquímicos en la pared celular y la matriz extracelular de cada microalga.

En base a esto se plantea como Objetivo General un estudio comparativo de las principales características ultraestructurales y fisiológico-moleculares, centrado en la pared celular y la matriz extracelular de las microalgas liquénicas *Csol* (*Coccomyxa simplex*) y TR9 (*Trebouxia* sp.) aisladas y expuestas a varios ciclos de desecación-rehidratación.

Los objetivos específicos se han dividido en dos bloques, uno correspondiente a la pared celular y otro, a la matriz extracelular.

Objetivos específicos para la pared celular

- Análisis detallado de la composición de la pared celular de TR9 y *Csol* antes (control, totalmente hidratado) y después de cuatro ciclos desecación/rehidratación. En general, se separarán las principales fracciones de polisacáridos matriciales y estructurales para la posterior determinación de la composición y ligación glicosídica por técnicas de GC-MS.
- Estudiar los posibles cambios en la citoarquitectura de TR9 y *Csol* durante la desecación/rehidratación, mediante TEM, SEM y microscopía confocal. El propósito de este objetivo es correlacionar las diferencias a nivel bioquímico-molecular con la capacidad de plegamiento controlado de la pared celular y de preservación de la integridad de las estructuras celulares básicas en las dos microalgas a estudiar.

Objetivos específicos para la matriz extracelular

- Análisis general de los diferentes componentes que forman parte de la matriz extracelular de TR9 y *Csol* en condiciones control y después de cuatro ciclos desecación/rehidratación, tales como polisacáridos, ácidos urónicos, proteínas y polisacáridos sulfatados.
- En relación con los polisacáridos neutros, se analizarán las principales fracciones para identificar su composición y ligación glicosídica. Determinación estructural mediante la purificación de posibles polisacáridos sulfatados para su posterior análisis mediante técnicas

como RMN, composición y ligación glicosídica por GC-MS.

- Análisis comparativo de los perfiles exoproteómicos de *Trebouxia* sp. TR9 y *Coccomyxa simplex*, en condiciones control y tras cuatro ciclos de desecación/rehidratación por medio de purificación de exoproteínas y su posterior análisis mediante LC-MS/MS, y empleo de herramientas bioinformáticas con el fin de identificar las exoproteínas, analizar sus propiedades y asignarles posibles funciones.

Publicaciones que componen la Tesis Doctoral

PUBLICACIONES CIENTÍFICAS

González-Hourcade, M., Braga, M. R., del Campo, E. M., Ascaso, C., Patiño, C. and Casano, L. M. (2020) Ultrastructural and biochemical analyses reveal cell wall remodelling in lichen-forming microalgae submitted to cyclic desiccation-rehydration. *Ann Bot,* 125(3), 459-469.

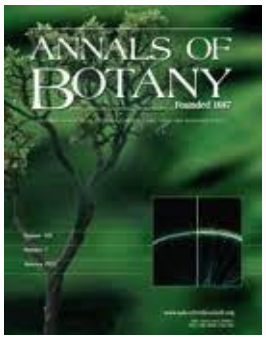

Revista científica	Annals of Botany
Factor de impacto de los últimos 5 años (2019).	4,689
Cuartil y position (2019)	Q1 (27/234)

González-Hourcade, M., del Campo, E. M., Braga, M. R., Salgado, A. and Casano, L. M. (2020) Disentangling the role of extracellular polysaccharides in desiccation tolerance in lichen-forming microalgae. First evidence of sulfated polysaccharides and ancient sulfotransferase genes. *Environ Microbiol* (En impresión).

Revista científica	Environmental Microbiology
Factor de impacto de los últimos 5 años (2019).	5,453
Cuartil y position (2019)	Q1 (27/135)

González-Hourcade, M., del Campo, E. M., and Casano, L. M. (2020) The under-explored extracellular proteome of aero-terrestrial microalgae provides clues on different mechanisms of desiccation tolerance in non-model organisms. *Plant Mol Biol* (En revisión)

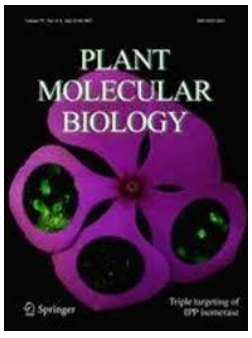

Revista científica	Plant Molecular Biology
Factor de impacto de los últimos 5 años (2019).	4,065
Cuartil y position (2019)	Q1 (42/234)

Primer artículo

Ultrastructural and biochemical analyses reveal cell wall remodelling in lichen-forming microalgae submitted to cyclic desiccation-rehydration

Annals of Botany **125**: 459–469, 2020
doi: 10.1093/aob/mcz181, available online at www.academic.oup.com/aob

ANNALS OF BOTANY
Founded 1887

Ultrastructural and biochemical analyses reveal cell wall remodelling in lichen-forming microalgae submitted to cyclic desiccation–rehydration

María González-Hourcade[1], Marcia R. Braga[2], Eva M. del Campo[1], Carmen Ascaso[3], Cristina Patiño[4] and Leonardo M. Casano[1,*]

[1]University of Alcalá, Department of Life Sciences, 28871-Alcalá de Henares, Madrid, Spain, [2]Institute of Botany, Department of Plant Physiology and Biochemistry, 04301-012 São Paulo, SP, Brazil, [3]Museo Nacional de Ciencias Naturales, CSIC, Department of Biogeochemistry and Microbial Ecology, c/Serrano 115, 28006, Madrid, Spain and [4]Centro Nacional de Biotecnología, CSIC, c/Darwin 3, 28049, Madrid, Spain
For correspondence. E-mail leonardo.casano@uah.es2020125**3459470*

Received: 10 September 2019 Returned for revision: 15 October 2019 Editorial decision: 25 October 2019 Accepted: 29 October 2019
Published electronically 4 November 2019

• **Background and Aims** One of the most distinctive features of desiccation-tolerant plants is their high cell wall (CW) flexibility. Most lichen microalgae can tolerate drastic dehydration–rehydration (D/R) conditions; however, their mechanisms of D/R tolerance are scarcely understood. We tested the hypothesis that D/R-tolerant microalgae would have flexible CWs due to species-specific CW ultrastructure and biochemical composition, which could be remodelled by exposure to cyclic D/R.
• **Methods** Two lichen microalgae, *Trebouxia* sp. TR9 (TR9, adapted to rapid D/R cycles) and *Coccomyxa simplex* (Csol, adapted to seasonal dry periods) were exposed to no or four cycles of desiccation [25–30 % RH (TR9) or 55–60 % RH (Csol)] and 16 h of rehydration (100 % RH). Low-temperature SEM, environmental SEM and freeze-substitution TEM were employed to visualize structural alterations induced by D/R. In addition, CWs were extracted and sequentially fractionated with hot water and KOH, and the gel permeation profile of polysaccharides was analysed in each fraction. The glycosyl composition and linkage of the main polysaccharides of each CW fraction were analysed by GC–MS.
• **Key Results** All ultrastructural analyses consistently showed that desiccation caused progressive cell shrinkage and deformation in both microalgae, which could be rapidly reversed when water availability increased. Notably, the plasma membrane of TR9 and Csol remained in close contact with the deformed CW. Exposure to D/R strongly altered the size distribution of TR9 hot-water-soluble polysaccharides, composed mainly of a β-3-linked rhamnogalactofuranan and Csol KOH-soluble β-glucans.
• **Conclusions** Cyclic D/R induces biochemical remodelling of the CW that could increase CW flexibility, allowing regulated shrinkage and expansion of D/R-tolerant microalgae.

Key Words: Cell wall, cell wall folding, cell wall remodelling, *Coccomyxa*, desiccation, desiccation tolerance, lichen, microalgae, *Trebouxia*.

INTRODUCTION

Lichens are mutualistic symbiotic systems in which at least two different organisms coexist: a fungus (mycobiont) and one or more photosynthetic partner that can belong to the cyanobacteria (cyanobiont) and/or the green algae (phycobiont). In some of these systems, the presence of two or more microalgae (Casano *et al.*, 2011), bacteria (Molins *et al.*, 2013) or yeasts (Aschenbrenner *et al.*, 2014) has recently been described. Lichens are found in a variety of environments that range from mild habitats such as humid tropical forests (Aragón *et al.*, 2016) to extreme ecosystems such as the Arctic (Ascaso *et al.*, 1990; Zhang *et al.*, 2015) and hot deserts (Vargas Castillo *et al.*, 2017), where vascular plants cannot grow (Fritsch and Haines, 1923; Belnap *et al.*, 2001).

Lichens and their green microalgae have both been described as poikilohydric organisms, meaning that they do not actively regulate their water content; consequently, they depend on the availability of water in the environment. Lichens can be exposed to long periods of water shortage, which causes protoplast desiccation, a potentially strong abiotic stress (Kranner *et al.*, 2008). When water becomes available again, the lichen thallus rehydrates, and after the first few minutes or hours of rehydration active metabolism is restored (Schroeter *et al.*, 1992; Tuba *et al.*, 1996). Accordingly, these organisms, adapted or acclimatized to alternating desiccation–rehydration (D/R) cycles, have developed desiccation tolerance (DT), defined as a set of strategies to cope with these extreme conditions, which permit survival with a cellular water content of ~5–10 % (Gaff, 1971; Holzinger and Karsten, 2013), in some cases for long periods (Kranner *et al.*, 2008).

Ramalina farinacea is an epiphytic fruticose lichen that is widely distributed in Mediterranean environments and is adapted to continuous rapid cycles of diurnal and/or seasonal desiccation and rehydration (Casano *et al.*, 2011) with an average relative humidity (RH) of ~25–30 %. *Solorina saccata* is a foliose lichen with a geographical distribution that encompasses

mild and cold areas, where it is normally protected in cracks of calcareous rocks, which predominantly present microenvironments with an RH of 55–60 % (during the dry season) or more. In a previous study (Centeno *et al.*, 2016), we studied the physiological responses of two lichen microalgae with a contrasting habitat preference, when exposed to desiccation below 25–30 % RH and then rehydrated. These were *Trebouxia* sp. TR9 (TR9), isolated from *R. farinacea*, and *Coccomyxa simplex* (Csol), obtained from *S. saccata*. The relative water content and water potential were recorded throughout the process together with sugar and primary metabolite profiles. Under these experimental conditions, both desiccation and rehydration occurred more rapidly in Csol than in TR9. Metabolomic analyses showed notable differences between the two microalgae, whereby TR9 was constitutively richer in polyols and capable of increasing synthesis of osmo-compatible solutes during desiccation, whereas Csol increased polyol synthesis under D/R. Although both microalgae are desiccation-tolerant, in TR9 this capacity seems to rely mainly on constitutive features, whereas in Csol a higher proportion of inducible mechanisms appears to play a role in DT.

The most studied desiccation-tolerant organisms are those known as 'resurrection plants', a group of angiosperms that activate physiological, structural and biochemical responses to cope with desiccation stress (Farrant *et al.*, 2017 and references therein). These plants and some charophyte algae have evolved flexible cell walls (CWs), with distinctive biochemical and ultrastructural features, that fold as the protoplast shrinks due to dehydration and expand during rehydration (Moore *et al.*, 2008*a*,*b*; Holzinger and Pichrtová, 2016). The immediate consequence of this CW flexibility is to prevent the mechanical stress occurring during dehydration in cells with a relatively rigid CW, which damages the subtle connections between plasma membrane and wall (Sherwin and Farrant, 1996; Vicré *et al.*, 2004; Moore *et al.*, 2006). Recently, Farrant *et al.* (2017) reported that the flexibility of the CWs of the resurrection plant *Craterostigma wilmsii* seems to increase under desiccation conditions due to changes in glycosyl composition and the molecular size of xyloglycans. The 'controlled collapse' of CWs and changes in CW thickness have also been observed in the green microalga *Klebsormidium* (Streptophyta) under similar conditions (Holzinger and Karsten, 2013).

Few studies have been conducted on CW polysaccharide composition in lichen-forming algae. Besides a very low content (or even absence) of cellulose, the predominance of β-galactofuranans has been reported in the photobionts of *Ramalina gracilis* and *Cladina confusa* (Cordeiro *et al.*, 2005, 2007). More recently, we analysed the ultrastructure and polysaccharide composition of the microalgae of *R. farinacea*. Two green microalgae (*Trebouxia jamesii* and TR9) with different CWs (Casano *et al.*, 2011) coexist in this epiphytic lichen. At the ultrastructural level, we observed four clearly differentiable layers in the *T. jamesii* CW, whereas TR9 showed a more diffuse structure in which only three layers could be distinguished. Fractionation of *T. jamesii* and TR9 CWs revealed a high proportion of galactose, xylose and rhamnose that was associated with a β-xylorhamnogalactofuranan present in the hot water fraction. Meanwhile, the alkaline fraction showed high proportions of galactose, glucose and mannose similar to those found in *Asterochloris erici* (Cordeiro *et al.*, 2007). In addition, a comparative analysis of TR9 and Csol CWs indicated that although both CWs had the same number of layers (three), these were thinner and more defined in Csol than in TR9 (Casano *et al.*, 2011, Álvarez *et al.*, 2015). Furthermore, glucose, mannose, galactose and rhamnose were the predominant monosaccharides in Csol, in contrast to the glycosyl composition of the TR9 CW. Some genera of Trebouxiophyceae, such as *Coccomyxa*, also present algaenans, highly aliphatic, insoluble, non-enzymatically hydrolysable biopolymers previously known as sporopollenin (Zhang and Volkman, 2017), in the outermost layer of their CWs (Honegger, 2012 and references therein). Algaenans could play a role associated with resistance to biotic and desiccation stress (Dunker and Wilhelm, 2018). The distribution of algaenans in the class Trebouxiophyceae is not uniform, since they have been found in the CWs of some species of *Coccomyxa* and *Myrmecia*, but their presence is controversial in the *Trebouxia* genus (Honegger and Brunner, 1981; König and Peveling, 1984).

It should be noted that analyses of algal CWs in general, and those of lichen microalgal CWs in particular, have primarily been performed with cells under control (hydrated) conditions rather than the cyclic D/R conditions that often occur in natural lichen habitats. This practice may fail to detect information on the degree of DT or acclimation responses. Therefore, our hypothesis was that lichen microalgae such as TR9 and Csol with distinctive DT strategies, probably resulting from adaptation/acclimation to contrasting environments, would have flexible CWs. However, this mechanical feature might vary between these two microalgae due to species-specific ultrastructural arrangement and biochemical composition, which in turn might be remodelled by exposure to cyclic D/R. In consequence, the aim of the present study was to investigate whether these lichen microalgae are capable of folding and expanding their CWs following protoplast contraction and expansion due to exposure to desiccation and rehydration, respectively. In addition, we sought to determine possible acclimation changes in CW polysaccharides after exposure to cyclic D/R in which each alga was desiccated under conditions similar to those found in their natural habitats (25–30 % RH for TR9, 55–60 % for Csol).

MATERIALS AND METHODS

Microalga isolation and culture

Trebouxia sp. TR9 microalga was isolated from the lichen *Ramalina farinacea* collected at Sª El Toro (Castellón, Spain; 39°54′16″ N, 0°48′220″ W) (Gasulla *et al.*, 2010). *Coccomyxa simplex* (formerly *C. solorinae-saccatae*, strain 216-12) was obtained from the SAG Culture Collection of Algae (Sammlung von Algenkulturen) at Göttingen University (Germany). According to this algal bank, Csol was isolated from the lichen *Solorina saccata* found in Großer St Bernhard, Switzerland (45°57′4″ N, 7°12′32″ W). Both microalgae were cultured under axenic conditions on small nylon squares (4 cm^2) in semisolid supplemented Bold 3N medium (Bold and Parker, 1962), inside a growth chamber at 15 °C under a 14-h/10-h light/dark cycle (light conditions: 25 µmol m^{-2} s^{-1}).

D/R treatment

Nylon squares containing 3-week-old cultures of Csol and TR9 (~180–200 and 200–300 mg FW, respectively) were removed from the culture medium and placed in a climatic chamber (K110; Pol-eko-Aparatura, Poland) for the four D/R cycles. The desiccation conditions, established as optimal for each microalga in previous experiments (Hell *et al.*, 2019), were 25–30 % RH for TR9 and 55 % RH for Csol cultures at 25 °C for 8 h. Afterwards, the cultures were transferred to Petri dishes with a semisolid medium, composed of 1.5 % agar in distilled water, at 100 % RH and 20 °C for 16 h. At the indicated times, samples were collected from the desiccation or rehydration treatment and weighed prior to subsequent microscopic analyses or CW extraction. Fully hydrated cells prior to D/R cycles were considered the control condition.

Structural analyses

For transmission electron microscopy (TEM) analysis, TR9 and Csol samples before and after four D/R cycles (in desiccated and rehydrated state) were high-pressure-frozen and freeze-substituted (Aichinger and Lütz-Meindl, 2005) with modifications. Samples were frozen in a Leica EM PACT2 high-pressure freezer and freeze-substituted with 1.5 % osmium tetroxide in acetone for 54 h at −90 °C then 4 h at −30 °C and 2 h at 4 °C in a Leica AFS2 freeze-substitution apparatus. After three washes with anhydrous acetone, samples were embedded in Epon 812 resin at room temperature and polymerized for 48 h at 60 °C. Seventy-nanometre sections were obtained in a Leica EM UC6 ultramicrotome and mounted on 200 mesh nickel grids, post-stained with 2 % (w/v) aqueous uranyl acetate and 2 % lead citrate and observed with a JEOL JEM 1011 (100 kV) electron microscope equipped with a Gatan Erlangshen ES1000W digital camera.

For low-temperature scanning electron microscopy (LTSEM), microalgae were observed by high-resolution field emission gun scanning electron microscopy (FEG-SEM) at low temperature before and after one cycle of D/R (in desiccated and rehydrated state). An AQUILO cryo preparation chamber (PP3010T, Quorum Technology) was connected to the FEG-SEM. Small samples of algal cultures were mounted using a mixture of 50 % Tissue Tek/50 % colloidal graphite and rapidly frozen under vacuum conditions. The cryo preparation chamber was maintained under high vacuum and cooled during fracturing, sublimation of surface ice and metal and carbon coating. Then, samples were transferred to a cold stage in the SEM chamber for FEG-ESEM analysis under cryogenic conditions.

Environmental scanning electron microscopy (ESEM) can be used to record secondary images under conditions of water vapour pressure and temperature up to water saturation (RH = 100 %). Algal samples were mounted on the stainless-steel stub with double-sided carbon adhesive and left to equilibrate at 5 °C for 15 min and then subjected to eight controlled vapour-pressure purges (from 99–100 % to 10 % and then from 10 % to 100 % RH), allowing the samples to equilibrate for several minutes at each RH level. Images were taken at each RH level. Samples of Csol were observed using a FEI Quanta 400 instrument under conditions of 15 kV acceleration potential and at a working distance of 5–10 nm. Samples of TR9 were visualized by means of field-emission gun high resolution ESEM (FEG-ESEM), using a QuemScan650F model (FEI, Netherlands) in environmental mode (10–4000 Pa). For this purpose, the GESED detector and 5–10 kV acceleration potential was applied.

The presence/absence of algaenans in the CW of both algal species was assessed by light microscopy (Eclipse Ci-L; Nikon) after crystal violet staining according to Zych *et al.* (2009).

Extraction and fractionation of CW components

After extraction of the extracellular polymeric substances attached to the external surface of the CW (Casano *et al.*, 2015), Csol and TR9 microalgae (1–5 g FW) were subjected to four cycles in a French press (1350 psi), which disrupted 95 % of the control cells in both algae. However, in cells exposed to D/R conditions, disruption was slightly less efficient since we observed a higher proportion of unbroken cells (~10–15 %). Cell walls were pelleted (10 000 *g*, 15 min at 4 °C) and washed with 30 mL of 100 mM NaCl and twice with ultrapure water. Cell debris was removed by successive washes with organic solvents: three times with 93 % ethanol (20 mL g^{-1} FW), once at room temperature overnight, once under the same conditions for 2 h and once at 80 °C with gentle stirring for 2 h; twice with chloroform:methanol 1:1 (v/v) (20 mL g^{-1} FW) with stirring for 1 h; and twice with pure acetone at room temperature for 8 h each time. Cell walls were filtered through glass-fibre filters (Merck Millipore), dried in an oven at 60 °C for 2 d and weighed.

Cell walls of TR9 and Csol were fractionated by successive extraction with ultrapure hot water (HW) and 10 % KOH (KOH) (Cordeiro *et al.*, 2005). Briefly, 120 mg of CW was suspended in 9 mL of ultrapure water and stirred at 100 °C for 4 h and then centrifuged (14 500 *g*, 5 min). This procedure was performed twice and the supernatants were combined, dialysed, freeze-dried and considered as the HW-soluble fraction. The insoluble material was suspended in 9 mL of 10 % KOH and maintained at room temperature overnight with gentle agitation. After centrifugation (14 500 *g*, 5 min), the insoluble material was re-extracted by stirring with 10 % KOH at 100 °C for 4 h. Combined KOH supernatants were neutralized with acetic acid and precipitated with 3 volumes of 93 % ethanol at 4 °C overnight. After centrifugation (21 000 *g*, 5 min) and washing with 93 % ethanol, the precipitate was dried, re-solubilized in ultrapure water and considered as the KOH-soluble fraction. Total neutral sugars were determined by the phenol-H_2SO_4 method (Dubois *et al.*, 1956) using glucose as standard.

Gel-permeation chromatography

Aliquots of HW- and KOH-soluble fractions (~2 mg of neutral sugars) were added to a 70.0 × 1.6 cm (ID) Sepharose 4B column C (General Electric Healthcare) equilibrated with 150 mM phosphate–citrate buffer (pH 5.2) and eluted with the same buffer. The amount of neutral carbohydrates in each 2-mL fraction was determined as described above. Dextrans of 9.3, 76, 156 and 2000 kDa (Sigma–Aldrich, St Louis, MO, USA)

were used as standards for column calibration. Based on the carbohydrate amounts recovered from the column, the most prominent peaks were selected. In cases of CW fractions with polydisperse profiles, we selected the fractions with the highest mass. Therefore, ten eluted peaks from HW- and KOH-soluble fractions from control and D/R TR9 and Csol algae were dialysed (cut-off 2000 kDa) against bi-distilled water and lyophilized to perform glycosyl composition and glycosyl linkage analyses.

Glycosyl composition analysis

Glycosyl composition of selected fractions was analysed by combined gas chromatography–mass spectrometry (GC–MS) of the per-*O*-trimethylsilyl derivatives of the monosaccharide methyl glycosides produced from the samples by acidic methanolysis as described previously by Santander *et al.* (2013). Briefly, ~100–400 µg of the sample was heated with 1 M HCl in MetOH at 80 °C for 17 h. Then, a re-N-acetylation was carried out with a mixture of MetOH, pyridine and acetic anhydride for 30 min. The solvents were evaporated and the samples were derivatized with Tri-Sil® (Pierce) at 80 °C for 30 min. The GC–MS analysis of the per-*O*-trimethylsilyl methyl glycosides was performed using an Agilent 7890A GC interfaced to a 5975C MSD, equipped with a Supelco Equity-1 fused silica capillary column (30 m × 0.25 mm ID).

Glycosyl linkage analysis

Six of the ten samples contained sufficient sample mass (~1 mg) to perform a glycosyl linkage analysis. These samples were permethylated and reduced twice and acetylated, and the resulting partially methylated alditol acetates were analysed by GC–MS according to Heiss *et al.* (2009) with a slight modification. Briefly, the samples were suspended in dimethyl sulphoxide and stirred for 1 d and then permethylated using potassium dimsyl anion and iodomethane, and, in the case of uronic acids, reduced with lithium borodeuteride. After sample clean-up, permethylated material was subjected to two rounds of treatment with sodium hydroxide (15 min) and methyl iodide (45 min). The permethylated material was hydrolysed using 2 M trifluoroacetic acid (2 h at 121 °C), reduced with sodium borodeuteride and acetylated using acetic anhydride/trifluoroacetic acid. The resulting partially methylated alditol acetates were analysed using an Agilent 7890A GC interfaced to a 5975C Mass Selective Detector in electron impact ionization mode; separation was performed in a 30-m Supelco SP-2331 bonded-phase fused silica capillary column.

RESULTS AND DISCUSSION

Structural changes during D/R in lichen microalgae

Compelling evidence has been reported in recent years of a positive causal relationship between the response of plants and algae to water deficit and the biophysical properties of their CWs (Moore *et al.*, 2008*a*,*b*; Shtein *et al.*, 2018). The first step of our investigation was to analyse the ultrastructural modifications occurring during desiccation and rehydration of fully hydrated TR9 and Csol cells.

Desiccation/rehydration-induced structural alterations in TR9 and Csol, especially in their CW and plasma membrane, were visualized by TEM, LTSEM and ESEM (Figs 1–5). The TEM and LTSEM images of TR9, taken after four and one D/R cycle(s) respectively, showed that desiccation caused progressive cell shrinkage and CW deformation, which could be rapidly reversed when water availability increased (Fig. 1A–F and Supplementary Data Fig. S1). These changes were also observed in Csol (Fig. 2A–F), even though this latter microalga seemed to recover to a slightly lesser extent upon rehydration compared with TR9 since several cells did not completely expand. This difference in degree of recovery after desiccation linked to CW features was also found when employing ESEM, which permits rapid changes in the RH to which cells are exposed during microscope observation (Fig. 3). Under these conditions, TR9 tolerated an RH as low as 10 % and recovered after desiccation for up to five relatively rapid D/R cycles (entire cycle 20–25 min) (Fig. 3, upper panels). In contrast, Csol did not tolerate such drastic desiccation conditions, requiring a higher RH (60–65 %) during desiccation in order to recover upon rehydration (Fig. 3, lower panels). These findings suggest that TR9 is better adapted to rapid changes in water status, whereas Csol seems to need slower desiccation, probably in order to activate certain tolerance features. Irrespective of this, when desiccation was conducted at RH or speed similar to that encountered in their respective habitats, TR9 (Fig. 4 and Supplementary Data Fig. S2) and Csol (Fig. 5) plasma membranes remained in close contact with the deformed CW.

Crystal violet staining revealed a profound difference in CW permeability between TR9 and Csol, as only 21 % of Csol cells allowed dye entry whereas almost all TR9 cells became stained (Supplementary Data Fig. S3). Since algaenan hinders the penetration of large molecules of crystal violet (Zych *et al.*, 2009), our result indicates the absence of this biopolymer in the TR9 CW and its presence in Csol. These findings support those reported by Honegger (2012) regarding the presence of algaenan in *Coccomyxa* microalgae. However, the presence of algaenan in the algal CW of *Trebouxia* species remains controversial. König and Peveling (1984) have reported its presence in several *Trebouxia* species, but Honegger and Brunner (1981) did not find any acetolysis-resistant material, a characteristic of algaenan, in almost the same algal species. Our results clearly indicate that the CW of *Trebouxia* sp. TR9 species did not contain this highly resistant polymer and they therefore support the notion that the presence of algaenans is associated with typical trilaminar CWs, such as those of *Coccomyxa* species. In addition, we observed that the presence/absence of algaenan in Csol and TR9 was not modified by exposure to cyclic D/R (data not shown).

The diffuse trilaminar organization of the TR9 CW observed before D/R was preserved during desiccation (Fig. 4 A, B, D, E). However, after rehydration the inner and outermost layers (L1 and L3, respectively) became thinner while the intermediate layer (L2) became slightly thicker, so that the entire CW appeared to have a relatively more defined trilaminar structure, although total CW thickness did not change

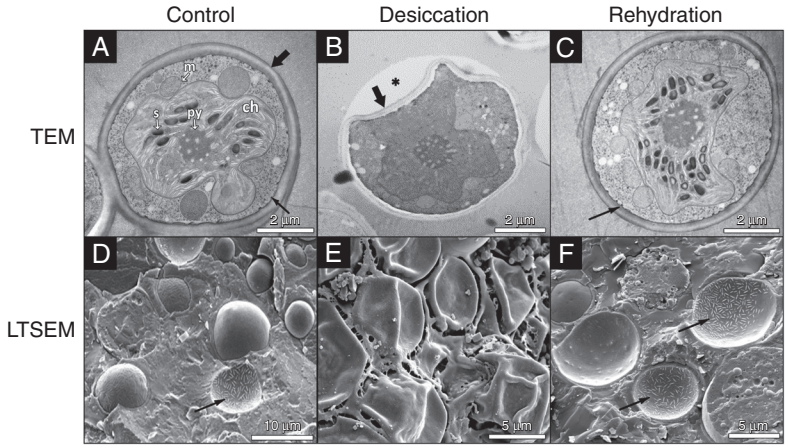

FIG. 1. TEM and LTSEM micrographs of *Trebouxia sp.* TR9 exposed to cyclic D/R. For TEM, TR9 cells were exposed to no D/R cycles (control, A) or four D/R cycles (desiccation, B; rehydration, C). For LTSEM, TR9 cells were exposed to no D/R cycles (control, D) or a single D/R cycle (desiccation, E; rehydration, F). Thick arrows indicate the CW and thin arrows mark plasmalemma invaginations. The asterisk in (B) indicates a gap between the Epon 812 resin and the CW, probably due to reduced adherence of the collapsed regions to the resin. Abbreviations in (A): ch, chloroplast; m, mitochondrion; py, pyrenoid; s, starch.

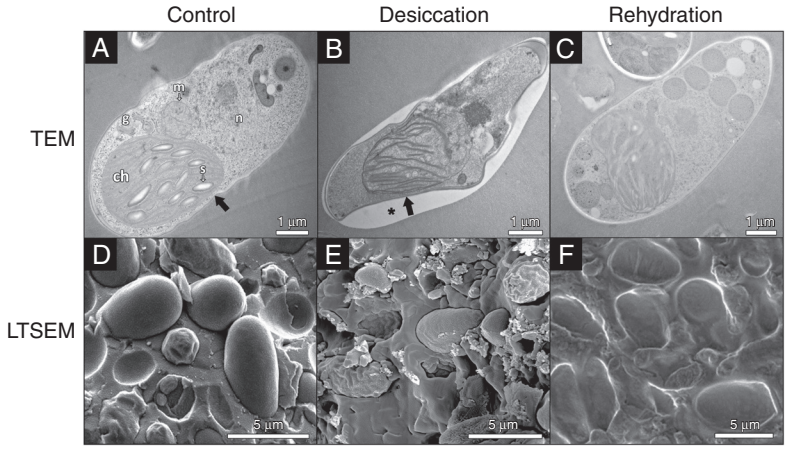

FIG. 2. TEM and LTSEM micrographs of *Coccomyxa simplex* exposed to cyclic D/R. For TEM, Csol cells were exposed to no D/R cycles (control, A) or four D/R cycles (desiccation, B; rehydration, C). For LTSEM, Csol cells were exposed no D/R cycles (control, D) or a single D/R cycle (desiccation, E; rehydration, F). Thick arrows indicate the CW. The asterisk in (B) indicates a gap between the Epon 812 resin and the CW, probably due to reduced adherence of the collapsed regions to the resin. Abbreviations in (A): ch, chloroplast; g, Golgi apparatus; m, mitochondrion; n, nucleus; s, starch.

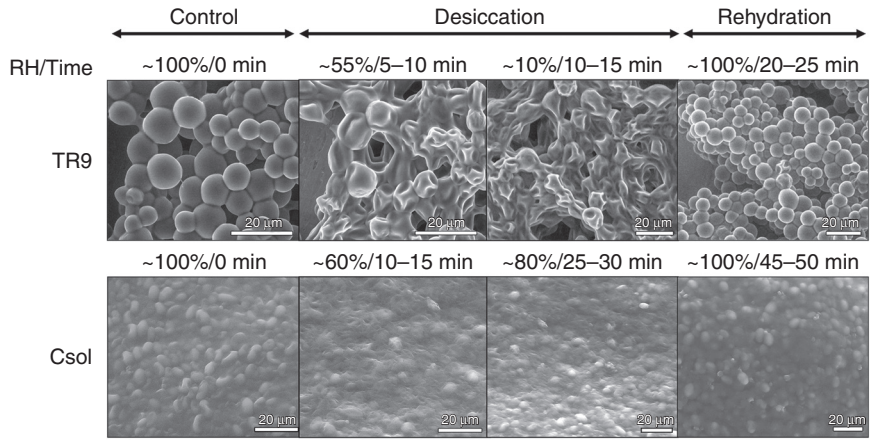

FIG. 3. ESEM micrographs of TR9 and Csol during a D/R cycle. Algal samples were left to equilibrate at 5 °C for 15 min and then subjected to eight controlled vapour pressure purges (from 99–100 % up to 10 % and then from 10 % to 100 % RH), allowing the samples to equilibrate for several minutes at each RH level. Images in the figure depict the key stages, timing and RH conditions during a D/R cycle, including the lowest RH below which Csol did not normally rehydrate, under ESEM conditions.

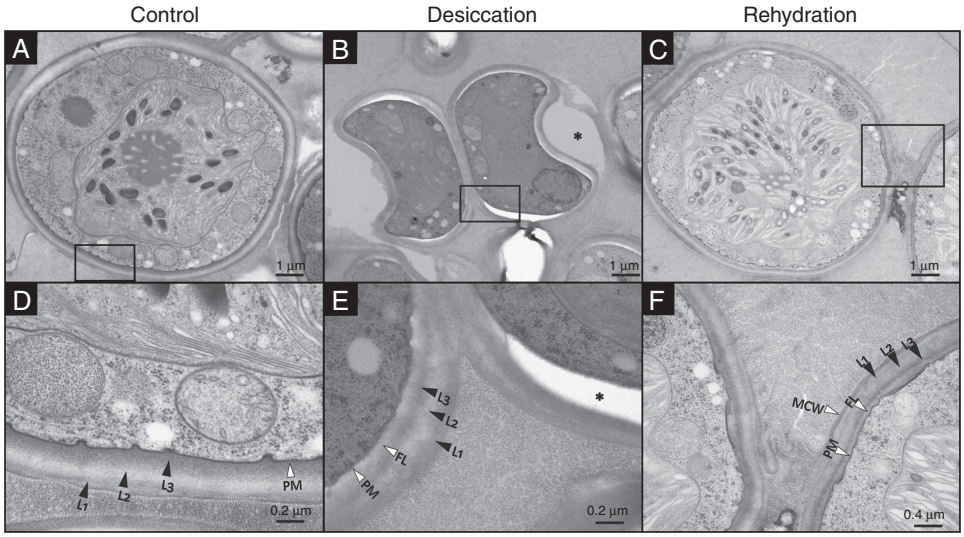

FIG. 4. TEM micrographs of TR9 sections with CW details during a D/R cycle. Rectangles in panels (A–C) indicate the areas shown at greater magnification in panels (D–F), respectively. The asterisk in (E) indicates a gap between the Epon 812 resin and the CW, probably due to reduced adherence of the collapsed regions to the resin. L1, L2 and L3 indicate the diffuse three-layer structure of the CW. FL, fibrillar layer; PM, plasma membrane; MCW, mother cell wall.

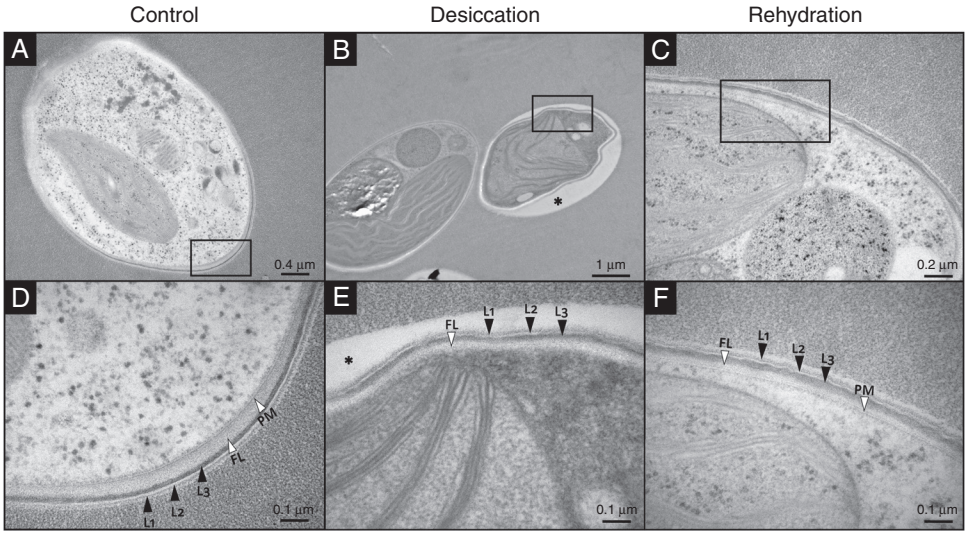

FIG. 5. TEM micrographs of Csol sections with CW details during a D/R cycle. Rectangles in panels (A–C) indicate the areas shown at higher magnification in panels (D–F), respectively. The asterisk in (B) and (E) indicates a gap between the Epon 812 resin and the CW, probably due to reduced adherence of the collapsed regions to the resin. L1, L2 and L3 indicate the typical three-laminar organization of the CW. FL, fibrillar layer; PM, plasma membrane.

significantly during D/R (Fig. 4 C, F and Supplementary Data Fig. S4). In contrast, the CW thickness of Csol decreased significantly during desiccation and recovered upon rehydration, but no apparent changes in its well-defined trilaminar structure were observed under D/R (Fig. 5 and Supplementary Data Fig. S4). In desiccation-tolerant moss protonemata, dehydration induces marked cytological alterations, including CW folding and changes in thickness (Pressel and Duckett, 2010).

Early studies on drying seeds by Webb and Arnott (1982) revealed that the 'controlled collapse' of the CW was necessary to maintain structural organization and cell viability in the desiccated state. Importantly, they found that CW deformation occurred in a species-specific manner and was related to the biochemical composition of the CW. This notion has now been extended to other desiccation-tolerant organisms (Shtein *et al.*, 2018), such as resurrection plants, in which the presence of plasticizing polysaccharides such as arabinans confers high flexibility on their CWs (Moore *et al.*, 2008*a*).

Cell wall biochemistry

Cell wall polysaccharides are constantly remodelled by several enzymes to adjust CW mechanical properties to changes in internal and external environmental conditions (Simmons *et al.*, 2015 and references therein). The ultrastructural adjustments observed in TR9 and Csol CWs during D/R strongly suggest that at least some of the main CW components were subjected to biochemical remodelling. Therefore, we conducted a comparative analysis of the polysaccharides in CW fractions from the two microalgae.

Fractionation of the CW yielded a significantly higher proportion of alkali-soluble (KOH) than hot-water-soluble (HW) polysaccharides in both TR9 and Csol under control conditions (T0). However, the KOH fraction in TR9 was 3.3 times higher than the HW one, whereas in Csol the latter was only 1.4 times higher than the former (Table 1). Exposure to four D/R cycles increased the proportion of HW polysaccharides in TR9, which contrasted with the reduction of both fractions in Csol.

The gel permeation profile of sugar-containing polymers in the HW fraction showed a main sharp peak of ~75 kDa in TR9 (Fig. 6A, peak 1) under control conditions (Table 1). After D/R cycles, we observed a marked shift in polymer distribution towards molecules of higher (to a greater extent) and lower molecular mass than 75 kDa (Fig. 6 A, Table 1). Previous glycosyl composition and linkage analyses of the crude CW of (control) TR9 algae indicated the predominance of a 3-linked galactofuranan substituted at the 6 position by rhamnosyl residues (Casano *et al.*, 2015). In this study, the polysaccharide(s) corresponding to peak 1 obtained by gel filtration chromatography of HW polymers showed galactose,

TABLE 1. *Effects of cyclic D/R on yield, molecular mass and glycosyl composition of cell wall polysaccharides of TR9 and Csol phycobionts. Cell walls were isolated before (T0) and after four D/R cycles, and fractionated sequentially with hot water (HW) and alkali (KOH). Each fraction was submitted to gel filtration chromatography on a Sepharose 4B column. Glycosyl composition analysis of selected fractions was performed by combined GC–MS of the per-*O*-trimethylsilyl derivatives of the monosaccharide methyl glycosides (Santander et al., 2013)*

Species	Treatment	Fraction	Fraction yield (% of CW mass)	Selected peak	Average molecular mass (kDa)	Monosaccharides (mol %)						
						Ara	Rha	Fuc	Xyl	Man	Gal	Glc
TR9	T0	HW	10.6	1	75	3.4	10.1	–	4.1	3.2	55.0	24.3
		KOH	35.6	3	174	1.3	23.6	–	39.5	0.6	30.7	4.4
	D/R	HW	14.6	2	103	–	32.5	–	8.0	–	59.5	–
		KOH	34.2	4	19	4.3	10.9	–	49.6	3.6	29.6	1.9
Csol	T0	HW	13.5	5	47	3.7	18.6	18.6	30.5	17.0	8.0	
		KOH	18.6	6a	174	–	–	–	–	–	4.5	95.5
				6b	61	–	4.5	4.7	8.3	–	6.4	76.1
				6c	5.2	1.2	1.5	7.3	7.8	9.1	8.1	65.2
	D/R	HW	5.5	–								
		KOH	10.1	7a	103	–	–	–	–	20.5	15.4	64.1
				7b	3.7	–	–	–	–	–	–	100

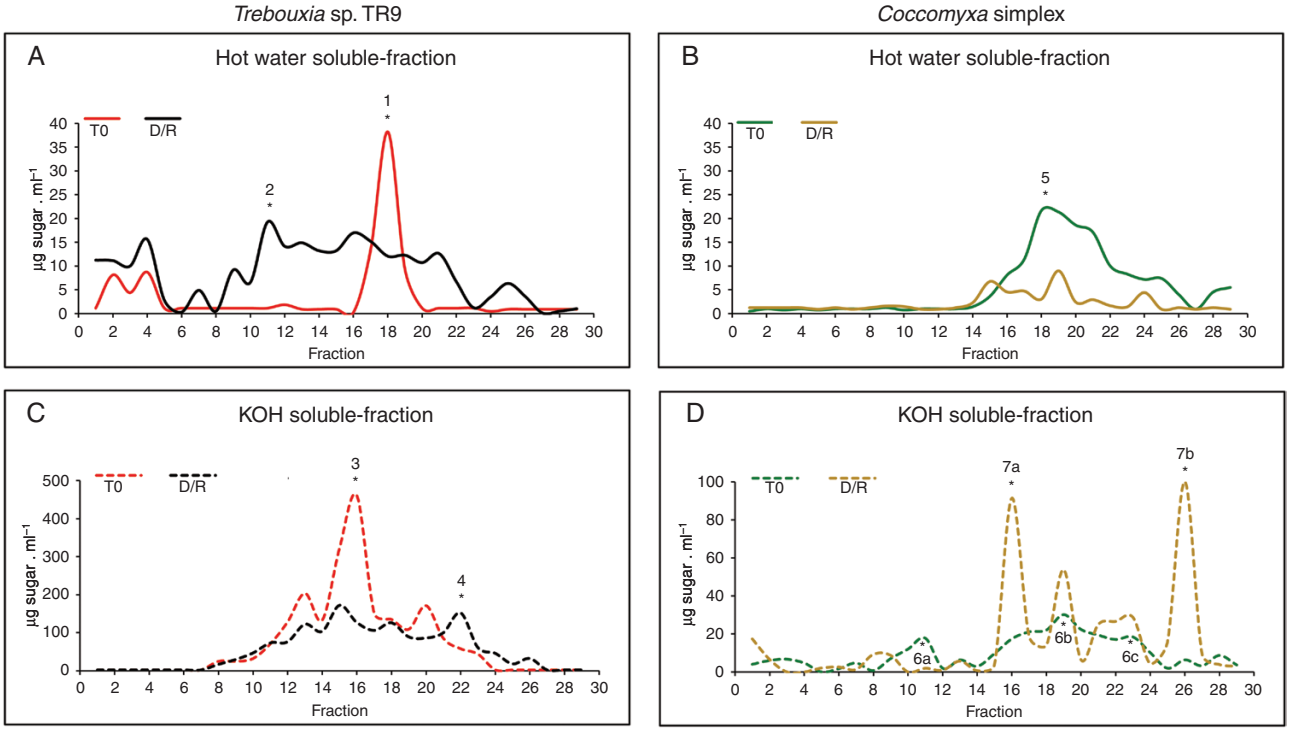

FIG. 6. Effects of four D/R cycles on the molecular mass profile of polysaccharides present in CW fractions of TR9 and Csol microalgae. Sepharose 4B chromatography of polysaccharides from each CW fraction was performed at least three times with at least two different CW preparations from independent TR9 and Csol cultures, under both control and D/R conditions. The chromatographic profile of each polysaccharide fraction did not differ by more than 5 % (in molecular mass) among replicates and with respect to those depicted in the figure. T0 corresponds to cell wall fractions before submitting to D/R cycles. The asterisks indicate fractions selected for glycosyl composition and glycosyl linkage analyses.

TABLE 2. *Glycosyl linkage analysis of CW polysaccharides of TR9 and Csol microalgae before and after cyclic D/R. Peak fractions of gel permeation chromatography were dialysed, freeze-concentrated, permethylated, depolymerized, reduced and acetylated. The resulting partially methylated alditol acetates were analysed by GC–MS as described by York et al. (1985). Peaks 2 and 5 corresponded to hot-water-soluble polysaccharides and peaks 4, 6 and 7 to KOH-soluble ones (for details see Table 1)*

Linkage	*Trebouxia sp. TR9*		*Coccomyxa simplex*					
	Peak 2	Peak 4	Peak 5	Peak 6a	Peak 6b	Peak 6c	Peak 7a	Peak 7b
	(mol %)							
t-Ara*f*	–	0.8	–	–	–	–	–	–
t-Xyl*p*	5.7	3.0	3.5	2.1	1.1	–	–	–
2-Rha*p*	10.9	1.2	7.9	3.1	0.7	–	–	–
t-Rha*p*	–	–	1.3	0.3	–	–	–	–
2-Man*p*	–	–	3.7	1.5	1.1	–	0.8	–
3-Rha*p*	–	1.3	13.8	6.6	2.0	–	–	–
t-Man*p*	–	–	0.4	0.1	1.3	–	–	–
3-Man*p*	–	–	bql	bql	bql	–	2.9	–
t-Glc*p*	6.1	0.5	–	4.3	7.1	16.9	48.1	91.2
t-Fuc*p*	–	–	4.0	–	0.1	–	–	–
3-Fuc*p*	–	–	–	0.3	1.9	–	3.8	–
t-Gal*f*	–	10.4	–	0.6	–	–	–	–
4-Fuc*p*	–	–	–	0.5	–	–	–	–
3,4-Fuc*p*	–	–	5.6	6.7	3.5	–	–	–
t-Gal*p*	–	1.2	2.0	1.1	4.9	–	–	–
3-Ara*p*	–	–	4.3	2.7	–	–	–	–
3-Ara*p* or 4-Ara*f*	–	–	–	–	1.6	–	–	–
t-Ara*p*	–	–	0.9	0.9	0.2	–	–	–
3-Xyl*p*	–	–	2.0	2.0	0.9	–	–	–
4-Xyl*p*	–	1.2	4.4	5.8	3.1	11.0	–	–
2-Rha*p*	–	–	7.9	–	–	–	–	–
3,4-Rha*p*	–	–	1.5	0.4	–	–	–	–
2,3-Rha*p*	14.7	1.1	6.0	4.2	0.5	–	–	–
2-Glc*p*	–	–	2.4	–	–	–	–	–
3-Glc*p*	–	–	–	0.3	0.4	–	–	–
3-Glc*f*	–	–	2.1	1.8	–	–	–	–
4-Rha*p*	–	–	–	–	–	–	–	–
4-Man*p*	–	5.9	–	0.9	2.5	8.7	8.4	–
3-Gal*f*	53.2	–	–	0.8	–	–	–	–
3-Hex*f**	–	21.5	–	–	–	–	–	–
4-Gal*p*	1.5	31.3	1.4	0.5	1.5	–	2.0	–
4-Glc*p*	5.3	1.4	3.2	26.0	42.0	57.4	27.1	8.8
6-Gal*f*	2.7	–	–	–	–	–	–	–
6-Glc*p*	–	–	–	–	0.5	–	–	–
6-Gal*p*	–	–	7.1	3.2	3.8	–	6.9	–
6-Man*p*	–	–	0.1	–	0.3	–	–	–
6-Hex*f**	–	2.8	–	–	–	–	–	–
3-Gal*p*	–	–	0.8	–	3.0	5.9	–	–
2,3-Glc*p*	–	2.1	–	–	–	–	–	–
2,4-Glc*p*	–	–	–	0.5	1.4	–	–	–
2,3-Man*p*	–	–	1.0	1.0	0.5	–	–	–
2,4-Man*p*	–	–	9.4	4.2	2.5	–	–	–
2,6-Man*p*	–	0.3	0.1	–	–	–	–	–
3,4-Man*p*	–	–	0.7	0.5	–	–	–	–
3,6-Man*p*	–	–	–	–	0.6	–	–	–
2,3,6-Man*p*	–	–	0.1	0.1	bql	–	–	–
2,4,6-Man*p*	–	–	0.4	0.3	0.5	–	–	–
3,4,6-Man*p*	–	–	7.5	1.0	4.8	–	–	–
3,4-Gal*p*	–	1.0	–	–	–	–	–	–
3,6-Gal*p*	–	1.4	1.6	0.2	0.6	–	–	–
3,6-Hex*f**	–	2.2	–	–	–	–	–	–
4,6-Gal*p*	–	9.0	0.3	–	–	–	–	–
3,4-Glc*p*	–	–	–	5.0	4.0	–	–	–
4,6-Glc*p*	–	–	0.3	5.1	4.0	–	–	–
2,3,4-Glc*p*	–	–	–	0.6	06	–	–	–
3,4,6-Gal*p*	–	0.5	–	–	–	–	–	–
3,4,6-Glc*p*	–	–	–	1.0	0.6	–	–	–

*Probably galactofuranosyl residues; – not detected; bql, below the quantification level.

glucose and rhamnose as the main monosaccharides (Table 1). Although the amount of carbohydrate recovered from peak 1 was insufficient to perform a glycosyl linkage analysis, its high galactose and rhamnose content resembled that of 3-linked galactofuranan. This is in line with the observation that the polydispersion caused by exposure to D/R cycles generated a peak of high molecular mass (peak 2, Fig. 6 A) predominantly formed by 2,3-linked galactofuranosyl and 2,3-linked rhamnopyranosyl residues (Table 2).

Under control conditions, the KOH fraction of TR9 showed polymers ranging from 146 to 47 kDa with a main peak at 103 kDa (Fig. 6 C, Table 1). Exposure to cyclic D/R did not seem to significantly alter the molecular mass pattern of the total polymers in TR9, except for the appearance of a low molecular mass peak (peak 4, Fig. 6 C, Table 1). A glycosyl composition analysis of peak 3 (control TR9) revealed a high content of xylose besides galactose and rhamnose (Table 1). Peak 4 showed an increased proportion of xylose and a lower content of rhamnose compared with KOH, under control conditions (Table 1). A methylation analysis showed that peak 4 consisted of a 4-linked galactopyranan substituted at *O*-6, *O*-3 and *O*-3,6 positions, a 3-linked galactofuranan and 4-linked xylopyranosyl molecules (Table 2).

A quite different scenario was found in HW and KOH polysaccharides from the Csol CW. Under control conditions, polysaccharide polydispersion was observed in both fractions, with a prevalence of medium to lower molecular mass polymers in the HW fraction, ranging from 103 to 4.3 kDa (Fig. 6 B), and a broader dispersion in the KOH fraction (Fig. 6 D). No marked qualitative changes in the molecular mass pattern of HW sugar-containing polymers was found as a consequence of cyclic D/R, but we did observe a generalized decrease in their abundance (Fig. 6 B), which is consistent with the reduced yield of the HW fraction (Table 1).

According to Centeno *et al.* (2016), glucose, mannose, galactose and rhamnose are the predominant neutral sugars present in the crude CW of Csol, although arabinose, xylose and fucose are also present. Glycosyl linkage analysis indicated the presence of a non-branched glucan with the main chain composed of 4-linked glucopyranosyl residues and a 4-linked mannan poorly substituted at the *O*-2 or *O*-3 position, probably by galactosyl or mannosyl residues. In the present study, HW peak 5 was mainly composed of xylose and almost equal proportions of rhamnose, fucose and mannose (Table 1). The glycosyl linkage analysis suggested the presence of linear xylans, as indicated by the presence of 3- and 4-Xyl*p* residues and two mannans: a 2-linked polymer highly substituted mainly at position 4 and a 3-linked one highly branched at the 4- and 6-positions in this peak (Table 2). Within the KOH-soluble polymers of control Csol, peak 6a presented a high proportion of glucose followed by a lower amount of galactose (Table 1), which seemed to compose a 4-linked glucan branched at *O*-3 and *O*-6 positions. The existence of 4-Gal*p* and 3-Gal*f* residues indicated the presence of galactans as minor components of this peak (Table 2). Peak 6b appeared to contain a 4-linked glucan similar to that found in peak 6a but less branched (one substitution at every ten Glc*p* residues, instead of every five residues) (Table 2). A linear 4-linked glucan was the main component of peak 6c, but 4-linked xylan and mannan and a 3-linked galactan were also found in lower amounts.

In contrast to what was observed in the HW fraction, exposure to cyclic D/R significantly altered the molecular size pattern of KOH polymers in the Csol CW, changing from a polydisperse distribution under control conditions to some sharp peaks from 103 to 3.7 kDa (peaks 7a and 7b, respectively, Fig. 6 D, Table 1) after D/R. Glucose was the main component of peak 7a, which seemed to be represented by a polymer of 4-linked Glc*p*. Polysaccharides formed by 4-Man*p* and 6-Gal*p* were also found in peak 7a (Table 2). Meanwhile, peak 7b was almost exclusively formed by a glucan, in which the high proportion of t-Glc*p* residues suggested the presence of amylose-like polysaccharide (Tables 1 and 2). Amylose has been reported as a polymer that adheres to CWs during polysaccharide extraction from lichen phycobionts (Cordeiro *et al.*, 2008).

Results from the present study confirm our previous findings with crude CWs of the same microalgae under control conditions (Casano *et al.*, 2015; Centeno *et al.*, 2016) and extend them towards a more detailed analysis of CW components and how these are modified in response to cyclic D/R. Farrant *et al.* (2017) recently reported that the flexibility of *Craterostigma wilmsii* CWs seems to be modulated during desiccation. The proportion of glucose decreases and that of galactose increases as substituent in xyloglycans. These polysaccharides also change their degree of polymerization, moving from large to shorter chains and thus increasing CW flexibility under desiccation conditions (Farrant *et al.*, 2017). In our study, an analogous remodelling was observed due to changes in the alkaline-soluble polysaccharides extracted during the relatively slow and mild desiccation of Csol. In contrast, more marked changes were observed in the TR9 water-soluble fraction during fast and drastic desiccation, as the main medium molecular mass polysaccharide found in control cells changed to a complex mixture of different-sized polysaccharides. After D/R cycles, the degree of polymerization of Csol β-glucans decreased. Biochemical remodelling of the CW appears to play a crucial role in controlling its biomechanical properties, helping lichen microalgae to cope with rapid changes in the cell's hydric status. This study also supports the notion that CW remodelling is an active and species-specific process, induced by exposure to desiccation conditions similar to those encountered in the natural habitats in which each alga/lichen thrives.

SUPPLEMENTARY DATA

Supplementary data are available online at https://academic.oup.com/aob and consist of the following. Figure S1: extended TEM micrograph of TR9 under control conditions, showing detail of characteristic invaginations. Fig. S2: extended LTSEM micrograph of TR9 under desiccation conditions. Fig. S3: microscopic images of TR9 and Csol cells stained with 0.2 % crystal violet for 24 h. Fig. S4: effects of desiccation and rehydration on cell wall thickness of Csol and TR9 microalgae.

FUNDING

This research was supported by grants from the Spanish Ministry of Science, Innovation and Universities (CGL2016-80259-P), (PGC2018-094076-B-I00 to C.A.), Fundação de Amparo a Pesquisa do Estado de São Paulo, Brazil (2017/50341-0 to M.R.B.) and Conselho Nacional de Desenvolvimento Científico e Tecnológico, Brazil (305542/2016–8 to M.R.B.).

ACKNOWLEDGEMENTS

We thank Parastoo Azadi at the Complex Carbohydrate Research Center for glycosyl composition and linkage analyses, which were partially supported by a grant from the Chemical Sciences, Geosciences and Biosciences Division, Office of Basic Energy Sciences, U.S. Department of Energy (DE-SC0015662). ESEM and LTSEM observations were conducted under the guidance of Dr Sanchez Almazo at the Microscopy Service, Granada University Centre for Scientific Instrumentation (Spain).

LITERATURE CITED

Aichinger N, Lütz-Meindl U. 2005. Organelle interactions and possible degradation pathways visualized in high-pressure frozen algal cells. *Journal of Microscopy* **219**: 86–94.

Álvarez R, del Hoyo A, Díaz-Rodríguez C, *et al.* 2015. Lichen rehydration in heavy metal polluted environments: Pb modulates the oxidative response of both *Ramalina farinacea* thalli and its isolated microalgae. *Microbial Ecology* **69**: 698–709.

Aragón G, Belichón M, Martínez I, Prieto M. 2016. A survey method for assessing the richness of epiphytic lichens using growth forms. *Ecological Indicators* **62**: 101–105.

Ascaso C, Sancho LG, Rodríguez-Pascual C. 1990. The weathering action of saxicolous lichens in maritime Antarctica. *Polar Biology* **11**: 33–39.

Aschenbrenner IA, Cardinale M, Berg G, Grube M. 2014. Microbial cargo: do bacteria on symbiotic propagules reinforce the microbiome of lichens? *Environmental Microbiology* **16**: 3743–3752.

Belnap J, Büdel B, Lange OL. 2001. Biological soil crusts: characteristics and distribution. In: Belnap J, Lange OL, eds. *Biological soil crusts: structure, function, and management*. Berlin: Springer, 3–30.

Bold HC, Parker BC. 1962. Some supplementary attributes in the classification of *Chlorococcum* species. *Archiv Für Mikrobiologie* **42**: 267–288.

Casano LM, del Campo EM, García-Breijo FJ, *et al.* 2011. Two *Trebouxia* algae with different physiological performances are ever-present in lichen thalli of *Ramalina farinacea.* Coexistence versus competition? *Environmental Microbiology* **13**: 806–818.

Casano LM, Braga MR, Álvarez R, del Campo EM, Barreno E. 2015. Differences in the cell walls and extracellular polymers of the two *Trebouxia* microalgae coexisting in the lichen *Ramalina farinacea* are consistent with their distinct capacity to immobilize extracellular Pb. *Plant Science* **236**: 195–204.

Centeno DC, Hell AF, Braga MR, del Campo EM, Casano LM. 2016. Contrasting strategies used by lichen microalgae to cope with desiccation-rehydration stress revealed by metabolite profiling and cell wall analysis. *Environmental Microbiology* **18**: 1546–1560.

Cordeiro LMC, Carbonero ER, Sassaki GL, *et al.* 2005. A fungus-type β-galactofuranan in the cultivated *Trebouxia* photobiont of the lichen *Ramalina gracilis*. *FEMS Microbiology Letters* **244**: 193–198.

Cordeiro LMC, de Oliveira SM, Buchi DF, Iacomini M. 2008. Galactofuranose-rich heteropolysaccharide from Trebouxia sp., photobiont of the lichen Ramalina gracilis and its effect on macrophage activation. *International Journal of Biological Macromolecules* **42**: 436–440.

Cordeiro LMC, Sassaki GL, Iacomini M. 2007. First report on polysaccharides of *Asterochloris* and their potential role in the lichen symbiosis. *International Journal of Biological Macromolecules* **41**: 193–197.

Dubois M, Gilles KA, Hamilton JK, Rebers PA, Smith F. 1956. Colorimetric method for determination of sugars and related substances. *Analytical Chemistry* **28**: 350–356.

Dunker S, Wilhelm C. 2018. Cell wall structure of coccoid green algae as an important trade-off between biotic interference mechanisms and multidimensional cell growth. *Frontiers in Microbiology* **13**: 719.

Farrant JM, Cooper K, Dace HJW, Bentley J, Hilgart A. 2017. Desiccation tolerance. In: Shabala S, ed. *Plant stress physiology*. Boston: CABI Publishers, 217–252.

Fritsch F, Haines F. 1923. The moisture-relations of terrestrial algae. II. The changes during exposure to drought and treatment with hypertonic solutions. *Annals of Botany* **37**: 683–728.

Gaff DF. 1971. Desiccation-tolerant flowering plants in southern Africa. *Science* **174**: 1033–1034.

Gasulla F, Guéra A, Barreno E. 2010. A simple and rapid method for isolating lichen photobionts. *Symbiosis* **51**: 175–179.

Heiss C, Stacey Klutts J, Wang Z, Doering TL, Azadi P. 2009. The structure of *Cryptococcus neoformans* galactoxylomannan contains β-D-glucuronic acid. *Carbohydrate Research* **344**: 915–920.

Hell AF, Gasulla F, González-Hourcade M, del Campo EM, Centeno DC, Casano LM. 2019. Tolerance to cyclic desiccation in lichen microalgae is related to habitat preference and involves specific priming of the antioxidant system. *Plant & Cell Physiology* **60**: 1880–1891.

Holzinger A, Karsten U. 2013. Desiccation stress and tolerance in green algae: consequences for ultrastructure, physiological and molecular mechanisms. *Frontiers in Plant Science* **4**: 327.

Holzinger A, Pichrtová M. 2016. Abiotic stress tolerance of charophyte green algae: new challenges for omics techniques. *Frontiers in Plant Science* **7**: 678.

Honegger R. 2012. The symbiotic phenotype of lichen-forming Ascomycetes and their endo- and epibionts. In: Hock B, ed. *Fungal associations*, 2nd edn. Berlin: Springer, 287–339.

Honegger R, Brunner U. 1981. Sporopollenin in the cell walls of *Coccomyxa* and *Myrmecia* phycobionts of various lichens: an ultrastructural and chemical investigation. *Canadian Journal of Botany* **59**: 2713–2734.

König J, Peveling E. 1984. Cell walls of the phycobionts *Trebouxia* and *Pseudotrebouxia*: constituents and their localization. *The Lichenologist* **16**: 129–144.

Kranner I, Beckett R, Hochman A, Nash TH. 2008. Desiccation-tolerance in lichens: a review. *The Bryologist* **111**: 576–593.

Molins A, García-Breijo FJ, Reig-Armiñana J, del Campo EM, Casano LM, Barreno E. 2013. Coexistence of different intrathalline symbiotic algae and bacterial biofilms in the foliose Canarian lichen *Parmotrema pseudotinctorum*. *Vieraea* **41**: 349–370.

Moore JP, Nguema-Ona E, Chevalier L, *et al.* 2006. Response of the leaf cell wall to desiccation in the resurrection plant *Myrothamnus flabellifolius*. *Plant Physiology* **141**: 651–662.

Moore JP, Farrant JM, Driouich A. 2008*a*. A role for pectin-associated arabinans in maintaining the flexibility of the plant cell wall during water deficit stress. *Plant Signaling and Behavior* **3**: 102–104.

Moore JP, Vicré-Gibouin M, Farrant JM, Driouich A. 2008*b*. Adaptations of higher plant cell walls to water loss: drought vs desiccation. *Physiologia Plantarum* **134**: 237–245.

Pressel S, Duckett JG. 2010. Cytological insights into the desiccation biology of a model system: moss protonemata. *New Phytologist* **185**: 944–963.

Santander J, Martin T, Loh A, Pohlenz C, Gatlin D, Curtiss R. 2013. Mechanisms of intrinsic resistance to antimicrobial peptides of *Edwardsiella ictaluri* and its influence on fish gut inflammation and virulence. *Microbiology* **159**: 1471–1486.

Schroeter B, Green TGA, Seppelt RD, Kappen L. 1992. Monitoring photosynthetic activity of crustose lichens using a PAM-2000 fluorescence system. *Oecologia* **92**: 457–462.

Sherwin HW, Farrant JM. 1996. Differences in rehydration of three different desiccation tolerant species. *Annals of Botany*. **78**: 703–710.

Shtein I, Bar-On B, Popper ZA. 2018. Plant and algal structure: from cell walls to biomechanical function. *Physiologia Plantarum* **164**: 56–66.

Simmons TJ, Mohler KE, Holland C, Goubet F, Franková L, Houston DR, Hudson AD, Meulewaeter F, Fry SC. 2015. Hetero-trans-β-glucanase, an enzyme unique to Equisetum plants, functionalizes cellulose. *Plant Journal* **83**: 753–769.

Tuba Z, Csitanlan Z, Proctor M. 1996. Photosynthetic responses of a moss, *Tortula ruralis*, ssp. *Ruralis,* and the lichens *Cladonia convolute* and *C. Furcata* to water deficit and short periods of desiccation, and their ecophysiological significance: a baseline study at present-day CO2 concentration. *New Phytologist* **133**: 353–361.

Vargas Castillo R, Stanton D, Nelson PR. 2017. Aportes al conocimiento de la biota liquénica del oasis de neblina de Alto Patache, desierto de Atacama. *Revista de Geografía Norte Grande* **68**: 49–64.

Vicré M, Lerouxel O, Farrant J, Lerouge P, Driouich A. 2004. Composition and desiccation-induced alterations of the cell wall in the resurrection plant *Craterostigma wilmsii*. *Physiologia Plantarum* **120**: 229–239.

Webb M, Arnott H. 1982. Cell wall conformation in dry seeds in relation to the preservation of structural integrity during desiccation. *American Journal of Botany* **69**: 1657–1668.

York WS, Darvill AG, McNeil M, Stevenson TT, Albersheim P. 1985. Isolation and characterisation of plant cell walls and cell wall

components. In: Weissbach A, Weissbach H, eds. *Methods in enzymology*, Orlando: Academic Press Inc., 3–40.

Zhang T, Wei XL, Zhang YQ, Liu HY, Yu LY. 2015. Diversity and distribution of lichen-associated fungi in the Ny-Ålesund Region (Svalbard, High Arctic) as revealed by 454 pyrosequencing. *Scientific Reports* **5**: 14850.

Zhang Z, Volkman JK. 2017. Algaenan structure in the microalga *Nannochloropsis oculata* characterized from stepwise pyrolysis. *Organic Geochemistry* **104**: 1–7.

Zych M, Burczyk J, Kotowska M, *et al.* 2009. Differences in staining of the unicellular algae Chlorococcales as a function of algaenan content. *Acta Agronomica Hungarica*. **57**: 377–381.

Segundo artículo

Disentangling the role of extracellular polysaccharides in desiccation tolerance in lichen-forming microalgae. First evidence of sulfated polysaccharides and ancient sulfotransferase genes

environmental microbiology

Environmental Microbiology (2020) **00**(00), 00–00 doi:10.1111/1462-2920.15043

Disentangling the role of extracellular polysaccharides in desiccation tolerance in lichen-forming microalgae. First evidence of sulfated polysaccharides and ancient sulfotransferase genes

María González-Hourcade,[1] Eva M. del Campo ,[1] Marcia R. Braga ,[2] Antonio Salgado [3] and Leonardo M. Casano [1*]

[1]*University of Alcalá, Department of Life Sciences, Alcalá de Henares, Madrid, 28871, Spain.*

[2]*Department of Plant Physiology and Biochemistry, Institute of Botany, São Paulo, SP, 04301-012, Brazil.*

[3]*Centro de Espectroscopía de RMN (CERMN), Faculty of Pharmacy, University of Alcalá, Alcalá de Henares, Madrid, 28805, Spain.*

Summary

***Trebouxia* sp. TR9 and *Coccomyxa simplex* are desiccation-tolerant microalgae with flexible cell walls, which undergo species-specific remodelling during dehydration–rehydration (D/R) due to their distinct ultrastructure and biochemical composition. Here, we tested the hypothesis that extracellular polysaccharides excreted by each microalga could be quantitatively and/or qualitatively modified by D/R. Extracellular polysaccharides were analysed by size exclusion and anion exchange chromatography, specific stains after gel electrophoresis and gas chromatography/mass spectrometry of trimethylsilyl derivatives (to determine their monosaccharide composition). The structure of a TR9-sulfated polymer was deduced from nuclear magnetic resonance (NMR) analyses. In addition, sugar-sulfotransferase encoding genes were identified in both microalgae, and their expression was measured by RT-qPCR. D/R did not alter the polydispersed profile of extracellular polysaccharides in either microalga but did induce quantitative changes in several peaks. Furthermore, medium-low-sized uronic acid-containing polysaccharides were almost completely substituted by higher molecular mass carbohydrates after D/R. Sulfated polysaccharide(s) were detected, for the first time, in the extracellular polymeric substances of both microalgae, but only increased significantly in TR9 after cyclic D/R, which induced a sugar-sulfotransferase gene and accumulated sulfated ß-D-galactofuranan(s). Biochemical remodelling of extracellular polysaccharides in aeroterrestrial desiccation-tolerant microalgae is species-specific and seems to play a role in the response to changes in environmental water availability.**

Received 28 February, 2020; revised 9 April, 2020; accepted 23 April, 2020. *For correspondence. E-mail leonardo.casano@uah.es, Tel. +34 918856432.

Introduction

The presence of extracellular polymeric substances (EPS) has commonly been associated with bacteria since they are the main components of biofilms. Nowadays, it is known that microalgae also produce high quantities of these materials, which are mainly composed of heterogeneous high molecular mass polysaccharides and proteins released into the environment. Polysaccharides usually account for at least 50%–60% of total EPS and are composed of long-chain repeating units of five major neutral monosaccharides, represented mainly by glucose, galactose, arabinose, mannose and fucose (Moore and Tischer, 1964; Raveendran *et al*., 2013). The amount and composition of EPS depend on the microalgal species and are also influenced by their physiological performance, since abiotic stresses (Markou and Nerantzis, 2013) such as desiccation, nitrogen-limited medium or red and blue light (Han *et al*., 2014) increase their production.

Microalgal EPS also contain low proportions of uronic acids as well as organic (methyl, amino) and inorganic (sulfate) functional groups as chemical substituents in polysaccharides that can affect their physical and biological properties (Allard and Casadevall, 1990). Meanwhile, sulfated polysaccharides (SPs) contain some of their sugar residues as half esters of sulfuric acid. They are widely distributed in the EPS of a variety of organisms, from echinoderms (Mourão and Pereira, 1999) to mammals (Raveendran *et al*., 2013). SPs have been intensively studied since they present a wide spectrum of

bioactivities and have considerable pharmaceutical potential (Liu *et al*., 2016; Xiao and Zheng, 2016). In addition, SPs have hydrophilic properties due to the presence of negative charges, thus contributing to endow EPS with a gel-like consistency. Importantly, their high water-retention capacity may be crucial to prevent sudden changes in cell hydric status in organisms such as aeroterrestrial and intertidal algae that are subjected to cyclic desiccation/rehydration conditions. Moreover, SPs have an affinity for positively charged particles such as heavy metals (Burdin and Bird, 1994; Güven *et al*., 1995; De Philippis *et al*., 2003) and are thus suitable for bioremediation (Liu *et al*., 2016).

SPs have also been reported in algae, mostly in seaweed and aquatic microalgae, and based on their algal origin are called agarans, carrageenans, fucoidans and ulvans (Guangling *et al*., 2011; Cunha and Grenha, 2016). Although sulfotransferases are widespread enzymes responsible for sulfate esterification of SPs, few studies have addressed plant sulfotransferases (Hernández-Sebastià *et al*., 2008). No evidence has been obtained of the presence of SPs in aeroterrestrial microalgae (Baudelet *et al*., 2017) or the activity of sugar sulfotransferases in these organisms.

Many aeroterrestrial microalgae present a symbiotic lifestyle, establishing mutualistic associations with fungi-forming lichens. The fungus (mycobiont) comprises almost the entire lichen biomass (more than 90%) and provides protection against abiotic and biotic stresses (Becket *et al*., 2008). The lichen thallus can contain one or more species of photosynthetic partners (photobionts), represented by cyanobacteria or eukaryotic green microalgae (Casano *et al*., 2011). Lichens and their green microalgae are poikilohydric organisms since their water content is mainly determined by environmental water availability, and most of them are desiccation-tolerant. Desiccation tolerance has been defined as a set of strategies that permit survival with a cellular water content of approximately 5%–10% (Kranner *et al*., 2008). Indeed, most green microalgae in lichens have developed species-specific desiccation tolerance mechanisms to cope with alternating desiccation–rehydration (D/R) cycles (Hell *et al*., 2019, and references therein).

Trebouxia sp. TR9 (TR9) and *Coccomyxa simplex* (Csol) are green microalgae isolated from the lichens *Ramalina farinacea* (L.) Ach. and *Solorina saccata* (L.) Ach., respectively. *Ramalina farinacea* is an epiphytic fruticose lichen that is widely distributed in Mediterranean environments and is adapted to continuous rapid cycles of diurnal and/or seasonal D/R (Centeno *et al*., 2016) with an average relative humidity (RH) of approximately 25%–30%. It presents high ecophysiological plasticity against stressful environmental conditions, such as dehydration during the summer and rehydration by dew or rain. Meanwhile, *S. saccata* is a foliose lichen with a geographical distribution that encompasses mild and cold areas, where it is normally protected because it inhabits cracks in calcareous rocks, which predominantly present microenvironments with a RH of 55%–60% (during the dry season) or more.

In previous studies, Casano *et al*. (2015) analysed the glycosyl composition and linkage of extracellular polysaccharides in fully hydrated cultures of TR9. The extracellular polysaccharides of TR9 are mainly composed of galactose and glucose, with lower proportions of rhamnose, mannose, arabinose, fucose and xylose. Subsequently, Centeno *et al*. (2016) compared extracellular polysaccharides in Csol and TR9 and found that polysaccharides from both microalgae are mainly composed of galactose, indicating the predominance of a galactan but with a more heterogeneous composition in Csol.

In a recent study on TR9 and Csol microalgae cell walls (González-Hourcade *et al*., 2020), we observed striking changes in their ultrastructure and marked polysaccharide remodelling induced by exposure to cyclic D/R. Previously, it was demonstrated that abiotic stressors such as heavy metals and dehydration increase the production of extracellular polysaccharides and change their monomeric composition in cyanobacteria (Knowles and Castenholz, 2008; Ozturk *et al*., 2014) and green microalgae (Casano *et al*., 2015). Based on this evidence, we hypothesised that exposure to species-specific D/R conditions might induce quantitative and/or qualitative changes in EPS polysaccharides in TR9 and Csol. Since microalgae thrive in contrasting habitats, it is highly plausible that each EPS remodelling would present a species-specific pattern due to the habitat preferences of each microalga. Therefore, the aim of the present study was to determine possible changes in some of the main biochemical features of TR9 and Csol extracellular polysaccharides induced by exposure to cyclic D/R. We focused on molecular profile, glycosyl composition, and the presence of charged molecules such as uronic acids and sulfated sugars, due to their potential effect on cell water retention and thus desiccation tolerance.

Results

D/R induces changes in molecular mass profile and composition of exopolymeric substances

In agreement with previous results (Centeno *et al*., 2016), EPS from fully hydrated (T0) TR9 and Csol microalgae were mainly composed of carbohydrates and proteins, which accounted for more than 60% and 6% of total EPS biomass respectively (Table 1). Uronic acids were also detected, indicating the acidic nature of at least some of these polymers. Although exposure to four D/R cycles

significantly increased the amount of protein in Csol (data not shown), no changes were observed in overall EPS production or carbohydrate content. In contrast, D/R treatment induced an increase in galactose (84% in TR9 and 69% in Csol) and a reduction in rhamnose (−94% in both microalgae) and glucose (−91% in TR9 and −46% in Csol). In addition, a 76% reduction in arabinose relative content was observed in Csol.

Extracellular polysaccharides from fully hydrated TR9 and Csol presented a polydispersed molecular mass profile when subjected to Sepharose 4B chromatography (Fig. 1A, B), although most TR9 extracellular polysaccharides occurred between 218 and 12.5 kDa (Fig. 1A). Polydispersion was also observed in uronic acid-containing polymers from TR9 extracellular polysaccharides (Fig. 1C), whereas most Csol acidic polysaccharides showed intermediate to low molecular masses (Fig. 1D). Cyclic D/R induced quantitative but not qualitative changes in the molecular mass profile of extracellular polysaccharides in both TR9 and Csol (Fig. 1A, B). In TR9, molecules between 218 and 12.5 kDa decreased, in contrast with the increase in polymers higher than 500 kDa. The reverse was observed in Csol, whereby medium- to lower-sized polysaccharides increased after cyclic D/R. Acidic polysaccharides showed distinct polydispersed profiles depending on algal species and treatment (Fig. 1C, D). In fully hydrated conditions, these carbohydrates ranged from more than 500 to less than 5 kDa in TR9, while in Csol they ranged from 240 to less than 5 kDa. Exposure to D/R caused a marked shift towards higher molecular mass acidic extracellular polysaccharides in Csol (Fig. 1D), contrasting with a less pronounced effect in TR9 (Fig. 1C). A trend towards an increase in uronic acid content in TR9 after D/R cycles (Table 1) was confirmed by electrophoresis using alcian blue as dye (Fig. 2A).

SPs are dynamic components of microalgal EPS

Sulfate was detected in the EPS of both microalgae, presenting a significant increase (145%) in TR9 after cyclic D/R (Table 1). This finding agrees with the electrophoretic profile depicted in Fig. 2B showing a purple toluidine blue stain in TR9, which indicates an increase in sulfated polymers after four D/R cycles. Sepharose-4B chromatography revealed polydispersed profiles of sulfated polymers in fully hydrated TR9 and Csol (Fig. 3A). An increase in low molecular mass (24–8.5 kDa) sulfate-containing polymers was only observed in TR9 after D/R cycles (Fig. 3A) and was confirmed through electrophoresis in agarose gel and toluidine blue staining (Fig. 3B).

In agreement with the above results, the ion-exchange-Q-Sepharose chromatography profiles revealed a higher proportion of SPs in TR9 subjected to D/R than in fully hydrated TR9 (Fig. S1). The enriched carbohydrate fractions from TR9 after D/R were grouped in pools A (Fractions 29–42), B (Fractions 51–63) and C (Fraction 75). Turbidimetry revealed a considerable amount of sulfate in pool B, which was then selected for further analyses.

Structural determination of SPs in Trebouxia sp. *TR9 by nuclear magnetic resonance*

The structure of the isolated compound(s) (sulfate-enriched Q-Sepharose peak B, see above) was

Table 1 Features of the EPS of *Trebouxia* sp. TR9 and *Coccomyxa simplex* microalgae.

Microalga	*Trebouxia* sp. TR9		*Coccomyxa simplex*	
Treatment	T0	D/R	T0	D/R
EPS yield (μg EPS/mg FW)	7.0 ± 0.7	8.0 ± 1.1	8.2 ± 2.5	7.4 ± 1.5
Neutral carbohydrates (%)	67.4 ± 6.0	62.3 ± 5.8	65.2 ± 6.0	61.0 ± 4.6
Uronic acid-containing polymers (%)	18.7 ± 6.5	22.8 ± 8.4	27.8 ± 8.1	21.4 ± 7.0
Sulfated sugar-containing polysaccharides (%)	9.2 ± 0.7	22.5 ± 1.1*	16.7 ± 2.5	13.8 ± 1.5
Sulfated/neutral polysaccharides ratio	0.14	0.36	0.26	0.23
Neutral monosaccharides (% Mol)				
Arabinose	1.2[a]	1.2	2.1[a]	0.5
Rhamnose	5.0[a]	0.3	13.9[a]	0.8
Fucose	0.4[a]	—	1.5[a]	0.9
Xylose	1.3[a]	1.5	3.3[a]	4.1
Mannose	2.8[a]	2.1	14.3[a]	13.7
Galactose	50.1[a]	92.4	42.4[a]	71.5
Glucose	28.3[a]	2.6	15.1[a]	8.2

T0: Control. Most of the general features of EPS are shown as mean ± standard error. Values of glycosyl composition of D/R-treated samples are means of two technical replicates (with less than 2% variation between them) of a combined sample of equal amounts of at least two independent EPS preparations. Asterisk indicates statistically significant difference between D/R and T0 ($p < 0.05$).
[a]Original results from Centeno *et al*., 2016.

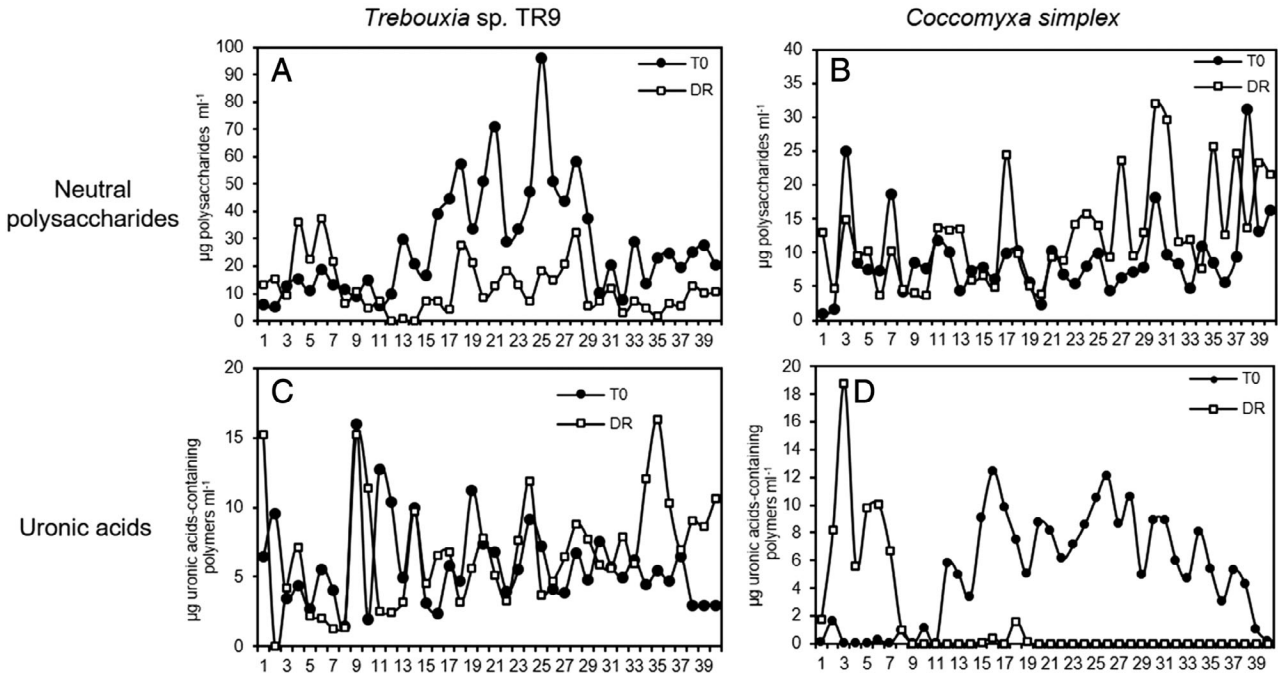

Figure 1 Effects of four D/R cycles on the molecular mass profile of principal components in the EPS of two microalgae species. T0: control. Sepharose 4B chromatography of each EPS was repeated at least three times using EPS preparations from independent TR9 and CsoI cultures exposed to both experimental conditions. Total neutral sugars (A, B) and uronic acids (C, D) were determined according to Dubois *et al*. (1956) and Filisetti-Cozzi and Carpita (1991), respectively. The chromatographic profiles of each EPS did not differ by more than 5% in molecular mass and by more than 12% in sugar/uronic acid content among replicates and with respect to those shown in the figure.

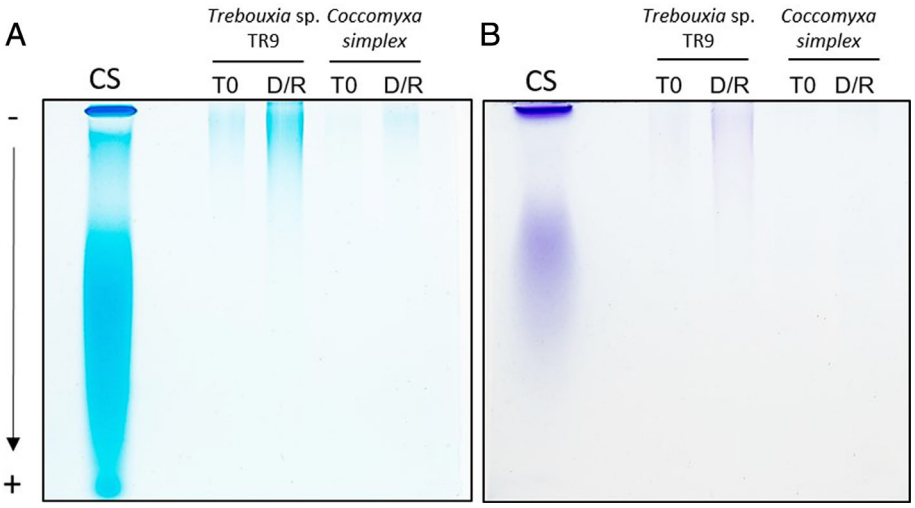

Figure 2 SDS-PAGE gel electrophoresis of crude EPS from *Trebouxia* sp. TR9 and *Coccomyxa simplex* for analysing negatively charged polysaccharides.
Images show representative gels of three to four electrophoresis from independent biological samples stained with Alcian blue (A) and Toluidine-O (B). T0: control; CS: chondroitin sulfate.

elucidated by means of monosaccharide composition analysis and nuclear magnetic resonance (NMR) data, and results for the former (Table 2) indicated that the SP pool was predominantly constituted by D-galactose (87.4% mol:mol).

The ^{1}H NMR spectrum of the sulfated sample from TR9 is shown in Fig. 4. The spectrum was poorly resolved and therefore no coupling constant information could be derived. Two main regions were distinguished, one at the 5.00–5.30 ppm interval and a second one between 3.50 and 4.20 ppm. In the first region, three rather sharp resonances were observed at 5.27, 5.19 and 5.04 ppm, which were assigned to anomeric protons. In the second region, associated with non-anomeric-carbohydrate hydrogens, the high degree of overlapping prevented individual signal assignments. A 2D TOCSY experiment proved of little help due to low resolution in the carbohydrate region (3.50–4.20 ppm). 1D TOCSY

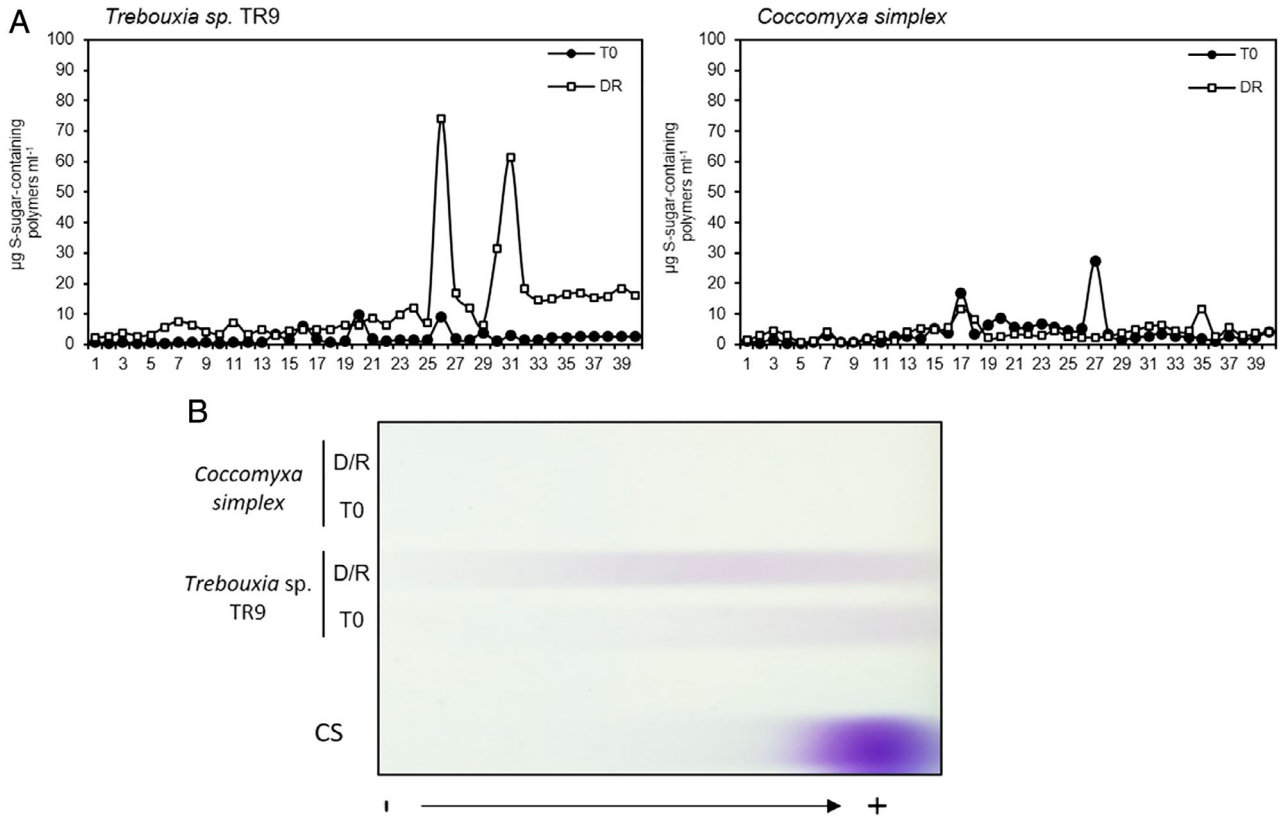

Figure 3 Molecular mass profile of SPs from crude EPS from *Trebouxia* sp. TR9 and *Coccomyxa simplex* separated by Sepharose 4B liquid chromatography (A) and by agarose gel electrophoresis and Toluidine-O staining (B).
Sepharose 4B chromatography of each EPS was repeated three times with biologically independent EPS preparations. The chromatographic profiles of each EPS did not differ by more than 6% in molecular mass and by more than 10% in sulfate content among replicates and with respect to those shown in the figure. Sulfate content of each fraction was quantified according to Terho and Hartiala (1971) and Kolmert *et al*. (2000). The image in (B) is representative of three electrophoretic profiles from independent biological samples. T0: control; CS: chondroitin sulfate.

Table 2 Glycosyl composition of the isolated SP(s) from *Trebouxia* sp. TR9 exposed to cyclic D/R conditions.

	S-polysac. TR9 D/R	
Monosaccharides	Mass (µg)	Mol %
Ribose	0.1	1.2
Arabinose	0.0	0.5
Rhamnose	ND	—
Fucose	ND	—
Xylose	0.5	5.4
Glucuronic acid	0.2	1.7
Galacturonic acid	ND	—
Mannose	0.1	0.9
Galactose	8.8	87.4
Glucose	0.3	2.8

Values are means of two technical replicates (with less than 2% variation between them) of a combined sample of two independent preparations of Q-Sepharose-purified SPs. ND, not detected.

experiments irradiating at the three anomeric hydrogens gave in each case a response to signals at ca. 4.14 ppm (Fig. S2).

The heteronuclear single quantum coherence (HSQC) experiment (Fig. S3A) yielded defined cross peaks, which led to partial carbohydrate identification by comparison with published data (Beier *et al*., 1980). The three ^{1}H peaks at 5.27, 5.19 and 5.05 ppm correlated to ^{13}C resonances at 107.8, 107.7 and 108.5 ppm, respectively, which were consistent with the anomeric positions of β-D-galactofuranosides. Other HSQC correlations, namely those at 4.13 ppm/81.7 ppm, 4.13 ppm/81.7 ppm, 4.13 ppm/81.7 ppm, 4.13 ppm/81.7 ppm and 3.66, 3.71 ppm/63.4 ppm were respectively assigned to the CH and CH_2 groups at Positions 2, 3, 4, 5 and 6 of β-D-galactofuranosides (Beier *et al*., 1980; Säwén *et al*., 2010). Interestingly, the small responses encountered in the 1D TOCSY experiments were compatible with ß-D-galactofuranoses. The chemical shifts in anomeric signals at 5.19 and 5.05 ppm were consistent with a →5)-β-D-Gal*f*-(1→6)-β-D-Gal*f*-(1→ linear scaffold. This finding was further corroborated by other $^{1}H/^{13}C$ chemical shift pairs, for instance, those at 3.70–3.80 ppm/61–63 ppm and 3.95 ppm/76–78 ppm and attributed to the 6-CH_2 and

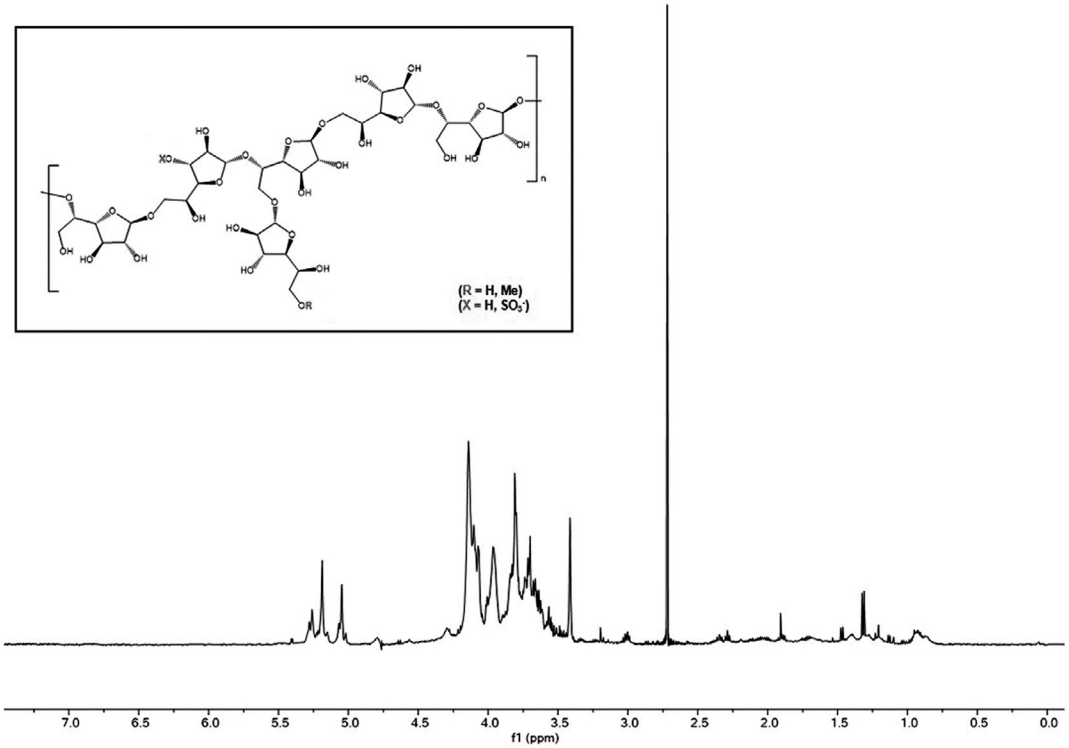

Figure 4 ^{1}H PRESAT spectrum (D2O, 500 MHz) and tentative structure of isolated sulfated polymer from *Trebouxia* sp. TR9 after exposure to cyclic desiccation/rehydration conditions.

5-CH groups of a β-D-Gal*f* residue involved in a 1→5 glycosidic linkage. Other ^{1}H/^{13}C pairs, i.e., those at 3.56, 3.61 ppm/74.0 ppm and 3.41 ppm/59.0 ppm, were assigned to the CH_2 and CH_3 groups of a β-D-Gal*f* moiety with a methoxy group at the 6-CH_2OH position (Pathak *et al*., 2001). Therefore, a structure compatible with our data would be [(1→5)-β-D-Gal*f*-(1→6)-β-D-Gal*f*] with 6-O-methyl-ß-D-galactofuranose residues, either as part of the main scaffold or as peripheral substituents (Fig. 4).

NMR experiments did not yield clear signals attributable to sulfated carbohydrate residues (δ^{1}H 4.5–4.8 ppm). However, the proximity of the large residual HDO signal hampered the detection of weak, low-intensity ^{1}H resonances between 4.6 and 4.9 ppm. A small broad signal at 4.56 ppm was observed in the ^{1}H NMR spectrum and also two small singlets at 4.63 and 4.64 ppm in the ^{1}H PRESAT experiment: these ^{1}H chemical shifts were consistent with sulfonated carbohydrates. Interestingly, a 2D TOCSY PRESAT experiment (Fig. S3B) corroborated these findings, supporting the presence of sulfate substituents in the compound, albeit in low proportion. A TOCSY cross-peak between the signals at 4.54 and 4.12 ppm is shown in Fig. S3B (inset). Assuming that the resonance at 4.12 ppm was due to β-D-Gal*f* H-2, as suggested by the 1D TOCSY experiments (Fig. S2), sulfation may have occurred at 3-OH of β-D-Gal*f*.

Desiccation induces expression of a sulfotransferase gene in TR9

Our finding that sulfate-containing polysaccharides were only observed in TR9 after D/R cycles prompted us to search for transcripts encoding for sulfotransferases in customized databases of transcript sequences from TR9 and Csol. We identified a single transcript encoding a sulfotransferase for each alga. Both transcript sequences were annotated and submitted to GenBank (accession nos. MN954666 and MN954665 respectively). The sequences of both proteins resulting from each transcript had similar lengths of 600 aa and 591 aa for TR9 and Csol respectively (Fig. 5A, C). Protein motif predictions revealed the presence of a signal peptide at the N-terminus for a secretory pathway. In the C-terminus, a conserved Sulfotransfer_3 domain was predicted (PF13469, e-value = $2.3e^{-31}$). A motif consisting of tetratricopeptide repeats (TPRs) upstream of the sulfotransferase domain was also predicted. TR9 and Csol sulfotransferases have a roughly spherical structure with a lateral motif consisting of four parallel β-sheets flanked by α-helices. The catalytic domain consists of a five-stranded parallel β-sheet, laterally flanked by α-helices (Fig. 5B, D). To elucidate any differential expression of sulfotransferase genes after D/R treatment compared with control conditions, we performed transcript

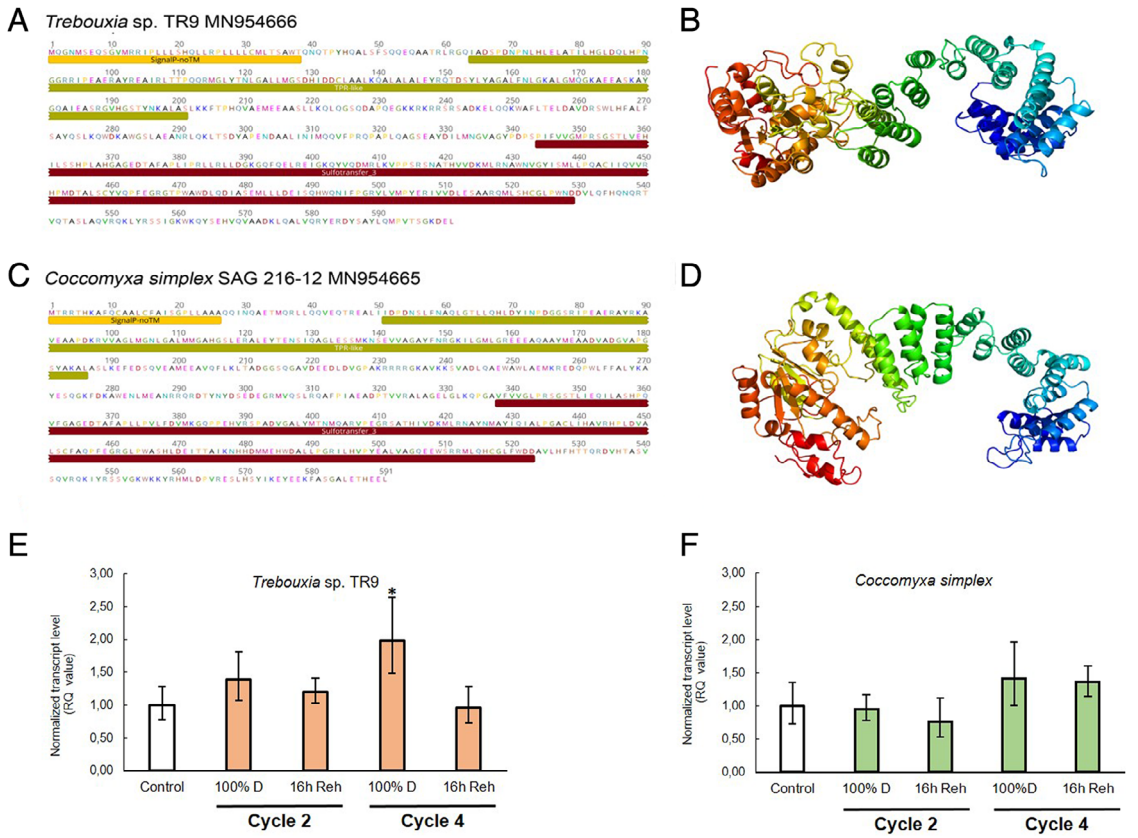

Figure 5 Primary (A, C) and secondary (B, D) structures of the sulfotransferase proteins encoded in the nuclear genome from *Trebouxia* sp. TR9 and *Coccomyxa simplex* resulting from translation of the reconstructed mRNA.
Changes in the transcript levels of sulfotransferase encoding genes from TR9 and Csol microalgae exposed to cyclic D/R (E, F). Values were calculated with $2^{-\Delta\Delta Ct}$ relative quantification for five biological replicates. Error bars show the standard error. D, desiccation; Reh, rehydration. Asterisk indicates statistically significant difference between treatments and control ($p < 0.05$).

quantification by real-time PCR (qPCR). No significant changes were observed in the sulfotransferase transcript level of Csol during cyclic D/R, whereas the TR9 sulfotransferase gene presented a transient transcriptional induction by desiccation in the fourth cycle (Fig. 5E, F). These results are consistent with the increase in low molecular mass sulfate-containing polymers only observed in TR9 after D/R cycles (Fig. 3A) and reinforce the notion that SPs play an important role in the EPS of TR9 during desiccation.

A TBLASTN search in the NCBI databases for sulfotransferases in other organisms, using the TR9 sequence as a query indicated the presence of similar proteins (more than 26% identity compared with the homologous sequence from TR9 and e-value below $1e^{-5}$) with a sulfotransferase domain and other highly conserved domains in a variety of organisms, including archaea, bacteria, cyanobacteria, green algae, animals and a single plant (Fig. S4). The retrieved sulfotransferases presented different additional motifs depending on the group of organisms (Fig. 6): (i) a signal peptide at the N-terminus was found only in green algae and animals and (ii) a TPR motif upstream of the sulfotransferase domain in all organisms except animals. The longest protein sequence with 1083 aa (accession no. GAT44054) was found in the basidiomycete *Mycena chlorophos* (34.49% identical residues compared with the homologous sequence from TR9 and e-value of $3e^{-50}$). This protein included seven transmembrane domains, which were absent in all the other organisms studied, together with a TPR motif upstream of a sulfotransferase motif. The shortest protein, with ca. 400 aa, was found in animals with a sulfotransferase motif occupying almost the entire sequence and a signal peptide at the N-terminus. Interestingly, searches for terrestrial plants yielded no results except for the resurrection plant *Dorcoceras hygrometricum* (accession nos. KZV43544 and KZV42185). In this plant species, we found two sulfotransferases with e-values below $4e^{-20}$. One of these had an additional alpha-galactosidase-like motif. The phylogenetic relationships between the sulfotransferases retrieved for different groups of organisms, including archaea, bacteria, cyanobacteria, green

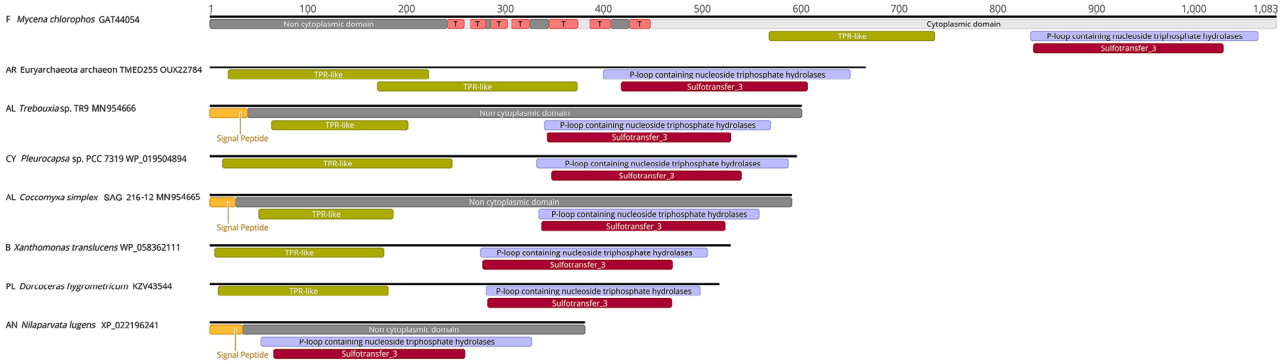

Figure 6 Identified motifs and signal peptides from sulfotransferase sequences from several organisms including *Trebouxia sp*. TR9 and *Coccomyxa simplex*.

algae, plants, fungi and animals, showed a well-defined clade including sulfotransferases from photosynthetic eukaryotes (Fig. 7). This clade was more closely related to cyanobacterial sulfotransferases than to those from heterotrophic eukaryotes such as fungi and animals. Interestingly, sulfotransferases similar to those found in TR9 and Csol are present in several green algae and other diverse, phylogenetically distant groups of organisms, but not in plants or red algae included in the NCBI except *D. hygrometricum*. Indeed, none of the 245 sulfotransferases identified in the complete genomes of four *Gossypium* species (Wang *et al*., 2019) is similar to those described here for TR9 and Csol.

Discussion

Microalgae and cyanobacteria produce EPS forming a mucous mass surrounding cells or a group of cells. Microorganism EPS can present different biological properties depending on the characteristics of the secreted polymers, including cell adhesion, biofilm cohesion and cell aggregation, water retention and sorption of organic compounds and inorganic ions (Xiao and Zheng, 2016 and references therein). Extracellular carbohydrates in green algae, and particularly in Trebouxiophyceae, have generally received little research attention. However, the presence of EPS was recently reported in lichen-forming aeroterrestrial microalgae (Casano *et al*., 2015; Centeno *et al*., 2016). These studies, which investigated the chemical composition of EPS in fully hydrated phycobionts of *R. farinacea* (*Trebouxia* sp. TR1 and *T*. sp. TR9) and *S. saccata* (Csol), found marked quantitative and qualitative differences in exopolysaccharides between algal species, which were probably related to the water regime of their respective habitats. In the present study, we compared TR9 and Csol focusing on the effects of cyclic D/R on their water-soluble exopolysaccharides, including sulfated polymer(s), a still unexplored aspect in these microalgae.

A range of evidence indicates that EPS synthesis can be modulated in response to stress: (i) it has been suggested that EPS function as ROS scavengers following oxidative stress (Tannin-Spitz *et al*., 2005; Li *et al*., 2011); (ii) exposure to toxic metals can either increase EPS accumulation in tolerant organisms (Casano *et al*., 2015) or reduce it in sensitive ones (Lim *et al*., 2006) and (iii) the desiccation tolerance of aeroterrestrial cyanobacteria largely depends on the presence of EPS (Mazor *et al*., 1996; Knowles and Castenholz, 2008).

In both TR9 and Csol, exposure to D/R did not alter the polydispersed profile of EPS polysaccharides but did induce quantitative changes in several peaks (Fig. 1A, B). In TR9, exposure to D/R caused a shift towards higher molecular mass, while in Csol, medium- to low-sized neutral polysaccharides increased. In contrast, the medium- to low-sized uronic acid-containing polysaccharides in Csol EPS were almost completely substituted by higher molecular mass carbohydrates after cyclic D/R (Fig. 1D). A previous glycosyl linkage analysis revealed that a 3-linked galactan and a highly branched 3, 4, 6-galactan were the predominant components of TR9 and Csol EPS respectively (Casano *et al*., 2015; Centeno *et al*., 2016). Rhamnose-containing carbohydrates were also described as forming part of the EPS in both algae. Thus, the increase in galactose and marked decrease in rhamnose and glucose after cyclic D/R observed in this study (Table 1) suggest an increase in galactose-containing polymers to the detriment of rhamnose- and glucose-forming polymers in the EPS of both microalgae. In accordance with this finding, changes in the monomeric composition of EPS polysaccharides have previously been reported in cyanobacteria under dehydration (Knowles and Castenholz, 2008; Ozturk *et al*., 2014). Liu *et al*. (2017) have reported that coordination of EPS flexibility and rigidity (facilitated by a ß-galactosidase) seems to be crucial in order for *Nostoc flagelliforme* to thrive during cycles of rehydration and desiccation, respectively. Desiccation tolerance in *Botryococcus braunii*, a

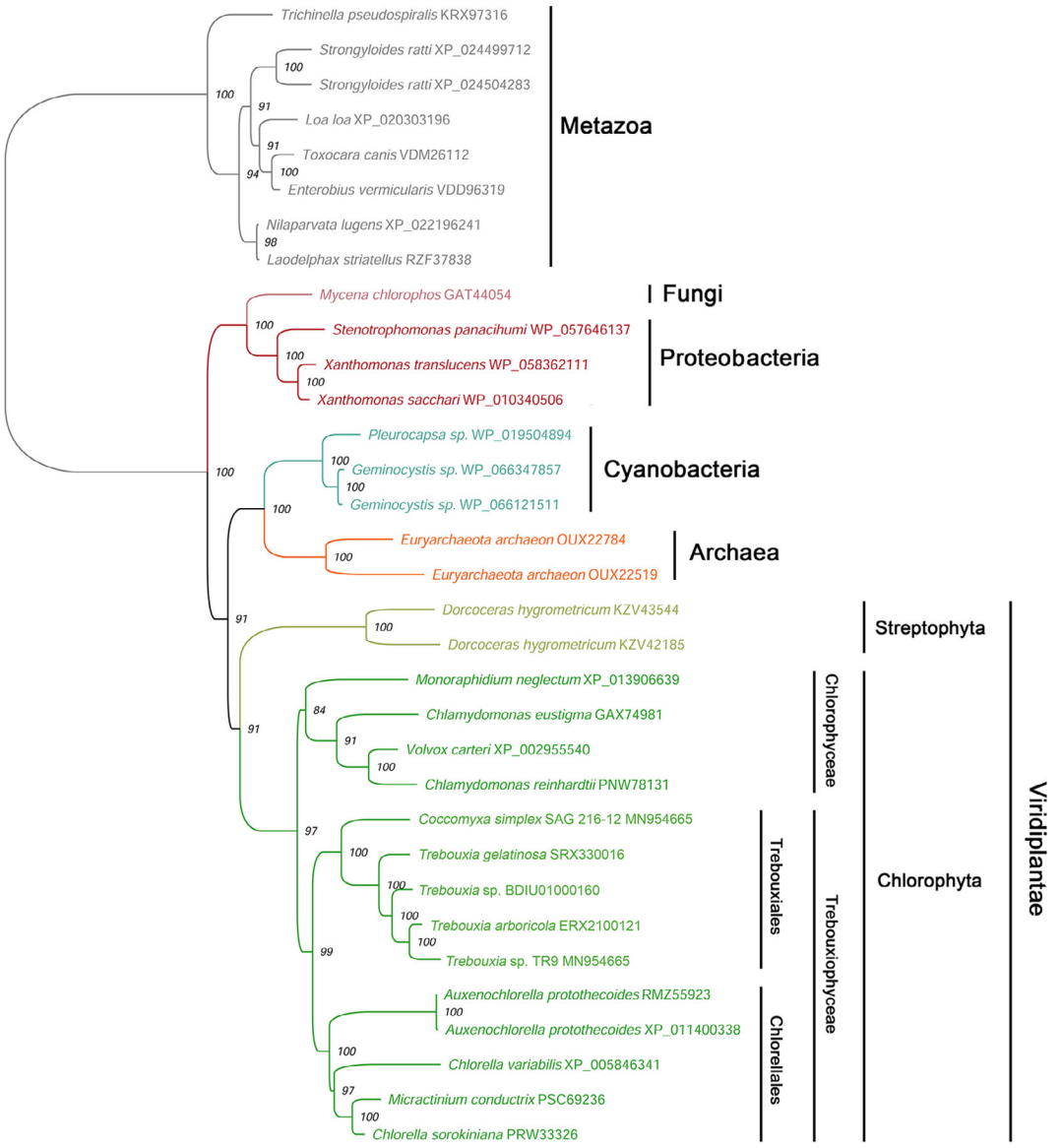

Figure 7 Phylogenetic tree inferred using the ML method, based on alignment of the concatenated amino acid sequences resulting from the translation of several organisms including *Trebouxia* sp. TR9 and *Coccomyxa simplex*.
Note: bootstrap values are shown in the nodes of the tree. The scale bar indicates substitutions/site.

Trebouxiophycean taxon closely related to TR9 and Csol (Martínez-Alberola *et al*., 2019), depends on its extracellular substances (Demura *et al*., 2014). Recently, González-Hourcade *et al*. (2020) observed that exposure to cyclic D/R induces marked cell wall polysaccharide remodelling and striking changes in the cell ultrastructure of TR9 and Csol. Together, these results indicate that modifications in polysaccharides, as components of cell walls and/or EPS, are species-specific and play a role in the microalgae response to changes in environmental water availability, contributing to their desiccation tolerance. The acclimation process of the cell wall and EPS of lichen algae in their biological context may be influenced to some extent by the interaction with the mycobiont in the lichen thallus. However, it is highly probable that the biochemical remodelling of these cellular components observed in isolated algae (González-Hourcade *et al*., 2020; this work) faithfully reflects their natural acclimation to cyclic D/R. This suggestion is based on the similarities in the ultrastructural changes found between isolated (González-Hourcade *et al*., 2020) and lichenized algae (Brown *et al*., 1987) exposed to desiccation.

It has been proposed that the presence of SPs in marine plants is a consequence of physiological adaptation to high-salinity environments (Aquino *et al*., 2011).

However, more recently, SPs have also been found in some freshwater green algae such as *Cladophora surera* (Arata *et al*., 2017) and freshwater plants such as *Eicchornia crassipes* (Dantas-Santos *et al*., 2012). Here, we provide the first evidence of sulfated exopolymers in the EPS of two aeroterrestrial lichen algae, TR9 and Csol. In TR9, sulfated exopolymers are constituted, at least in part, by polysaccharides, as indicated by turbidimetric, in-gel and NMR analyses (Figs. 2-4, S2, S3 and Table 2). Based on a glycosyl composition analysis, galactans seem to be the predominant component of TR9 SPs. According to NMR results, the molecular structure of isolated SP of TR9 would be [(1→5)-ß-D-Gal*f*-(1→6)-ß-D-Gal*f*] (Fig. 4). This structure is similar to that found in mycolyl-arabinogalactan complexes that form part of the cellular envelope of several mycobacteria species (Jarlier and Nikaido, 1994; Bhowruth *et al*., 2008), which consists of β-D-galactofuranoses with alternating 1→5 and 1→6 linkages (Fig. 4). On the other hand, even though sulfated galactans seem to be absent in terrestrial plants, they are widely distributed in a range of organisms from animals (including both terrestrial and marine species) to marine autotrophs, including both angiosperms and algae. Galactose sulfation is a chemical modification with considerable physiological impact, since, e.g., it can increase the affinity of carbohydrate moieties for certain binding proteins and thus confer greater specificity to molecular interactions (Pomin, 2016), and sulfated groups constitute the main sites for water (and cation) retention in polysaccharides (Wang *et al*., 2013). Therefore, the differences in sulfate content between TR9 and Csol under fully hydrated and D/R conditions suggest that each alga has a distinct strategy for coping with desiccation stress.

Carbohydrate sulfation is catalysed by carbohydrate sulfotransferases, while modification of sulfate residues in SPs is presumably catalysed by sulphatases (Ho, 2015). In spite of the diversity of sulfotransferase substrates and physiological functions, these enzymes conserve certain amino acid sequences across all kingdoms (Hernández-Sebastià *et al*., 2008). Thanks to the presence of these conserved domains, it is possible to classify sulfotransferases into families and search for similar sequences with bioinformatic tools. The Sulfotransfer_3 domain found in the TR9 and Csol microalgae sulfotransferases is also present in the human heparan sulfate (HS) 3-O-sulfotransferase isoform 3 (3-OST-3), which transfers a sulfuryl group to a specific glucosamine in HS (Moon *et al*., 2004). The presence of a signal peptide for a secretory pathway suggests that TR9 and Csol enzymes may be extracellular, membrane-attached proteins or soluble proteins within either the endoplasmic reticulum or Golgi apparatus. An extracellular location and membrane attachment can both be excluded since they do not appear in the exoproteome (data not shown) nor do they have transmembrane domains. It is likely that TR9 and Csol sulfotransferases are located within either the endoplasmic reticulum or Golgi apparatus, as described for enzymes that catalyse oligosaccharide sulfation in animals (Honke and Taniguchi, 2002). The TPR motif found in sulfotransferases from TR9, Csol and other groups of organisms is probably involved in protein–protein interactions (Cerveny *et al*., 2013), which are crucial in plant cell physiology and development. Moreover, many of them are also involved in coordinating these interactions and hormonal signalling in plants under stress conditions (Sharma and Pandey, 2016).

In this study, phylogenetic reconstruction based on amino acid sequences of sulfotransferases yielded some interesting clues about the evolution of these enzymes in TR9 and Csol. In our phylogenetic tree, the relationships between green algal sulfotransferases were consistent with those between green algal groups in previously published phylogenetic reconstructions (e.g. Martínez-Alberola *et al*., 2019, 2020). Sulfotransferases found in photosynthetic eukaryotes could be considered of archaeal/cyanobacterial origin, whereas those found in the heterotrophic eukaryote *M*. *chlorophos* may be of proteobacterial origin. One possible scenario for the origin of the studied sulfotransferases in photosynthetic eukaryotes and the fungus *M*. *chlorophos* may be as a consequence of organelle endosymbiosis (chloroplast in photosynthetic eukaryotes and mitochondria in the fungus) and probable subsequent horizontal gene transfer events, as previously proposed for the origin and evolution of other proteins (e.g., Anantharaman *et al*., 2002; Koonin and Aravind, 2002). Such events were probably followed by the recruitment of new domains as a signal peptide in the case of photosynthetic eukaryotes or transmembrane domains in the case of *M*. *chlorophos*. In this respect, it is interesting to note that sulfotransferases from photosynthetic eukaryotes have an eukaryotic signal peptide as those found in the plant *D*. *hygrometricum*, one of them has an additional alpha-galactosidase-like motif not found in prokaryotic sulfotransferases. Our phylogenetic reconstruction also suggests that cyanobacterial sulfotransferases may be of archaeal origin and significantly different from the sulfotransferases found in *Proteobacteria*, as postulated for the origin and evolution of other proteins (e.g. Jeter *et al*., 2019). More importantly, sulfotransferases similar to those found in TR9 and Csol are present in several green algae and various other phylogenetically distant groups of organisms, but not in all plants included in the NCBI except the resurrection plant *D*. *hygrometricum*. This observation, together with the presence of similar sulfotransferases in a sole fungus from among all the fungi included in the NCBI databases, suggests an ancient origin for the

studied sulfotransferases and subsequent gene loss in selected lineages.

Expression analyses of sulfotransferase genes indicated an increase in TR9 but not in Csol transcript levels. This finding suggests that SPs play an important role in the TR9 EPS during desiccation and is consistent with the fact that while TR9 lives in environments with rapid and extreme desiccation cycles, Csol is generally found in areas with slow D/R cycles. Both microalgae seem to be able to survive successive D/R cycles but deploy different strategies. In Csol, the presence of a thin cell wall with algaenans, as demonstrated in previous studies (González-Hourcade *et al*., 2020), can increase impermeability and retard drying. In TR9, the abundance of extracellular SPs, which can retain water during drying, may compensate for the absence of a more impermeable and rigid cell wall. Given that sulfate content and sulfotransferase transcript levels after D/R remained unchanged in Csol but increased in TR9, it is reasonable to surmise that TR9 may modulate the number of sulfated groups to better cope with sudden changes in water availability.

In recent years, several lines of evidence have indicated that the exopolysaccharides synthesized by extremophiles possess valuable distinctive characteristics with therapeutic potential and promising biotechnological applications (Wang *et al*., 2018). Currently, the application of enzymatic sulfation to polysaccharides remains limited due to the often scarce availability of sulfotransferases (Bedini *et al*., 2017). Therefore, future research on sulfonated exopolysaccharides and carbohydrate sulfotransferase genes in poorly studied extremophiles such as aeroterrestrial lichen algae may contribute not only to elucidate their biological significance but also to produce new potentially useful sulfated polymers through enzymatic synthesis.

Experimental procedures

Microalgae isolation and culture: D/R treatment

The *Trebouxia sp*. TR9 microalga was isolated from the lichen *R. farinacea* as previously described (Casano *et al*., 2011). *Coccomyxa simplex* (Csol) was obtained from the Sammlung von Algenkulturen at the Gottingen University (strain 216-12, Germany). According to this algal bank, Csol was isolated from the lichen *S. saccata*. Both microalgae were cultured under axenic conditions on semi-solid Bold 3N medium as described elsewhere (Centeno *et al*., 2016). D/R treatment was carried out following the procedure previously described by González-Hourcade *et al*. (2020). Briefly, 3-week-old cultures were subjected to four D/R cycles, in which desiccation conditions were 33% RH for TR9 and 55% RH for Csol cultures at 25°C for 8 h, under light. Afterwards, the cultures were transferred to Petri dishes with a semi-solid medium consisting solely of 1.5% agar in distilled water, in 100% RH at 15°C for 16 h (6-h light + 10-h darkness). Fully hydrated cells prior to D/R cycles were considered the control condition (T0).

Extraction of EPS: Sugar determinations

EPS accumulated on the outer microalgae surface were obtained by incubation of cells using gentle agitation with ultrapure water containing 1% phenylmethylsulphonyl fluoride and 0.1% inhibitor protease cocktail (Sigma-Aldrich, USA) at 40°C (20 ml g FW cell^{-1}) for 40 min. The supernatant was recovered by centrifugation at 5000*g* for 10 min at 4°C, filtered through glass fibre filters (Merck Millipore), dialysed against distilled water in Slice-A-Lyzer G2 Dialysis Cassettes (Thermo Scientific) (cut-off 2000) and freeze-dried. Total neutral sugars were determined by the phenol-H_2SO_4 method (Dubois *et al*., 1956) using glucose as standard, while uronic acids were determined according to the method described by Filisetti-Cozzi and Carpita (1991), using glucuronic acid (Sigma-Aldrich) as standard. Sulfate content was quantified by acid prehydrolysis (Terho and Hartiala, 1971) and then by the turbidimetric method described by Kolmert *et al*. (2000), using K_2SO_4 as standard.

Gel permeation chromatography

About 2 mg of either crude EPS or SPs was applied to a Sepharose 4B 70 × 16 cm (length × ID) Column C (General Electric Healthcare) equilibrated with 150 mM phosphate–citrate buffer (pH 5.2) and eluted with the same buffer. Forty 2-ml fractions were collected, and the amount of total carbohydrates, uronic acids and sulfate in each fraction was determined as described above. Dextrans of 9.3, 76, 156 and 2000 kDa (Sigma-Aldrich) were used as standards for column calibration.

Purification of SPs by anion exchange chromatography

Crude EPS were dissolved in distilled water (25 mg/25 ml), centrifuged at 15,000*g* for 5 min, and the supernatant was applied to a column (4.8 × 30 cm, Sigma-Aldrich) of Q-Sepharose Fast Flow (Amersham Biosciences, Sweden) equilibrated with distilled water. The charged substances were eluted with a linear gradient of 0–4 M NaCl at a flow rate of 2 ml min^{-1}. Eighty 5-ml fractions were collected, and their carbohydrate content was estimated by the phenol-H_2SO_4 method (Dubois *et al*., 1956). The fractions with high sugar yield were further assayed for their sulfate content using the method described by Kolmert *et al*. (2000), and those showing a

high sulfate concentration were pooled according to their Q-Sepharose elution profile, dialysed against distilled water and lyophilised as described above. Ionic strength during anionic chromatography was monitored by measuring the electric conductivity of each fraction.

Analysis of sulfated polymers by polyacrylamide and agarose gel electrophoresis

The presence of sulfated polymers in EPS from TR9 and Csol was also explored using toluidine blue staining. This dye can bind to both neutral and SPs, forming either blue or purple complexes respectively (Schmitz *et al*., 2010; Dantas-Santos *et al*., 2012; Sridharan and Shankar, 2012). Therefore, samples equivalent to 50 μg of total sugars were applied on 1.5% agarose gel (8 × 10 cm) and electrophoresed using a 0.01 M Tris/acetate running buffer (pH 8.3). After running at 90 V for 1 h, gels were stained with 0.01% toluidine blue O solution in 3% acetic acid/0.5% Triton X-100 overnight and de-stained in 3% acetic acid (Suresh *et al*., 2013).

In other experiments, samples from Q-Sepharose peak fractions (usually containing 50 μg of crude polysaccharides) were applied on 12.5% polyacrylamide gels (1.5 mm thickness), as described by Laemmli (1970). Electrophoresis was performed at 100 V for 2 h and acidic charged polymers were visualized using the staining procedure described by Zacharius *et al*. (1969), with modifications. Briefly, gels were pretreated with 1% periodic (w/v) acid in 3% acetic (v/v) acid followed by 0.5% sodium metabisulfite and stained with 0.5% alcian blue in 3% acetic acid and 25% isopropanol for 1 h. The gel was washed in the same solution without alcian blue. In order to preferentially reveal sulfate-containing polymers, parallel gels were stained with 0.01% toluidine blue O in 3% acetic acid/0.5% Triton X-100 overnight and de-stained with 3% acetic acid (Suresh *et al*., 2013). Chondroitin sulfate (Sigma-Aldrich) was used as standard.

Glycosyl composition of EPS and sulfated polymers

The glycosyl composition of TR9 and Csol crude EPS after four D/R cycles and of Q-Sepharose-purified SPs from TR9 after four D/R cycles was analysed by combined gas chromatography/mass spectrometry (GC/MS) of the per-*O*-trimethylsilyl derivatives of the monosaccharide methyl glycosides produced from the samples by acidic methanolysis, as described previously by Santander *et al*. (2013). Briefly, 1.5–3 mg of the samples were heated with methanolic HCl at 80°C for 17 h. After solvent removal, the samples were treated with a mixture of methanol, pyridine and acetic anhydride for 30 min. The solvents were evaporated, and the samples were derivatized with Tri-Sil® (Pierce) at 80°C for 30 min. GC/MS analysis of the TMS methyl glycosides was performed on an Agilent 7890A GC interfaced to a 5975C MSD, using an Supelco Equity-1 fused silica capillary column (30 m × 0.25 mm ID).

Nuclear magnetic resonance experiments

Deuterated water (99.8% deuteration) was supplied by Sigma-Aldrich (Madrid, Spain). A Varian INNOVA 500 NMR System (Varian, Palo Alto, CA, USA), fitted with an inverse 5 mm HCX 500 MHz probehead, z-gradient module and variable temperature unit, was used for all NMR experiments. The spectrometer resonance frequency for ^{1}H was 499.58 MHz. The ^{1}H 90° hard pulse was optimized and set to 8.4 μs (58 dB). The spectral width for the ^{1}H NMR experiment was 8012.8 Hz, and 32,768 acquisition points were recorded. Thirty-two scans with a 25-s interscan delay were acquired. A 0.50 Hz line broadening function was applied before processing. Selective 1D TOCSY experiments were performed with a spin lock time of 80 ms. For the HSQC experiment, the spectral widths were 3205 and 22,612 Hz in the F2 and F1 frequency domains respectively. The data were acquired with 256 t1 increments with 32 transients per t1 increment and with a 1.0 s interpulse delay. A 1-s presaturation pulse at the HDO signal (4.78 ppm) for solvent suppression was applied. Residual dimethylsulphoxide was used as internal standard for both ^{1}H and ^{13}C chemical shifts (2.71 and 39.39 ppm respectively). All experiments were recorded at 25°C. All NMR data were processed using the MestReNova software (version 14.1.1., Mestrelab Research SL, Santiago de Compostela, Spain).

Identification, sulfotransferase enzyme modelling and gene expression analysis

Transcripts encoding sulfotransferase enzymes from TR9 and Csol were identified by performing a search within customized databases of transcript sequences from both algal species, which are stored on our computers at the University of Alcalá. A sulfotransferase sequence from the Trebouxiophyceae *Micractinium conductrix* (accession no. PSC67312) was used as a query in TBLASTN searches (Gish and States, 1993) with Geneious Prime 2019.9.3 (Kearse *et al*., 2012). As a result, two transcripts were identified as the products of the expression of sulfotransferase genes, one from TR9 and the other from Csol. These sequences were used to obtain two pairs of primers for sulfotransferase transcript quantification by real-time PCR (qPCR) (Table S1). Both strands of the resulting PCR products were sequenced with an ABI 3130 Genetic Analyzer using the ABI BigDyeTM Terminator Cycle Sequencing Ready Reaction kit (Applied

Biosystems, CA, USA) to confirm their correctness. The sulfotransferase enzyme sequences from additional *Trebouxia* algae were obtained by translating the corresponding transcripts reconstructed from reads available in the Sequence Read Archive of the NCBI. This was the case of *Trebouxia arboricola* (accession no. ERX2100121) and *Trebouxia gelatinosa* (accession no. SRX330016). In the case of *Trebouxia* sp. TZW2008, the sulfotransferase enzyme sequence was deduced from the genomic sequence available at the NCBI (TZW2008_contig_201, whole genome shotgun sequence, accession no. BDIU01000160.1).

RNA extraction and qPCR

Total RNA was extracted from algal cultures (100–200 mg FW) following the protocol described by Jones *et al*. (1985), using five biological replicates of each experimental condition and two technical replicates. RNA was quantified using a NanoDrop ND-1000TM spectrophotometer (Daemyung, Korea), and DNA contaminants were degraded using the DNAse I RNA-free kit (Invitrogen, CA, USA). The complementary DNA (cDNA) was synthesized with the RevertAid First Strand cDNA Synthesis kit (Thermo Fisher Scientific, Madison, USA) using the supplied oligo-dT primer according to the manufacturer's instructions. PCR amplifications were performed in a 10-μl total volume containing 1 μl of 10-fold diluted cDNA, 0.5 μl of each primer and 5 μl 2X Fast SYBR-Green Master Mix (Foster City, CA, USA), using a 7500 Fast Real-Time PCR system (Applied Biosystems) under standard apparatus conditions. The absence of nonspecific PCR products and primer dimers was verified by dissociation curves and agarose gel electrophoresis. The amplification efficiency of each set of primers was confirmed as being higher than 95% according to the standard curve method described by da Costa *et al*. (2015). Transcript quantification was normalized to Ap47 (Clathrin adaptor complexes subunit) and Act (Actin) as reference genes following the strategy proposed by Vandesompele *et al*. (2002). Quantification of sulfotransferase transcript levels was performed at 0, 2 and 4 cycles of D/R because transcriptional changes could occur before it was possible to observe metabolic response.

Phylogenetic analyses

Phylogenetic reconstructions were performed based on the alignment of 33 amino acid sequences of sulfotransferases arranged into multiple sequence alignments (MSA) using MAFFT version 7 (Katoh and Standley, 2013) on the Guidance web server (Penn *et al*., 2010). The GUIDANCE2 algorithm was used to create a SuperMSA by concatenating the default MSA and alternative 50 MSAs. All data sets were subjected to maximum likelihood (ML) with PhyML (Guindon *et al*., 2010) using the LG + G + I + F (Le and Gascuel, 2008) substitution model selected as the best model with 'Smart Model Selection' (Lefort *et al*., 2017). Bootstrap supports (Felsenstein, 1985) were calculated to estimate the robustness of the clades from 100 replicates of the data. Trees were displayed with FigTree v.1.3 (Rambaut, 2008).

Additional analyses

Searches for possible transit peptides were performed with TargetP 1.1 (Emanuelsson *et al*., 2007) and Phobius (Kall *et al*., 2004). Protein motif predictions were performed by comparison against the NCBI-CDD motif library (Marchler-Bauer *et al*., 2017), using the GenomeNet protein motif search service (https://www.ncbi.nlm.nih.gov/cdd). Protein structures were computed using phyre2 (Kelley *et al*., 2015) and graphically visualized with RasMol (Sayle and Milner-White, 1995). Protein alignments were performed with Muscle 3.6 (Edgar, 2004), using Geneious Prime 2019.9.3 (Kearse *et al*., 2012).

Acknowledgements

This research was funded by grants from the Spanish Ministry of Science, Innovation and Universities (CGL2016-80259-P). Glycosyl composition analyses were partially funded by a grant from the Chemical Sciences, Geosciences and Biosciences Division, Office of Basic Energy Sciences, U.S. Department of Energy (DE-SC0015662) to Parastoo Azadi at the Complex Carbohydrate Research Centre (University of Georgia, USA). M.R. Braga is grateful to the Conselho Nacional de Desenvolvimento Científico e Tecnológico, Brazil, for research fellowships (305542/2016-8, 312414/2019-2) and the Fundação de Amparo a Pesquisa do Estado de São Paulo, Brazil, for a grant (2017/50341-0).

References

Allard, B., and Casadevall, E. (1990) Carbohydrate composition and characterization of sugars from the green microalga *Botryococcus braunii*. *Phytochemistry* **29**: 1875–1878.

Anantharaman, V., Koonin, E.V., and Aravind, L. (2002) Comparative genomics and evolution of proteins involved in RNA metabolism. *Nucleic Acids Res* **30**: 1427–1464.

Aquino, R.S., Gravitol, C., and Mourão, P.A.S. (2011) Rising from the sea: correlations between sulfated polysaccharides and salinity in plants. *PLoS One* **6**: e18862.

Arata, P.X., Alberghina, J., Confalonieri, V., Errea, M.I., Estevez, J.M., and Ciancia, M. (2017) Sulfated

polysaccharides in the freshwater green macroalga *Cladophora surera* not linked to salinity adaptation. *Front Plant Sc* **13**: 1927.

Baudelet, P.H., Ricochon, G., Michel, L., and Muniglia, L. (2017) A new insight into cell walls of Chlorophyta. *Algal Res* **25**: 333–371.

Becket, R.P., Kranner, I., and Minibayeva, F.V. (2008) Stress physiology and the symbiosis. In *Lichen Biology*, Nash, T. H., III (ed). Cambridge, UK: Cambridge University Press, pp. 184–151.

Bedini, E., Laezza, A., Parrilli, M., and Iadonisi, A. (2017) A review of chemical methods for the selective sulfation and desulfation of polysaccharides. *Carbohydr Polym* **174**: 1224–1239.

Beier, R.C., Mundy, B.P., and Strobel, G.A. (1980) Assignment of anomeric configuration and identification of carbohydrate residues by ^{13}C NMR. 1. Galacto- and glucopyranosides and furanosides. *Can J Chem* **58**: 2800–2807.

Bhowruth, V., Alderwick, L.J., Brown, A.K., Bhatt, A., and Besra, G.S. (2008) Tuberculosis: a balanced diet of lipids and carbohydrates. *Biochem Soc Trans* **36**: 555–565.

Brown, D.H., Rapsch, S., Beckett, A., and Ascaso, C. (1987) The effect of desiccation on cell shape in the lichen *Parmelia sulcata* Taylor. *New Phytol* **105**: 295–299.

Burdin, K.S., and Bird, K.T. (1994) Heavy metal accumulation by carrageenan and agar producing algae. *Bot Mar* **37**: 467–470.

Casano, L.M., Del Campo, E.M., García-Breijo, F.J., Reig-Armiñana, J., Gasulla, F., Del Hoyo, A., and Barreno, E. (2011) Two *Trebouxia* algae with different physiological performances are ever-present in lichen thalli of *Ramalina farinacea*. Coexistence versus competition? *Environ Microbiol* **13**: 806–818.

Casano, L.M., Braga, M.R., Álvarez, R., Del Campo, E.M., and Barreno, E. (2015) Differences in the cell walls and extracellular polymers of the two *Trebouxia* microalgae coexisting in the lichen *Ramalina farinacea* are consistent with their distinct capacity to immobilize extracellular Pb. *Plant Sci* **236**: 195–204.

Centeno, D.C., Hell, A.F., Braga, M.R., Del Campo, E.M., and Casano, L.M. (2016) Contrasting strategies used by lichen microalgae to cope with desiccation-rehydration stress revealed by metabolite profiling and cell wall analysis. *Environ Microbiol* **18**: 1546–1560.

Cerveny, L., Straskova, A., Dankova, V., Hartlova, A., Ceckova, M., Staud, F., and Stulik, J. (2013) Tetratricopeptide repeat motifs in the world of bacterial pathogens: role in virulence mechanisms. *Infect Immun* **81**: 629–635.

da Costa, M., Duro, N., Batista-Santos, P., Ramalho, J.C., and Ribeiro-Barros, A.I. (2015) Validation of candidate reference genes for qRT-PCR studies in symbiotic and non-symbiotic *Casuarina glauca* Sieb. Ex Spreng. Under salinity conditions. *Symbiosis* **66**: 21–35.

Cunha, L., and Grenha, A. (2016) Sulfated seaweed polysaccharides as multifunctional materials in drug delivery applications. *Mar Drugs* **14**: 42–82.

Dantas-Santos, N., Gomes, D.L., Costa, L.S., Cordeiro, S.L., Costa, M.S., Trindade, E.S., *et al*. (2012) Freshwater plants synthesize sulfated polysaccharides: heterogalactans from water hyacinth (*Eicchornia crassipes*). *Int J Mol Sci* **13**: 961–976.

De Philippis, R., Paperi, R., Sili, C., and Vincenzini, M. (2003) Assessment of the metal removal capability of two capsulated cyanobacteria, *Cyanospira capsulata* and *Nostoc PCC7936*. *J Appl Phycol* **15**: 155–161.

Demura, M., Ioki, M., Kawachi, M., Nakajima, N., and Watanabe, M.M. (2014) Desiccation tolerance of *Botryococcus braunii* (Trebouxiophyceae, Chlorophyta) and extreme temperature tolerance of dehydrated cells. *J Appl Phycol* **26**: 49–53.

Dubois, M., Gilles, K.A., Hamilton, J.K., Rebers, P.A., and Smith, F. (1956) Colorimetric method for determination of sugars and related substances. *Anal Chem* **28**: 350–356.

Edgar, R.C. (2004) MUSCLE: multiple sequence alignment with high accuracy and high throughput. *Nucleic Acids Res* **32**: 1792–1797.

Emanuelsson, O., Brunak, S., von Heijne, G., and Nielsen, H. (2007) Locating proteins in the cell using TargetP, SignalP and related tools. *Nat Protoc* **2**: 953–971.

Felsenstein, J. (1985) Confidence limits on phylogenies: an approach using the bootstrap. *Evolution* **39**: 783–791.

Filisetti-Cozzi, T.M., and Carpita, N.C. (1991) Measurement of uronic acids without interference from neutral sugars. *Anal Biochem* **197**: 157–162.

Gish, W., & States, D. J. (1993). Identification of protein coding regions by database similarity search. *Nature Genetics*, **3**: 266–272.

González-Hourcade, M., Braga, M.R., Del Campo, E.M., Ascaso, C., Patiño, C., and Casano, L.M. (2020) Ultrastructural and biochemical analyses reveal cell wall remodelling in lichen-forming microalga submitted to cyclic desiccation-rehydration. *Ann Bot* **125**: 459–469.

Guangling, J., Guangli, Y., Junzeng, Z., and Ewart, H.S. (2011) Chemical structures and bioactivities of sulphated polysaccharides from marine algae. *Mar Drugs* **9**: 196–233.

Guindon, S., Dufayard, J.F., Lefort, V., Anisimova, M., Hordijk, W., and Gascuel, O. (2010) New algorithms and methods to estimate maximum-likelihood phylogenies: assessing the performance of PhyML 3.0. *Syst Biol* **59**: 307–321.

Güven, K.C., Akyüz, K., and Yurdun, T. (1995) Selectivity of heavy metal binding by algal polysaccharides. *Toxicol Environ Chem* **47**: 65–70.

Han, P.P., Sun, Y., Shi-ru, J., Zong, C., and Tan, A. (2014) Effects of light wavelengths on extracellular and capsular polysaccharide production by *Nostoc flagelliforme*. *Carbohydr Polym* **152**: 145–151.

Hell, A.F., Gasulla, F., González-Hourcade, M., Del Campo, E.M., Centeno, D.C., and Casano, L.M. (2019) Tolerance to cyclic desiccation in lichen microalgae is related to habitat preference and involves specific priming of the antioxidant system. *Plant Cell Physiol* **60**: 1880–1891.

Hernández-Sebastià, C., Varin, L., and Marsolais, F. (2008) Sulfotransferases from plants, algae and phototrophic bacteria. In *Sulfur Metabolism in Phototrophic Organisms*, Hell, R., Dahl, C., and Leustek, T. (eds). Dordrecht, The Netherlands: Springer, pp. 111–130.

Ho, C.L. (2015) Phylogeny of algal sequences encoding carbohydrate sulfotransferases, formylglycine-dependent sulfatases, and putative sulfatase modifying factors. *Front Plant Sci* **6**: 1057.

Honke, K., and Taniguchi, N. (2002) Sulfotransferases and sulfated oligosaccharides. *Med Res Rev* **22**: 637–654.

Jarlier, V., and Nikaido, H. (1994) Micobacterial cell wall: structure and role in natural resistance to antibiotics. *FEMS Microbiol Lett* **123**: 11–18.

Jeter, V.L., Mattes, T.A., Beattie, N.R., and Escalante-Semerena, J.C. (2019) A new class of phosphoribosyltransferases involved in cobamide biosynthesis is found in methanogenic archaea and cyanobacteria. *Biochemistry* **58**: 951–964.

Jones, J.D., Dunsmuir, P., and Bedbrook, J. (1985) High level expression of introduced chimaeric genes in regenerated transformed plants. *EMBO J* **4**: 2411–2418.

Kall, L., Krogh, A., and Sonnhammer, E.L. (2004) A combined transmembrane topology and signal peptide prediction method. *J Mol Biol* **338**: 1027–1036.

Katoh K., and Standley D.M. (2013). MAFFT multiple sequence alignment Software version 7: improvements in performance and usability. *Molecular Biology and Evolution*, **30**: 772–780. http://dx.doi.org/10.1093/molbev/mst010.

Kearse, M., Moir, R., Wilson, A., Stones-Havas, S., Cheung, M., Sturrock, S., *et al*. (2012) Geneious basic: an integrated and extendable desktop software platform for the organization and analysis of sequence data. *Bioinformatics* **28**: 1647–1649.

Kelley, L.A., Mezulis, S., Yates, C.M., Wass, M.N., and Sternberg, M.J. (2015) The Phyre2 web portal for protein modeling, prediction and analysis. *Nat Protoc* **10**: 845–858.

Knowles, E.J., and Castenholz, R.W. (2008) Effect of exogenous extracellular polysaccharides on the desiccation and freezing tolerance of rock-inhabiting phototrophic microorganisms. *FEMS Microbiol Ecol* **66**: 261–270.

Kolmert, Å., Wikström, P., and Hallberg, K.B. (2000) A fast and simple turbidimetric method for the determination of sulfate in sulfate-reducing bacterial cultures. *J Microbiol Methods* **41**: 179–184.

Koonin, E.V., and Aravind, L. (2002) Origin and evolution of eukaryotic apoptosis: the bacterial connection. *Cell Death Differ* **9**: 394–404.

Kranner, I., Beckett, R., Hochman, A., and Nash, T.H. (2008) Desiccation-tolerance in lichens: a review. *Bryologist* **111**: 576–593.

Laemmli, U.K. (1970) Cleavage of structural proteins during the assembly of the head of bacteriophage T4. *Nature* **227**: 680–685.

Le, S.Q., and Gascuel, O. (2008) An improved general amino acid replacement matrix. *Mol Biol Evol* **25**: 1307–1320.

Lefort, V., Longueville, J.E., and Gascuel, O. (2017) SMS: smart model selection in PhyML. *Mol Biol Evol* **34**: 2422–2424.

Li, H., Xu, J., Liu, Y., Ai, S., Qin, F., Li, Z., *et al*. (2011) Antioxidant and moisture-retention activities of the polysaccharide from *Nostoc commune*. *Carbohydr Polym* **83**: 1821–1827.

Lim, C.Y., Yoo, Y.H., Sidhartan, M., Ma, C.W., Bang, I.C., Kim, J.M., *et al*. (2006) Effects of copper(I) oxide on growth and biochemical compositions of two marine microalgae. *J Environ Biol* **27**: 461–466.

Liu, Q.M., Yang, Y., Maleki, S.J., Alcocer, M., Xu, S.S., Shi, C.L., *et al*. (2016) Anti-food allergic activity of sulfated polysaccharide from *Gracilaria lemaneiformis* is dependent on immunosuppression and inhibition of p38 MAPK. *J Agri Food Chem* **64**: 4536–4544.

Liu, W., Cui, L., Xu, H., Zhu, Z., and Gao, X. (2017) Flexibility-rigidity coordination of the dense exopolysaccharide matrix in terrestrial cyanobacteria acclimated to periodic desiccation. *Appl Environ Microbiol* **83**: e01619-17.

Marchler-Bauer, A., Bo, Y., Han, L., He, J., Lanczycki, C.J., Lu, S., *et al*. (2017) CDD/SPARCLE: functional classification of proteins via subfamily domain architectures. *Nucleic Acids Res* **45**: D200–D203.

Markou, G., and Nerantzis, E. (2013) Microalgae for high-value compounds and biofuels production: a review with focus on cultivation under stress conditions. *Biotechnol Adv* **31**: 1532–1542.

Martínez-Alberola, F., Barreno, E., Casano, L.M., Gasulla, F., Molins, A., and Del Campo, E.M. (2019) Dynamic evolution of mitochondrial genomes in Trebouxiophyceae, including the first completely assembled mtDNA from a lichen-symbiont microalga (*Trebouxia* sp. TR9). *Sci Rep* **9**: 8209.

Martínez-Alberola, F., Barreno, E., Casano, L.M., Gasulla, F., Molins, A., Moya, P., *et al*. (2020) The chloroplast genome of the lichen-symbiont microalga *Trebouxia* sp. TR9 (Trebouxiophyceae, Chlorophyta) shows short inverted repeats with a single gene and loss of the rps4 gene, which is encoded by the nucleus. *J Phycol* **56**: 170–184.

Mazor, G., Kidron, G.J., Vonshak, A., and Abeliovich, A. (1996) The role of cyanobacterial exopolysaccharides in structuring desert microbial crusts. *FEMS Microbiol Ecol* **21**: 121–130.

Moon, A.F., Edavettal, S.C., Krahn, J.M., Munoz, E.M., Negishi, M., Linhardt, R.J., *et al*. (2004) Structural analysis of the sulfotransferase (3-o-sulfotransferase isoform 3) involved in the biosynthesis of an entry receptor for herpes simplex virus 1. *J Biol Chem* **279**: 45185–45193.

Moore, B.G., and Tischer, R.G. (1964) Extracellular polysaccharides of algae: effects on life-support systems. *Science* **145**: 586–587.

Mourão, P.A., and Pereira, M.S. (1999) Searching for alternatives to heparin: sulfated fucans from marine invertebrates. *Trends Cardiovasc Med* **9**: 225–232.

Ozturk, S., Aslim, B., Suludere, Z., and Tan, S. (2014) Metal removal of cyanobacterial exopolysaccharides by uronic acid content and monosaccharide composition. *Carbohydr Polym* **101**: 265–271.

Pathak, A.K., Pathak, V., Seitz, L., Maddry, J.A., Gurcha, S. S., Besra, G.S., *et al*. (2001) Studies on (β,1→5) and (β,1→6) linked Octyl Galf disaccharides as substrates for mycobacterial galactosyltransferase activity. *Bioorg Med Chem* **9**: 3129–3143.

Penn, O., Privman, E., Ashkenazy, H., Landan, G., Graur, D., and Pupko, T. (2010) GUIDANCE: a web server for assessing alignment confidence scores. *Nucleic Acids Res* **38**: W23–W28.

Pomin, V.H. (2016) Phylogeny, structure, function, biosynthesis and evolution of sulfated galactose-containing glycans. *Int J Biol Macromol* **84**: 372–379.

Rambaut, A. (2008) FigTree: Tree figure drawing tool. Version 1.3.1.

Raveendran, S., Yoshida, Y., Maekawa, T., and Kumar, D.S. (2013) Pharmaceutically versatile sulfated polysaccharide based bionano platforms. *Nanomedicine* **5**: 605–626.

Santander, J., Martin, T., Loh, A., Pohlenz, C., Gatlin, D., and Curtiss, R. (2013) Mechanisms of intrinsic resistance to antimicrobial peptides of *Edwardsiella ictaluri* and its influence on fish gut inflammation and virulence. *Microbiology* **159**: 1471–1486.

Säwén, E., Huttunen, E., Zhang, X., Yang, Z., and Widmalm, G. (2010) Structural analysis of the exopolysaccharide produced by Streptococcus thermophilus ST1 solely by NMR spectroscopy. *J Biomol NMR* **47**: 125–134.

Sayle, R.A., and Milner-White, E.J. (1995) RASMOL: biomolecular graphics for all. *Trends Biochem Sci* **20**: 374–376.

Schmitz, N., Laverty, S., Fraus, V.B., and Aigner, T. (2010) Basic methods in histopathology of joint tissues. *Osteoarthritis Cartilage* **18**: S113–S116.

Sharma, M., and Pandey, G.K. (2016) Expansion and function of repeat domain proteins during stress and development in plants. *Front Plant Sci* **6**: 1218. https://doi.org/10.3389/fpls.2015.01218.

Sridharan, G., and Shankar, A.A. (2012) Toluidine blue: a review of its chemistry and clinical utility. *J Oral Maxillofac Pathol* **16**: 251–255.

Suresh, V., Senthilkumar, N., Thangam, R., Rajkumar, M., Anbazhagan, C., Rengasamy, R., *et al*. (2013) Separation, purification and preliminary characterization of sulfated polysaccharides from *Sargassum plagiophyllum* and its in vitro anticancer and antioxidant activity. *Process Biochem* **48**: 364–373.

Tannin-Spitz, T., Bergman, M., van Moppes, D., Grossman, S., and Arad, S. (2005) Antioxidant activity of the polysaccharide of the red microalga *Porphyridium* sp. *J Appl Phycol* **17**: 215–222.

Terho, T.T., and Hartiala, K. (1971) Method for determination of the sulfate content of glycosaminoglycans. *Anal Biochem* **41**: 471–476.

Vandesompele, J., De Preter, K., Pattyn, F., Poppe, B., Van Roy, N., De Paepe, A., and Speleman, F. (2002) Accurate normalization of real-time quantitative RT-PCR data by geometric averaging of multiple internal control genes. *Genome Biol* **3**: research0034.1.

Wang, X., Zhang, Z., Yao, Z., Zhao, M., and Qi, H. (2013) Sulfation, anticoagulant and antioxidant activities of polysaccharide from green algae *Enteromorpha linza*. *Int J Biol Macromol* **58**: 225–230.

Wang, J., Salem, D.R., and Sani, R.K. (2018) Extremophilic exopolysaccharides: a review and new perspectives on engineering strategies and applications. *Carbohydr Polym* **205**: 8–26.

Wang, L., Liu, X., Wang, X., Pan, Z., Geng, X., Chen, B., *et al*. (2019) Identification and characterization analysis of sulfotransferases (SOTs) gene family in cotton (*Gossypium*) and its involvement in fiber development. *BMC Plant Biol* **19**: 595.

Xiao, R., and Zheng, Y. (2016) Overview of microalgal extracellular polymeric substances (EPS) and their applications. *Biotechnol Adv* **34**: 1225–1244.

Zacharius, R.M., Zell, T.E., Morrison, J.H., and Woodlock, J.J. (1969) Glycoprotein staining following electrophoresis on acrylamide gels. *Anal Biochem* **30**: 148–152.

Supporting Information

Additional Supporting Information may be found in the online version of this article at the publisher's web-site:

Table S1 Oligonucleotide sequences of sulfotransferases employed for transcript quantification by real-time PCR. F, forward; R, reverse. pb, pair of bases.

Fig. S1 Anionic profile of EPS from crude EPS from *Trebouxia* sp. TR9 under control conditions (A) and after exposure to desiccation-rehydration conditions (B) separated by Q-Sepharose chromatography.

Fig. S2 ^{1}H NMR PRESAT spectrum (D_2O, 500 MHz) (a), and 1D TOCSY spectra (D_2O, 500 MHz) after selective irradiation at 5.26 (b), 5.18 (c) and 5.05 ppm (d) from *Trebouxia* sp. TR9 in desiccation/rehydration conditions.

Fig S3 HSQCED PRESAT spectrum (D_2O, 500 MHz) (A) TOCSY PRESAT spectrum (D_2O, 500 MHz) (inset: cross peaks probably due to sulfated positions) (B) of isolated sulfated polymer from *Trebouxia* sp. TR9 in desiccation/rehydration conditions.

Fig. S4 Alignment of sulfotransferase amino acid sequences from several organisms including *Trebouxia* sp. TR9 and *Coccomyxa simplex*, showing conserved regions. The brown bar indicates the Sulfotransfer_3 domain.

Tercer artículo

The under-explored extracellular proteome of aero-terrestrial microalgae provides clues on different mechanisms of desiccation tolerance in non-model organisms

Plant Molecular Biology

The under-explored extracellular proteome of aero-terrestrial microalgae provides clues on different mechanisms of desiccation tolerance in non-model organisms

--Manuscript Draft--

Manuscript Number:	
Full Title:	The under-explored extracellular proteome of aero-terrestrial microalgae provides clues on different mechanisms of desiccation tolerance in non-model organisms
Article Type:	Original Article
Keywords:	exoproteome; extracellular; desiccation; rehydration; secretome; microalgae; Coccomyxa simplex; Trebouxia sp.
Corresponding Author:	Eva Maria del Campo Universidad de Alcala Alcala de Henares, Madrid SPAIN
Corresponding Author Secondary Information:	
Corresponding Author's Institution:	Universidad de Alcala
Corresponding Author's Secondary Institution:	
First Author:	Maria Gonzalez-Hourcade
First Author Secondary Information:	
Order of Authors:	Maria Gonzalez-Hourcade
	Eva Maria del Campo
	Leonardo Mario Casano
Order of Authors Secondary Information:	
Funding Information:	Ministerio de Ciencia, Innovación y Universidades (CGL2016-80259-P) — Dr. Leonardo Mario Casano
Abstract:	Trebouxia sp. (TR9) and Coccomyxa simplex (Csol) are desiccation-tolerant lichen microalgae with different adaptive strategies in accordance with the prevailing conditions of their habitats. The remodelling of cell wall and extracellular polysaccharides depending on water availability are key elements in the tolerance to desiccation of both microalgae. Currently, there is no information about the extracellular proteins of these algae and other aero-terrestrial microalgae in response to limited water availability. To our knowledge, this is the first report on the exoproteome of aeroterrestrial microalgae subjected to cyclic desiccation/rehydration. LC-MS/MS and bioinformatic analyses of the extracellular proteins in the two lichen microalgae submitted to four desiccation/rehydration cycles allowed the compilation of 111 and 121 identified proteins for TR9 and Csol, respectively. Both sets of exoproteins shared a variety of predicted biological functions but showed a constitutive expression in Csol and partially inducible in TR9. In both algae, the exoproteomes included a number of proteins of unknown functions, some of which could be considered as small intrinsically disordered proteins related with desiccation tolerant organisms. Differences in the composition and the expression pattern between the studied exoproteomes would be oriented to preserve the biochemical and biophysical properties of the extracellular structures under the different conditions of water availability in which each alga thrives.
Suggested Reviewers:	Richard Beckett beckett@nu.ac.za
	Gerd Jürgens gerd.juergens@zmbp.uni-tuebingen.de

	Robert Sharp sharpr@missouri.edu
	Ramesh Katam Ramesh.katam@famu.edu

TITLE: The under-explored extracellular proteome of aero-terrestrial microalgae provides clues on different mechanisms of desiccation tolerance in non-model organisms

María González-Hourcade (0000-0001-5484-2615), Eva M. del Campo (0000-0003-4796-6227), Leonardo M. Casano (0000-0002-2304-7317)

University of Alcalá, Dept. of Life Sciences, 28805, Alcalá de Henares (Madrid), Spain.

Running title: Exo-proteomics of aero-terrestrial microalgae

Abstract

Key Message Comparative exoproteome analysis between two aero-terrestrial microalgae show similar protein repertoires but different expression patterns in response to cyclic desiccation/rehydration probably oriented to preserve the extracellular structures during drying.

Abstract *Trebouxia* sp. (TR9) and *Coccomyxa simplex* (Csol) are desiccation-tolerant lichen microalgae with different adaptive strategies in accordance with the prevailing conditions of their habitats. The remodelling of cell wall and extracellular polysaccharides depending on water availability are key elements in the tolerance to desiccation of both microalgae. Currently, there is no information about the extracellular proteins of these algae and other aero-terrestrial microalgae in response to limited water availability. To our knowledge, this is the first report on the exoproteome of aeroterrestrial microalgae subjected to cyclic desiccation/rehydration. LC-MS/MS and bioinformatic analyses of the extracellular proteins in the two lichen microalgae submitted to four desiccation/rehydration cycles allowed the compilation of 111 and 121 identified proteins for TR9 and Csol, respectively. Both sets of exoproteins shared a variety of predicted biological functions but showed a constitutive expression in Csol and partially inducible in TR9. In both algae, the exoproteomes included a number of proteins of unknown functions, some of which could be considered as small intrinsically disordered proteins related with desiccation tolerant organisms. Differences in the composition and the expression pattern between the studied exoproteomes would be oriented to preserve the biochemical and biophysical properties of the extracellular structures under the different conditions of water availability in which each alga thrives.

Keywords: exoproteome, extracellular, desiccation, rehydration, secretome, microalgae, *Coccomyxa simplex*, *Trebouxia sp.*

Introduction

Extracellular polymeric substances (EPS) are highly hydrated polymers produced by a wide range of microorganisms. Microbial EPS facilitate water retention, cell adhesion, signalling and protection from abiotic and biotic environmental stresses. This mucous mass surrounding cells or group of cells is mainly composed by complex polysaccharides and proteins (Costa *et al.*, 2018). In spite of the high diversity of substances secreted beyond the plasma membrane, secretomics is usually considered within the frame of proteomics as a compilation of proteins exported into the extracellular space (Vincent *et al.*, 2020). In plants, the secretome is usually considered as the population of proteins exported into the extracellular space including cell wall proteins as well as non-cell wall extracellular proteins (Krause *et al.*, 2013; Vincent *et al.*, 2020) despite plants also secreting a wide variety of molecules including polysaccharides, metabolites, phytohormones and nucleic acids (Vincent *et al.*, 2020). In any case, plant secretomes are involved in a variety of processes other than cell-wall remodelling, including signalling, development and stress responses (Delaunois *et al.*, 2014). Comparative studies of secretomes from plants under diverse stressful conditions showed changes in the abundance of apoplastic enzymes involved in oxide-reductions, carbohydrate metabolism, and protein processing, which reveal the significant role of the apoplast in plant stress signal reception and response (Tanveer *et al.*, 2014). Plant cell wall and the extracellular matrix (ECM) or EPS constitute the front-line defence under stress conditions. Specially in desiccation tolerant plants, the controlled deformation of their flexible cell walls prevents the extreme mechanical stress provoked by dehydration (Chen *et al.*, 2020).

Microalgae have attracted attention, as they produce a diversity of EPS that form a hydrated biofilm matrix. Microalgal EPS are mainly composed of polysaccharides, proteins,

nucleic acids and lipids. Compared to polysaccharides from terrestrial plants, fungi and macroalgae, microbial polysaccharides have probably the highest structural and functional diversity (reviewed in Pierre *et al.*, 2019 and Xiao and Zheng, 2016). Microalgal EPS contain proteins interacting with polysaccharides and other substances to form a stable EPS matrix, however little is known of the chemistry and function of exoproteins, in general, and of the extracellular enzymes in particular. The limited available data on EPS proteins from green algae indicates an important interspecific variability. *Clorella vulgaris* has higher protein content than *Chodatella* sp. and the cyanobacterium *Microcystis* sp., which has higher polysaccharide content (Chiou *et al.*, 2010). In *Dunaliella tertiolecta*, carbohydrates predominated while protein was found to be the minor component of EPS (Geun Goo *et al.*, 2013). In *Chlorella* sp. and *Micractinium* sp., the N availability and the cultivation stage significantly affect the EPS protein content in a species-specific manner (Wang *et al.*, 2014). The exoproteome of the freshwater chlorophyte *Chlamydomonas reinhardtii* has few cell wall associated proteins and is mainly composed of a variety of hydroxyproline-rich glycoproteins forming a relatively simple cell wall matrix along with flagellar proteins and peptidases (Baba *et al.*, 2011). In brown algae, *Ectocarpus siliculosus* and *Saccharina japonica* show exoproteomes composed of very similar protein repertories, which were partially common with those of other multicellular organisms including land plants, fungi and animals (Terauchi *et al.*, 2017). The exoproteome of the charophycean *Penium margaritaceum* is more closely related to those of land plants than to those of chlorophytes (Ruiz-May *et al.*, 2018). These findings support the hypothesis that many of the proteins associated with plant cell wall remodelling as well as other extracellular proteins evolved prior to the colonization of terrestrial habitats (Ruíz-May *et al.,*2018).

Probably, the less studied exoproteins are those from aero-terrestrial microalgae, in general, and lichen forming algae in particular. Lichens are poikilohydric because they cannot

actively regulate their water content, and thus are frequently facing dehydration stress. Most lichens are desiccation tolerant, since they have evolutionarily acquired a set of strategies/mechanisms allowing the survival in anabiosis with a cellular water content of approximately 5-10% (Kranner *et al.*, 2008). This capacity is not only inherent to the mycobionts but also to the lichen microalgae. Indeed, it was recently revealed that two lichen microalgae belonging to different genera, *Coccomyxa simplex* (Csol) and *Trebouxia* sp. (TR9) have developed species-specific mechanisms of desiccation tolerance (DT) to cope with alternating desiccation-rehydration (D/R) cycles (Hell *et al.*, 2019). Differences in strategies to cope with dehydration stress between TR9 and Csol seem to be strongly linked with the ecological context in which each alga thrives. The former is adapted to Mediterranean environments with an average relative humidity (RH) of approx. 25-30% and relatively rapid cycles of daily and/or seasonal D/R (Centeno *et al.*, 2016). In contrast, the lichen *Solorina saccata* from which Csol was obtained, thrives in mild and cold areas with a RH of at least 55-60% (during the dry season). A detailed study on the hydric behaviour and the physiological performance of TR9 and Csol clearly indicated a higher DT of the former than the later, since TR9 fully recovered from more drastic conditions of drying (i.e. low air relative humidity and rapid dehydration) than Csol (Hell *et al.,* 2019). However, each microalga was able to recover its photosynthetic capacity upon rehydration, when subjected to desiccation conditions resembling those of their natural habitats. Within the diverse mechanisms of DT orchestrated by TR9 and Csol, the desiccation-induced ultrastructural changes of cell wall and the biochemical remodelling of cell wall polysaccharides seemed to play a crucial role (González-Hourcade *et al.*, 2020b). The cell wall of fully hydrated TR9 is mainly composed of poorly branched galactans with the predominance of a hot-water-soluble 75 kDa rhamno-galactofuranan and alkali-soluble galactans with substitutions of rhamnosyl, xylosyl and mannosyl residues (Casano *et al.,* 2015; González-Hourcade *et al.,* 2020b). Exposure to cyclic

D/R causes marked changes especially in the hot-water-soluble galactans that increase in abundance and appear as a population of polymers with higher (to a greater extent) and lower molecular mass than 75 kDa, in which mannosyl substitutions are absent. In contrast to TR9, the cell wall of fully hydrated Csol is mainly composed of polysaccharides showing a polydispersed and broad molecular mass profile (Centeno *et al.,* 2016; González-Hourcade *et al.,* 2020b). The main hot-water-soluble polymers are linear xylans and two highly substituted mannans, while poorly substituted 4-linked glucans account for most alkali-soluble polysaccharides. Cyclic D/R only produces a generalized quantitative decrease without qualitative changes in the hot-water-soluble polysaccharides; however, it significantly modifies the KOH-soluble 4-linked glucans, changing from a polydispersed molecular mass distribution to some discrete polymers within 103 to 3.7 kDa (González-Hourcade *et al.,* 2020a).

TR9 and Csol algae also produced EPS including polysaccharides and proteins as the main components (Casano *et al.*, 2015; Centeno *et al.*, 2016). The TR9 EPS show predominance of poorly substituted galactans resembling the cell wall polysaccharides, although with a lower content of rhamnose, xylose, and mannose (Casano et al., 2015). Galactans are also the main components of the Csol EPS; even though they are much more heterogeneous than TR9 EPS. A highly branched manno-galactan and a 2-linked rhamnan account for most Csol EPS polysaccharides (Centeno *et al.,* 2016). Importantly, the EPS of both microalgae contain uronic acids and sulfated sugars, although the amount of uronic acids per cell unit is 1.5-fold higher in TR9 than in Csol (Centeno *et al.,* 2016). Cyclic D/R does not modify the polydispersed molecular mass distribution of EPS polymers of both microalgae but provokes changes in the abundance of several polysaccharides (González-Hourcade *et al.,* 2020a). However, in Csol, the medium-low-sized uronic acid-containing polysaccharides present in hydrated cells are substituted by higher molecular mass carbohydrates after D/R. Sulfated polysaccharide(s) increase after cyclic D/R

only in TR9.Interestingly, species-specific modifications in EPS carbohydrates seemed to contribute to DT including an increase of sulfated polysaccharides in TR9 (González-Hourcade *et al.*, 2020a). The exoproteins of TR9 and Csol have been preliminary studied by 2D-SDS-PAGE (Centeno *et al.*, 2016). An average of 70 spots were detected in each exoproteome, which contrast with the higher size of exoproteomes of other organisms (e.g. 135 proteins in *Anabaena* sp., (Oliveira *et al.*, 2015). Importantly, those data were obtained only from algal cells under control (fully hydrated) conditions. Furthermore, previous studies showed that two different species of lichen microalgae, TR9 and *Trebouxia* sp. TR1, produced different amounts of EPS that contained proteins with distinct polypeptide patterns, probably related with different capabilities of extracellular Pb retention (Casano *et al.*, 2015).

Based on the mentioned evidence, we hypothesized that, in lichen algae, the biochemical diversity the cell wall and EPS and the species-specific remodelling of extracellular polymers involved in the DT: (i) implies the participation of a wide range of species-specific cell wall/EPS-modifying enzymes present in the exoproteome of each alga; and (ii) the exposition to species-specific conditions of D/R could induce quantitative and/or qualitative changes in the exoproteome of each alga. Therefore, the objective of the present study was to characterize in detail the proteins contained in the EPS of TR9 and Csol, and search for possible changes in their levels after cyclic D/R to gain knowledge on the composition, structure and function of EPS proteins from lichen algae in relation with their most outstanding feature, the desiccation tolerance.

Materials and methods

Microalgae isolation and culture and desiccation-rehydration treatments

Trebouxia sp. TR9 was isolated from the lichen *Ramalina farinacea* according to (Casano *et al.*, 2011), and *Coccomyxa simplex* (Csol) (*Coccomyxa solorina* according to Malavasi *et al.*, 2016) was obtained from Sammlung von Algenkulturen at Göttingen University (Germany) (strain 216-12). Both microalgae were axenically cultured on small nylon square membranes in semi-solid Bold 3N medium (Bold and Parker, 1962) for three weeks prior treatments in a growth chamber as previously described (Centeno *et al.*, 2016). Algal cultures were subjected to four D/R cycles. Desiccation (D) conditions consisted of 33% RH for TR9 and 55% RH for Csol cultures at 25°C for 8h, under light. Rehydration (R) was performed by transferring the cultures to Petri dishes with a semi-solid medium composed by 1.5% agar in distilled water with 100% RH at 15 °C for 16 h (6h light + 10h darkness). Fully hydrated cells prior to D/R cycles were considered the control condition (T0).

Extraction of exoproteome from *Trebouxia* sp. TR9 and *Coccomyxa simplex*

Extracellular proteins accumulated on the outer microalgae surface were obtained by incubation of cells by gentle agitation with ultrapure water containing 1% phenylmethylsulfonyl fluoride and 0.1% inhibitor protease cocktail (Sigma-Aldrich Co., USA) at 40ºC (20 ml. g FW cell^{-1}) for 40 min. The supernatant was recovered by centrifugation at 5000 ×g for 10 min at 4°C, filtered through glass fiber filters (Merck Millipore, USA), dialyzed against distilled water in Slice-A-Lyzer Dialysis Cassettes G2 (Thermo Scientific, USA) (cut off 2000) and freeze-dried. Total protein content was determined by Bradford method (Bradford, 1976) using bovine serum albumin as standard.

Protein identification by LC-MS/MS

Information on exoproteomes was obtained on the basis of protein identification by analyses by liquid nano-chromatography coupled to a high-resolution mass spectrometer (LC-MS/MS).

Samples of water-soluble exoproteins corresponding to both Csol and TR9 prior desiccation (T0) and after four cycles of D/R (DR) were processed by LC-MS/MS including three biological replicates of each sample. Proteins were cleaned by loading each 25µg sample into a concentrating gel and then digested with trypsin. Peptides were extracted with acetonitrile, dried by vacuum centrifugation and reconstituted in 30 µl and stored at -20 ° C until analysis. Peptides were analyzed by liquid nano-chromatography (nano Easy-nLC 1000, Thermo Scientific) coupled to a high-resolution mass spectrometer Q-Exactive HF (Thermo Scientific, Bremen, Germany). The nano-HPLC was coupled online to the nanoelectric source of the Q-exactive HF mass spectrometer in which the peptides were analyzed after entering by electrospray ionization using the integrated tip in the analytical column. The peptides were detected in a m/z mass range of 350-2000 Da. MS/MS data were acquired in the Data-dependent acquisition (DDA) mode of the MS. The obtained MS/MS spectra were analyzed with the software Proteome Discoverer 2.2 (Thermo Scientific) using SEQUEST as a search engine based on a database including sequences of proteins obtained from the translation of the identified ORFs in previous transcriptomic analyses. The percolator algorithm was used to estimate the FDR (false positive rate) and was filtered by a q-value <0.01 for the proteins identified with high confidence.

Estimation of the abundance of identified proteins

To determine the abundances of the peptides and the identified proteins, a processing was carried out that begins with the recalibration of the masses by means of a quick search with Sequest HT against the appropriate database and an alignment of the chromatograms of the samples. Subsequently, the alignment of retention times between the different samples analyzed for the quantification of the precursor ions was performed, considering the unique peptides and razor peptides (peptides shared between a group of proteins) that are present in at least 50 % of replicas, regardless of modified peptides. Finally, the total amount of protein between the different samples

was normalized using the total abundance of all peptides. The ratios of the peptides were calculated as the geometric median of the ratios of these in the different biological replicas. The protein ratio was calculated as the geometric median of the peptide group ratios. To test whether the abundance of a protein varies among replicas, the statistical test of Variance Analysis (ANOVA) was used to estimate the probability that these measures are different among the three replicas. The observed differences were considered significant if the p-value obtained was below 0.05. To rule out the false-positive changes estimated by the p-value, for a given level of FDR, the p-value was corrected, by the Benjamini-Hochberg method (Benjamini and Hochberg, 1995), obtaining an adjusted p-value also called q-value, which better controls the FDR. Additionally, a series of filters were applied to determine if a protein is expressed differentially between conditions: abundance ratio variability, which is the variability of the ratios calculated in percentage and must have a value below 30% and above 0%; p-value and q-value <0.05 to obtain statistical significance. Proteins that meet a p-value <0.05 and $\log_2$FC ≥0.6 (FC ≥ 1.5) are considered differentially abundant proteins. Volcano Plot was used to represent the results of the statistical tests applied (-log P-value) against the $\log_2$ratio, Fold Change (FC) of the calculated protein.

***In silico* identification and analysis of extracellular proteins**

The identification of transcripts coding for extracellular proteins from TR9 and Csol was performed by searching among customized databases compiling transcript sequences from both algal species, which are housed in our computers in the University of Alcalá. Identification of the candidate coding regions (open reading frames or ORFs) was performed with Transdecoder (https://github.com/TransDecoder/TransDecoder/wiki). Predictions of extracellular proteins were performed using the SignalP 5.0 (Nielsen *et al.*, 2019) and TargetP 2.0 (Almagro-Armenteros *et al.*, 2019) and Predisi (Hiller *et al.*, 2004) with default parameters. Proteins containing

transmembrane domain (s) according to Phobius (Kall *et al.*, 2007) were excluded. Cello v.2.5 for sub cellular location prediction was used for removing ER targeting proteins (Yu *et al.*, 2006). Additionally, BLASTp searches were performed against the Plant Secretome and Subcellular Proteome KnowledgeBase (PlantSecKB) using each protein sequence as query (Lum *et al.*, 2014). Functional annotation of extracellular proteins was performed on the basis of NT, NR, GO, KOG, KEGG, UniprotKB and InterPro functional databases performing a batch CD-Search against the Conserved Domain Database (CDD) from the NCBI (Marchler-Bauer *et al.*, 2017), KofamKOALA (https://www.genome.jp/tools/kofamkoala/), MOTIF Search (https://www.genome.jp/tools/motif/), Interproscan 5 (Jones *et al.*, 2014), and BLASTp (Altschul *et al.*, 1990). Isoelectric Point of proteins were predicted with Protein Isoelectric Point predictor provided by Sequence Manipulation Suite v2 (Stothard, 2000).

Results

Exoproteome protein repertoires of TR9 and Csol

In the present study 21-day-old *in vitro* cultured TR9 and Csol algae were used as biological material for obtaining water-soluble extracellular proteins which were subsequently analyzed by LC-MS/MS. Samples obtained from cells undergoing four D/R cycles and from fully hydrated cells prior to D/R cycles (T0) were used for assessing possible changes induced by cyclic desiccation at exoproteome level. Our analyses allowed the identification of 2,503 and 2,614 proteins for TR9 and Csol, respectively. However, only 111 and 121 proteins for TR9 (ExoTR9) and Csol (ExoCsol), respectively, were classified as “bona fide” exoproteins after screening with diverse bioinformatic tools (Tables 1 and 2). Predictions were based on the detection of a signal peptide specific for the secretory pathway with five different tools. Firstly, Predisi, SignalP 5.0, TargetP 2.0 and Phobius were used for secretory signal peptide predictions. The later program

was also employed to exclude proteins containing transmembrane domain (s) and Cello v.2.5, to remove ER targeting proteins. Finally, blast searches were performed against PlantSecKB.

ExoTR9 and ExoCsol proteins showed similar size distributions (Fig. 1A, Tables 1 and 2) with lengths ranging from 200 to 500 aa for approximately half of them. Most of the exoproteins where acidic with isoelectric points (IP) ranging from 3 to 6 in both algal species (Fig. 1B, Tables 1 and 2), especially in TR9 with more proteins with IP below 5 (79 out of 147) than Csol (58 out of 179). Manual annotation of each set of putative extracellular proteins allowed us to attribute putative functions to 79 and 83 proteins in ExoTR9 and ExoCsol, respectively (Fig. 2, Tables 1 and 2). The remaining 32 and 38 proteins (from TR9 and Csol, respectively) had unknown function. Approximately a third of the extracellular proteins were predicted as hydrolases in both TR9 (37 out of 111) and Csol (44 out of 121), most of them being glycosidases and proteases.

Pairwise comparisons among each set of exoproteins revealed the existence of isoforms, which are the result of the expression of genes with one or more paralog(s) in the genome of each algal species. Specifically, we found isoforms for 10 and 11 proteins in TR9 and Csol, respectively (annotated as a, b, c and d in Tables 1 and 2). In all cases, the resulting pairwise alignments had E-values under 1e-25 and similarity above 40%. Generally, we found only two isoforms per protein. However, up to four isoforms were found for a Glycosyl hydrolase in TR9 (TR9_013) and an Endo-1,4-β-mannosidase in Csol (CSOL_011). Isoforms were found in proteins with a variety of functions including expansins, glycosidases, hydrolases, phosphatases and proteases among others. More than a half of proteins having isoforms in Csol were shared with TR9 (6 out of 11) and nearly all the proteins having isoforms in TR9 were shared with Csol (8 out of 10). Shared proteins with isoforms have mainly hydrolytic activities including glycosidases, proteases and other hydrolases.

Exploration of possible homologous proteins among the exoproteomes of green algae and land plants

Blast searches (E-values below 0.01, http://proteomics.ysu.edu/blast/blast.html) against secretomes of diverse organisms including plants (PlantSecKB), fungi (FunSekKB) and protists (ProtSecKB) available at http://proteomics.ysu.edu/secretomes indicated that at least 99 and 116 proteins from TR9 and Csol exoproteomes, respectively, are similar to proteins from any of the above referred secretomes (Fig. 3, Tables S1 and S2). The remaining proteins were not similar to any other in the studied secretomes. Most of the TR9 and Csol exoproteins were 74.77 % and 90.08 % similar, respectively, to those of plant (including land plants and green algae) exoproteomes, while only six and ten exoproteins of TR9, and two and five of Csol were similar to those of protists and fungi, respectively (Table S1 and S2). Csol showed a higher amount of exoproteins similar to those exclusive of green algae (56 out of 121) than TR9 (29 out of 111), while the number of exoproteins similar to those exclusive of land plants was higher in TR9 (24 out of 111) than in Csol (9 out of 121). Moreover, TR9 had a higher number of exoproteins similar to those from land plants, fungi or protists than Csol.

A more detailed exploration of possible homologous proteins among the exoproteomes of green algae and land plants available in PlantSecKB was made (Fig. 4, Table S1 and S2). The selected algal species were the Trebouxiophyceae *Coccomyxa* sp. C169, *Chlorella variabilis*, and the Chlorophyceae *Chlamydomonas reinhardtii* whereas the selected plant species were the spermatophytes *Arabidopsis thaliana*, *Oryza sativa* and the monilophytes *Selaginella moellendorffii* and *Physcomitrella patens*. The exoproteome of each organism was retrieved by selecting the option of "curated secreted" for *A. thaliana* and *Oryza sativa* and "highly likely secreted" for the remaining species. After Blastp searches with E-values under 1e-25, a total of 23 out of 99 and 47 out of 105 proteins, excluding isoforms, were shared with green algae but not

with land plants in TR9 and Csol, respectively. By contrast, only five and two proteins were shared with land plants but not with green algae in TR9 and Csol, respectively. These proteins included hydrolases of sugars or lipids in both algae and a glyoxal oxidase only in TR9. The proteins shared among both lichen algae and land plants were 12 and 15 for TR9 and Csol, respectively. An additional comparison with the fungus *Agaricus bisporus* resulted in the sharing of ten and seven proteins with TR9 and Csol, respectively. These proteins included glycosidases, isomerases, oxidoreductases, phosphatases and proteases. All of them were homologous of land plants or algae proteins (from green algal species different than the three above mentioned), except TR9_042, a phosphodiesterase/alkaline phosphatase that exclusively shared TR9 and *A. bisporus* in our study. A comparison with the resurrection plant *Dorcoceras hygrometricum* was also performed. Since the exoproteome of this land plant is not available in the PlantSecKB, we manually selected the exoproteins among the proteins available for this species in GenBank following the same procedure as for TR9 and Csol in this study. We found five proteins shared among TR9, Csol and *D. hygrometricum* (three proteases, a phosphatase and a SOUL-domain-containing protein).

Summing up, from the comparison of the exoproteome of TR9 and Csol with those from other organisms can be pointed out some remarkable findings. (1) proteins involved in cell adhesion and expansins were exclusively shared with other Trebouxiophyceae algae (Fig. 4); (2) TR9 showed more exoproteins similar to those from land plants, fungi or protists than Csol, while this alga had a higher proportion of exoproteins similar to those from other algae; (3) the TR9 exoproteome contained a higher number of glycosidases and phosphatases typical of land plants and fungi instead of green algae compared with the Csol exoproteome.

Expression profiles of extracellular proteins after cyclic D/R in TR9 and Csol

In order to address the underlying mechanisms that sustain the different degrees of desiccation toleranceDT of TR9 and Csol, focused on the remodelling of the cell wall and EPS, weThe comparisoned of the abundance of exoproteins before and after cyclic desiccation. In TR9, 23 out of the 111 exoproteins increased after four D/R cycles (Fig. 5 and Table 3) . By contrast, in Csol the amount of all 121 exoproteins remained unchanged after D/R treatment. Sixteen out of 23 exoproteins whose levels increase after D/R treatments are predicted to be involved in a variety of biological functions (Fig. 5 and Table 3). However, the possible biological function of seven of them remains unknown.

In a general view, there are a number of diverse predicted glycosidases, including glycosyl hydrolases and other carbohydrate related enzymes, and expansins in the exoproteome of both TR9 and Csol in control (T0) and after D/R conditions (Table 1, 2 and 3). These features strongly suggest that each microalga is constitutively provided with the main enzymatic tools for performing the biochemical remodelling of the cell wall and EPS outlined in the Introduction. This is very important in organisms that perform rapid changes on their extracellular polysaccharides, as the lichen algae under study. The TR9_011 protein was identified as an endo-1,4-β-mannosidase, had two isoforms (a and b) (Table 1). After D/R treatment, the amount of TR9_011a increased whereas TR9_010b remained unchanged. The exoproteome of Csol contained a homologous protein (CSOL_011) with four different isoforms (Table 2), whose abundance remained unchanged after D/R treatment. Blast searches using PlantSecKB and FunSecKB databases revealed the existence of homologous proteins (E-values under 1e-25) in several taxa including green algae such as *Coccomyxa subellipsoidea* C-169 (accession I0YJN3 in UniprotKB) and *Chlorella variabilis* (accession E1ZL99 in UniprotKB), land plants such as *Arabidopsis thaliana* (accession Q9M0H6 in UniprotKB) and the basidiomycete *Agaricus bisporus* (accession K9I320 in UniprotKB). The second up-regulated glycosidase (TR9_013) had

four isoforms (Table 3) but only one of them (TR9_013d) increased after D/R treatment. This protein was also present in ExoCsol (CSOL_009) which remained unchanged after D/R treatments. Blastp searches against the NCBI (all non-redundant GenBank CDS translations+PDB+SwissProt+PIR+PRF excluding environmental samples from WGS projects) rendered positive results against Chlorophyta algae and bacteria (the best scores had E-values under 1e-80 and similarities above 35%). The TR9_013d protein showed 42% similarity (E-value of 1e-16) with a major extracellular endoglucanase from the bacterium *Xanthomonas campestris* (XccCel5A protein, accession P19487). The third up-regulated glycosidase after D/R treatments was TR9_016. This protein showed 44% similarity (E-value of 3e-08) with a type II chitinase from *Oryza sativa* after Blasp searches against PlantsecKB database (Rcb4 protein, accession Q9AT30). Indeed, TR9_016 was classified as a member of the family GH18 after CD-Search against the Conserved Domain Database (CDD) from the NCBI. The GH18 type II chitinases hydrolyze chitin, an abundant polymer of β-1,4-linked N-acetylglucosamine (GlcNAc), which is a major component of the cell wall of fungi.

Half of the eight different putative proteases identified in ExoTR9 were up-regulated after D/R treatment: TR9_047, TR9_053b, TR9_050 and TR9_051 (Table 3). TR9_047 was identified a cysteine proteinase with two isoforms, one of which (TR9_047a) remained unchanged whereas the other (TR9_047b) increased after D/R. Both isoforms were similar to the Cysteine proteinase RD21 (responsive-to-desiccation-21) of *A. thaliana* (accession Q9LT78 for UniprotKB and At3g19390) with similarities of 49.45% (E-values of 9e-137 and 2e-112 for TR9_047a and TR9_047b, respectively). Two serine proteases were up-regulated in TR9 after exposition to cyclic D/R. One of them is TR9_053b, similar to the serine carboxypeptidase BRS1 (brassinosteroid insensitive 1 suppressor) of *A. thaliana*. The other one is TR9_051, similar to Subtilisin-like proteases from diverse organisms including prokaryotes such as *Bacillus subtilis*,

whose Subtilisin E (UniprotKB accession P04189) has 32.63% similarity with TR9_051 (E-value of 1e-38). Subtilisin E is an extracellular serine protease associated with sporulation (Piggot and Coote, 1976). TR9_051 was also 30.61% similar (E-value 9e-05) to a Senescence-Associated Subtilisin Protease SASP from *A. thaliana* (UniprotKB accession Q9LVJ1). TR9_050 was predicted to be similar (24.07% similarity, E-values of 1e-51) to the metalloaminopeptidase APM1 from *A. thaliana* (accession Q8VZH2 for UniprotKB) and from very distant taxa such as animals. For instance, the human Aminopeptidase (Uniprot accession P15144) showed 26.96% similarity and E-value of 4e-40. One predicted protease inhibitor was also up-regulated after D/R treatment in TR9. The TR9_045 protein is 46.88% similar (E-value 4e-13) to the extracellular Subtilisin-chymotrypsin inhibitor WSCI (UniprotKB accession P82977) from *Triticum aestivum*.

Some proteins putatively involved in the extracellular formation of H_2O_2 increased after D/R treatments in TR9. One of them is TR9_036 that showed 28.57% similarity (E-value of 9e-41) with a glyoxal oxidase from the lignin-degrading basidiomycete *Phanerochaete chrysosporium* (GenBank accession ABD61572). As far as we know this is the first report of an extracellular glyoxal oxidase in a green alga. Another is TR9_055, which showed 39% similarity (E-value of 4e-04) with a germin-like protein from *A. thaliana* (UniprotKB accession O65252).

Notably, both TR9 and Csol exoproteomes contain many IDP proteins within the "uncharacterized" set (Tables 1 and 2). However, only TR9_075, TR9_079, TR9_085, TR9_086, TR9_088, TR9_094 are small, hydrophilic proteins, with very little sequence similarity to each other (except for TR9_079a and TR9_079b), up-regulated in response to cyclic D/R. The assignment of a biological function to all the uncharacterized proteins could provide new insight into the underlying mechanisms of the DT response in photosynthetic eukaryotes. This may also be useful for the modification of metabolic processes in the extracellular matrix for agricultural and industrial purposes.

Discussion

In the last few years, technological advancements in proteomics and the sequencing of whole genomes and transcriptomes have enabled the first large-scale secretome analyses. It has been demonstrated that the type of sample and its preparation are critical steps for the subsequent proteomic analyses, data processing and interpretation, which mainly involve bioinformatics (Krause *et al.*, 2013; Vincent *et al.*, 2020). In this study, we performed an intensive bioinformatic analysis of proteomic data obtained after protein processing by LC-MS/MS to select probable extracellular proteins in two microalgae (TR9 and Csol). Such analyses allowed to ascribe two sets of more than a hundred proteins to the exoproteomes from each microalgae, which were manually annotated. Most of the proteins with any predicted function are quite similar to those of most plant exoproteomes with a large variety of hydrolytic enzymes and other enzymes such as isomerases, oxidoreductases, phosphatases, phosphorylases, kinases and transferases, among others (Vincent *et al.*, 2020).

Previous preliminary analyses of the extracellular polymeric substances (EPS) including both carbohydrates and proteins of fully hydrated microalgae, showed quantitative and qualitative differences between TR9 and Csol (Casano et al., 2015; Centeno *et al.*, 2016). 2D-electrophoresis of extracellular proteins showed different amounts of distinguishable spots arranged in distinct polypeptide patterns for each microalga. In that first approximation and according to data shown in this study, the exoproteomes from each algal species are found to be highly acidic with IPs ranging from 3.0 to 4.5 and 3.8 to 4.7 in TR9 and Csol, respectively. As mentioned in more detail in the Introduction, galactans predominate within the carbohydrates of the cell wall and EPS of Csol and TR9 (Casano *et al.,* 2015), and are submitted to species-specific remodelling during cyclic D/R in both microalgae (González-Hourcade *et al.*, 2020a). The remodelling of extracellular polysaccharides involves diverse glycosidases, some of which were preliminary

identified after 2D electrophoresis in TR9 and Csol (Centeno *et al.*, 2016). In this study, a number of putative glycosidases are shown to be constitutively expressed in both TR9 and Csol microalgae. However, certain glycosidases including an endo-1,4-beta-mannosidase, an endoglucanase and a chitinase are upregulated after D/R treatments, only in TR9. In land plants, β-mannosidases catalyse random hydrolysis of (1-4)-β-D-mannosidic bonds in mannans, galactomannans and glucomannans and show divergent expression patterns for individual genes suggesting their involvement in diverse biological processes (Yuan *et al.*, 2007). The higher content of mannose-containing polysaccharides in the cell wall and EPS of Csol compared to TR9 (González-Hourcade *et al.,* 2020b) is consistent with the more diverse β-mannosidase genes/isoforms and the constitutive expression of all of them in Csol. In TR9, the D/R-induced increase of a mannosidase isozyme (TR9_011a) may be related to the remodelling of cell wall polysaccharides going from mannose-containing polysaccharides in control cells to a complex mixture of polysaccharides without mannose after D/R (González-Hourcade *et al.,* 2020b). It should be stressed that TR9 is adapted to faster and more drastic changes in water availability compared to Csol, which supports the notion that the cell wall of TR9 should be able to fold very rapidly and to a greater extent than the cell wall of Csol (González-Hourcade *et al.,* 2020b).

The cell wall of TR9 contains very low amounts of cellulose-like polymers (Casano *et al.*, 2015), which could be the substrate of the up-regulated TR9 glycosidase (TR9_013d) similar to the major extracellular endoglucanase from the bacterium *Xanthomonas campestris* (XccCel5A). This endoglucanase catalyses the endo-hydrolysis of (1-4)-β-D-glucosidic linkages in cellulose, cereal β-D-glucans and lichenin (Rosseto *et al.*, 2016). Lichenin is common component of the mycobiont cell wall (Stone, 2009). TR9 also showed the upregulation of an extracellular chitinase (TR9_016) and a chitin deacetylase (TR9_018). Chitinases have been found as common dehydration-responsive cell wall proteins in *Zea mays* (Zhu *et al.*, 2007),

Cynodon dactylon (Ye *et al.*, 2015)*, Vicia faba* (Li *et al.*, 2018)*, Arachis duranensis* (Carmo *et al.*, 2019) and *Cicer arietinum* (Gupta *et al.*, 2020) among others. Chitin is a major component of the cell wall of fungi and also supports and organizes their extracellular matrices (Steinfeld *et al.,* 2019). Lichenin is common component of the mycobiont cell wall (Stone, 2009). Thus, the induction of the extracellular chitinase and chitin deacetylase along with the endoglycosidase acting on lichenin in TR9, could be relevant for the mycobiont-phycobiont interaction in the context of rapid D/R cycles. Under these conditions, TR9 cells fold and expand as their water content falls and rises, respectively, in a matter of minutes or hours, compromising the stability of the close contact between the fungus haustoria or hyphae and the algal cell wall. Therefore, the over expression of those enzymes could be a mechanism to provoke a controlled loosening of the mycobiont cell wall that may preserve the physical and physiological interaction between mycobiont and microalgae.

Along with glucosidases, proteases and protease inhibitors constitute most of the proteins with predicted functions in both TR9 and Csol exoproteomes. The presence of a number of constitutively expressed proteases of diverse types and modes of action and protease inhibitors, indicate that exoproteins are subjected to controlled hydrolysis accomplished in the extracellular space in both algae. All the putative proteolytic enzymes and protease inhibitors are constitutively expressed in Csol whereas a significant number of proteases including a cysteine proteinase, two serine proteases and a metalloaminopeptidase and a protease inhibitor are induced only in TR9 after D/R. A number of diverse proteases similar to upregulated proteins in TR9 are related to drought stress in plants. The D/R-upregulated TR9_047b protein is similar to the cysteine proteinase RD21 (responsive-to-desiccation-21) of *A. thaliana*, which is specifically induced by water stress (Shinozaki and Yamaguchi-Shinozaki, 1997). Some serine carboxypeptidases related to drought tolerance such as subtilisin proteases from *A. thaliana* (Wang *et al.*, 2018) and

Physcomitrella patens (Wang *et al.*, 2009) are similar to the upregulated TR9_051 protein. Metallopeptidases of the M1 family similar to the upregulated protein TR9_050, are involved in seed development (Teale and Palme, 2018) and in response to desiccation (Kidrič *et al.*, 2014). Similarly, the D/R-induced TR9_045 protein is similar to extracellular subtilisin-chymotrypsin inhibitor WSCI, a drought-responsive protein detected in wheat grain (Hajheidari *et al.*, 2007). The increase of both a subtilisin and a subtilisin inhibitor in TR9 after D/R treatments, would seem somewhat contradictory. However, this phenomenon has been already reported in proteomic analyses in land plants subjected to water deficit such as *Lupinus albus* (Pinheiro *et al.*, 2005) and *A. thaliana* (Bray, 2002). In general, subtilisins are involved in non-selective protein degradation (Schaller, 2004). Thus, the interaction of a protease and their inhibitor in TR9 suggests a mechanism for keeping proteolysis under control. Proteins can be damaged by ROS generated in the extracellular space of TR9 and Csol microalgae even though both algae have a strong intracellular antioxidant system constitutively expressed, which is reinforced by antioxidant enzymes and non-enzymatic compounds induced during cyclic D/R (Centeno *et al.*, 2016; Hell *et al.*, 2019). Thus, proteases and protease inhibitors can play an important role as second line components of the extracellular antioxidant protection system during D/R in lichen algae as previously demonstrated for e.g. the resurrection plant *R. servica* (Augusti *et al.,* 2001; Sgherri *et al.,* 2004; Kidrič *et al.,* 2014).

Studies about extracellular ROS metabolism in lichens showed an increase of extracellular superoxide upon D/R (Beckett *et al.*, 2003; Minibayeva and Beckett, 2001). In the resurrection plant *Ramonda nathaliae*, Jovanović *et al.* (2011) proposed that controlled generation of ROS is crucial in sensing dehydration and inducing cellular responses. Plants can enzymatically produce ROS towards or within their apoplastic space in a highly regulated manner (Kärkönen and Kuchitsu, 2015). One of these ROS-producing enzymes are glyoxal oxidases,

which oxidise simple aldehydes to the corresponding carboxylic acids in a reaction that couples O_2 consumption with H_2O_2 formation (Vanden Wymelenberg *et al.*, 2006). Other enzymes able to catalyse the formation of H_2O_2 are extracellular germin-like proteins (GLPs) functioning as Mn-dependent superoxide dismutases and oxalate oxidases (Davidson *et al.*, 2009; Pei *et al.*, 2019 and cites therein), which are upregulated in response to biotic and abiotic stressors (Davidson et al., 2009; Pei *et al.,* 2019 and cites therein). As stated in previous paragraphs, the upregulated proteins TR9_036 and TR9_055 were found to be similar to plant glyoxal oxidases and GLPs, respectively, and thus may produce extracellular H_2O_2. This ROS can be converted in hydroxyl radicals through Fenton or Haber-Weiss reactions, which could cause polysaccharide scission and, therefore, cell wall loosening (e.g. Liszkay *et al.*, 2004; Müller *et al.*, 2009; Schopfer, 2001). It seems reasonable to assume that some of the changes observed in the molecular size (not accompanied by variations in monosaccharide composition) of cell wall and EPS polysaccharides that sustain the outstanding flexibility of TR9 could be related to the action of H_2O_2-generating enzymes induced upon cyclic D/R.

It is widely accepted that unicellular organisms such as yeast and green algae can form multicellular clumps surrounded by an ECM under adverse conditions (Smukalla et al., 2008). In each algal group, the ECM has different composition. In ulvophytes, the abundance of uronic acid-rich and/or sulfated polysaccharides in the cell wall matrix may indicate that these strongly anionic polymers have an important role in the formation and maintenance of the multicellular form (Domozych and Domozych, 2014). Recently, sulfated polysaccharide(s) were detected in the EPS of both TR9 and Csol microalgae. Unlike Csol, the induction of a sugar-sulfotransferase gene was observed in TR9 after cyclic D/R resulting in the increased accumulation of sulfated ß-D-galactofuranan(s) (González-Hourcade *et al.,* 2020a). The transition from an unicellular lifestyle to a multicellular one implies self-recognition, self-interaction and adhesion. In this

study, NCBI blastp research revealed that the over-expressed protein TR9_029 was 28% similar (E-value 2e-09) to a fucolectin-1-like from the fish *Sinocyclocheilus rhinocerous* (GenBank accession XP_016384390). We speculate that this lectin may mediate self-recognition and self-interaction among algal cells forming cell aggregates and/or maintaining the pre-existent cell-cell contacts after D/R. These intercellular tight contacts seem to be highly relevant for both TR9 and Csol (and probably to the lichen symbiosis) as indicated by the constitutive presence of several putative adhesins or cell-adhesion-related proteins in both exoproteomes (Tables 1 and 2). As examples, TR9_002 and CSOL_003 were identified to have a Fasciclin 1 (FAS1) domain, which is a structural motif of extracellular proteins in all kingdoms of life. FAS1 proteins are often implicated in the interaction between the cell and the ECM.

Along with well-studied proteins, desiccation tolerant organisms across all kingdoms of life produce and employ a number of less known, more specialized and intrinsically disordered proteins (IDPs) to survive in dried state (Boothby and Pielak, 2017). IDPs are small, often hydrophilic, disordered proteins with very little sequence similarity to each other both within and between species, which are often induced in response to desiccation but can also be constitutively expressed at high levels. It has been proposed diverse mechanisms for their protective functions including water retention acting as hydration buffers, or as classic chaperones in maintenance of structures and cellular components, in ROS scavenging among others. In several cases IDPs are essential, sufficient, or both for mediating DT (Boothby and Pielak, 2017; Koshland and Tapia, 2019). The assignment of a biological function to all the uncharacterized proteins could provide new insight into the underlying mechanisms of the DT response in photosynthetic eukaryotes. This may also be useful for the modification of metabolic processes in the extracellular matrix for agricultural and industrial purposes.

Conclusions

Trebouxia sp. TR9 and *Coccomyxa* simplex are good examples of desiccation-tolerant microalgae that deploy different adaptive strategies in accordance with the prevailing conditions of their habitats. TR9 lives in environments with fast and drastic changes of water availability whereas Csol is generally found in more protected and humid areas. The different flexibility of cell walls and properties of extracellular polysaccharides, which are remodelled in response to cyclic dehydration/rehydration, are key elements in the tolerance to desiccation of both microalgae. The analysis of the extracellular proteome performed in the present study suggests that Csol is provided with a repertory of extracellular hydrolases, which are constitutively expressed. Most of such extracellular hydrolases are proteases and glycosidases, which are thought to carry out the turnover of polysaccharides and proteins under non- stress conditions as well as the remodelling of extracellular polymers during changes in water availability. TR9 has a quite similar repertory of extracellular enzymatic activities including a number of hydrolases and other enzymes, some of which are over-expressed in response to changes in water availability. Certain over-expressed proteins seem to be very ancient and evolved prior to the colonization of terrestrial habitats by plants. Such proteins participate in key biological functions including (i) remodelling of cell wall and extracellular polysaccharides by glycosidases, (ii) control the steady-state levels of exoproteins by proteases, (iii) enzymatic production of hydrogen peroxide and (iv) maintenance of water homeostasis by intrinsically disordered proteins. Further biochemical experimentation will be needed to confirm the actual catalytic activity of the putative enzymes found in this study. Our results suggest that the activity of most of the extracellular enzymatic activities would be oriented to preserve the biochemical and biophysical properties of the extracellular structures, thus ameliorating the impact of desiccation on the algal cell and probably on its interaction with the mycobiont. Additionally, a number of proteins whose function remains unknown were found,

some of which could be considered as small intrinsically disordered proteins related with desiccation tolerant organisms.

Acknowledgments

This study was supported by a grant from the Spanish Ministry of Science, Innovation and Universities [CGL2016-80259-P]. We thank the Proteomic Service of the Universidad Complutense de Madrid (Madrid, Spain) for the LC-MS/MS analyses of exoproteins from TR9 and Csol algae, and Gabriel Casano for the English revision of the manuscript.

References

Almagro-Armenteros JJ, Tsirigos KD, Sønderby CK, Petersen TN, Winther O, Brunak S, von Heijne G, Nielsen H (2019) SignalP 5.0 improves signal peptide predictions using deep neural networks. Nat Biotechnol 37(4):420-423. 10.1038/s41587-019-0036-z

Altschul SF, Gish W, Miller W, Myers EW, Lipman DJ (1990) Basic local alignment search tool. J Mol Biol 215(3):403-410. 10.1016/S0022-2836(05)80360-2

Augusti A, Scartazza A, Navari-Izzo F, Sgherri CL, Stevanovic B, Brugnoli E (2001) Photosystem II photochemical efficiency, zeaxanthin and antioxidant contents in the poikilohydric *Ramonda serbica* during dehydration and rehydration. Photosynth Res 67(1-2):79-88. 10.1023/A:1010692632408

Baba M, Suzuki I, Shiraiwa Y (2011) Proteomic analysis of high-CO(2)-inducible extracellular proteins in the unicellular green alga, *Chlamydomonas reinhardtii*. Plant Cell Physiol 52(8):1302-1314. 10.1093/pcp/pcr078

Beckett RP, Minibayeva FV, Vylegzhanina NN, Tolpysheva T (2003) High rates of extracellular superoxide production by lichens in the suborder Peltigerineae correlate with indices of high metabolic activity. Plant Cell Environ 26(11):1827-1837. 10.1046/j.1365-3040.2003.01099.x

Benjamini Y, Hochberg Y (1995) Controlling the false discovery rate: a practical and powerful approach to multiple testing. J R Stat Soc Series B Stat Methodol 57(1):289-300. 10.1111/j.2517-6161.1995.tb02031.x

Bold HC, Parker BC (1962) Some supplementary attributes in the classification of *Chlorococcum* species. Arch Mikrobiol 42:267-288. 10.1007/bf00422045

Boothby TC, Pielak GJ (2017) intrinsically disordered proteins and DT: Elucidating functional and mechanistic underpinnings of anhydrobiosis. Bioessays 39(11):10. 10.1002/bies.201700119

Bradford MM (1976) A rapid and sensitive method for the quantitation of microgram quantities of protein utilizing the principle of protein-dye binding. Anal Biochem 72:248-254. 10.1006/abio.1976.9999

Bray EA (2002) Classification of genes differentially expressed during water-deficit stress in *Arabidopsis thaliana*: an analysis using microarray and differential expression data. Ann Bot 89 Spec No:803-811. 10.1093/aob/mcf104

Carmo LST, Martins ACQ, Martins CCC, Passos MAS, Silva LP, Araujo ACG, Brasileiro ACM, Miller RNG, Guimaraes PM, Mehta A (2019) Comparative proteomics and gene expression analysis in *Arachis duranensis* reveal stress response proteins associated to drought tolerance. J Proteomics 192:299-310. 10.1016/j.jprot.2018.09.011

Casano LM, Braga MR, Álvarez R, del Campo EM, Barreno E (2015) Differences in the cell walls and extracellular polymers of the two *Trebouxia* microalgae coexisting in the lichen *Ramalina farinacea* are consistent with their distinct capacity to immobilize extracellular Pb. Plant Sci 236:195-204. 10.1016/j.plantsci.2015.04.003

Casano LM, del Campo EM, García-Breijo FJ, Reig-Arminana J, Gasulla F, Del Hoyo A, Guéra A, Barreno E (2011) Two *Trebouxia* algae with different physiological performances are ever-present in lichen thalli of *Ramalina farinacea*. Coexistence versus competition? Environ Microbiol 13(3):806-818. 10.1111/j.1462-2920.2010.02386.x

Centeno DC, Hell AF, Braga MR, del Campo EM, Casano LM (2016) Contrasting strategies used by lichen microalgae to cope with desiccation-rehydration stress revealed by metabolite

profiling and cell wall analysis. Environ Microbiol 18(5):1546-1560. 10.1111/1462-2920.13249

Chen P, Jung NU, Giarola V, Bartels D (2020) The dynamic responses of cell walls in resurrection plants during dehydration and rehydration. Front Plant Sci10:1698. 10.3389/fpls.2019.01698

Chiou Y, Hsieh M, Yeh H (2010) Effect of algal extracellular polymer substances on UF membrane fouling. Desalination 250:648-652. 10.1016/j.desal.2008.02.043

Costa OYA, Raaijmakers JM, Kuramae EE (2018) Microbial extracellular polymeric substances: ecological function and impact on soil aggregation. Front Microbiol 9:1636. 10.3389/fmicb.2018.01636

Davidson R, Reeves P, Manosalva P, Leach J (2009) Germins: A diverse protein family important for crop improvement. Plant Sci 177(6):499-510. 10.1016/j.plantsci.2009.08.012

Delaunois B, Jeandet P, Clément C, Baillieul F, Dorey S, Cordelier S (2014) Uncovering plant-pathogen crosstalk through apoplastic proteomic studies. Front Plant Sci 5:249. 10.3389/fpls.2014.00249

Domozych, D. S., and Domozych, C. E. (2014). Multicellularity in green algae: upsizing in a walled complex. Front. Plant Sci. 5:649. 10.3389/fpls.2014.00649

Geun Goo B, Baek G, Jin Choi D, Il Park Y, Synytsya A, Bleha R, Ho Seong D, Lee C, Kweon Park J (2013) Characterization of a renewable extracellular polysaccharide from defatted microalgae *Dunaliella tertiolecta*. Bioresour Technol 129:343-350. 10.1016/j.biortech.2012.11.077

González-Hourcade M, Braga MR, del Campo EM, Ascaso C, Patino C, Casano LM (2020a) Ultrastructural and biochemical analyses reveal cell wall remodelling in lichen-forming microalgae submitted to cyclic desiccation-rehydration. Ann Bot 125(3):459-469. 2020. 10.1093/aob/mcz181

González-Hourcade M, del Campo EM, Braga MR, Salgado A, Casano LM (2020b) Disentangling the role of extracellular polysaccharides in DT in lichen-forming microalgae. First evidence of sulfated polysaccharides and ancient sulfotransferase genes. Environ Microbiol. (In press). 10.1111/1462-2920.15043

Gupta S, Mishra SK, Misra S, Pandey V, Agrawal L, Nautiyal CS, Chauhan PS (2020) Revealing the complexity of protein abundance in chickpea root under drought-stress using a comparative proteomics approach. Plant Physiol Biochem 151:88-102. 10.1016/j.plaphy.2020.03.005

Hajheidari M, Eivazi A, Buchanan BB, Wong JH, Majidi I, Salekdeh GH (2007) Proteomics uncovers a role for redox in drought tolerance in wheat. J Proteome Res 6(4):1451-1460. 10.1021/pr060570j

Hell AF, Gasulla F, Gonzáez-Hourcade MA, del Campo EM, Centeno DC, Casano LM (2019) Tolerance to cyclic desiccation in lichen microalgae is related to habitat preference and involves specific priming of the antioxidant system. Plant Cell Physiol 60(8):1880-1891. 10.1093/pcp/pcz103

Hiller K, Grote A, Scheer M, Munch R, Jahn D (2004) PrediSi: prediction of signal peptides and their cleavage positions. Nucleic Acids Res 32(Web Server issue):W375-9.10.1093/nar/gkh378

Jones P, Binns D, Chang HY, Fraser M, Li W, McAnulla C, McWilliam H, Maslen J, Mitchell A, Nuka G, Pesseat S, Quinn AF, Sangrador-Vegas A, Scheremetjew M, Yong SY, López R, Hunter S (2014) InterProScan 5: genome-scale protein function classification. Bioinformatics 30(9):1236-1240. 10.1093/bioinformatics/btu031

Jovanović Ž, Rakić T, Stevanović B, Radović S (2011) Characterization of oxidative and antioxidative events during dehydration and rehydration of resurrection plant *Ramonda nathaliae*. Plant Growth Regul 64(3):231-240. 10.1007/s10725-011-9563-4

Kall L, Krogh A, Sonnhammer EL (2007) Advantages of combined transmembrane topology and signal peptide prediction--the Phobius web server. Nucleic Acids Res 35(Web Server issue):W429-32. 10.1093/nar/gkm256

Kärkönen A, Kuchitsu K (2015) Reactive oxygen species in cell wall metabolism and development in plants. Phytochemistry 112:22-32. 10.1016/j.phytochem.2014.09.016

Kidrič M, Sabotič J, Stevanović B (2014) Desiccation tolerance of the resurrection plant *Ramonda serbica* is associated with dehydration-dependent changes in levels of proteolytic activities. J Plant Physiol 171(12):998-1002. 10.1016/j.jplph.2014.03.011

Koshland D, Tapia H (2019) Desiccation tolerance: an unusual window into stress biology. Mol Biol Cell 30(6):737-741. 10.1091/mbc.E17-04-0257

Kranner I, Beckett R, Hochman A, Nash TH (2008) Desiccation-tolerance in lichens: a review. Bryologist 111:576-594. 10.1639/0007-2745-111.4.576

Krause C, Richter S, Knoll C, Jurgens G (2013) Plant secretome - from cellular process to biological activity. Biochim Biophys Acta 1834(11):2429-2441. 10.1016/j.bbapap.2013.03.024

Li P, Zhang Y, Wu X, Liu Y (2018) Drought stress impact on leaf proteome variations of faba bean (*Vicia faba* L.) in the Qinghai-Tibet Plateau of China. 3 Biotech 8(2):110-018-1088-3. 10.1007/s13205-018-1088-3

Liszkay A, van der Zalm E, Schopfer P (2004) Production of reactive oxygen intermediates (O2˙−, H2O2, and ˙OH) by maize roots and their role in wall loosening and elongation growth. Plant Physiol 136(2):3114. 10.1104/pp.104.044784

Lum G, Meinken J, Orr J, Frazier S, Min XJ (2014) PlantSecKB: the plant secretome and subcellular proteome knowledgebase. Comput Mol Biol 4(1): 1-17. 10.5376/cmb.2014.04.0001

Malavasi V, Skaloud P, Rindi F, Tempesta S, Paoletti M, Pasqualetti M (2016) DNA-based taxonomy in ecologically versatile microalgae: a re-evaluation of the species concept within the coccoid green algal genus *Coccomyxa* (Trebouxiophyceae, Chlorophyta). PLoS One 11(3):e0151137. 10.1371/journal.pone.0151137

Marchler-Bauer A, Bo Y, Han L, He J, Lanczycki CJ, Lu S, Chitsaz F, Derbyshire MK, Geer RC, Gonzales NR, Gwadz M, Hurwitz DI, Lu F, Marchler GH, Song JS, Thanki N, Wang Z, Yamashita RA, Zhang D, Zheng C, Geer LY, Bryant SH (2017) CDD/SPARCLE: functional classification of proteins via subfamily domain architectures. Nucleic Acids Res 45(D1):D200-D203. 10.1093/nar/gkw1129

Minibayeva F, Beckett RP (2001) High rates of extracellular superoxide production in bryophytes and lichens, and an oxidative burst in response to rehydration following desiccation. New Phytol 152(2):333-341. 10.1046/j.0028-646X.2001.00256.x

Müller K, Linkies A, Vreeburg RAM, Fry SC, Krieger-Liszkay A, Leubner-Metzger G (2009) In vivo cell wall loosening by hydroxyl radicals during cress seed germination and elongation growth. Plant Physiol 150(4):1855. 10.1104/pp.109.139204

Nielsen H, Tsirigos KD, Brunak S, von Heijne G (2019) A brief history of protein sorting prediction. Protein J 38(3):200-216. 10.1007/s10930-019-09838-3

Oliveira P, Martins NM, Santos M, Couto NA, Wright PC, Tamagnini P (2015) The Anabaena sp. PCC 7120 exoproteome: Taking a peek outside the box. Life (Basel) 5(1):130-163. 10.3390/life5010130

Pei Y, Li X, Zhu Y, Ge X, Sun Y, Liu N, Jia Y, Li F, Hou Y (2019) GhABP19, a Novel germin-like protein from *Gossypium hirsutum*, plays an important role in the regulation of resistance to Verticillium and Fusarium Wilt Pathogens. Front Plant Sci 10:583. 10.3389/fpls.2019.00583

Pierre G, Delattre C, Dubessay P, Jubeau S, Vialleix C, Cadoret JP, Probert I, Michaud P (2019) What is in store for EPS microalgae in the next decade? Molecules :24(23):4296. 10.3390/molecules24234296.

Piggot PJ, Coote JG (1976) Genetic aspects of bacterial endospore formation. Bacteriol Rev 40(4):908-962.

Pinheiro C, Kehr J, Ricardo CP (2005) Effect of water stress on lupin stem protein analysed by two-dimensional gel electrophoresis. Planta 221(5):716-728. 10.1007/s00425-004-1478-0

Rosseto FR, Manzine LR, de Oliveira Neto M, Polikarpov I (2016) Biophysical and biochemical studies of a major endoglucanase secreted by *Xanthomonas campestris* pv. campestris. Enzyme Microb Technol 91:1-7. 10.1016/j.enzmictec.2016.05.007

Ruíz-May E, Sorensen I, Fei Z, Zhang S, Domozych DS, Rose JKC (2018) The Secretome and N-glycosylation profiles of the Charophycean green alga, *Penium margaritaceum*, resemble those of Embryophytes. Proteomes 6(2):10.3390/proteomes6020014.

Schaller A (2004) A cut above the rest: the regulatory function of plant proteases. Planta 220(2):183-197. 10.1007/s00425-004-1407-2

Schopfer P (2001) Hydroxyl radical-induced cell-wall loosening in vitro and in vivo: Implications for the control of elongation growth. Plant J 28:679-688. 10.1046/j.1365-313x.2001.01187.x

Sgherri C, Stevanovic B, Navari-Izzo F (2004) Role of phenolics in the antioxidative status of the resurrection plant *Ramonda serbica* during dehydration and rehydration. Physiol Plantarum 122(4):478-485. 10.1111/j.1399-3054.2004.00428.x

Shinozaki K, Yamaguchi-Shinozaki K (1997) Gene expression and signal transduction in water-stress response. Plant Physiol 115(2):327-334. 10.1104/pp.115.2.327

Smukalla S, Caldara M, Pochet N et al. (2008) FLO1 is a variable green beard gene that drives biofilm-like cooperation in budding yeast. Cells 135: 726–737. 10.1016/j.cell.2008.09.037

Steinfeld L, Vafaei A, Rösner J, Merzendorfer H. (2019) Chitin prevalence and function in bacteria, fungi and protists. Adv Exp Med Biol. 1142:19-59. 10.1007/978-981-13-7318-3_3

Stone BA (2009) Chemistry of β-Glucans. In: Bacic A, Fincher GB and Stone BA (eds) Chemistry, biochemistry, and biology of 1-3 beta glucans and related polysaccharides. Academic Press, pp 5-46.

Stothard P (2000) The sequence manipulation suite: JavaScript programs for analyzing and formatting protein and DNA sequences. Biotechniques 28(6).1102-1104. 10.2144/00286ir01

Tanveer T, Shaheen K, Parveen S, Kazi AG, Ahmad P (2014) Plant secretomics: identification, isolation, and biological significance under environmental stress. Plant Signal Behav 9(8):e29426. 10.4161/psb.29426

Teale W, Palme K (2018) Naphthylphthalamic acid and the mechanism of polar auxin transport. J Exp Bot 69(2):303-312. 10.1093/jxb/erx323

Terauchi M, Yamagishi T, Hanyuda T, Kawai H (2017) Genome-wide computational analysis of the secretome of brown algae (Phaeophyceae). Mar Genomics 32:49-59. 10.1016/j.margen.2016.12.002

Vanden Wymelenberg A, Sabat G, Mozuch M, Kersten PJ, Cullen D, Blanchette RA (2006) Structure, organization, and transcriptional regulation of a family of copper radical oxidase

genes in the lignin-degrading basidiomycete *Phanerochaete chrysosporium*. Appl Environ Microbiol 72(7):4871-4877. 10.1128/AEM.00375-06

Vincent D, Rafiqi M, Job D (2020) The multiple facets of plant-fungal interactions revealed through plant and fungal secretomics. Front Plant Sci 10:1626. 10.3389/fpls.2019.01626

Wang M, Kuo-Dahab WC, Dolan S, Park C (2014) Kinetics of nutrient removal and expression of extracellular polymeric substances of the microalgae, *Chlorella* sp. and *Micractinium* sp., in wastewater treatment. Bioresour Technol 154:131-137. 10.1016/j.biortech.2013.12.047

Wang Q, Guo Q, Guo Y, Yang J, Wang M, Duan X, Niu J, Liu S, Zhang J, Lu Y, Hou Z, Miao W, Wang X, Kong W, Xu X, Wu Y, Rui Q, La H (2018) *Arabidopsis* subtilase SASP is involved in the regulation of ABA signaling and drought tolerance by interacting with OPEN STOMATA 1. J Exp Bot 69(18):4403-4417. 10.1093/jxb/ery205

Wang XQ, Yang PF, Liu Z, Liu WZ, Hu Y, Chen H, Kuang TY, Pei ZM, Shen SH, He YK (2009) Exploring the mechanism of *Physcomitrella patens* desiccation tolerance through a proteomic strategy. Plant Physiol 149(4):1739-1750. 10.1104/pp.108.131714

Xiao R, Zheng Y (2016) Overview of microalgal extracellular polymeric substances (EPS) and their applications. Biotechnol Adv 34(7):1225-1244. 10.1016/j.biotechadv.2016.08.004

Ye T, Shi H, Wang Y, Chan Z (2015) Contrasting changes caused by drought and submergence stresses in bermudagrass (*Cynodon dactylon*). Front Plant Sci 6:951. 10.3389/fpls.2015.00951

Yu CS, Chen YC, Lu CH, Hwang JK (2006) Prediction of protein subcellular localization. Proteins 64(3):643-651. 10.1002/prot.21018

Yuan JS, Yang X, Lai J, Lin H, Cheng ZM, Nonogaki H, Chen F (2007) The endo-beta-mannanase gene families in *Arabidopsis*, rice, and poplar. Funct Integr Genomics 7(1):1-16. 10.1007/s10142-006-0034-3

Zhu J, Álvarez S, Marsh EL, Lenoble ME, Cho IJ, Sivaguru M, Chen S, Nguyen HT, Wu Y, Schachtman DP, Sharp RE (2007) Cell wall proteome in the maize primary root elongation zone. II. Region-specific changes in water soluble and lightly ionically bound proteins under water deficit. Plant Physiol 145(4):1533-1548. 10.1104/pp.107.107250

Figure legends

Figure 1: Distribution of protein lengths (A) and isoelectric points (B) of proteins identified in the EPS of TR9 and Csol.

Figure 2: Distribution of functional categories of proteins identified in the EPS of TR9 and Csol.

Figure 3: Distribution of proteins identified in the EPS of TR9 and Csol similar to proteins contained in the secretomes of PlantsecKB from different groups of organisms: only chlorophytes (ALG), only land plants (PLN), both chlorophytes and land plants (VIR), protists (PRO), fungi (FUN) and not shared with any organism (NO).

Figure 4: Functional categorization proteins identified in the EPS of TR9 and Csol shared with the secretomes of different organisms accessible at PlantsecKB. Proteins identified in the EPS of TR9 (left) and Csol (right) which are shared with the secretomes contained in PlantsecKB from different organisms: *Agaricus bisporus* (AGA), *Dorcoceras hygrometricum* (DHY), *Physcomitrella patens* (PPA), *Selaginella moellendorffii* (SMO), *Oryza sativa* (OSA), *Arabidopsis thaliana* (ATH) *Coccomyxa* sp. C169 (C169), *Coccomyxa simplex* (Csol), *Trebouxia* sp. TR9 (TR9), *Chlorella variabilis* (CVA) and *Chlamydomonas reinhardtii* (CRE).

Figure 5: Functional categorization proteins up-regulated in the EPS of TR9.

Table S1: List of proteins identified in the EPS of TR9 indicating UniprotKB accessions of homologous proteins contained in the secretomes of PlantsecKB from different organisms: *Chlamydomonas reinhardtii* (CRE), *Chlorella variabilis* (CVA), *Coccomyxa* sp. C169 (C169), *Coccomyxa simplex* (Csol), *Dorcoceras hygrometricum* (DHY), *Oryza sativa* (OSA), *Arabidopsis thaliana* (ATH), *Physcomitrella patens* (PPA), *Selaginella moellendorffii* (SMO) and *Agaricus bisporus* (AGA). Only similar to chlorophytes (ALG), only similar to land plants (PLN), similar to both chlorophytes and land plants (VIR), similar to fungi (FUN), similar to protists (PRO).

Table S2: List of proteins identified in the EPS of Csol indicating UniprotKB accessions of homologous proteins contained in the secretomes of PlantsecKB from different organisms: *Chlamydomonas reinhardtii* (CRE), *Chlorella variabilis* (CVA), *Coccomyxa* sp. C169 (C169), *Coccomyxa simplex* (Csol), *Dorcoceras hygrometricum* (DHY), *Oryza sativa* (OSA), *Arabidopsis thaliana* (ATH), *Physcomitrella patens* (PPA), *Selaginella moellendorffii* (SMO) and *Agaricus bisporus* (AGA). Only similar to chlorophytes (ALG), only similar to land plants (PLN), similar to both chlorophytes and land plants (VIR), similar to fungi (FUN), similar to protists (PRO).

Key Message

Comparative exoproteome analysis between two aero-terrestrial microalgae show similar protein repertoires but different expression patterns in response to cyclic desiccation/rehydration probably oriented to preserve the extracellular structures during drying.

Author's contribution

LMC conceived and designed the research, MGH and LMC conducted experiments, MGH and EMC analyzed the data, MGH, EMC and LMC wrote the manuscript. All authors read and approved the manuscript.

Table 1: List of proteins identified in the EPS of *Trebouxia* sp. TR9 indicating physicochemical properties and predicted functions. [a]Accessions for the Conserved Domains Database from the NCBI (https://www.ncbi.nlm.nih.gov/cdd). [b]Accessions for UniprotKB (https://www.uniprot.org/). [c]Accessions for Genbank (https://www.ncbi.nlm.nih.gov/genbank/).

ID	Accession	Starting sequence	Length (aa)	IP	Function	Definition	From	To	E-Value	Domain accession
TR9_001	MT438941	MQRVNALVLL	590	4.6	Adhesion	Adhesin	248	446	0.000248549	[a]PRK09752
TR9_002	MT438942	MAQAMRLTLA	318	3.69	Adhesion	Fasciclin domain	52	186	1.1e-22	[a]pfam02469
TR9_003a	MT438943	MRFAAALVLT	424	4.05	Expansins	Expansin	4	419	1e-107	[b]I0YNK2
TR9_003b	MT438944	MSVTCCYFAA	461	4.05	Expansins	Expansin	64	259	2e-11	[b]A8IDR1
TR9_004	MT438945	MSLYSMSLVL	194	3.98	Expansins	Expansin (Barwin-like endoglucanase)	21	192	5e-38	[a]PLN00050
TR9_005	MT438946	MGLSSAAALL	415	4.03	Expansins	Peptidoglycan-binding domain	117	248	1.1e-07	[a]COG4305
TR9_006	MT438947	MRGLLTGLAA	723	4.88	Glycosidases	Alpha-L-arabinofuranosidase	298	712	8.8e-42	[a]COG3534
TR9_007	MT438948	MSSSLELILV	771	5.09	Glycosidases	Alpha-mannosidase	29	317	6.4e-61	[a]cd10791
TR9_008	MT438949	MASLRVFGLI	571	3.98	Glycosidases	Alpha-trehalase	34	559	0	[a]PLN02567
TR9_009	MT438950	MIWLVTLCLI	900	6.07	Glycosidases	Beta-L-arabinofuranosidase	32	691	4.2e-113	[a]pfam07944
TR9_010	MT438951	MIKLCGLILF	782	6.3	Glycosidases	Beta-xylosidase	32	762	9.7e-168	[a]PLN03080
TR9_011a	MT438952	MIGGGWQTVV	537	5.66	Glycosidases	Endo-1,4-beta-mannosidase	119	383	5.9e-27	[a]COG3934
TR9_011b	MT438953	MKAVAVLLAL	463	4.17	Glycosidases	Glycosyl hydrolase	19	442	1e-59	[b]I0YJN3
TR9_012	MT438954	MESHTQHALF	427	4.23	Glycosidases	Endoglucanase E-like	162	409	9.5e-15	[a]cd01831
TR9_013a	MT438955	MLRNAIQAAW	1230	3.9	Glycosidases	Glycosyl hydrolase	55	579	1e-92	[b]I0Z322
TR9_013b	MT438956	MAVICRAVVA	847	3.82	Glycosidases	Glycosyl hydrolase	166	844	1e-90	[b]I0Z322
TR9_013c	MT438957	MTRQLPLFIS	736	4.44	Glycosidases	Glycosyl hydrolase	273	728	1e-86	[b]I0Z322
TR9_013d	MT438958	MKTVVGIVGF	692	6.79	Glycosidases	Glycosyl hydrolase	275	682	1e-60	[b]I0Z322
TR9_014	MT438959	MQTPNFALFI	264	7.17	Glycosidases	Glycosyl hydrolase	56	261	2.4e-43	[b]pfam11790
TR9_015	MT438960	MQQAKQQLYS	468	4.38	Glycosidases	Glycosyl hydrolase	18	378	6.0e-27	[b]M5GGD2
TR9_016	MT438961	MLHCSARPRC	369	4.22	Glycosidases	Glycosyl hydrolase GH18	51	253	1.6e-08	[a]cl10447
TR9_017	MT438962	MGFAQFPDNL	1062	4.72	Glycosidases	Maltase-glucoamylase	326	723	0	[a]cd06602
TR9_018	MT438963	MAGFRGILPL	522	3.92	Hydrolase	Chitin deacetylase	10	443	0.001	[b]L7J1N6
TR9_019	MT438964	MKWSPQIRLQ	363	6.11	Hydrolases	Chlorophyllase I	64	297	3e-13	[b]A8J2S9
TR9_020	MT438965	MSVKMQLLHA	309	3.9	Hydrolases	Dienelactone hydrolase	43	288	6.1e-19	[a]COG0412
TR9_021	MT438966	MVVRWAVLLS	297	7.23	Hydrolases	Glyoxylase or a related metal-dependent hydrolase	47	290	8.9e-17	[a]COG0491
TR9_022	MT438967	MPYPRDCTML	263	5.1	Hydrolases	Kynurenine formamidase	48	262	6.93691e-30	[a]COG1878
TR9_023	MT438968	MFARFVALLT	580	4.16	Hydrolases	Lipase (class 3)	434	568	1.75776e-21	[a]cd00519
TR9_024	MT438969	MQFSLQRLVA	728	6.4	Hydrolases	Neutral/alkaline non-lysosomal ceramidase	26	542	0	[b]pfam04734
TR9_025	MT438970	MKLLCLALAL	207	10.09	Isomerases	Cyclophilin_ABH_Like: Cyclophilin A	35	199	2.25026e-99	[a]cd01926
TR9_026	MT438971	MSHELCTISL	154	4.54	Isomerases	Galactose mutarotase_like	30	152	1.74656e-53	[a]cd09019
TR9_027	MT438972	SSFCLTLIWP	168	8.37	Isomerases	Protein disulfide isomerase	50	156	1e-33	[b]A8JBH7
TR9_028	MT438973	MHRTEMLPAD	1895	6.06	Lectins	Calcium-binding EGF-like domain / Root-specific lectin	764/364	794/563	8.75965e-05	[a]pfam07974/[b]P15312
TR9_029	MT438974	MHRFYCAVVA	438	4.89	Lectins	eel-Fucolectin Tachylectin-4 Pentaxrin-1 Domain	236	433	2.4e-12	[a]smart00607
TR9_030	MT438975	MRTAAALVTC	696	4.56	Lectins	Lectin	244	354	0.0006	[b]Q0JF21
TR9_031	MT438976	MIVVRTPCVL	469	4.01	Lectins	Ricin-type beta-trefoil lectin domain	49	124	1.40987e-05	[b]pfam00652
TR9_032	MT438977	MASYKMMLAM	151	4.81	Oxidoreductases	Antibiotic biosynthesis monooxygenase	61	127	1.13491e-10	[a]pfam03992
TR9_033	MT438978	MRRRTCISSA	726	4.58	Oxidoreductases	Copper amine oxidase	358	719	2.33407e-80	[a]pfam01179
TR9_034	MT438979	MAAQRAMLLL	718	4.54	Oxidoreductases	Cupredoxin domain of the bacterial laccases	66	212	9.87136e-16	[a]cd13853
TR9_035	MT438980	MARATLVAFT	514	3.99	Oxidoreductases	FAD/FMN-containing dehydrogenase	67	495	5.1e-21	[a]COG0277

TR9_036	MT438981	MSCRNLLLIC	639	4.38	Oxidoreductases	Galactose oxidase Glioxal oxidase	529	624	2.6e-27	[a]cd02851
TR9_037	MT438982	MARINSFSGC	457	4.28	Oxidoreductases	Glucose/arabinose dehydrogenase	19	414	1.63418e-44	[a]COG2133
TR9_038	MT438983	MPGMCRDACR	485	5.55	Oxidoreductases	PAP2, haloperoxidase_like	228	464	4.28191e-45	[a]cd03398
TR9_039	MT438984	LTCRICCNTL	162	6.74	Oxidoreductases	Stellacyanin is a subclass of phytocyanins	53	145	2.52191e-07	[a]cd13920
TR9_040	MT438985	MRKTTMSWIK	362	7.98	Phosphatases	Histidine phosphatase	118	341	2.56639e-13	[a]cd07067
TR9_041a	MT438986	MARSAMPYVS	782	4.68	Phosphatases	Metallo-dependent phosphatase	49	680	1e-118	[b]I0Z217
TR9_041b	MT438987	MSRAWRNAPA	744	4.6	Phosphatases	Metallo-dependent phosphatase	1	628	1e-114	[b]I0Z217
TR9_042	MT438988	MQIYLRSPTR	674	5.17	Phosphatases	Phosphodiesterase/alkaline phosphatase D	27	606	4.81446e-82	[a]COG3540
TR9_043	MT438989	MVIMQRLSAC	714	4.1	Phosphatases	Purple acid phosphatase	244	592	4.83305e-78	[a]cd00839
TR9_044	MT438990	MRHCLHLTST	225	6.97	Protease inhibitors	Cystatin/monellin	13	223	3e-52	[b]I0YL91
TR9_045	MT438991	MRKGTAIVSA	131	5.91	Protease inhibitors	Potato inhibitor I family	69	131	7.3e-23	[b]pfam00280
TR9_046	MT438992	MQSAALFAMV	335	6.06	Proteases	Cathepsin X	50	302	8.49768e-76	[a]cd02698
TR9_047a	MT438993	MRCQVAGLLL	489	4.86	Proteases	Cysteine protease	32	442	1e-112	[b]A5HIJ6
TR9_047b	MT438994	ITMRVKLACI	414	4.54	Proteases	Cysteine protease	52	408	5e-99	[b]A8I5R9
TR9_048	MT438995	MALLKHSMRM	609	4.2	Proteases	Lysosomal pro-X carboxypeptidase	28	551	3e-32	[b]B9SX01
TR9_049	MT438996	MRLHACIALA	684	4.5	Proteases	PA_VSR: Protease-associated	51	192	2.39526e-29	[a]cd02125
TR9_050	MT438997	MGLRNMPFYL	1064	4.3	Proteases	Peptidase M1 aminopeptidase	62	516	3.7e-95	[a]cd09601
TR9_051	MT438998	MQGPAAYACR	564	4.31	Proteases	Peptidase S8 family	242	509	7.0e-100	[a]cd07473
TR9_052	MT438999	MNMMRSTSLI	515	4.5	Proteases	Phytepsin	62	513	6.58538e-178	[a]cd06098
TR9_053a	MT439000	MAGGLAAFAA	496	5.06	Proteases	Serine carboxypeptidase	50	492	7.76224e-176	[a]pfam00450
TR9_053b	MT439001	MLKLIWLATF	488	6.36	Proteases	Serine carboxypeptidase	35	483	1e-124	[b]Q8L7B2
TR9_054	MT439002	MVAGQYLALF	225	5.51	Seed storage	Cupin	66	182	3.5345e-21	[a]smart00835
TR9_055	MT439003	MAASIPFIVL	209	4.19	Seed storage	Probable germin-like protein subfamily	10	171	4e-04	[b]O65252
TR9_056	MT439004	MSCSSAVAAV	354	3.88	Transferases	Fatty acyltransferase-like	30	317	8.98653e-56	[a]cd01846
TR9_057	MT439005	MIEADRAGGR	374	6.3	Transferases	Glycosyltransferase family 8	58	300	4.35909e-07	[a]cd00505
TR9_058	MT439006	MRSYFGVVFA	168	4.35	Transferases	Phosphatidylinositol/phosphatidylglycerol transfer protein	22	138	3.96299e-20	[a]cd00917
TR9_059	MT439007	MKVKLGYSLL	1053	4.92	Other	Cysteine rich repeat	629	686	6.25522e-11	[a]pfam00839
TR9_060	MT439008	MAKVLCTAAV	428	3.92	Other	Desiccation-related protein PCC13-62	68	335	5e-28	[b]Q10LK1
TR9_061	MT439009	MKVSVATVAL	358	4.04	Other	Ferritin/ribonucleotide reductase-like protein	20	215	1e-08	[b]G3JG31
TR9_062	MT439010	SFSHSSWTLV	111	7.5	Other	Dynein light chain	23	111	1.2267e-65	[a]PTZ00059
TR9_063	MT439011	MLTSPKTFVS	558	3.9	Other	Nitrous oxide reductase family maturation protein NosD	226	345	6.37435e-05	[a]TIGR04247
TR9_064	MT439012	MQNRVLLLNW	320	4.49	Other	PAN/APPLE-like domain	228	275	4.76073e-08	[a]pfam14295
TR9_065	MT439013	QQRSMTASQL	580	4.11	Other	Periplasmic binding protein TroA_d	208	316	2.17658e-05	[a]cd01141
TR9_066	MT439014	MGARICLSAV	693	3.91	Other	Probable pectinesterase/pectinesterase inhibitor	532	624	3.81817e-05	[a]PLN02217
TR9_067	MT439015	MQSEFLAWLA	144	7.13	Other	Rab GTPase family 1	27	113	7.53911e-59	[a]cd01869
TR9_068	MT439016	MHYWILVVLC	563	4.28	Other	RING finger (key role in the ubiquitination pathway)	515	561	1.84371e-11	[a]cd16714
TR9_069	MT439017	MQHISRLARN	284	6.39	Other	Solanesyl diphosphate synthase-like protein	89	264	2e-27	[b]D7FMC2
TR9_070	MT439018	SFIVQLNFST	301	6.23	Other	Urea carboxylase-associated protein 2	70	272	7.43879e-12	[a]TIGR03425
TR9_071a	MT439019	MRQQICSLNF	491	7.03	Unknown	Uncharacterized protein	21	277	3e-05	[b]M7V4X6
TR9_071b	MT439020	MTHTDSRNKM	427	4	Unknown	Uncharacterized protein	47	427	6.45e-127	[d]KAA6427183
TR9_071c	MT439021	MFRTSQLTLL	472	4.3	Unknown	Uncharacterized protein	63	457	0.004	[b]F7WBJ3
TR9_072	MT439022	MQAQHCFISL	282	4.9	Unknown	Protein of unknown function (DUF3455)	97	255	4.23068e-07	[a]pfam11937
TR9_073a	MT439023	MKPGPGIAFT	224	7.63	Unknown	SOUL-domain-containing protein	28	212	6e-54	[b]I0YVE6
TR9_073b	MT439024	MKASLVATCL	254	5.07	Unknown	SOUL-domain-containing protein	37	222	3e-40	[b]I0YT62
TR9_074	MT439025	QLIAAQAPCI	387	5.73	Unknown	Uncharacterized protein	79	384	2e-79	[b]E1ZD15
TR9_075	MT439026	MVVVICRTSV	225	4.62	Unknown	Uncharacterized protein	41	225	1.2e-72	[c]KAA6429616

TR9_076	MT439027	MTMSLGLVLP	279	3.32	Unknown	Uncharacterized protein	52	279	2.48e-53	[c]KAA6420823
TR9_077	MT439028	MARKVLYIVL	214	7.01	Unknown	Uncharacterized protein	61	214	8e-53	[c]KAA6428896
TR9_078	MT439029	MPSGKVSTLL	542	7.47	Unknown	Uncharacterized protein	66	533	2.18012e-48	[a]COG5361
TR9_079a	MT439030	MASHANCILA	151	4.37	Unknown	Uncharacterized protein	29	123	2.9e-38	[c]KAA6426885
TR9_079b	MT439031	MRTAVLCALL	159	4.25	Unknown	Uncharacterized protein	61	156	1.2e-26	[c]KAA6426885
TR9_080	MT439032	MLTCRDLTAV	171	3.99	Unknown	Uncharacterized protein	87	171	1.09e-35	[c]KAA6429357
TR9_081	MT439033	MQLYAHVCGV	225	3.91	Unknown	Uncharacterized protein	7	225	4e-33	[b]I0Z8F9
TR9_082	MT439034	MLSQHFLCAL	173	6.24	Unknown	Uncharacterized protein	37	171	7e-28	[b]A0A0G4GJN4
TR9_083	MT439035	MRTAVFIVCC	236	4.35	Unknown	Uncharacterized protein	92	217	1.19e-18	[c]KAA6429868
TR9_084	MT439036	MKASHHKAGT	463	6.5	Unknown	Uncharacterized protein	35	448	5e-17	[b]I0YJF6
TR9_085	MT439037	MSARIQQLLV	242	4.11	Unknown	Uncharacterized protein	33	221	3e-06	[b]G2YCB8
TR9_086	MT439038	MRCLLFVISL	149	7.63	Unknown	Uncharacterized protein	20	136	0.001	[b]C1E490
TR9_087	MT439039	MSHHLLVRLV	634	4.33	Unknown	Uncharacterized protein	328	558	0.002	[b]M7SHU2
TR9_088	MT439040	MWAKCVRQFQ	232	7.38	Unknown	Uncharacterized protein	38	154	0.002	[b]E1ZTR2
TR9_089	MT439041	MRSHKQCTPL	358	9.45	Unknown	Uncharacterized protein	138	308	0.002	[b]E1Z4F6
TR9_090	MT439042	MYMPTVSKGF	436	4.32	Unknown	Uncharacterized protein	102	145	0.00393714	[a]cd17767
TR9_091	MT439043	MPFKRLTLLW	391	5.21	Unknown	Uncharacterized protein	58	149	0.004	[b]B9H8C9
TR9_092	MT439044	MHTVRFSRMR	394	4.38	Unknown	Uncharacterized protein	37	152	0.004	[b]C4XZ24
TR9_093	MT439045	MVPSRVGIYG	427	9.93	Unknown	Uncharacterized protein	325	424	0.007	[b]I0YXQ0
TR9_094	MT439046	MKVAYLLSTL	390	4.12	Unknown	Uncharacterized protein	6	275	0.008	[b]D8UCR1
TR9_095	MT439047	MTVIAPQAVS	858	4.39	Unknown	Uncharacterized protein	137	247	0.009	[b]R7SVP1
TR9_096	MT439048	MSCTRSVIAI	554	4.3	Unknown	Uncharacterized protein	334	549	2.86822e-036	[a]pfam11790
TR9_097	MT439049	MFSKYRACAC	244	3.89	Unknown	Uncharacterized protein	--	--	--	--
TR9_098	MT439050	MAPALVTLKA	146	4.65	Unknown	Uncharacterized protein	--	--	--	--
TR9_099	MT439051	MMLAWLLSLY	110	4.77	Unknown	Uncharacterized protein	--	--	--	--

Table 2: List of proteins identified in the EPS of Coccomyxa simplex SAG 216-12 indicating physicochemical properties and predicted functions. [a]Accessions for the Conserved Domains Database from the NCBI (https://www.ncbi.nlm.nih.gov/cdd). [b]Accessions for UniprotKB (https://www.uniprot.org/). [c]Accessions for Genbank (https://www.ncbi.nlm.nih.gov/genbank/).

ID	Accession	Starting sequence	Length (aa)	IP	Function	Definition	From	To	E-Value	Domain accession
CSOL_001	MT438820	MFQLMAFIRS	369	6.64	Adhesion	Bacterial Ig-like domain	57	154	2.87e-05	[a]pfam16640
CSOL_002	MT438821	MRQHRQAHMC	490	4.71	Adhesion	Cysteine rich repeat	192	243	4.10e-08	[a]pfam00839
CSOL_003	MT438822	MRKRLDSLSV	257	5.28	Adhesion	Fasciclin domain	311	448	1.34e-16	[a]pfam02469
CSOL_004	MT438823	MAPKSALAVL	646	9.17	Adhesion	MAEBL domain	76	401	3.09e-05	[a]PTZ00121
CSOL_005	MT438824	MTPILAFAVL	297	4.95	Adhesion	Putative auto-transporter adhesin	34	217	7.27e-10	[a]pfam10988
CSOL_006	MT438825	MHSLELICCV	587	8.24	Expansins	Expansin-like B1	6	249	8.35e-15	[a]PLN03023
CSOL_007a	MT438826	MQAILLIGVA	704	4.34	Expansins	Peptidoglycan-binding domain, expansin	105	237	7.85e-15	[a]COG4305
CSOL_007b	MT438827	MTPFGALLAF	396	4.92	Expansins	Peptidoglycan-binding domain, expansin	68	245	4.41e-07	[a]COG4305
CSOL_008	MT438828	MEIQKKITIA	1139	6.1	Glycosidases	Alpha-mannosidase	38	331	3.85e-140	[a]cd10810
CSOL_009	MT438829	MVTMQLCFLV	729	4.42	Glycosidases	Cellulase (glycosyl hydrolase family 5)	282	643	5.29e-08	[a]pfam00150
CSOL_010	MT438830	MGMQQYCYLR	492	4.68	Glycosidases	Cellulase (glycosyl hydrolase family 5)	79	356	1.89e-13	[a]pfam00150
CSOL_011a	MT438831	MISARFLVVV	723	4.46	Glycosidases	Endo-1,4-beta-mannosidase	123	471	2.95e-24	[a]COG3934
CSOL_011b	MT438832	MAIANCQRGL	686	5.75	Glycosidases	Endo-1,4-beta-mannosidase	50	364	2.15e-21	[a]COG3934
CSOL_011c	MT438833	MGVSLPRTSV	514	5.44	Glycosidases	Endo-1,4-beta-mannosidase	75	377	2.36e-19	[a]COG3934
CSOL_011d	MT438834	MFITRSTSAV	622	5.1	Glycosidases	Endo-1,4-beta-mannosidase	42	375	3.84e-15	[a]COG3934
CSOL_012	MT438835	MLKTTAFFVL	396	5.99	Glycosidases	Glycoside hydrolase	1	283	1.00e-84	[b]I0YJN3
CSOL_013	MT438836	MYRSREVMGL	352	6.5	Glycosidases	Glycoside hydrolase	33	143	7.00e-05	[b]I0Z322
CSOL_014	MT438837	MGATALLPLA	421	4.89	Glycosidases	Glycosyl hydrolase family 18	56	318	4.94e-17	[a]pfam00704
CSOL_015a	MT438838	MASASKRQQR	1214	6.21	Glycosidases	Maltase-glucoamylase	339	728	0	[a]cd06602
CSOL_015b	MT438839	MAAMQEFICF	1019	5.02	Glycosidases	Maltase-glucoamylase	320	706	0	[a]cd06602

CSOL_016	MT438840	MPAVKMSNHM	887	6.02	Glycosidases	Pectate lyase	692	820	7.21e-06	[a]pfam13229
CSOL_017	MT438841	MPAISQLSVA	555	4.96	Glycosidases	Pectinacetylesterase	66	365	4.69e-53	[a]pfam03283
CSOL_018	MT438842	MRSPELYRLV	467	5.46	Glycosidases	Similarity with Pectate lyases	240	400	0.000973156	[a]pfam13229
CSOL_019	MT438843	MHSAIQLLLV	416	5.82	Hydrolases	Bicupin	63	392	3.41e-65	[a]TIGR03404
CSOL_020	MT438844	MGRLYLVTLL	310	6.11	Hydrolases	Dienelactone hydrolase	39	269	5.53e-28	[a]COG0412
CSOL_021	MT438845	MGRSLGCLLF	453	5.12	Hydrolases	Fatty acyltransferase	22	315	4.43e-27	[a]cd01846
CSOL_022	MT438846	MARRIALLFA	405	5.1	Hydrolases	Indole acetimide hydrolase	63	576	2.46e-56	[a]PRK07488
CSOL_023	MT438847	MQILLQLAVV	282	5.35	Hydrolases	Isoamyl-acetate hydrolyzing esterase	42	247	9.55e-86	[a]cd01838
CSOL_024	MT438848	MALLMHRMLP	153	4.95	Hydrolases	Kynurenine formamidase	43	255	1.48e-26	[a]COG1878
CSOL_025	MT438849	MFKLAIIFVA	294	4.82	Hydrolases	Lipase (class 3)	217	370	9.66e-32	[a]cd00519
CSOL_026	MT438850	MKGVTRQIFA	323	5.81	Hydrolases	NodB (polysaccharide deacetylase)	44	242	2.96e-32	[a]cd10959
CSOL_027a	MT438851	MRSSLTVVLC	224	5.8	Hydrolases	PAF-acetylhydrolase	31	278	7.31e-36	[a]cd01820
CSOL_027b	MT438852	MMRYIAALLL	333	6.16	Hydrolases	PAF-acetylhydrolase	38	277	3.33e-28	[a]cd01820
CSOL_027c	MT438853	MVCALVAVLL	285	4.77	Hydrolases	PAF-acetylhydrolase	34	264	2.68e-27	[a]cd01820
CSOL_028	MT438854	MLLATKPILL	573	5.54	Hydrolases	Phospholipase B	30	550	0	[b]pfam04916
CSOL_029	MT438855	MVRSALLALC	204	9.11	Isomerases	Cyclophilin A	32	197	8.73e-108	[a]cd01926
CSOL_030	MT438856	MAGGQLRTSL	392	5.76	Isomerases	Galactose mutarotase	37	375	3.72e-147	[a]cd09019
CSOL_031	MT438857	MKCSSVLLVA	142	8.04	Isomerases	Protein disulfide-isomerase	28	129	4.13e-41	[a]cd03005
CSOL_032	MT438858	MAVSCRLSVL	394	6.1	Oxidoreductases	Ascorbate peroxidase and cytochrome C peroxidase	170	385	7.39e-29	[a]cd00691
CSOL_033	MT438859	MVSFTQVLAI	171	4.45	Oxidoreductases	Electron transfer DM13 (likely to function as cytochromes)	45	139	1.36e-14	[a]smart00686
CSOL_034	MT438860	MKMFSIYKMK	195	5.07	Oxidoreductases	Endoplasmic reticulum protein 19 (ERp19) family	59	158	3.78e-26	[a]cd02959
CSOL_035	MT438861	MNSFVLIGLM	436	4.21	Oxidoreductases	FAD/FMN-containing dehydrogenase	82	501	8.41e-34	[a]COG0277
CSOL_036	MT438862	MLSLKLVGLL	420	5.16	Oxidoreductases	Glucose/arabinose dehydrogenase	28	397	3.93e-57	[a]COG2133
CSOL_037	MT438863	MENIQRLAWT	682	6.32	Oxidoreductases	L-ascorbate oxidase	39	658	7.04e-117	[a]TIGR03388
CSOL_038	MT438864	MVSRLKIGLC	607	5.98	Oxidoreductases	Sugar 1,4-lactone oxidases	44	271	3.41e-19	[a]TIGR01678
CSOL_039	MT438865	MRALLIAAAV	492	5.57	Phosphatases	Homo sapiens acid phosphatase 5	124	447	7.52e-38	[a]cd07378

CSOL_040	MT438866	MELSSIKPMR	723	5.47	Phosphatases	Purple acid phosphatase	307	595	7.57e-81	[a]cd00839
CSOL_041	MT438867	MQPPLGSRIT	342	7.33	Phosphorylases/Kinases	Nucleoside phosphorylase	74	175	0.00092567	[a]COG0775
CSOL_042	MT438868	MVSGLRGLLA	807	4.28	Protease inhibitors	Potato inhibitor I family	213	275	2.78e-15	[a]pfam00280
CSOL_043a	MT438869	MVKHGVLVGC	342	5.74	Proteases	Cathepsin X	63	307	2.02e-116	[a]cd02698
CSOL_043b	MT438870	MATYLLLLVA	401	5.09	Proteases	Cathepsin X	52	309	4.39e-79	[a]cd02698
CSOL_044	MT438871	MRNSCSSFVL	381	4.98	Proteases	Eukaryotic aspartyl protease	49	376	5.03e-82	[a]pfam00026
CSOL_045	MT438872	MAPARYLVLP	591	4.3	Proteases	Imelysin peptidase	37	244	2.68e-19	[a]pfam09375
CSOL_046a	MT438873	MRAVILALGL	709	4.7	Proteases	Papain family cysteine protease	136	350	5.49e-111	[a]pfam00112
CSOL_046b	MT438874	MLPRFLIVVV	402	4.44	Proteases	Papain family cysteine protease	138	350	1.68e-100	[a]pfam00112
CSOL_046c	MT438875	MCSRGCVAAL	401	4.64	Proteases	Peptidase C1A subfamily	137	369	2.59e-82	[a]cd02248
CSOL_047	MT438876	MATSRVQSAI	375	7.18	Proteases	Pepsin-like aspartic proteases	62	414	5.45e-53	[a]cd05471
CSOL_048	MT438877	MRRSNVRLFT	1290	4.65	Proteases	Peptidase S8 family domain in Subtilisin-like proteins	175	407	1.10e-108	[a]cd07473
CSOL_049	MT438878	MMAWAGVSLL	794	4.73	Proteases	Prolyl oligopeptidase PreP	62	776	6.96e-145	[a]COG1505
CSOL_050	MT438879	MKGMLAIVVT	538	4.81	Proteases	Serine carboxypeptidase	67	523	4.52e-170	[a]pfam00450
CSOL_051	MT438880	MVSADRAAIW	784	6.06	Proteases	Trypsin-like peptidase domain	286	458	2.11e-07	[a]pfam13365
CSOL_052	MT438881	MRTRLVACTS	582	7.19	Proteases	V8-like Glu-specific endopeptidase	134	389	1.17e-19	[a]COG3591
CSOL_053	MT438882	MGRFLCALTV	987	5.32	Seed storage	Cupin	67	182	1.29e-18	[a]smart00835
CSOL_054	MT438883	MNSIKLIAFG	134	7.46	Transferases	Lecithin:cholesterol acyltransferase	62	388	1.18e-55	[b]pfam02450
CSOL_055	MT438884	MKSQACIALL	157	4.54	Transferases	Domain involved in innate immunity and lipid metabolism	23	139	5.91e-22	[a]smart00737
CSOL_056	MT438885	MLLFTLCALG	323	4.7	Other	Ankyrin repeat (signal transduction)	85	213	1.02e-08	[a]COG0666
CSOL_057	MT438886	MGRSWVQIRC	409	7.33	Other	Carbonic anhydrase alpha	90	324	4.96e-36	[a]cd03124
CSOL_058	MT438887	MSRSALTLAI	404	8.63	Other	Foam promoting protein (Precursor) (CFG1)	50	250	6.00e-04	[b]B1A0U2
CSOL_059a	MT438888	MALILALVAS	287	4.35	Other	Ferritin-like domain	22	189	4.62e-46	[a]pfam13668
CSOL_059b	MT438889	MYGSDTICAG	516	5.39	Other	Ferritin-like domain	24	186	1.44006e-043	[a]pfam13668
CSOL_060	MT438890	MASDRSQMCA	285	4.74	Other	Oxidative stress defense protein	66	222	9.88e-10	[a]PRK11087

CSOL_061	MT438891	MKALAWFSLL	378	5.96	Other	PAN domain (protein-protein or protein-carbohydrate interactions)	65	104	3.38e-05	[a]pfam14295
CSOL_062	MT438892	MVRVLAATAV	463	7.09	Other	PAN domain (protein-protein or protein-carbohydrate interactions)	388	434	7.01e-05	[a]pfam14295
CSOL_063	MT438893	MSSSIFLTLA	176	6.09	Other	PAN domain (protein-protein or protein-carbohydrate interactions)	92	148	0.000128321	[a]pfam14295
CSOL_064	MT438894	MWLATHRLCC	326	6.89	Other	Phosphate transporter	37	243	1.43e-47	[a]cd13565
CSOL_065	MT438895	MRLPPLSGLT	611	6.49	Other	Phosphate-induced protein 1	351	571	1.78e-18	[a]pfam04674
CSOL_066	MT438896	MRCLAASLIA	212	4.94	Other	Phosphatidyl Ethanolamine-Binding Protein	55	206	2.23e-42	[a]cd00866
CSOL_067	MT438897	MTFKVALALV	495	5.77	Other	Receptor L domain	254	368	2.69e-06	[a]pfam01030
CSOL_068	MT438898	MRFSTLSWAL	281	4.71	Other	Ribonuclease T2 (secreted RNAse)	48	229	1.57e-51	[a]cd01061
CSOL_069	MT438899	MGSLVRGLVL	508	5.56	Other	SOUL heme-binding protein (signaling)	32	204	9.16e-65	[a]pfam04832
CSOL_070	MT438900	MMKLAIVLFL	228	6.91	Other	Stigma-specific protein (controls exudate secretion)	182	225	1.16e-09	[a]pfam04885
CSOL_071	MT438901	MLRQLLVVLL	404	4.8	Other	Stress up-regulated Nod 19	64	368	3.93e-28	[a]pfam07712
CSOL_072	MT438902	SYQRRALLTL	112	6.25	Other	Ubiquitin-like (Ubl) domain	36	107	7.49e-28	[a]cd16116
CSOL_073	MT438903	MVHLHRPAIV	681	5.83	Unknown	Uncharacterized protein	119	707	0	[c]XP_005644381
CSOL_074	MT438904	MRLMHWAVAA	426	5.33	Unknown	Uncharacterized protein	25	426	0	[b]I0YNK2
CSOL_075	MT438905	MAAQQTSFLL	570	7.18	Unknown	Uncharacterized protein	38	471	0	[b]I0Z3I2
CSOL_076	MT438906	MWELCTFVVL	624	4.67	Unknown	Uncharacterized protein	1	611	0	[b]I0YJ50
CSOL_077	MT438907	MGRAGGVCTA	625	6.64	Unknown	Uncharacterized protein	1	624	0	[b]I0YIJ4
CSOL_078	MT438908	MRFIAAVALL	375	9.48	Unknown	Uncharacterized protein	1	375	1.00e-173	[b]I0YZ62
CSOL_079	MT438909	MANLKAILIL	379	4.69	Unknown	Uncharacterized protein	1	379	1.00e-149	[b]I0Z321
CSOL_080a	MT438910	MERSHIRRAA	470	7.32	Unknown	Uncharacterized protein	23	438	1.00e-126	[b]I0YJ96
CSOL_080b	MT438911	MGRIRGSRLL	552	5.24	Unknown	Uncharacterized protein	313	552	6.00e-85	[b]I0YJ96
CSOL_080c	MT438912	MARCHLAAAS	469	8.24	Unknown	Uncharacterized protein	27	460	7.00e-73	[b]I0YJ96
CSOL_081	MT438913	MAFRYLALVP	213	7.77	Unknown	Uncharacterized protein	1	289	3.62e-124	[c]XP_005651627
CSOL_082	MT438914	MASSGLRFAG	301	5.73	Unknown	Uncharacterized protein	7	301	1.00e-121	[b]I0YRQ2
CSOL_083a	MT438915	MQRIAVLFLF	284	5.37	Unknown	Uncharacterized protein	1	263	1.00e-113	[b]I0YKS0
CSOL_083b	MT438916	MRIFTIIAGL	286	6.74	Unknown	Uncharacterized protein	23	253	2.00e-63	[b]I0YKS0

CSOL_084a	MT438917	MAARAVLILA	258	4.84	Unknown	Uncharacterized protein	1	258	1.00e-110	[b]I0YLX2
CSOL_084b	MT438918	MAAQAILFLA	279	5.65	Unknown	Uncharacterized protein	25	229	2.00e-86	[b]I0YLX2
CSOL_085	MT438919	MGLKICGIVS	167	8.23	Unknown	Uncharacterized protein	1	213	1.00e-105	[b]I0YTL7
CSOL_086	MT438920	MGLFLLAALA	375	7.11	Unknown	Uncharacterized protein	12	269	1.00e-103	[b]I0Z6A7
CSOL_087	MT438921	MVLRHFQALL	471	6.62	Unknown	Uncharacterized protein	3	111	6.00e-75	[b]J3N8P0
CSOL_088	MT438922	MTTLKFLALV	238	7.59	Unknown	Uncharacterized protein	1	222	6.00e-74	[b]I0Z2H5
CSOL_089a	MT438923	MRSTLVIAMI	422	6.13	Unknown	Uncharacterized protein	1	129	1.00e-59	[b]I0Z979
CSOL_089b	MT438924	MTATRYAVSA	130	7.9	Unknown	Uncharacterized protein	22	130	3.00e-20	[b]I0Z979
CSOL_090	MT438925	MNKLLIALVA	118	7.97	Unknown	Uncharacterized protein	20	118	1.00e-40	[b]I0YJR5
CSOL_091	MT438926	MVHIIGKASF	418	7.15	Unknown	Uncharacterized protein	79	172	4.00e-21	[b]I0YK40
CSOL_092	MT438927	MNTTAVFLLV	149	4.34	Unknown	Uncharacterized protein	1	149	1.00e-17	[b]I0YW26
CSOL_093	MT438928	MKKHIILAVA	281	5.94	Unknown	Uncharacterized protein	78	135	1.00e-14	[b]I0YNT4
CSOL_094	MT438929	MVAAMDSKMM	144	6.12	Unknown	Uncharacterized protein	42	132	7.00e-12	[b]I0YK40
CSOL_095	MT438930	MMQGFQFLWM	309	5.71	Unknown	Uncharacterized protein	121	285	2.00e-10	[b]I0YW16
CSOL_096	MT438931	MGTMRARATT	485	3.9	Unknown	Uncharacterized protein	265	470	2.00e-07	[b]I0Z2M2
CSOL_097	MT438932	MTLGGASPLK	639	5.74	Unknown	Uncharacterized protein	467	590	1.00e-05	[b]A0A067C9Y0
CSOL_098	MT438933	MRLLLVCILA	226	4.48	Unknown	Uncharacterized protein	4	196	4.00e-05	[b]E1ZGH7
CSOL_099	MT438934	MARLWGAALL	283	4.84	Unknown	Uncharacterized protein	49	150	0.00136656	[a]PRK10856
CSOL_100	MT438935	MTRRQGADQL	150	9.16	Unknown	Uncharacterized protein	97	130	0.00310502	[a]COG4099
CSOL_101	MT438936	MLALKQACAA	525	4.95	Unknown	Uncharacterized protein	76	186	0.00323126	[a]pfam12740
CSOL_102	MT438937	MFSSRRAFVC	379	6.5	Unknown	Uncharacterized protein	108	206	0.00816807	[a]PLN02629
CSOL_103	MT438938	MMSKAPYRRS	269	8.32	Unknown	Uncharacterized protein	55	100	0.00932326	[a]cd00064
CSOL_104	MT438939	MAVIASRGAN	420	6.62	Unknown	Uncharacterized protein	---	---	---	---
CSOL_105	MT438940	MASRPSLLAG	307	6.52	Unknown	Uncharacterized protein	8	307	1.00e-131	[a]I0YRQ3

Table 3: List of differentially expressed proteins identified in the EPS of *Trebouxia* sp. TR9.

ID	Accession	Function	Definition	Expression	Abundance Ratio (log2): (DR) / (T0)	Abundance Ratio P-Value
TR9_011a	MT438952	Glycosidases	Endo-1,4-beta-mannosidase	UP	1.73	0.02218746
TR9_013d	MT438958	Glycosidases	Glycoside hydrolase	UP	1.58	0.04370915
TR9_016	MT438961	Glycosidases	Glycosyl hydrolase GH18	UP	1.68	0.02425582
TR9_018	MT438963	Glycosidases	Glycoside hydrolase	UP	1.71	0.02246178
TR9_019	MT438964	Other	Chlorophyllase I	UP	3.28	0.00005830
TR9_024	MT438969	Hydrolases	Neutral/alkaline non-lysosomal ceramidase	UP	1.34	0.04148034
TR9_029	MT438974	Lectins	eel-Fucolectin	UP	2.02	0.01405157
TR9_035	MT438980	Oxidoreductases	FAD/FMN-containing dehydrogenase	UP	3.16	0.00011482
TR9_036	MT438981	Oxidoreductases	Galactose oxidase	UP	1.82	0.01652966
TR9_045	MT438991	Protease inhibitors	Potato inhibitor I family (Proteinase inhibitor)	UP	1.51	0.03094566
TR9_047b	MT438994	Proteases	Cysteine protease	UP	1.73	0.03349551
TR9_050	MT438997	Proteases	Peptidase M1 aminopeptidase	UP	2.18	0.00769083
TR9_051	MT438998	Proteases	Peptidase S8 family domain	UP	2.06	0.00793157
TR9_053b	MT439001	Proteases	Serine carboxypeptidase	UP	1.75	0.01107544
TR9_055	MT439003	Seed storage	Cupin	UP	3.44	0.00003987
TR9_071a	MT439019	Unknown	Uncharacterized protein	UP	1.42	0.04771957
TR9_075	MT439026	Unknown	Uncharacterized protein	UP	1.95	0.00559478
TR9_079a	MT439030	Unknown	Uncharacterized protein	UP	2.02	0.00826465
TR9_079b	MT439031	Unknown	Uncharacterized protein	UP	1.85	0.02393809
TR9_085	MT439037	Unknown	Uncharacterized protein	UP	1.57	0.03294702
TR9_086	MT439038	Unknown	Predicted protein	UP	1.63	0.03114887
TR9_088	MT439040	Unknown	Putative uncharacterized protein	UP	1.81	0.01207804
TR9_094	MT439046	Unknown	Putative uncharacterized protein	UP	1.49	0.03076886

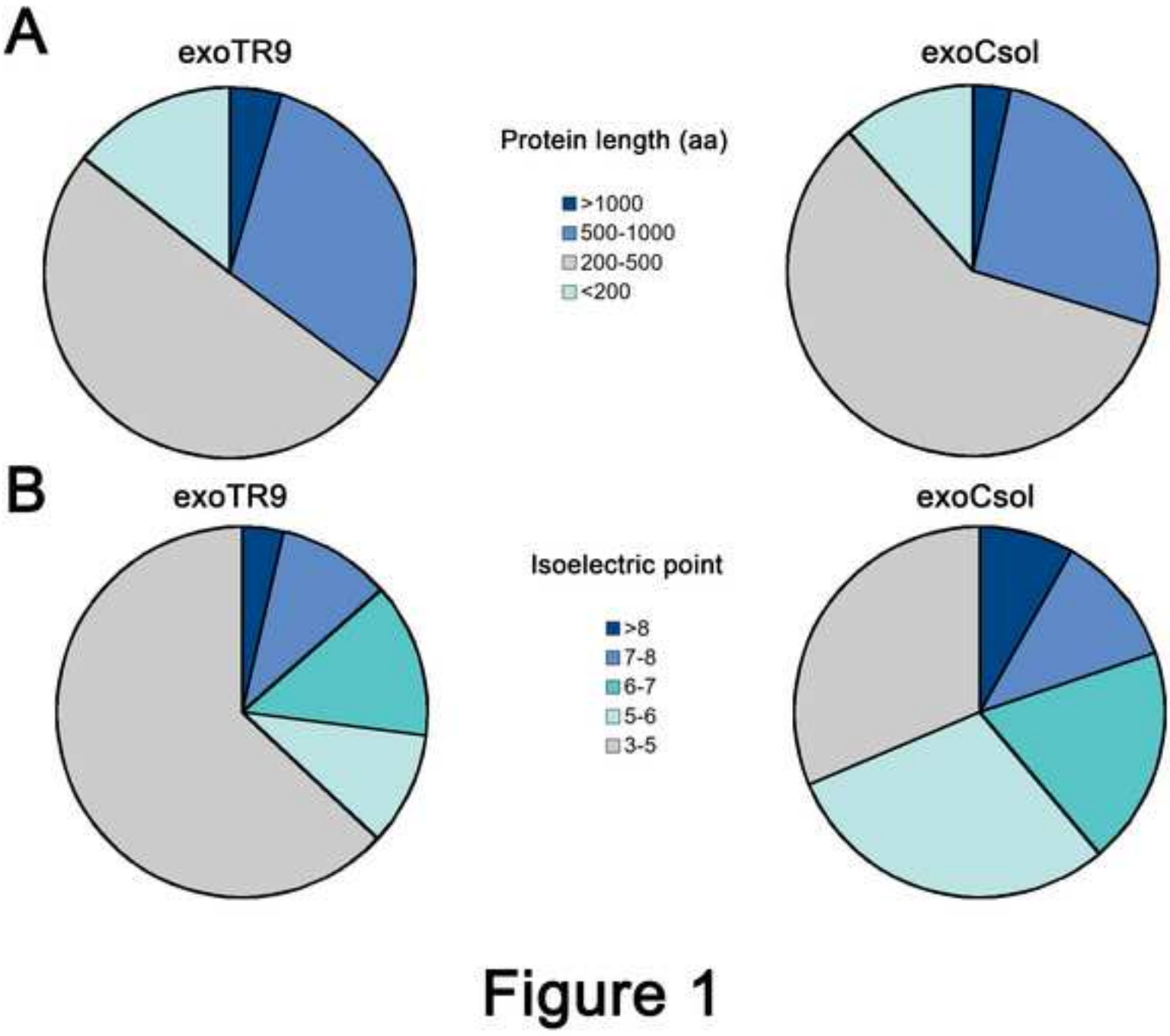

Figure 1

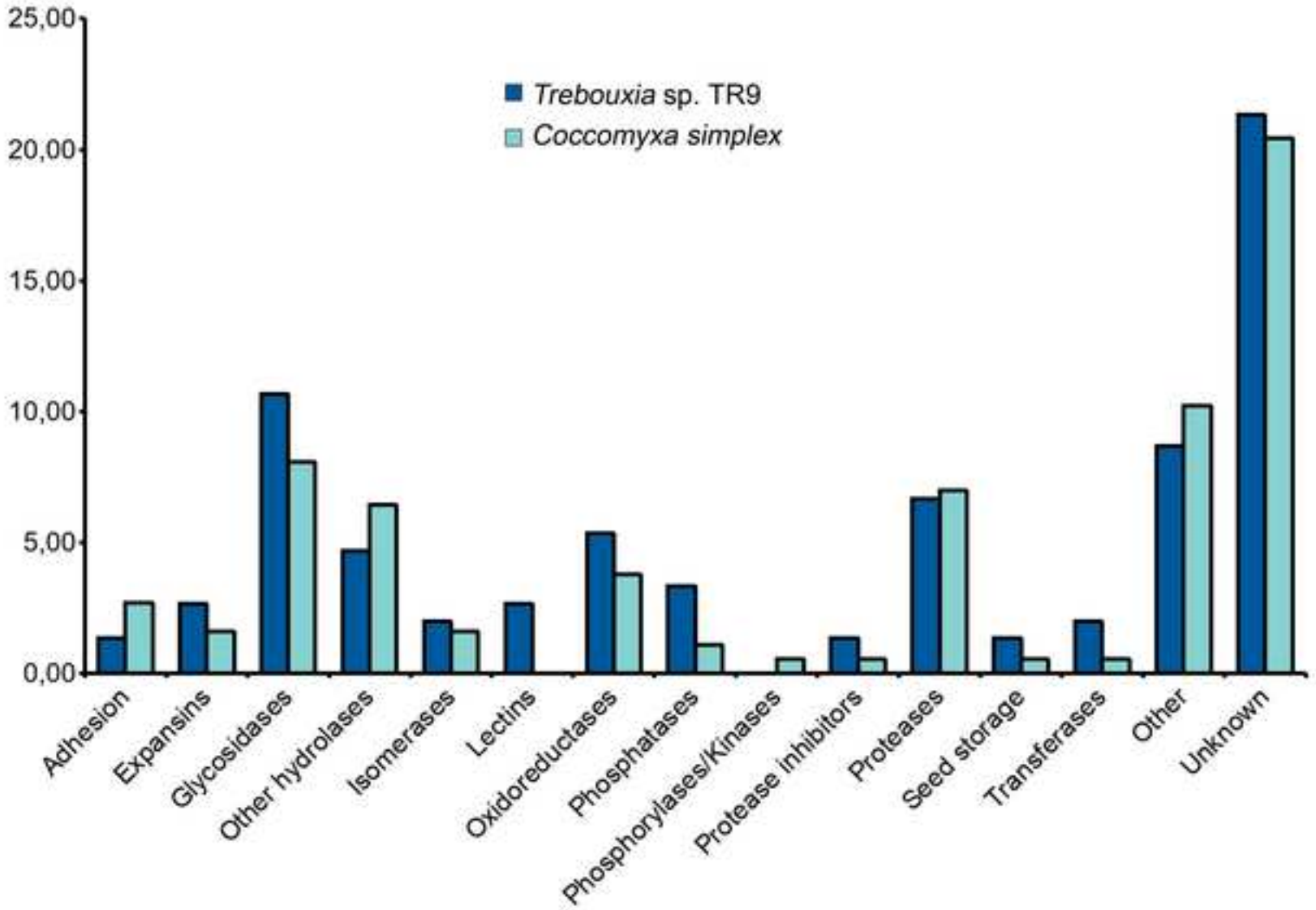

Figure 2

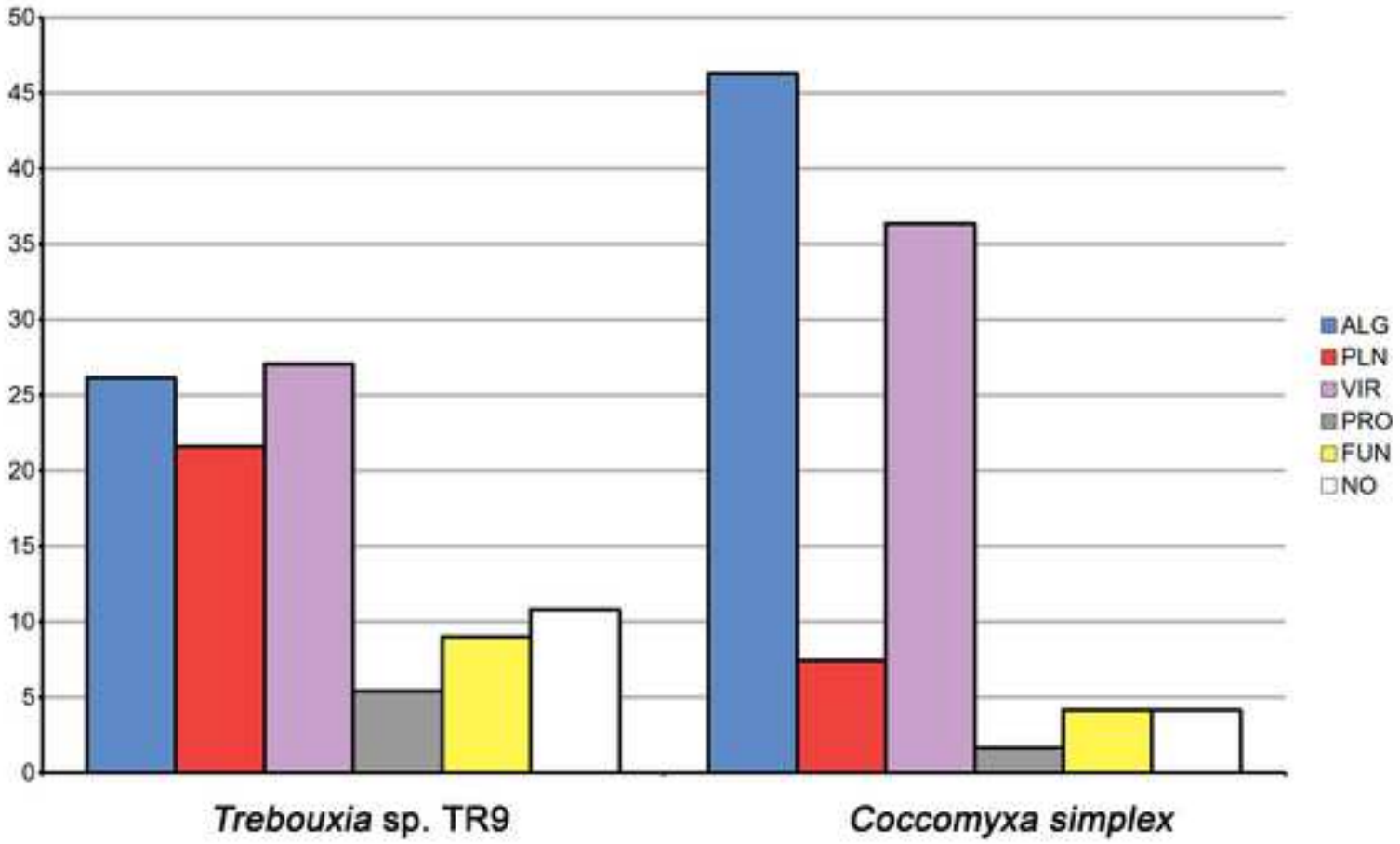

Figure 3

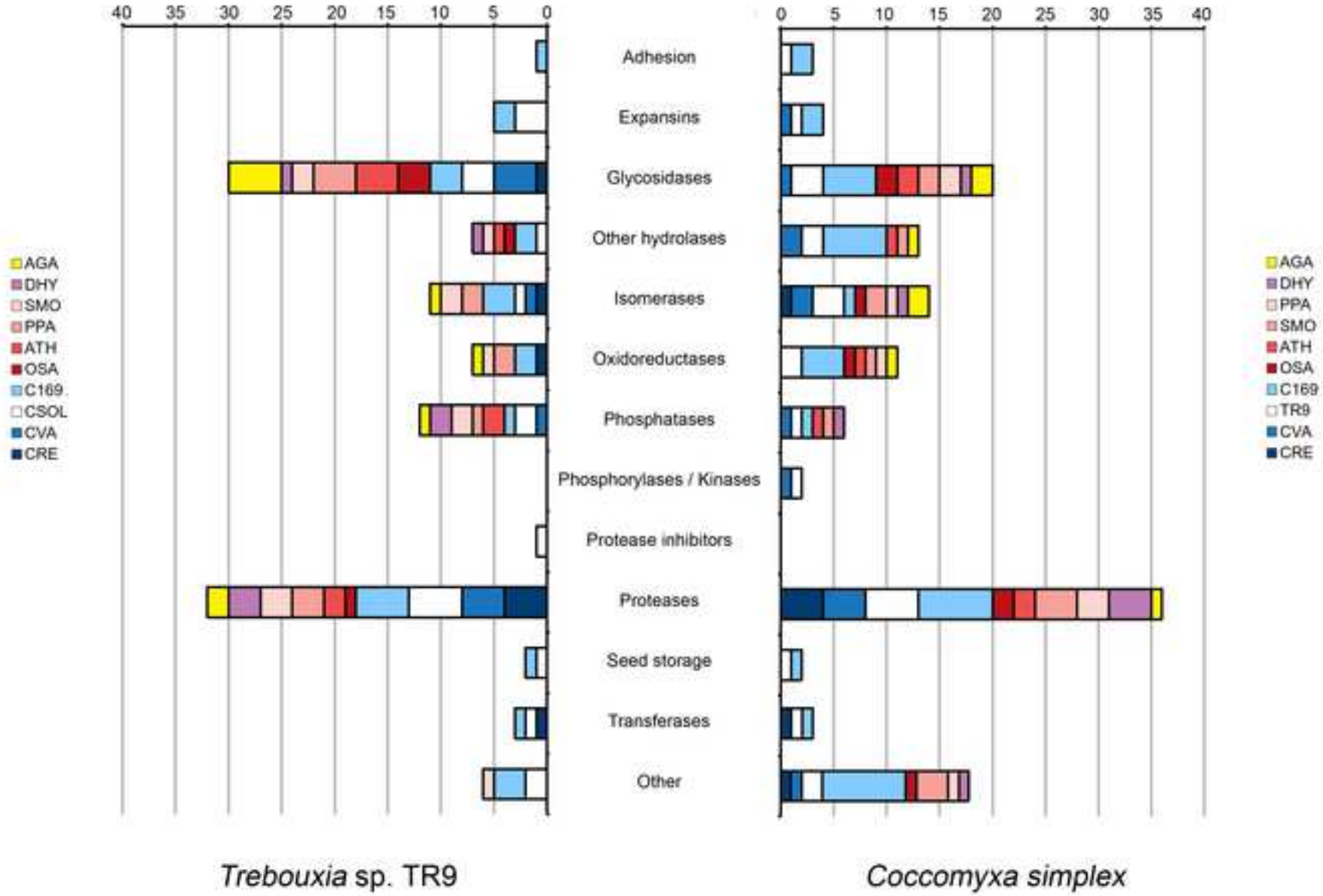
40 35 30 25 20 15 10 5 0
0 5 10 15 20 25 30 35 40
AGA
DHY
SMO
PPA
ATH
OSA
C169
CSOL
CVA
CRE
Adhesion
Expansins
Glycosidases
Other hydrolases
Isomerases
Oxidoreductases
Phosphatases
Phosphorylases / Kinases
Protease inhibitors
Proteases
Seed storage
Transferases
Other
AGA
DHY
PPA
SMO
ATH
OSA
C169
TR9
CVA
CRE
Trebouxia sp. TR9
Coccomyxa simplex

Figure 4

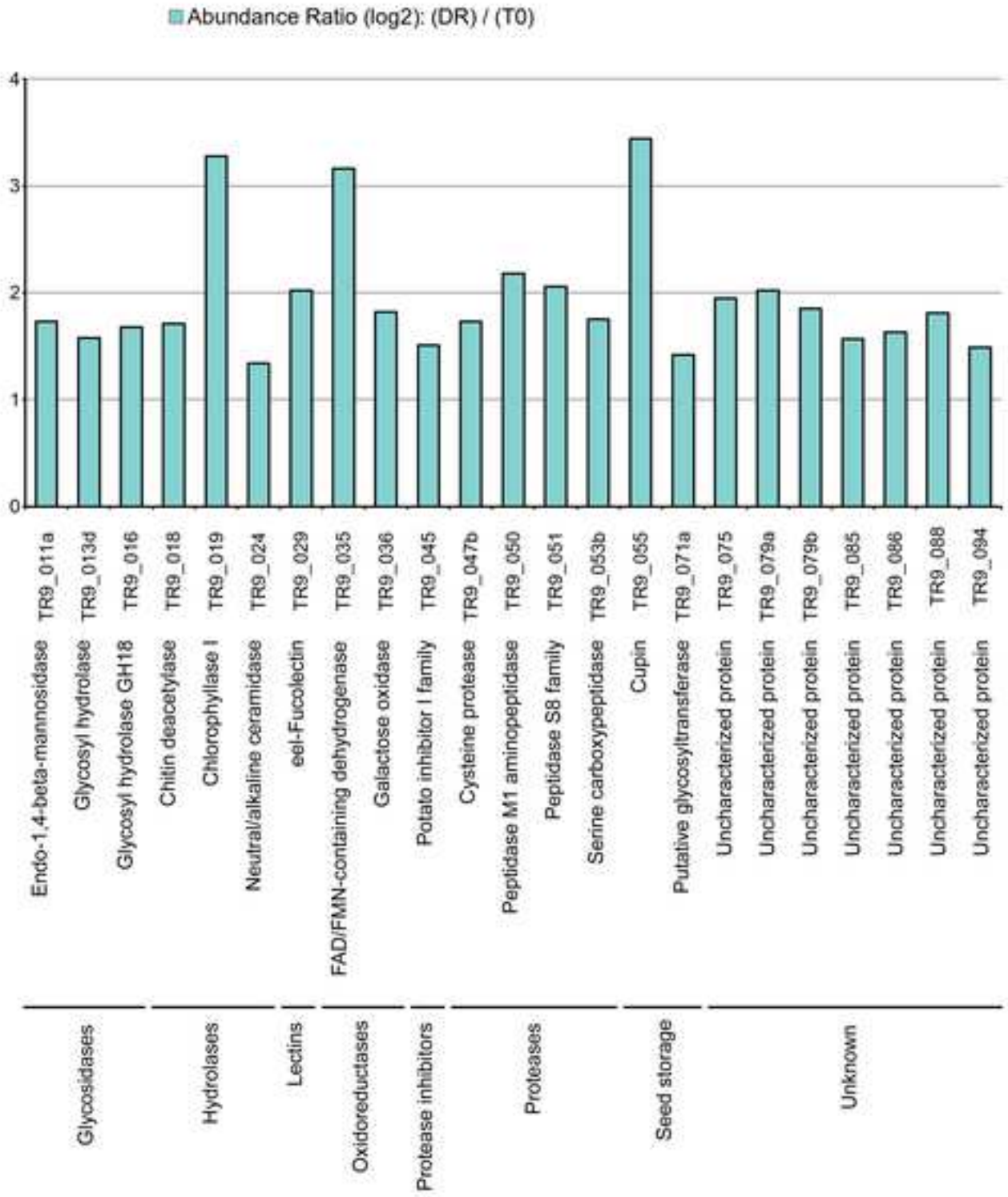
Abundance Ratio (log2): (DR) / (T0)
4
3
2
1
0
Endo-1,4-beta-mannosidase TR9_011a
Glycosyl hydrolase TR9_013d
Glycosyl hydrolase GH18 TR9_016
Chitin deacetylase TR9_018
Chlorophyllase I TR9_019
Neutral/alkaline ceramidase TR9_024
eel-Fucolectin TR9_029
FAD/FMN-containing dehydrogenase TR9_035
Galactose oxidase TR9_036
Potato inhibitor I family TR9_045
Cysteine protease TR9_047b
Peptidase M1 aminopeptidase TR9_050
Peptidase S8 family TR9_051
Serine carboxypeptidase TR9_053b
Cupin TR9_055
Putative glycosyltransferase TR9_071a
Uncharacterized protein TR9_075
Uncharacterized protein TR9_079a
Uncharacterized protein TR9_079b
Uncharacterized protein TR9_085
Uncharacterized protein TR9_086
Uncharacterized protein TR9_088
Uncharacterized protein TR9_094
Glycosidases
Hydrolases
Lectins
Oxidoreductases
Protease inhibitors
Proteases
Seed storage
Unknown

Figure 5

Consideraciones finales y Conclusiones

Consideraciones finales

Los resultados obtenidos durante la ejecución de la presente Tesis Doctoral han sido publicados previamente (González-Hourcade *et al.,* 2020 a, b) o han sido enviados y están actualmente en revisión para su publicación (González-Hourcade *et al.,* 2020, en revisión). En conjunto, estas aportaciones confirman, profundizan en el análisis detallado y extienden los hallazgos iniciales del grupo PlantStres sobre la pared celular y polímeros extracelulares en las dos microalgas liquénicas *Trebouxia* sp. TR9 y *Coccomyxa simplex* (Casano *et al.,* 2011, 2015; Centeno *et al.,* 2016). El primero de los artículos de esta Tesis está dedicado al estudio pormenorizado de los cambios ultraestructurales y bioquímicos en los polisacáridos de la pared celular como consecuencia de la exposición a la desecación cíclica. Los dos artículos siguientes hacen referencia al análisis de diferentes componentes de la matriz extracelular. En el primero de estos (González-Hourcade *et al.,* 2020b) se estudian los polisacáridos extracelulares y su remodelación bioquímica inducida por la desecación cíclica, y en el segundo (González-Hourcade *et al.,* 2020, en revisión) se caracterizan las exoproteínas y su posible implicación en la remodelación de la pared y de los polímeros extracelulares.

Brevemente, TR9 y *Csol* presentan estrategias bioquímico-moleculares y estructurales diferentes a nivel de su pared celular y matriz extracelular que les permite hacer frente a la desecación cíclica en sus respectivos hábitats. Por ello, TR9, un alga típicamente mediterránea, posee una pared celular más gruesa, pero de ultraestructura difusa y significativamente más flexible (Fig.1), que le permite responder rápidamente a cambios bruscos y drásticos en el contenido hídrico intracelular. Estas propiedades biomecánicas de la pared celular de TR9 parecen sustentarse en una composición química característica de esta alga, que sufre una evidente remodelación por exposición a desecación cíclica. En condiciones control la pared está fundamentalmente formada por un ramno-galactofuranano matricial de tamaño molecular intermedio y por galactanos estructurales altamente sustituidos por manosa, xilosa y ramnosa; mientras que, tras la desecación cíclica, cambia el perfil molecular del ramno-galactofuranano y disminuye el grado de sustitución de los galactanos estructurales.

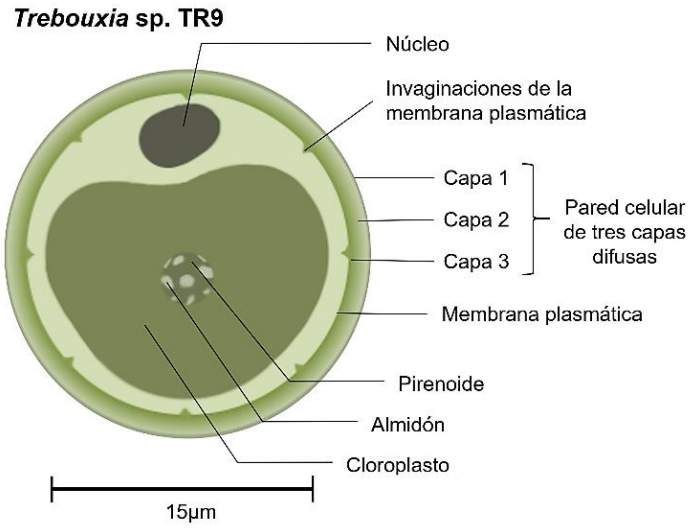

Figura 1. Representación esquemática celular y detalles de la pared celular de *Trebouxia* sp. TR9

Por otra parte, *Csol* habita en un ambiente relativamente más húmedo y protegido, con ciclos de desecación más lentos que los que soporta TR9. Esta sería la razón por la cual *Csol* presenta una estrategia de tolerancia distinta y que incluye una pared celular delgada, formada por capas bien definidas, incluyendo los algaenanos (Fig.2), los cuales confieren una menor flexibilidad y permiten un plegamiento más limitado que en TR9.

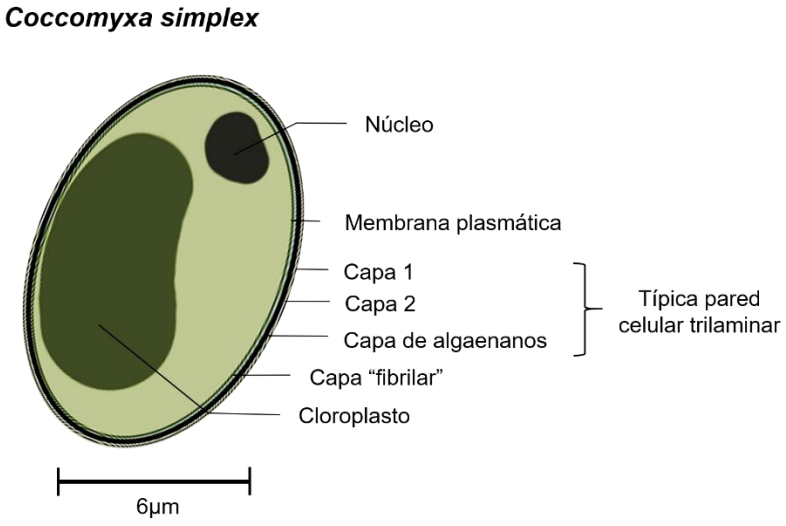

Figura 2. Representación esquemática celular y detalles de la pared celular de *Coccomyxa simplex.*

Esto se debe, al menos en parte, a su peculiar composición, en la cual xilanos y mananos matriciales junto con ß-glucanos estructurales, todos de perfil molecular disperso, son los componentes principales cuando *Csol* se

encuentra completamente hidratada. El efecto más notable de la desecación cíclica es la aparición de varios ß-glucanos estructurales con masas moleculares bien definidas.

Con respecto a la matriz extracelular, TR9 contiene predominantemente homogalactanos con escasas sustituciones de residuos de ramnosa, xilosa y manosa. Además, esta matriz es rica en ácidos urónicos y polisacáridos sulfatados que, por sus cargas negativas presentan una gran capacidad de retención de agua y evitan una deshidratación excesivamente rápida. *Csol* también incluye galactanos como componentes principales de los exopolisacáridos, aunque tiene una composición más heterogénea que TR9, puesto que, presenta más ramificaciones de manosa y ramnosa. La matriz extracelular de *Csol* es relativamente menos abundante que la de TR9, pero también contiene ácidos urónicos y polisacáridos sulfatados, aunque estos últimos no cambian tras la desecación cíclica, indicando que en *Csol* la deshidratación es más lenta, por lo que no requeriría una gran capacidad de retención de agua a nivel extracelular.

Estas remodelaciones bioquímico-estructurales tanto de los polisacáridos de la pared celular como los de la matriz extracelular, se producen principalmente por la acción concertada de las hidrolasas extracelulares, cuyos niveles estacionarios podrían estar modulados por la acción conjunta de proteasas e inhibidores de proteasas. Estas exoproteínas, entre las que se incluyen las glicosidasas, exoenzimas asociadas a carbohidratos y proteasas, se han descrito en los exoproteomas de ambas algas, conservándose tras la desecación cíclica. Sin embargo, cada alga presenta un patrón de expresión diferente. *Csol* mostraría una estrategia de expresión constitutiva, mientras que, el exoproteoma de TR9 parece ser parcialmente inducible por la desecación. Esta especie está adaptada a cambios más rápidos en la disponibilidad de agua y por ello, su respuesta debe ser más rápida, involucrando cambios más profundos en la pared celular, que la de *Csol*. Esta podría ser la razón por la que TR9 sobreexpresa 23 de sus 111 exoproteínas, muchas de las cuales están relacionadas con la hidrólisis de carbohidratos y proteínas.

Conclusiones

Las principales conclusiones de la presente Tesis Doctoral son:

1. Ambos ficobiontes, *Trebouxia* sp. TR9 y *Coccomyxa simplex*, presentan una pared celular cuya ultraestructura y composición en polisacáridos es característica de cada especie. La desecación cíclica induce la remodelación bioquímica en la pared celular, mejorando probablemente sus propiedades biomecánicas y su capacidad para plegarse a medida que el protoplasto celular se contrae.
2. TR9 muestra una pared celular robusta y sin una organización definida, pero más flexible y una capacidad de respuesta más rápida que *Csol*. El cambio bioquímico más destacable está relacionado con una reducción en el nivel de polimerización de sus principales polisacáridos estructurales, sustituyendo al principal ramno-galactofuranano de células totalmente hidratadas por una mayoría de galactanos de bajo peso molecular.
3. *Csol* presenta una pared celular fina y con una clara organización en capas incluyendo algaenanos, lo que le provee de una característica impermeable que le permitiría desarrollar una desecación intracelular relativamente lenta, en comparación con TR9. El aumento de la concentración de glucosa y galactosa en sustitución de los xilanos de la condición control, es uno de los aspectos más notables en cuanto a cambios en la composición de la pared celular.
4. Los polisacáridos extracelulares de TR9 son cuantitativa y cualitativamente diferentes como a los de *Csol*, en condiciones de completa hidratación. Ambas especies, tras la exposición a la desecación, cambian de una composición glicosídica altamente heterogénea a una relativamente homogénea en la que la galactosa es el principal monosacárido.
5. Las dos algas poseen exopolímeros sulfatados, pero solo TR9, aumenta la presencia de polisacáridos sulfatados extracelulares en condiciones desecación cíclica, lo cual le conferiría una mayor capacidad para retener agua y por lo tanto una ventaja adaptativa frente ciclos rápidos de desecación/rehidratación

6. Las sulfotransferasas responsables de la sulfatación de los azúcares en ambas algas, presentan un origen ancestral y sin similitudes con otras enzimas con funciones similares en otras especies de algas de estilo de vida acuática ni de plantas vasculares.
7. Los exoproteomas de TR9 y *Csol* contienen 111 y 121 proteínas, respectivamente, distribuidas en proporciones similares entre diferentes grupos funcionales, siendo las glicosidasas y proteasas los conjuntos más abundantes y probablemente más relevantes por sus funciones en el metabolismo de polisacáridos y proteínas extracelulares. Otras exoproteínas menos abundantes intervienen en funciones fundamentales como la interacción célula-célula, el metabolismo de ROS y la expansión celular. Aproximadamente un tercio de las exoproteínas de ambas algas presentan funciones desconocidas hasta la fecha, y algunas de éstas también han sido observadas en otros organismos tolerantes a la desecación.
8. A nivel de exoproteoma, cada microalga responde de modo diferente frente a la desecación cíclica. Mientras TR9 incrementa la expresión de ciertas proteínas, *Csol* presenta un patrón de expresión constitutivo para todas sus exoproteínas.

En conjunto, los datos aportados en la presente Tesis Doctoral contribuyen a esclarecer, al tiempo que originan nuevas preguntas, las peculiares características ultraestructurales y bioquímicas de la pared celular y la matriz extracelular de las microalgas liquénicas, y su relevante y compleja participación en la capacidad de estos organismos para tolerar profundos cambios en su contenido hídrico.

Bibliografía

Ahmadjian, V. (1995) Lichens are more important than you think. *BioScience* 45: 123-124.

Ahmadjian, V. (1993) The lichen symbiosis. New York: John Willey & Sons, Inc.

Ahmadjian, V. (1988) The lichen alga Trebouxia: does it occur free-living? *Plant Syst* Evol 158: 243-247

Ahmadjian, V. (1982) Algal/fungal symbioses. *Progr Phycol Res*, pp 179-233.

Ahmadjian, V. (1960) Some New and Interesting Species of *Trebouxia*, a Genus of Lichenized Algae. *Am J Bot* 47(8), 677.

Alpert, P. (2006). Constraints of tolerance: why are desiccation-tolerant organisms so small or rare? *J Exp Biol* 209: 1575-1584.

Armstrong, R.A. (2017) Adaptation of Lichens to Extreme Conditions. In *Plant Adaptation Strategies in Changing Environment*. Shukla V., Kumar S., Kumar N. (eds.) Springer, Singapore, pp. 1-27.

Asada, K. (1999). The water-water cycle in chloroplasts: Scavenging of Active Oxygens and Dissipation of Excess Photons. *Annu Rev Plant Phys* 50: 601-639.

Aschenbrenner, I.A., Cardinale, M., Berg, G., and Grube, M. (2014). Microbial cargo: do bacteria on symbiotic propagules reinforce the microbiome of lichens? *Environ Microbiol* 16: 3743-3752.

Baudelet, P.H., Ricochon, G., Michel, L., and Muniglia, L. (2017). A new insight into cell walls of Chlorophyta. *Algal Res* 25: 333-371.

Beckett, R.P., Kranner, I., and Minibayeva, F.V. (2008). Stress physiology and the symbiosis. In *Lichen Biology*, Nash, T.H.III (ed). Cambridge, UK: Cambridge University Press, pp. 184-151.

Boscaiu, M., Mora, E., Fola, O., Scridon, S., Llinares, J., and Vicente, O . (2009). Osmolyte accumulation on xerophytes as a response to environmental stress. *Bull UASVM Hort* 66(1): 96-102.

Brunner, U., and Honegger, R. (1985). Chemical and ultrastructural studies on the distribution of sporopolleininlike biopolymers in six genera of lichen phycobiontes. *Can J Bot* 63: 2221-2230.

Büdel, B. (1992). Taxonomy of lichenized procaryotic blue-green algae. In *Algae and Symbioses.* Reisser, W.*,* ed. Bristol: Biopress Limited. pp. 301-324.

Buitink, J., and Leprince, O. (2004) Glass formation in plant anhydrobiotes: survival in the dry state. *Cryobiol* 48: 215-228

del Campo, E.M., Catalá, S., Gimeno, J. *et al.* (2013) The genetic structure of the cosmopolitan three-partner lichen *Ramalina farinacea* evidences the concerted diversification of symbionts.*FEMS Microbiol Ecol* 83: 310-323.

del Campo, E.M., Gimeno, J., Casano, L.M., *et al.* (2010) South European populations of *Ramalina farinacea* (L.) Ach. share different *Trebouxia* algae. In *Bibliotheca Lichenolgica.* Nash, T.H.III (ed.), 105. Stuttgart: Schweizerbart science publishers, pp. 247- 256.

Casano, L.M., Braga, M.R., Álvarez, R., del Campo, E.M., and Barreno E. (2015). Differences in the cell walls and extracellular polymers of the two *Trebouxia* microalgae coexisting in the lichen *Ramalina farinacea* are consistent with their distinct capacity to immobilize extracellular Pb. *Plant Sci* 236: 195-204.

Casano, L.M., del Campo, E.M., García-Breijo, F.J., *et al.* (2011). Two *Trebouxia* algae with different physiological performances are ever-present in lichen thalli of *Ramalina farinacea.* Coexistence versus competition? *Environ Microbiol* 13: 806-818.

Casano, L.M., Gomez, L.D., Lascano, H.R., Gonzalez, C.A., and Trippi, V.S. (1997). Inactivation and degradation of CuZn-SOD by active oxygen species in wheat chloroplasts exposed to photooxidative stress. *Plant Cell Physiol* 38: 433-440.

Centeno, D.C., Hell, A.F., Braga, M.R., del Campo, E.M., and Casano, L.M. (2016). Contrasting strategies used by lichen microalgae to cope with desiccation/rehydration stress revealed by metabolite profiling and cell wall analysis. *Environ Microbiol* 18: 1546-1560.

Chiou ,Y., Hsieh, M., and Yeh, H. (2010) Effect of algal extracellular polymer substances on UF membrane fouling. *Desalination* 250: 648-652.

Cordeiro, L.M.C., Carbonero, E.R., Sassaki, G.L., *et al.* (2005). A fungus-type β-galactofuranan in the cultivated *Trebouxia* photobiont of the lichen *Ramalina gracilis*. *FEMS Microbiol Lett* 244: 193-198.

Cordeiro LMC, de Oliveira SM, Buchi DF, Iacomini M. 2008. Galactofuranose-rich heteropolysaccharide from *Trebouxia* sp., photobiont of the lichen *Ramalina gracilis* and its effect on macrophage activation. *Int J Biol Macromol* 42: 436-440.

Cordeiro, L.M.C., Sassaki, G.L., and Iacomini, M. (2007). First report on polysaccharides of *Asterochloris* and their potential role in the lichen symbiosis. *Int J Biol Macromol* 41: 193-197.

Cunha, L., and Grenha, A. (2016) Sulfated seaweed polysaccharides as multifunctional materials in drug delivery applications. *Mar Drugs* 14: 42-82.

Cybulska, J., Halaj, M., Cepák, V., Lukavský, J., and Capek, P. (2016). Nanostructure features of microalgae biopolymer. *Starch* 68: 629-636.

Darienko, T., Gustavs, L., Eggert, A., Wolf, W., and Pröschold, T. (2015) Evaluating the Species Boundaries of Green Microalgae (*Coccomyxa*, Trebouxiophyceae, Chlorophyta) Using Integrative Taxonomy and DNA Barcoding with Further

Implications for the Species Identification in Environmental Samples. *PLoS One*. *10*(6):e0127838.

DePriest, P.T. (2004) Early molecular investigations of lichen-forming symbionts: 1986-2001. *Annu Rev Microbiol* 58: 273-301.

Dertli, E., Mayer, M. J., and Narbad, A. (2015) Impact of the exopolysaccharide layer on biofilms, adhesion and resistance to stress in *Lactobacillus johnsonii* FI9785. *BMC Microbiol* 15: 8.

Díaz, E., Vicente-Manzanares, M., Legaz, M. *et al.* (2015) A cyanobacterial β-actin-like protein, responsible for lichenized *Nostoc* sp. motility towards a fungal lectin. *Acta Physiol Plant* 37, 249

Duan, Y.H., Guo, J., Ding, K., *et al.* (2011) Characterization of a wheat HSP70 gene and its expression in response to stripe rust infection and abiotic stresses. *Mol Biol Rep* 38: 301-307.

Duarte, M.E.R., Cardoso, M.A., Noseda, M.D. and Cerezo, A.S. (2001) Structural studies on fucoidans from the brown seaweed *Sargassum stenophyllum*. *Carbohydr. Res.* 333: 281-293.

Erokhina, L.G., Shatilovich, A.V., Kaminskaya, O.P., and Gilichinskii, D.A. (2004) Spectral properties of the green alga *Trebouxia*, a phycobiont of cryptoendolithic lichens in the Antarctic Dry Valley. *Microbiol*, 73(4), 420-424.

Fait, A., Angelovici, R., Less, H., Ohad, I., Urbanczyk-Wochniak, E., Fernie, A.R., and Galili, G. (2006) *Arabidopsis* seed development and germination is associated with temporally distinct metabolic switches. *Plant Physiol* 142: 839-854.

Farrant, J.M., Vander Willigen, C., Loffell, D.A., Bartsch, S., and Whittaker, A. (2003) An investigation into the role of light during desiccation of three angiosperm resurrection plants. *Plant Cell Environ* 26: 1275-1286.

Foyer, C., Lelandais, M., Galap, C., and Kunert, K.J. (1991) Effects of elevated cytosolic glutathione reductase activity on the cellular glutathione pool and photosynthesis in leaves under normal and stress conditions. *Plant Physiol*. 97(3): 863-872.

Friedl, T., & Büdel, B. (2008). Photobionts. In *Lichen Biology*. Nash, T.H.III (ed.) Cambridge: Cambridge University Press pp. 9-26.

Friedl, T., and Rokitta, C. (1997) Species relationships in the lichen alga *Trebouxia* (Chlorophyta, Trebouxiophyceae): molecular phylogenetic analyses of nuclear-encoded large subunit rRNA gene sequences. *Symbiosis* 23: 125-148.

Friedl T. (1987) Thallus development and phycobionts of the parasitic lichen *Diploschistes muscorum*. *Lichenologist*, 19: 183-191.

Gasulla, F., de Nova, P.G., Esteban-Carrasco, A., Zapata, J.M., Barreno, E., and Guera, A. (2009) Dehydration rate and time of desiccation affect recovery of the lichen alga *Trebouxia erici*: alternative and classical protective mechanisms. *Planta* 231: 195-208.

Gray, A.P, Lucas, I.A.N., Seed, R., and Richardson, C.A. (1999) *Mytilus edulis chilensis* infested with *Coccomyxa parasitica* (Chlorococcales, Coccomyxaceae). *J Mollus Stud* 65(3): 289-294.

Halliwell, B., and Cross, C.E. (1994) Oxygen-derived species: their relation to human disease and environmental stress. *Environ Health Perspect* 102(Suppl 10): 5-12.

Helm, R.F., and Potts, M. (2012) Extracellular matrix (ECM), In *Ecology of cyanobacteria II*. Springer Verlag, Berlin, Germany. pp 461-480.

Holzinger, A., and Karsten, U. (2013) Desiccation stress and tolerance in green algae: consequences for ultrastructure, physiological and molecular mechanisms. *Front Plant Sci* 4: 327.

Honegger, R. (2009) Lichen-forming fungi and their photobionts. In *Plant relationships*. Springer, Berlin/Heidelberg, pp 307-333.

Honegger, R. (2008) Morphogenesis. In *Lichen biology. 2nd. ed*., Nash, T.H.III. (ed.). Cambridge University Press, Cambridge y Nueva York. pp 69-93.

Honegger R, Peter, M. and Scherrer, S. (1996) Drought-induced structural alterations at the mycobiont-photobiont interface in a range of foliose macrolichens. *Protoplasma* 190: 221-232.

Honegger, R. (1991) Functional aspects of the lichen symbiosis. *Annu Rev Plant Biol* 42: 553-578.

Honegger R, and Brunner, U. (1981) Sporopollenin in the cell walls of *Coccomyxa* and *Myrmecia* phycobionts of various lichens: an ultrastructural and chemical investigation. *Can J Botany* 59: 2713-2734.

Inupakutika, M.A., Sengupta, S., Devireddy, A.R., Azad, R.K., and Mittler, R. (2016) The evolution of reactive oxygen species metabolism. *J Exp Bot* 67: 5933-5943.

Jiao, G., Yu, G., Zhang, J., and Ewart, H. S. (2011) Chemical structures and bioactivities of sulfated polysaccharides from marine algae. *Mar drugs*, 9(2), 196-223.

Jones, L., and McQueen-Mason, S. (2004) A role for expansins in dehydration and rehydration of the resurrection plant *Craterostigma plantagineum. FEBS Lett* 559:61-65.

Karsten, U., and Holzinger, A. (2012) Light, temperature and desiccation effects on photosynthetic activity and drought-induced ultrastructural changes in the green alga *Klebsormidium dissectum* (Streptophyta) from a high alpine soil crust. *Microb Ecol* 63: 51-63.

Kirk, P.M., Cannon, P.F., Minter, D.W. and Stalpers, J.A. (2008) Dictionary of the Fungi. 10th Edition, Wallingford, CABI, 22.

König, J., and Peveling, E. (1984) Cell walls of the phycobionts *Trebouxia* and *Pseudotrebouxia*: constituents and their localization. *The Lichenologist* 16: 129-144.

Kranner, I., Beckett, R., Hochman, A., and Nash, T.H.III. (2008) Desiccation-tolerance in lichens: a review. *The Bryologist* 111: 576-593.

Kumar, M., Sundaram, S., Gnansounou, E., Larroche, C., and Thakur, I.S. (2018) Carbon dioxide capture, storage and production of biofuel and biomaterials by bacteria: A review. *Bioresource Technol* 247: 1059-1068.

Lahaye, M., and Robic, A. (2007) Structure and function properties of Ulvan, a polysaccharide from green seaweeds. *Biomacromolecules* 8: 1765-1774.

Lahaye, M., Ray, B., Baumberger, S., Quemener, B., and Axelos, M.A.V. (1996) Chemical characterisation and gelling properties of cell wall polysaccharides from species of *Ulva* (Ulvales, Chlorophyta). *Hydrobiologia* 326: 473-480.

Laufer, Z., Beckett, R.P., Minibayeva, F.V., Luthje, S., and Bottger, M. (2006) Occurrence of laccases in lichenized ascomycetes of the *Peltigerineae*. *Mycol Res* 110: 846-853.

Leavitt, S.D., Kraichak, E., Nelsen, M.P., *et al.* (2015) Fungal specificity and selectivity for algae play a major role in determining lichen partnerships across diverse ecogeographic regions in the lichen-forming family *Parmeliaceae* (Ascomycota). *Mol Ecol* 24: 3779-3797.

Liu, Q.M., Yang, Y., Maleki, S.J., Alcocer, M., Xu, S.S., Shi, C.L., *et al.* (2016) Anti-food allergic activity of sulfated polysaccharide from Gracilaria lemaneiformis is dependent on immunosuppression and inhibition of p38 MAPK. *J Agri Food Chem* 64: 4536-4544.

Lombardi AT, Hidalgo TM, Vieira AA. (2005) Copper complexing properties of dissolved organic materials exuded by the freshwater microalgae Scenedesmus acuminatus (Chlorophyceae). Chemosphere; 60(4):453-459.

Lombardi, A.T., and Vieira, A.A. (1999) Lead- and copper-complexing extracellular ligands released by *Kirchneriella aperta* (Chloroccocales, Chlorophyta), *Phycologia* 38:4, 283-288.

Lu, Z.J., and Neumann, P.M. (1998) Water stressed maize, barley and rice seedlings show species diversity in mechanisms of leaf growth inhibition. *J Exp* Bot 49: 1945-1952.

Lutzoni, F., and Vilgalys, R. (1995) *Omphalina* (Basidiomycota, Agaricales) as a model system for the study of coevolution in lichens. *Cryptogam Bot* 5: 71-81.

Malavasi, V., Škaloud, P., Rindi, F., Tempesta, S., Paoletti, M., and Pasqualetti, M. (2016) DNA-Based Taxonomy in Ecologically Versatile Microalgae: A Re-Evaluation of the Species Concept within the Coccoid Green Algal Genus *Coccomyxa* (Trebouxiophyceae, Chlorophyta). *PLoS One* 11(3).

Mann, E.E., and Wozniak, D.J. (2012) *Pseudomonas* biofilm matrix composition and niche biology. *FEMS Microbiol Rev* 36: 893-916.

McCoy, G. (1977) Nutritional, morphological, and physiological characteristics of *Trentepohlia* (I.U. 1227) in axenic culture on defined media: Oregon State University.

McKinnell, J.P., and Percival, E. (1962) Structural investigations o the water-soluble polysaccharide of the green seaweed *Enteromorpha compressa*. *J Chem Soc* , 3141-3148.

Mittler, R. (2002) Oxidative stress, antioxidants and stress tolerance. *Trends Plant Sci* 7: 405-410.

Molins, A., García-Breijo, F.J., Reig-Armiñana, J., del Campo, E.M., Casano, L.M., and Barreno, E. (2013) Coexistence of different intrathalline symbiotic algae and bacterial biofilms in the foliose Canarian lichen *Parmotrema pseudotinctorum. Vieraea* 41: 349-370.

Moore, J.P., Vicré-Gibouin, M., Farrant, J.M., and Driouich, A. (2008) Adaptations of higher plant cell walls to water loss: drought vs desiccation. *Physiol Plantarum* 134: 237-245.

Moore, B.G., and Tischer, R.G. (1964) Extracellular polysaccharides of algae: effects on life-support systems. *Science* 145: 586-587.

Mukhtar, A., Garty, J., and Galun, M. (1994) Does the lichen alga *Trebouxia* occur free-living in nature: further inmmunological evidence. *Symbiosis* 17: 247-253.

Munns, R., Passioura, J.B., Guo, J.M., Chazen, O., and Cramer, G.R. (2000) Water relations and leaf expansion: importance of time scale. *J Exp Bot* 51:1495-1504.

Nash, T.H.III. (2008) Lichen Biology", 2th Edition, Cambridge University Press, Cambridge.

Noda, K., Ohno, N., Tanaka, K., *et al.* (1996) A water-soluble antitumor glycoprotein from *Chlorella vulgaris*. *Planta Med*. 62(5): 423-426.

Peksa, O., and Skaloud, P. (2011) Do photobionts influence the ecology of lichens? A case study of environmental preferences in symbiotic green alga *Asterochloris* (Trebouxiophyceae). *Mol Ecol* 20(18): 3936-3948.

Perez-Garcia, O., Escalante, F.M, de-Bashan, L.E., and Bashan, Y. (2011) Heterotrophic cultures of microalgae: metabolism and potential products. *Water Res*. 45 (1):11-36.

Peveling, E., and Galum, M. (1976) Electron-microscopical studies on the phycobiont *Coccomyxa Schmidle*. *New Phytol* 77: 713-718.

Popper, Z.A., Michel, G., Herve, C., *et al.* (2011) Evolution and diversity of plant cell walls: from algae to flowering plants. *Annu Rev Plant Biol* 62: 567-590.

Printzen, C., Fernández-Mendoza, F., Muggia, L., Berg, G., and Grube, M. (2012) Alphaproteobacterial communities in geographically distant populations of the lichen *Cetraria aculeata*. FEMS Microbiol Ecol 82: 316-325.

Puymaly, A.D. (1924) Le Chlorococcum humicola (Nag.) *Rabenh. Revue Algologique* 1: 107-114.

Raveendran, S., Yoshida, Y., Maekawa, T., and Kumar, D.S. (2013) Pharmaceutically versatile sulfated polysaccharide based bionano platforms. *Nanomedicine* 5: 605-626.

Rai, A.N. (2002) Cyanolichens: nitrogen metabolism. In *Cyanobacteria in Symbiosis*, Rai, A.N. Bergman, B., and Rasmussen, U. (eds). Dordrecht: Kluwer Academic. pp. 97-115.

Rambold, G. and Triebel, D. (1992) The inter-lecanoralean associations. *Bibliotheca Lichenologica* 48: 3-201.

Rikkinen, J., Oksanen, I. and Lohtander, K. (2002). Lichen guilds share related cyanobacterial symbionts. *Science*, 29 (5580), 357.

Rossi F., De Philippis R. (2016) Exocellular polysaccharides in microalgae and cyanobacteria: chemical features, role and enzymes and genes involved in their biosynthesis. *In The Physiology of Microalgae. Developments in Applied Phycology*, Borowitzka M., Beardall J., Raven J. (eds) Springer, Cham.

Ruíz-May, E., Sorensen, I., Fei, Z, Zhang, S., Domozych, D.S., and Rose, J.K.C. (2018) The secretome and n-glycosylation profiles of the charophycean green alga, *Penium margaritaceum*, resemble those of Embryophytes. *Proteomes* 6(2):10.3390/proteomes6020014.

Sacristán, M., Millanes, A.M., Legaz, M.E., and Vicente, C. (2006) A lichen lectin specifically binds to the alpha-1,4-polygalactoside moiety of urease located in the cell wall of homologous algae. *Plant Signal Behav*. 1(1): 23-27. doi:10.4161/psb.1.1.2276.

Saini K.C., Nayaka S., and Bast F. (2019) Diversity of Lichen Photobionts: Their Coevolution and Bioprospecting Potential. In *Microbial Diversity in Ecosystem Sustainability and Biotechnological Applications.* Satyanarayana T., Das S., and Johri B. (eds) Springer, Singapore. pp 307-323.

Singh, R.S., and Walia, A.K. (2014) Characteristics of lichen lectins and their role in symbiosis, *Symbiosis*, 62, 123-134.

Tamaru, Y., Takani, Y., Yoshida, T., and Sakamoto, T. (2005) Crucial role of extracelular polysaccharides in desiccation and freezing tolerance in the terrestrial cyanobacterium *Nostoc commune*. *Appl Environ Microbiol* 71: 7327-7333.

Tremouillaux-Guiller, J., and Huss, V.A. (2007) A cryptic intracellular green alga in *Ginkgo biloba*: ribosomal DNA markers reveal worldwide distribution. *Planta* 226: 553-557.

Tremouillaux-Guiller, J., Rohr, T., Rohr, R., and Huss, V.A. (2002) Discovery of an endophytic alga in *Ginkgo biloba*. *Am J Bot* 89: 727-733.

Tschermak-Woess, E. (1988) The algal partner. In *CRC Handbook of Lichenology*, Vol. 1, M. Galun, M. (ed.) pp. 39-92. Boca Raton: CRC Press.

Turetsky, M.R. (2003) The role of bryophytes in carbon and nitrogen cycling. *Bryologist* 106: 395-409.

Vicré, M., Lerouxel, O., Farrant, J., Lerouge, P., and Driouich, A. (2004) Composition and desiccation-induced alterations of the cell wall in the resurrection plant *Craterostigma wilmsii*. *Physiologia Plantarum* 120: 229-239.

Vicré, M., Sherwin, H.W., Driouich, A., Jaffer, M.A., and Farrant, J.M. (1999) Cell wall characteristics and structure of hydrated and dry leaves of the resurrection plant Craterostigma wilmsii, a microscopical study. *Plant Physiol* 155: 719-726.

Williams, L., Colesie, C., Ullmann, A., Westberg, M., Wedin, M., and Büdel, B. (2017) Lichen acclimation to changing environments: Photobiont switching vs. climate-specific uniqueness in *Psora decipiens*. *Ecol Evo* 7:2560- 2574.

Wingender, J., Neu, T. R., and Flemming, H.C. (eds.). (1999) Microbial Extracellular Polymeric Substances. Springer-Verlag Berlin Heidelberg.

Xiao, R., and Zheng, Y. (2016) Overview of microalgal extracellular polymeric substances (EPS) and their applications.*Biotechnol Adv* 34: 1225-1244.

Yancey, P.H., Clark, M.E., Hand, S.C., Bowlus, R.D., and Somero, G.N. (1982) Living with water stress: evolution of osmolyte systems. *Science* 217:1214-1222.

Anexo I. Ultrastructural and biochemical analyses reveal cell wall remodelling in lichen-forming microalgae submitted to cyclic desiccation–rehydration (Material Suplementario)

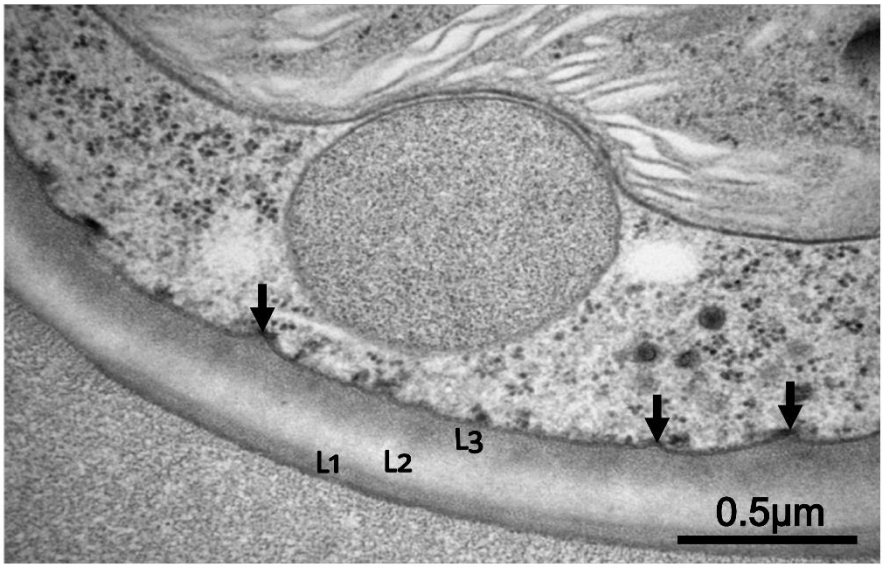

Figure S1: Extended TEM micrograph of TR9 under control conditions, showing detail of characteristic invaginations.

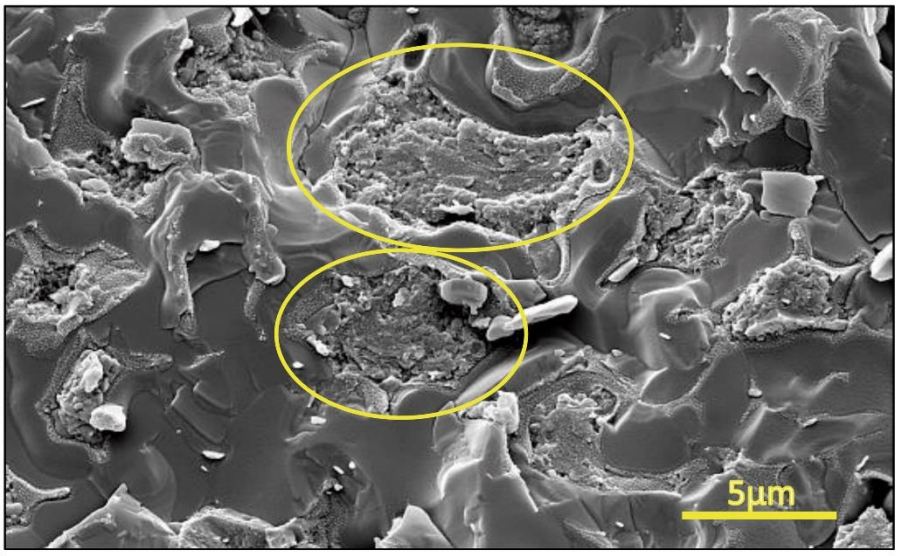

Figure S2: Extended LTSEM micrograph of TR9 under desiccation conditions.

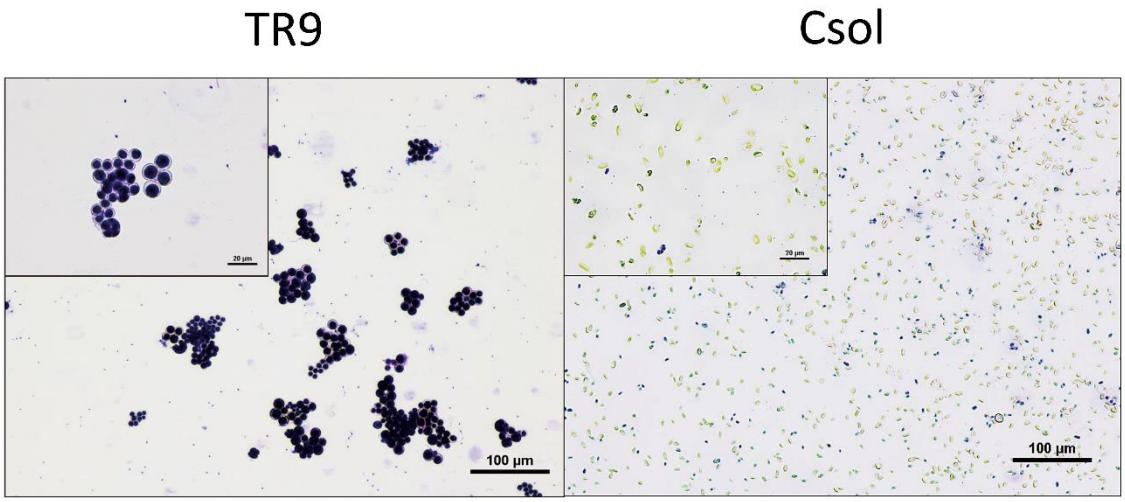

Figure S3: Microscopic images of TR9 and *Csol* cells stained with 0.2 % crystal violet for 24 h.

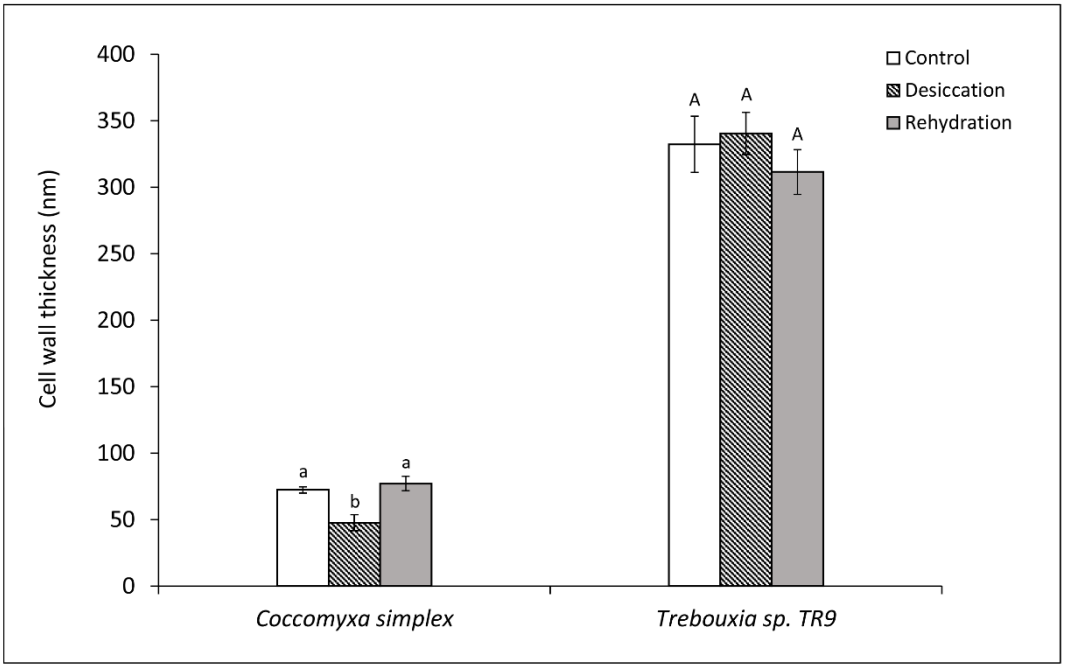

Figure S4: Effects of desiccation and rehydration on cell wall thickness of *Csol* and TR9 microalgae.

Anexo II. Disentangling the role of extracellular polysaccharides in desiccation tolerance in lichen-forming microalgae. First evidence of sulfated polysaccharides and ancient sulfotransferase genes. (Material Suplementario)

Table S1. Oligonucleotide sequences of sulfotransferases employed for transcript quantification by real-time PCR.

Transcript ID	Accession number	Primer sequences (5'-3')	Lenght (pb)
TR9_SulfoTransferase	MN954666	F: GTTCTTGTGATGCCCTACGA R:GTACGCTGGTTCTGATGGAA	82
Csol_SulfoTransferase	MN954665	F: CGGTGCTGTTTGATGTGATG R: GCATCTTGTCCACAATGTGC	96

F, forward; R, reverse. pb, pairs of bases of the amplified sequence.

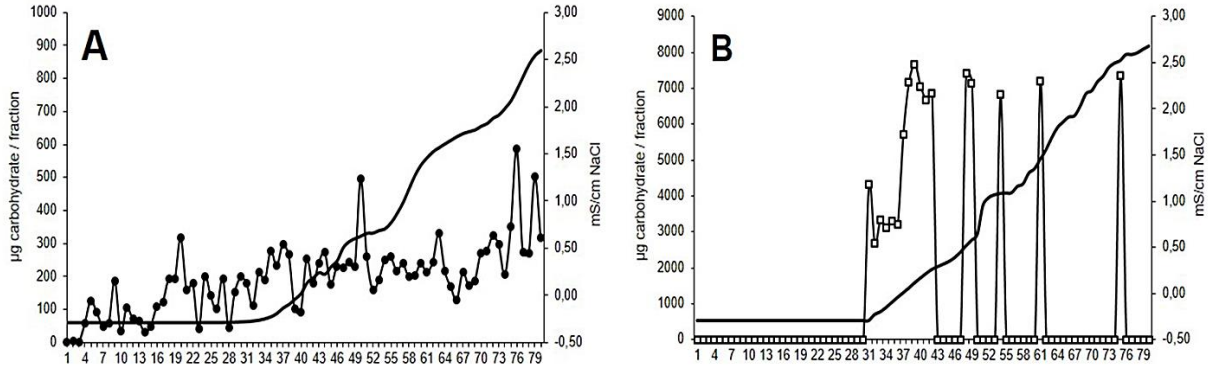

Fig. S1 Anionic profile of EPS from crude EPS from *Trebouxia* sp. TR9 under control conditions (A) and after exposure to desiccation-rehydration conditions (B) separated by Q-Sepharose chromatography.

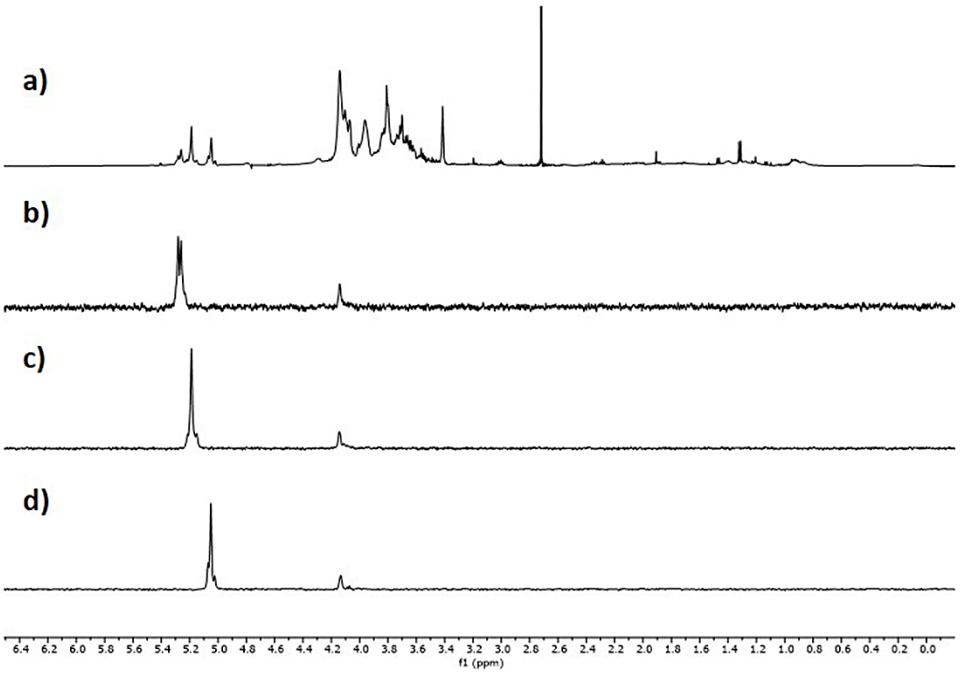

Fig. S2 ^{1}H NMR PRESAT spectrum (D_2O, 500 MHz) (a), and 1D TOCSY spectra (D_2O, 500 MHz) after selective irradiation at 5.26 (b), 5.18 (c) and 5.05 ppm (d) from *Trebouxia* sp. TR9 in desiccation/rehydration conditions.

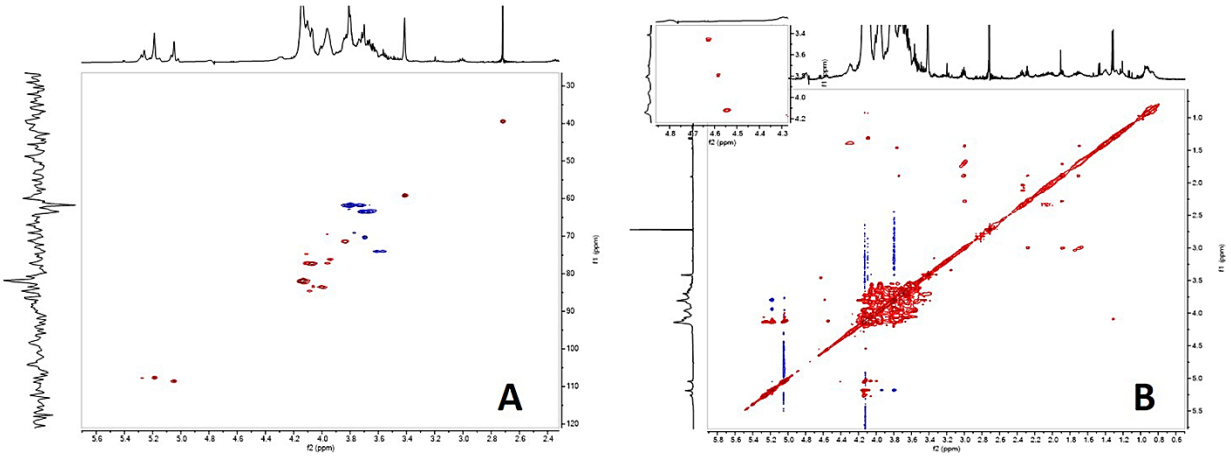

Fig S3 HSQCED PRESAT spectrum (D_2O, 500 MHz) (A) TOCSY PRESAT spectrum (D_2O, 500 MHz) (inset: cross peaks probably due to sulfated positions) (B) of isolated sulfated polymer from *Trebouxia* sp. TR9 in desiccation/rehydration conditions.

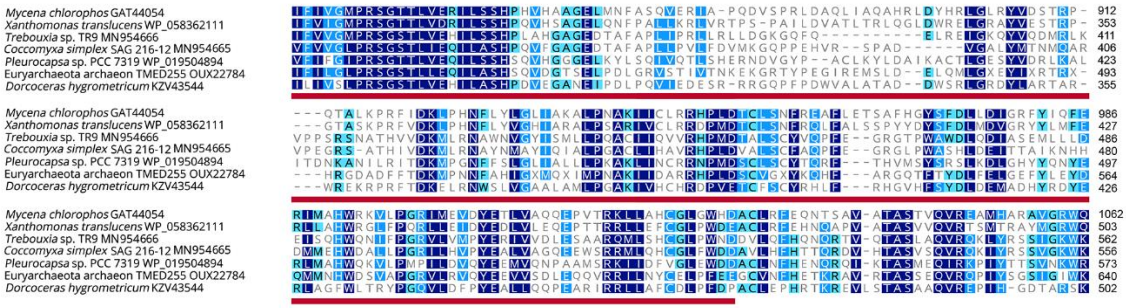

Fig. S4 Alignment of sulfotransferase amino acid sequences from several organisms including *Trebouxia* sp. TR9 and *Coccomyxa simplex*, showing conserved regions. The brown bar indicates the Sulfotransfer_3 domain.

Anexo III. The under-explored extracellular proteome of aero-terrestrial microalgae providesclues on different mechanisms of of desiccdesiccation tolerance in non-model organisms (Marterial Suplementario)del organisms (Material Suplementario)

Table S1: List of proteins identified in the EPS of *Trebouxia* sp. TR9 indicating UniprotKB accessions of orthologous proteins contained in the secretomes of PlantsecKB from different organisms: *Chlamydomonas reinhardtii* (CRE), *Chlorella variabilis* (CVA), *Coccomyxa* sp. C169 (C169), *Coccomyxa simplex* (Csol), *Dorcoceras hygrometricum* (DHY), *Oryza sativa* (OSA), *Arabidopsis thaliana* (ATH), *Physcomitrella patens* (PPA), *Selaginella moellendorffii* (SMO) and *Agaricus bisporus* (AGA). [a]Only similar to chlorophytes (ALG), only similar to land plants (PLN), similat to both chlorophytes and land plants (VIR), similar to fungi (FUN), similar to protists (PRO).

ID	Function	CRE	CVA	C169	CSOL	DHY	OSA	ATH	PPA	SMO	AGA	[a]Exoproteomes
TR9_001	Adhesion				CSOL-018							ALG
TR9_002	Adhesion											ALG
TR9_003a	Expansins			I0YNK2	CSOL-074							ALG
TR9_003b	Expansins											ALG
TR9_004	Expansins			I0YK61								ALG
TR9_005	Expansins			I0Z5V8	CSOL-007b							VIR
TR9_006	Glycosidases						Q2QY88	Q9SG80	A9TTS7		K9I2A0	VIR
TR9_007	Glycosidases		E1ZE88	I0Z5G3								ALG
TR9_008	Glycosidases								A9TAG6		K9I3G2	VIR
TR9_009	Glycosidases	A8IFS8	E1ZAH6									VIR
TR9_010	Glycosidases					KZV21210	Q6Z8I7	Q94KD8		D8SVP1	K9HTD7	PLN
TR9_011a	Glycosidases		E1ZL99	I0YJN3	CSOL-011b		Q0JKM9	Q9M0H6	A9REW6	D8T025	K9I320	VIR
TR9_011b	Glycosidases											VIR
TR9_012	Glycosidases											FUN
TR9_013a	Glycosidases			I0YKD8	CSOL-009							ALG
TR9_013b	Glycosidases											ALG
TR9_013c	Glycosidases											ALG
TR9_013d	Glycosidases											ALG
TR9_014	Glycosidases											FUN
TR9_015	Glycosidases											FUN
TR9_016	Glycosidases											PLN

TR9_017	Glycosidases		E1ZDJ3		CSOL-015a			Q9S7Y7	Q9AVC3		K9HP67	VIR
TR9_018	Hydrolase											ALG
TR9_019	Hydrolases											VIR
TR9_020	Hydrolases			I0Z7C1	CSOL-020							ALG
TR9_021	Hydrolases											ALG
TR9_022	Hydrolases				CSOL-024							PLN
TR9_023	Hydrolases											VIR
TR9_024	Hydrolases					KZV50574	Q0JL46	Q304B9		D8TDK8		PLN
TR9_025	Isomerases			I0YVA5	CSOL-029				A9SSY0	D8S966	K9I2R3	PLN
TR9_026	Isomerases				CSOL-030							VIR
TR9_027	Isomerases	A8JBH7	E1ZUD2		CSOL-031				A9SGV8	D8RRA3		PLN
TR9_028	Lectins											VIR
TR9_029	Lectins											PLN
TR9_030	Lectins											VIR
TR9_031	Lectins											PLN
TR9_032	Oxidoreductases											ALG
TR9_033	Oxidoreductases											PLN
TR9_034	Oxidoreductases											ALG
TR9_035	Oxidoreductases				CSOL-035							PLN
TR9_036	Oxidoreductases								A9RYW1	D8RH97	K9H789	PLN
TR9_037	Oxidoreductases				CSOL-036							ALG
TR9_038	Oxidoreductases	A8IDT6							A9TAS6			VIR
TR9_039	Oxidoreductases											VIR
TR9_040	Phosphatases											VIR
TR9_041a	Phosphatases		E1ZMF3	I0Z0Q6	CSOL-040	KZV48951		Q5MAU8	A9RY38	D8RA20		VIR
TR9_041b	Phosphatases											VIR
TR9_042	Phosphatases										K9HT88	FUN
TR9_043	Phosphatases			I0YPZ7		KZV16493		Q9LXI7		D8SYQ0		PLN
TR9_044	Protease inhibitors			I0YL91								VIR

TR9_045	Protease inhibitors											PLN
TR9_046	Proteases	A8JGQ3	E1ZFH9	I0YVT7	CSOL-043b							ALG
TR9_047a	Proteases	A8I5R9	E1Z6N8	I0YPQ4	CSOL-046a	KZV54558	Q076Q8		A9RNZ6	D8QW56		VIR
TR9_047b	Proteases											VIR
TR9_048	Proteases											PLN
TR9_049	Proteases											PLN
TR9_050	Proteases											PLN
TR9_051	Proteases		E1ZSU4	I0YKM3	CSOL-048							VIR
TR9_052	Proteases	Q7XB41	E1ZR39	I0YLR8	CSOL-044	KZV43689		Q9XEC4	A9SM45	D8QZN2	K9HNT0	VIR
TR9_053a	Proteases	A8HP98		I0YRC3	CSOL-007a	KZV51634		Q9M099	A9RCP9	D8QPJ4	K9HXS5	PLN
TR9_053b	Proteases											PLN
TR9_054	Seed storage			I0Z8V3	CSOL-053							VIR
TR9_055	Seed storage											PLN
TR9_056	Transferases											PLN
TR9_057	Transferases											PRO
TR9_058	Transferases	A8JEK5		I0YML6	CSOL-057							VIR
TR9_059	Other				CSOL-002							ALG
TR9_060	Other			I0Z8G7	**CSOL-059b**					D8R4F9		VIR
TR9_061	Other											VIR
TR9_062	Other											PLN
TR9_063	Other				**CSOL-018**							VIR
TR9_064	Other			I0YQC5								ALG
TR9_065	Other											VIR
TR9_066	Other											FUN
TR9_067	Other											PLN
TR9_068	Other											ALG
TR9_069	Other											PRO
TR9_070	Other											---
TR9_071a	Other											FUN
TR9_071b	Unknown											---

TR9_071c	Unknown								FUN
TR9_072	Unknown								PLN
TR9_073a	Unknown		E1ZFQ7	I0YVE6	CSOL-069	KZV19404		D8R2V0	ALG
TR9_073b	Unknown								ALG
TR9_074	Unknown	A8ICQ1	E1ZD15						ALG
TR9_075	Unknown								---
TR9_076	Unknown								---
TR9_077	Unknown								---
TR9_078	Unknown								ALG
TR9_079a	Unknown								---
TR9_079b	Unknown								---
TR9_080	Unknown								---
TR9_081	Unknown			I0Z8F9					ALG
TR9_082	Unknown								PRO
TR9_083	Unknown								---
TR9_084	Unknown								VIR
TR9_085	Unknown								PRO
TR9_086	Unknown								ALG
TR9_087	Unknown								PRO
TR9_088	Unknown								ALG
TR9_089	Unknown								FUN
TR9_090	Unknown		E1ZA60		CSOL-041				ALG
TR9_091	Unknown				CSOL-101				PLN
TR9_092	Unknown								FUN
TR9_093	Unknown								VIR
TR9_094	Unknown								PRO
TR9_095	Unknown								FUN
TR9_096	Unknown								ALG
TR9_097	Unknown								---
TR9_098	Unknown								---

TR9_099	Unknown	---

Table S2: List of proteins identified in the EPS of *Coccomyxa simplex* SAG 216-12 indicating UniprotKB accessions of orthologous proteins contained in the secretomes of PlantsecKB from different organisms: *Chlamydomonas reinhardtii* (CRE), *Chlorella variabilis* (CVA), *Coccomyxa* sp. C169 (C169), *Coccomyxa simplex* (Csol), *Dorcoceras hygrometricum* (DHY), *Oryza sativa* (OSA), *Arabidopsis thaliana* (ATH), *Physcomitrella patens* (PPA), *Selaginella moellendorffii* (SMO) and *Agaricus bisporus* (AGA). [a]Only similar to chlorophytes (ALG), only similar to land plants (PLN), similar to both chlorophytes and land plants (VIR), similar to fungi (FUN), similar to protists (PRO).

ID	FUNCTION	CRE	CVA	TR9	C169	DHY	OSA	ATH	SMO	PPA	AGA	[a]Exoproteomes
CSOL-001	Adhesion				I0Z3I6							ALG
CSOL-002	Adhesion			TR9_059								ALG
CSOL-003	Adhesion				I0YJF6							ALG
CSOL-004	Adhesion											PLN
CSOL-005	Adhesion											ALG
CSOL-006	Expansins		E1ZAG9		I0Z1H6							VIR
CSOL-007a	Expansins			TR9_005	I0Z5V8							VIR
CSOL-007b	Expansins											VIR
CSOL-008	Glycosidases					KZV33424	Q2R3E0		D8RSH3			PLN
CSOL-009	Glycosidases											ALG
CSOL-010	Glycosidases											VIR
CSOL-011a	Glycosidases			TR9_011a	I0YNM9		Q0JKM9	Q9FJZ3	D8RV06	A9REW6	K9I320	VIR
CSOL-011b	Glycosidases											VIR
CSOL-011c	Glycosidases											VIR
CSOL-011d	Glycosidases											VIR
CSOL-012	Glycosidases				I0Z4Y9							ALG
CSOL-013	Glycosidases				I0Z329							ALG
CSOL-014	Glycosidases				I0Z119							VIR
CSOL-015a	Glycosidases		E1ZDJ3	TR9_017				Q9S7Y7		A9SI09	K9I6V6	VIR
CSOL-015b	Glycosidases											VIR
CSOL-016	Glycosidases				I0YYG3							ALG
CSOL-017	Glycosidases											VIR
CSOL-018	Glycosidases			TR9_063								ALG
CSOL-019	Hydrolases				I0YWV8						K9I776	VIR
CSOL-020	Hydrolases			TR9_020	I0Z7C1							ALG
CSOL-021	Hydrolases											VIR
CSOL-022	Hydrolases		E1Z502		I0Z9F7				D8RLK4			VIR
CSOL-023	Hydrolases							Q9SRM5				PLN
CSOL-024	Hydrolases			TR9_022								PLN

CSOL-025	Hydrolases				I0Z737							VIR
CSOL-026	Hydrolases				I0Z6Z3							ALG
CSOL-027a	Hydrolases		E1ZCH2		I0Z6Z4							ALG
CSOL-027b	Hydrolases											ALG
CSOL-027c	Hydrolases											ALG
CSOL-028	Hydrolases											ALG
CSOL-029	Isomerases			TR9_025	I0YVA5				D8S966	A9SSY0	K9I2R3	PLN
CSOL-030	Isomerases		E1ZM99	TR9_026		KZV23333					K9HES8	VIR
CSOL-031	Isomerases	A8JBH7	E1ZUD2	TR9_027			Q75M08		D8RRA3			VIR
CSOL-032	Oxidoreductases				I0YKS3							VIR
CSOL-033	Oxidoreductases				I0YS94							ALG
CSOL-034	Oxidoreductases											VIR
CSOL-035	Oxidoreductases			TR9_035	I0YJ58							VIR
CSOL-036	Oxidoreductases			TR9_037								VIR
CSOL-037	Oxidoreductases				I0Z9F5		Q8RYM9	Q84J37	D8SRL2	A9SZY8	K9I022	VIR
CSOL-038	Oxidoreductases											VIR
CSOL-039	Phosphatases											VIR
CSOL-040	Phosphatases		E1ZMF3	TR9_041b	I0Z0Q6	KZV16493		Q5MAU8	D8RA20			VIR
CSOL-041	Phosphorylases/Kinases		E1ZA60	TR9_090								ALG
CSOL-042	Protease inhibitors											PLN
CSOL-043a	Proteases	A8JGQ3	E1ZFH9	TR9_046	I0Z479							VIR
CSOL-043b	Proteases											ALG
CSOL-044	Proteases	A8IT96	E1ZR39	TR9_052	I0YLR8	KZV43689		Q9XEC4	D8T8Z0	A9SM45	K9HPY6	VIR
CSOL-045	Proteases											PRO
CSOL-046a	Proteases	A8I5R9	E1Z6N8	TR9_047a	I0YPQ4	KZV54558	Q076Q8		D8QW56	A9RNZ6		VIR
CSOL-046b	Proteases											VIR
CSOL-046c	Proteases											VIR
CSOL-047	Proteases	A8HQ73				KZV51708	Q69QQ2		D8RQT8			VIR
CSOL-048	Proteases		E1ZSU4	TR9_051	I0YKM3							VIR
CSOL-049	Proteases				I0YUE2							ALG
CSOL-050	Proteases			TR9_053a	I0YRC3	KZV51634		Q9M099	D8SKY0	A9SNG8		PLN
CSOL-051	Proteases				I0YQR4							ALG
CSOL-052	Proteases											ALG
CSOL-053	Seed storage			TR9_054	I0Z8V3							VIR
CSOL-054	Transferases											PLN
CSOL-055	Other											PRO
CSOL-056	Other				I0YQ41							ALG

CSOL-057	Other	A8JEK5		TR9_058	I0YML6					VIR
CSOL-058	Other									FUN
CSOL-059a	Other			TR9_061	I0YQP4			D8R4F9		VIR
CSOL-059b	Other									VIR
CSOL-060	Other				I0Z143					ALG
CSOL-061	Other									ALG
CSOL-062	Other				I0YW16					ALG
CSOL-063	Other									ALG
CSOL-064	Other									ALG
CSOL-065	Other									PLN
CSOL-066	Other				I0Z732			D8QU61		VIR
CSOL-067	Other									ALG
CSOL-068	Other	A8IMY7					Q9FEG7		A9TXG9	VIR
CSOL-069	Other		E1ZFQ7	TR9_073a	I0YVE6	KZV19404		D8R2V0		VIR
CSOL-070	Other				I0YSQ3					VIR
CSOL-071	Other				I0YID5					VIR
CSOL-072	Other									PRO
CSOL-073	Unknown									---
CSOL-074	Unknown			TR9_003a	I0YNK2					ALG
CSOL-075	Unknown				I0Z3I2					ALG
CSOL-076	Unknown				I0YJ50					ALG
CSOL-077	Unknown									ALG
CSOL-078	Unknown				I0YZ62					ALG
CSOL-079	Unknown				I0Z321					ALG
CSOL-080a	Unknown				I0YJ96					ALG
CSOL-080b	Unknown									ALG
CSOL-080c	Unknown									ALG
CSOL-081	Unknown									---
CSOL-082	Unknown									ALG
CSOL-083a	Unknown				I0YKS0					ALG
CSOL-083b	Unknown									ALG
CSOL-084a	Unknown				I0YLX2					ALG
CSOL-084b	Unknown									ALG
CSOL-085	Unknown				I0YTL7					ALG
CSOL-086	Unknown				I0Z6A7					ALG
CSOL-087	Unknown									FUN
CSOL-088	Unknown				I0Z2H5					VIR

CSOL-089a	Unknown		I0Z979	ALG
CSOL-089b	Unknown			ALG
CSOL-090	Unknown		I0YJR5	ALG
CSOL-091	Unknown		I0YK40	ALG
CSOL-092	Unknown		I0YW26	ALG
CSOL-093	Unknown		I0YNT4	ALG
CSOL-094	Unknown			ALG
CSOL-095	Unknown			ALG
CSOL-096	Unknown			ALG
CSOL-097	Unknown			PRO
CSOL-098	Unknown			ALG
CSOL-099	Unknown		I0Z961	ALG
CSOL-100	Unknown			---
CSOL-101	Unknown	TR9_091		---
CSOL-102	Unknown			VIR
CSOL-103	Unknown			PRO
CSOL-104	Unknown			---
CSOL-105	Unknown			ALG

Anexo IV. Otras publicaciones y comunicaciones científicas relacionadas con la Tesis Doctoral.

1. **González-Hourcade, M.,** del Campo, E.M., Casano, LM. (2018). Desiccation-rehydration driven cell wall remodelling in lichen-forming microalgae. SEB's Annual Meeting. Florencia, Italia.

2. Póster. Gasulla, F., Hell, A.F., **González-Hourcade, M.,** del Campo, E.M., and Casano , L.M. (2018) Assessing the different degree of desiccation-tolerance of two lichen photobionts: response of the antioxidant system and gene regulation. In Resurrection plants: Hope for crop drought tolerance (ReHOPE) Plovdiv, Bulgaria. Federation of European Biochemical Societies.

3. **González-Hourcade, M**., del Campo, E.M., Casano, LM. (2019). Characterization of extracellular components in desiccation-tolerant lichen microalgae**.** XXII Symposium of Cryptogamic Botany. Lisboa, Portugal

4. **González-Hourcade, M.**, Braga, M.R., del Campo, E.M., Patiño, C., Ascaso, C., Casano, LM. (2019). Remodelación de la pared celular de microalgas liquénicas tolerantes a la desecación. En*: Séptimas Jornadas de Jóvenes Investigadores de la Universidad de Alcalá*, *Ciencias e Ingenierías* (Guerrero Ortega, A., Ros Magán, G., Ruiz Benito, P., Pascual Vives, F.,Tejedor Martínez, C., y Tabernero Magro, V. (eds)) (p.183) I.S.B.N.: 978-84-177729-43-1.

5. Hell, A.F., Gasulla, F., **González-Hourcade, M.,.**del Campo, E.M., Centeno, D.C., and Casano, L.M. (2019). Tolerance to cyclic desiccation in lichen microalgae is related to habitat preference and involves specific priming of the antioxidant system. *Plant Cell Physiol.* 60: 1880-1891.

6. Martínez-Alberola, F., Barreno, E., Casano, L.M., Gasulla, F., Molins, A., Moya, P., **González-Hourcade, M.,** and del Campo, E.M. (2020). The chloroplast genome of the lichen-symbiont microalga *Trebouxia* sp. TR9 (Trebouxiophyceae, Chlorophyta) shows short inverted repeats with a single gene and loss of the rps4 gene, which is encoded by the nucleus. *J Phycol* 56: 170-184.

PCP
PLANT & CELL PHYSIOLOGY

Tolerance to Cyclic Desiccation in Lichen Microalgae is Related to Habitat Preference and Involves Specific Priming of the Antioxidant System

Aline F. Hell[1,2], Francisco Gasulla[1], María González-Hourcade[1], Eva M. del Campo[1], Danilo C. Centeno[2] and Leonardo M. Casano [1,*]

[1]Department of Life Sciences, University of Alcalá, Alcalá de Henares, Madrid, Spain
[2]Centre of Natural Sciences and Humanities, Federal University of ABC, São Bernardo do Campo, SP, Brazil
*Corresponding author: E-mail, leonardo.casano@uah.es; Fax, +34-91-8855066.
(Received February 25, 2019; Accepted May 15, 2019)

Regular Paper

Oxidative stress is a crucial challenge for lichens exposed to cyclic desiccation and rehydration (D/R). However, strategies to overcome this potential stress are still being unraveled. Therefore, the physiological performance and antioxidant mechanisms of two lichen microalgae, *Trebouxia* sp. (TR9) and *Coccomyxa simplex* (Csol), were analyzed. TR9 was isolated from *Ramalina farinacea*, a Mediterranean fruticose epiphytic lichen adapted to xeric habitats, while Csol is the phycobiont of *Solorina saccata*, a foliaceous lichen that grows on humid rock crevices. The tolerance to desiccation of both species was tested by subjecting them to different drying conditions and to four consecutive daily cycles of D/R. Our results show that a relative humidity close to that of their habitats was crucial to maintain the photosynthetic rates. Concerning antioxidant enzymes, in general, manganese superoxide dismutases (MnSODs) were induced after desiccation and decreased after rehydration. In TR9, catalase (CAT)-A increased, and its activity was maintained after four cycles of D/R. Ascorbate peroxidase activity was detected only in Csol, while glutathione reductase increased only in TR9. Transcript levels of antioxidant enzymes indicate that most isoforms of MnSOD and FeSOD were induced by desiccation and repressed after rehydration. *CAT2* gene expression was also upregulated and maintained at higher levels even after four cycles of D/R in accordance with enzymatic activities. To our knowledge, this is the first study to include the complete set of the main antioxidant enzymes in desiccation-tolerant microalgae. The results highlight the species-specific induction of the antioxidant system during cyclic D/R, suggesting a priming of oxidative defence metabolism.

Keywords: Antioxidant • Coccomyxa • Desiccation tolerance • Lichen microalga • Priming • Trebouxia.

Introduction

The water status of lichens varies passively with surrounding environmental conditions as they are subject to continuous and relatively rapid cycles of desiccation and rehydration (D/R). During desiccation, most lichens enter into a latent state, named anhydrobiosis, until the water becomes available again and then they recover their normal metabolism. This behavior is lethal for most living beings; however, most lichens orchestrate a repertoire of physiological, biochemical and molecular mechanisms to prevent cellular damage during desiccation. In this context, some of the mechanisms include the accumulation of sugars, and some derivatives enable maintenance of cell membrane integrity and glass state formation (Centeno et al. 2016). In addition, the constitutive synthesis of late-embryogenesis-abundant proteins helps to prevent protein denaturation (Gasulla et al. 2009, Carniel et al. 2016), and the presence of polar oligogalactolipids preserves the thylakoid structure (Gasulla et al. 2016).

One of the most important challenges that lichens in general, and their microalgae in particular, have to cope with is the oxidative stress associated with changes in water content. Aerobic metabolism, such as photosynthesis and cell respiration, unavoidably and constantly generates reactive oxygen species (ROS) in chloroplasts, mitochondria, peroxisomes, etc. (Gill and Tuteja 2010, Inupakutika et al. 2016). Under optimal conditions, ROS do not cause cellular damage since they can be kept at life-compatible levels by antioxidant mechanisms (Inupakutika et al. 2016 and references therein). However, redox homeostasis can be perturbed by different stress factors such as D/R. During the initial part of their rapid dehydration and the first minutes upon rehydration, a burst of intracellular ROS occurs in lichen microalgae (Weissman et al. 2005a, Catalá et al. 2010, Álvarez et al. 2015). This occurs in part because lichen algae do not significantly modify their content of photosynthetic pigments during D/R. Therefore, the chloroplast can increase its ROS formation rate since CO_2 fixation is rapidly impaired, whereas light continues to be absorbed by chlorophyll and electrons transported to O_2 at both PSI and PSII (Mubarakshina Borisova et al. 2012, Roach and Krieger-Liszkay 2014, Smirnoff and Arnaud 2019), forming primarily singlet oxygen, superoxide anion radicals ($O_2^{\bullet -}$) and H_2O_2, and secondarily, hydroxyl radical ($OH^{\bullet}$), the most reactive and toxic ROS. In addition, $OH^{\bullet}$ can also be generated at a neutral pH by the Fenton reaction between H_2O_2 and $O_2^{\bullet -}$ catalyzed by transition metals such as Fe (Fe^{2+}, Fe^{3+}) (Inupakutika et al. 2016).

Plant Cell Physiol. 00(0): 1–12 (2019) doi:10.1093/pcp/pcz103, Advance Access publication on 24 May 2019, available online at https://academic.oup.com/pcp

The increased and unbalanced formation of ROS is thought to be one of the most important sources of damage to proteins, lipids and nucleic acids, which ultimately results in cellular injury and death (Gill and Tuteja 2010). Lichens employ several mechanisms to avoid ROS formation, such as the activation of the xanthophyll cycle (Fernández-Marín et al. 2010) and alternative mechanisms that dissipate the excess of energy during desiccation (Gasulla et al. 2009, Komura et al. 2010, Heber et al. 2011). Complementarily, scavenging of formed ROS can be carried out by enzymatic or nonenzymatic antioxidants. Among the nonenzymatic constituents, reduced glutathione (GSH) (Kranner et al. 2005), polyols, phenolic compounds and ascorbic acid (Centeno et al. 2016) are within the most important water-soluble antioxidants in lichens. The principal enzymatic constituents include superoxide dismutase (SOD), ascorbate peroxidase (APx), catalase (CAT), glutathione reductase (GR), monodehydroascorbate reductase and dehydroascorbate reductase. There is a profuse and compelling body of evidence that supports a positive correlation between drought resistance and the activity of the antioxidant system in vascular plants (e.g. Kranner et al. 2002, Farrant et al. 2003, Dinakar and Bartels 2013, Georgieva et al. 2017).

It could be expected that lichens as holobionts and their microalgae partners, in particular, show higher levels of desiccation tolerance (DT) and have higher antioxidant enzymatic activity than less-tolerant species. However, from the few comparative studies carried out with lichens and/or isolated photobionts, no clear relationship between DT and levels of antioxidant enzymes can be formed. Mayaba and Beckett (2001) observed that the activities of SOD, CAT and APx were similar under wetting and drying conditions in *Peltigera polydactyla*, *Ramalina celastri* and *Teloschistes capensis*, which thrive in moist, xeric and extremely xeric habitats, respectively. Kranner (2002) did not observe a correlation between GR activity and the different degrees of DT of three lichens, *Lobaria pulmonaria*, *P. polydactyla* and *Pseudevernia furfuracea*. Weissman et al. (2005b) even reported that after rehydration, *Ramalina lacera* loses almost all CAT activity, and SOD activity decreases by 50–70%. On the other hand, in cultured isolated photobionts, antioxidants and antioxidant-related activities seem to be less effective than those of lichenized photobionts, and a clear activation of the studied antioxidant enzymes in response to desiccation has not been observed (Kranner et al. 2005, Gasulla et al. 2009). Carniel et al. (2016) also observed, through a transcriptomic analysis, that only one antioxidant gene, a manganese superoxide dismutase (*MnSOD*), was overexpressed in the lichen alga *Trebouxia gelatinosa* in response to dehydration. More recently, the same group has confirmed this result and reported an increase in transcript levels corresponding to an APx during dehydration (Banchi et al. 2018). In summary, within the limits of these scarce and partial data, it seems clear that high concentrations of antioxidants and/or antioxidant enzyme activities do not indicate 'per se' that a species could be tolerant to desiccation-induced oxidative stress. Alternatively, and in line with the proposed by Kranner et al. (2002) and Kranner et al. (2003), the ability to maintain, during desiccation, or rapidly re-establish, during rehydration, some critical levels of antioxidants and enzyme activities seems to be characteristic of well-adapted species. Accordingly, recent results with the resurrection plant *Haberlea rhodopensis* demonstrated that the polyphenolic antioxidant and antioxidant enzymes involved in the ascorbate-glutathione cycle increased during desiccation, peaking at an air-dry state (Georgieva et al. 2017). It is proposed that the induction of antioxidant metabolism during dehydration can protect the plant from oxidative stress during drying and afterwards during the early stages of rehydration.

In the present study, we employed two microalgae, *Trebouxia* sp. TR9 (TR9) and *Coccomyxa simplex* (Csol), isolated from lichens with different hydric requirements. TR9 is a phycobiont of the lichen *Ramalina farinacea*, a Mediterranean epiphytic fruticose ascolichen that can withstand long desiccation periods and frequent daily D/R cycles. On the other hand, Csol was isolated from *Solorina saccata*, a foliaceous lichen that is widely distributed within relatively more humid areas from the Mediterranean mountains to the Arctic where it grows on calcareous rocks, typically in crevices and always under sheltered conditions (Krog and Swinscow 1986). In a previous study, performed with these algae species exposed to one cycle of desiccation at 25% relative humidity (RH) followed by rehydration at saturating humidity, metabolite profiling and cell wall analysis suggested that TR9 could be predisposed to tolerate desiccation mainly by constitutive mechanisms together with some inducible components (Centeno et al. 2016). In contrast, in Csol, inducible responses seem to play a more crucial role, suggesting that each microalga has evolved different strategies of DT according to the water regimen of their habitats. Although the ecology of *R. farinacea* and *S. saccata* and the physiological studies (Centeno et al. 2016) indicated that TR9 and Csol differ in their DT degree, it has never been empirically demonstrated. In addition, a common feature of studies concerning the effects of desiccation on isolated phycobionts is that algae are grown on semi-solid cultures for weeks and then submitted to a single cycle of D/R (e.g. Carniel et al. 2016, Centeno et al. 2016, Banchi et al. 2018). However, in their natural habitats, they are exposed to seasonal and/or almost continuous daily cycles of D/R. Thus, the initial steps in the present study were to test the tolerance of both phycobionts to different drying conditions. Thereafter, we followed an approach that tended to mimic the daily changes in the water regimen that the selected microalgae could experience in their natural habitat. TR9 and Csol underwent consecutive daily cycles of D/R under 'species-specific' conditions of dehydration for each alga (22–25% RH for TR9 and 55% RH for Csol) to further determine their degree of DT (estimated as recovery of photochemical efficiency upon rehydration). Additionally, we carried out a comparative analysis of the activity of the main antioxidant enzymes and their gene expression during four cycles of D/R to shed light on the role of the antioxidant system in the acquisition of DT in lichen algae.

Results and Discussion

Assessing the desiccation tolerance of TR9 and CsoI, two lichen microalgae with different habitat preferences, through their photosynthetic response to different environmental conditions

To assess the possible differences in the degree of DT between two ecologically distinct lichen microalgae, isolated TR9 and CsoI were dried and maintained up to 3 months in atmospheres with a RH of 22–25%, 37% (these RHs are within the range of RH during Mediterranean summer days) and 56% (this RH is within the range of that during summer days in *S. saccata* habitats). The capacity to recover the photosynthetic activity (estimated as the maximum quantum efficiency yield of PSII, F_v/F_m) upon rehydration was monitored up to 3 months (**Fig. 1A–C**). Isolated TR9 microalgae showed higher initial F_v/F_m rates (0.75) compared with CsoI microalgae (0.65). In addition, TR9 microalgae were capable of recovering the photosynthetic activity after desiccation for 1, 2 and 3 months, even when different air-dried conditions were applied (25%, 37% and 56% RH), showing a slight decrease over time (**Fig. 1A–C**). In contrast, CsoI microalgae showed a drastic drop in F_v/F_m ratio from the first month of exposure at both 25% and 37% RH (**Fig. 1A, B**), suggesting that the photosynthetic machinery of this species becomes irreversibly damaged during desiccation under such conditions. However, when exposed to 56% RH, CsoI microalgae demonstrated a better recovery of photosynthetic levels (**Fig. 1C**). These results support the idea that TR9 and CsoI microalgae have a higher physiological recovery when exposed to conditions similar to those of their natural habitats. TR9 is a phycobiont of *R. farinacea*, a lichen adapted to xeric habitats and usually subjected to daily/seasonal cycles of D/R, while CsoI thrives within *S. saccata*, a lichen that grows in relatively more humid areas (Krog and Swinscow 1986, Centeno et al. 2016). These results agree with those of Gray et al. (2007), who investigated the photorecovery of phylogenetically close desert and aquatic algae and found that dehydration-tolerant algae recovered photosynthesis upon rehydration from a desiccated state faster than their aquatic relatives.

In view of the abovementioned results and those from a previous study in which, when desiccated under 25% RH, CsoI lost water much faster than TR9 (Centeno et al. 2016), a new set of experiments was performed aiming to evaluate the hydric status and the photosynthetic recovery capacity after up to four cycles of D/R within a more natural context. Therefore, desiccation was performed under species-specific RH (25% to TR9 and 56% to CsoI) and two different drying velocities (slow and rapid). The results showed that there were no differences between the RWC (RWC) curves of both species; 50% of the total desiccation (50D) occurred after approximately 3–4 h at slow desiccation and between 1 and 2 h at rapid desiccation (**Fig. 1D, E**). These results contrast with previous results (Centeno et al. 2016) and emphasize the notion that the hydric behavior of each lichen algae seems to be highly dependent not only on the RH during desiccation in absolute terms but also on the temporal evolution of this parameter during drying.

Indeed, when submitted to rapid desiccation conditions along four D/R cycles, CsoI microalgae did not completely recover its initial F_v/F_m level, which seemed to decrease after subsequent cycles, reaching 0.379 after 16 h rehydration in the last cycle (**Fig. 1G**). In contrast, TR9 microalgae could maintain their photosynthetic activity even after four cycles of D/R (~0.700). In addition, TR9 appeared to recover the photosynthetic activity faster, with a complete recovery after 1 h of rehydration, while in CsoI, the recovery appeared to be progressive and partial (**Fig. 1G**). Additional experiments in which the F_v/F_m were also measured during four D/R cycles employing other RH conditions (RH 90–50%, 50%, 30% and 10%) yielded similar results (Supplementary Fig. S3). These data support the idea that TR9 microalgae fully recover their photosynthetic capacity independently of the humidity condition applied, contrasting with the more sensitive behavior of CsoI.

Moreover, when subjected to daily slow desiccation cycles in air-dried conditions similar to those of their natural habitat (**Fig. 1F**), both species were able to fully recover their photosynthetic rates after the four D/R cycles. In poikilohydric organisms, survival to desiccation is considered to rely on the presence of constitutive mechanisms and the induction of mechanisms of repair only after R (Oliver et al. 1998, Farrant and Moore 2011). Our results suggest that drying velocity may play a crucial role in CsoI microalgae function (**Fig. 1F, G**), which could be related to the induction of a protective system during the desiccation step.

Both microalgae presented low F_v/F_m when completely desiccated (100D) (**Fig. 1F, G**) under slow and rapid drying conditions. It is known that dehydration suppresses photosynthesis in both desiccation-sensitive and desiccation-tolerant algae (Kranner et al. 2003, Gray et al. 2007, Holzinger et al. 2014). However, as reported by Challabathula et al. (2018) 'although the photosynthetic rates decrease in both desiccation-tolerant and sensitive plants during drought, the remarkable difference lies in the complete recovery of photosynthesis after rehydration in desiccation-tolerant plants'.

On the molecular and cellular level, the desiccation process is associated with increased ROS formation as by-products of metabolism, particularly in the electron transport chains of respiration and photosynthesis (Kranner et al. 2008). In the same way, during rehydration, a rapid and important increase in ROS can also occur (Weissman et al. 2005a, Catalá et al. 2010, Álvarez et al. 2015). Therefore, within the wide range of DT mechanisms to cope with D/R, one of the most important is based on a coordinated regulation of the antioxidant system to preserve redox homeostasis (Alscher et al. 2002, Gechev et al. 2013).

The following step in our research was aimed at providing insights into the role of the antioxidant system as a species-specific strategy of TR9 and CsoI to cope with D/R. We carried out a comparative analysis of the activity of the main

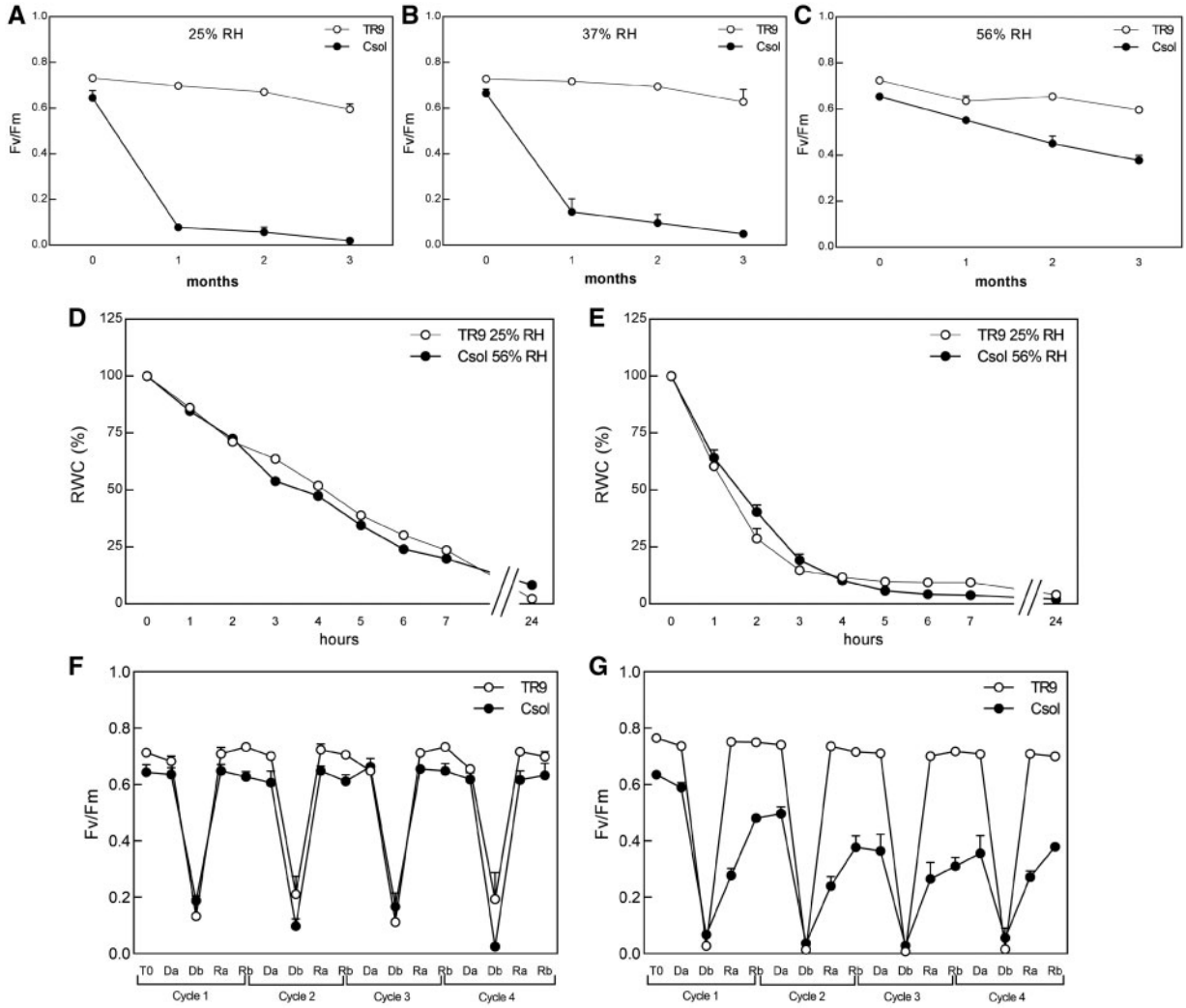

Fig. 1 Effects of the desiccation condition on the RWC and maximal photochemical yield of PSII (F_v/F_m) in TR9 and Csol microalgae. (A–C) F_v/F_m recovery after rehydration from desiccation under 25%, 37% and 56% RH for up to 3 months. RWC evolution at slow (D) and rapid desiccation (E) conditions. F_v/F_m changes in microalgae submitted to slow (F) and rapid (G) desiccation. Error bars show the standard error. T0, T0′ and T0″ indicate initial control, and controls of cycles 2 and 4, respectively; Da and Db indicate desiccation treatments with 50% and 100% of the minimal RWC value, respectively; Ra and Rb indicate treatments after 1 and 16 h of rehydration, respectively.

antioxidant enzymes and their gene expression during four cycles of D/R in these lichen algae.

Antioxidant enzyme response induced by desiccation-rehydration cycles

In resurrection plants, an increase in the antioxidant activities of APx, GR, SOD and CAT has been reported during dehydration. This activity can remain high at lower water contents (Farrant, 2000, Kranner et al. 2002, Farrant et al. 2003, Dinakar and Bartels 2013, Georgieva et al. 2017).

In lichens and their photobionts, antioxidant mechanisms include protective enzymes, such as SOD, CAT, peroxidases, GR and APx, in combination with nonenzymatic substances such as glutathione, α-tocopherol and ascorbic acid (Kranner et al. 2005, Kranner and Birtić 2005, Weissman et al. 2005a, Weissman et al. 2005b). SOD acts as the first line of defence by converting $O_2\bullet^-$ into H_2O_2, preventing the formation of highly toxic compounds. Then, CAT and APx transform H_2O_2 into water. On the other hand, GR, monodehydroascorbate reductase and dehydroascorbate reductase are involved in the regeneration of reduced glutatione and ascorbic acid (Inupakutika et al. 2016).

In the present study, the antioxidant enzyme activities were measured by spectrophotometric assay and zymogram analysis. In general, results indicate a diverse antioxidant response during the D/R cycle treatments.

SODs are a group of metallo-enzymes containing Fe, Mn or CuZn in their prosthetic group and are present in mitochondria, chloroplasts, cytosol, peroxisomes and apoplast (Alscher et al. 2002). There is no evidence of the presence of CuZnSOD isoforms, at least in most Chlorophyta algae (Inupakutika et al. 2016). The zymogram technique allowed us to separate the SOD isoforms according to their electrophoretic mobility into three groups of MnSODs, named MnSOD-A, MnSOD-B and MnSOD-C, and one FeSOD isoform (**Figs. 2A, 3A**). The activity

of each band/band group was estimated by image analysis (**Figs. 2B–E, 3B–E**). No clear trend was found regarding the SOD activity of TR9 photobionts (**Fig. 2A–E**), despite the increase in MnSOD-B and MnSOD-C isoforms, during cycles 2 and 4 (**Fig. 2C, D**). However, it is noteworthy that the increased values of T0′ and T0″ activities of both groups of MnSOD isoforms suggest an acclimation induced by successive cycles of D/R. On the other hand, changes in SOD activity were more striking in Csol photobionts. The activity of all isoforms, including FeSOD, clearly increased under desiccation and/or rehydration conditions but did not significantly change the initial activity levels of cycles 2 and 4 (T0′ and T0″, respectively, **Fig. 3B–E**). The different response at the level of SOD activity carried out by TR9 and Csol seems to reveal contrasting strategies from the first defence line of the antioxidant system on. Gasulla et al. (2009) found that SOD activity declined in *Asterochloris erici* during the desiccation period and during the first 24 h of recovery. A recovery in the antioxidant activity was observed only after 48 h at RH 67%.

CAT is involved in the rapid detoxification of H_2O_2 (Kranner et al. 2008), especially under conditions of high rates of H_2O_2 production (e.g. high SOD activity), due the low affinity for H_2O_2 of CAT (Smirnoff and Arnaud 2019). Their activity in lichens has been shown to vary greatly among species (Silberstein et al. 1996, Mayaba and Becket 2001, Weissman et al. 2005b). The activity of this enzyme was assayed by zymogram and semi-quantified as described for SOD. Zymograms revealed two bands of CAT isoforms in TR9 (**Fig. 2F**): CAT-A, which progressively increased during the second D/R cycle compared with the initial T0 and appeared to maintain its enzymatic activity during the subsequent D/R cycles (**Fig. 2G**). On the other hand, no significant differences were detected in the activity of the second isoform CAT-B (**Fig. 2H**). In contrast, no significant changes were observed in CAT activity (spectrometrically measured) in TR9 photobionts under Pb stress, which increases the production of ROS (Álvarez et al. 2012). Only one CAT isoform was found in Csol, which progressively increased through the four cycles of D/R (**Fig. 3F, G**).

APx is relatively specific to H_2O_2 since it does not metabolize other peroxides at high rates and participates in the 'ascorbate-glutathione' pathway in which H_2O_2 reduction is ultimately linked to NAD(P)H oxidation via ascorbate and glutathione pools (Noctor et al. 2012). According to previous results, no detectable levels of ascorbate were found in *Trebouxia* lichen photobionts (Kranner et al. 2005, Gasulla et al. 2009), including TR9 (Centeno et al. 2016). In this species, GR activity was characterized by a relatively low initial T0 level (0.051 ± 0.012 μmol NADPH·min^{-1}·mg^{-1}), which was significantly increased after D/R cycles 2 and 4 (**Fig. 2I**). A similar behavior was observed in the same microalgae exposed to other stressful conditions that

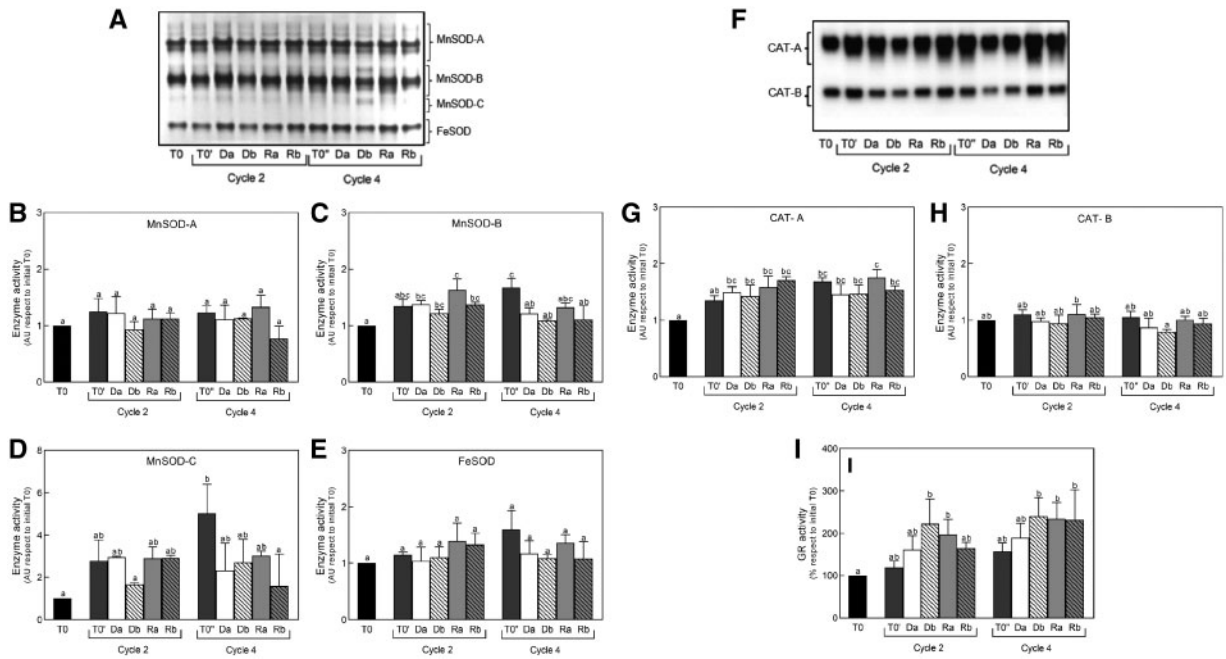

Fig. 2 Effects of cyclic desiccation-rehydration on SOD, CAT and GR activities in TR9 microalgae. (A) Image showing a representative SOD zymogram. SOD isoforms were grouped as indicated according their electrophoretic mobility and metal cofactor. (B–E) Enzyme activity of groups of SOD isoforms (MnSOD-A, MnSOD-B, MnSOD-C, FeSOD) calculated by the mean image analysis of three to six zymograms from independent biological samples. (F) Image depicting a representative CAT zymogram. (G, H) CAT activity was estimated from the image analysis of three to six zymograms from independent biological samples. Values in (B–E) and (G, H) are expressed in arbitrary units (AU). (I) Total GR activity determined by spectrophotometric assay. Values are expressed as percentages with respect to the initial T0 values (μmol NADPH·min^{-1}·mg^{-1} = 0.051 ± 0.012). Error bars show the standard error. Black bars indicate initial control treatment (T0); dark gray bars indicate controls of cycles 2 and 4 (T0′ and T0″, respectively); white solid and striped bars indicate desiccation treatments with 50% (Da) and 100% (Db) of the minimal RWC value, respectively; light gray solid and striped bars indicate treatments after 1 h (Ra) and 16 h (Rb) of rehydration, respectively.

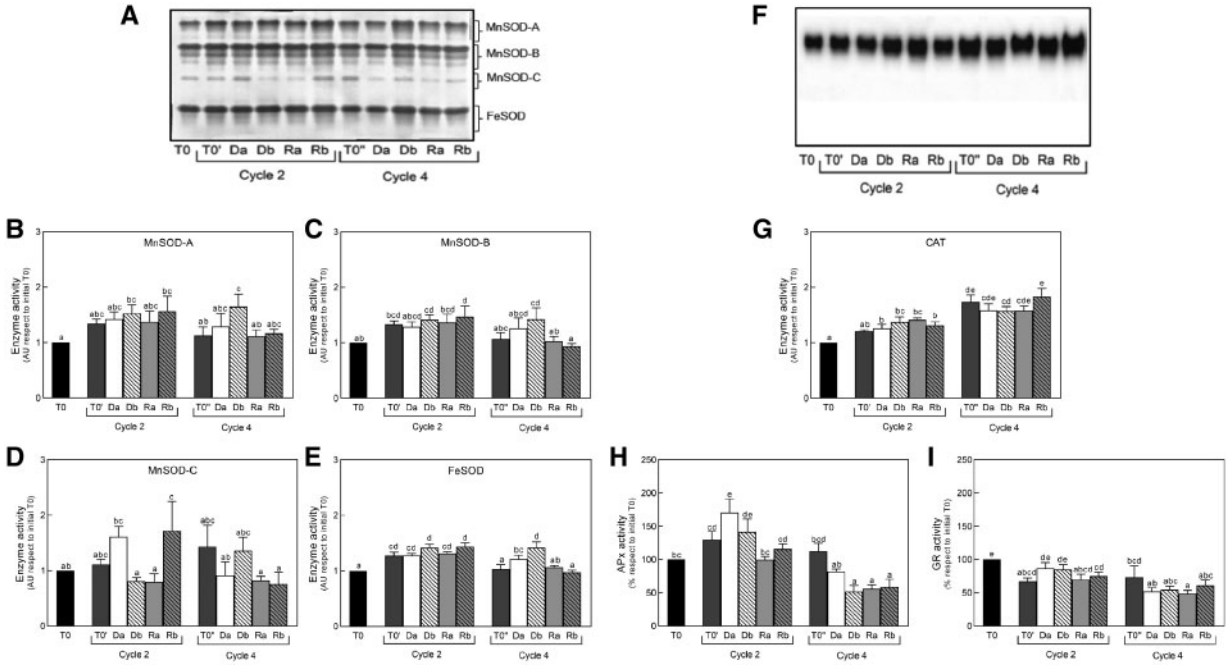

Fig. 3 Effects of cyclic desiccation-rehydration on SOD, CAT, Apx and GR activities in Csol microalgae. (A) Image showing a representative SOD zymogram in which the SOD isoforms were grouped as indicated in legend to **Fig. 2**. (B–E) Enzyme activity of groups of the SOD isoforms (MnSOD-A, MnSOD-B, MnSOD-C, FeSOD) calculated by the mean image analysis of three to six zymograms from independent biological samples. (F) Image depicting a representative CAT zymogram. (G) CAT activity was estimated from image analysis of three to six zymograms from independent biological samples. Values are expressed in AU. (H) Total Apx and (I) GR activity were determined by spectrophotometric assay. Values are expressed in percentages with respect to initial T0 values (μmol ascorbate·min^{-1}·mg^{-1} = 0.790 ± 0.207 and μmol NADPH·min^{-1}·mg^{-1} = 0.262 ± 0.098, respectively). Values represent the mean of three biological replicates of two independent experiments. Error bars show the standard error. Details of color and pattern of bars are given in the legend to **Fig. 2**.

promote ROS formation, such as Pb and xenobiotic treatments, in which GR activity was highly induced from low basal levels (del Hoyo et al. 2011, Álvarez et al. 2012).

On the other hand, Csol presented a marked increase in APx activity during desiccation of cycle 2, which then returned to the initial T0 (0.790 ± 0.207 μmol ascorbate·min^{-1}·mg^{-1}) levels during rehydration of the same cycle (**Fig. 3H**). A progressive decrease in APx activity was observed during cycle 4. Notably, Csol GR activity was characterized by a high initial level (0.262 ± 0.098 μmol NADPH·min^{-1}·mg^{-1}) that was approximately five times higher than that of TR9. In Csol, GR activity (**Fig. 3I**) showed a quite stable behavior during cycle 2, and a relative decrease in cycle 4 similar to that of APx activity. These results lead to the idea that, in the Csol photobiont, APx, GR and the 'ascorbate-glutathione' pathway could be relevant during the first cycles of D/R treatments, while SOD and CAT could play a more important role in later steps of cyclic D/R conditions.

The lack of ascorbate in TR9 photobionts, as shown previously (Centeno et al. 2016), and the induction of GR activity under cyclic D/R (this study) could indicate that this microalga uses, in addition to CAT, an alternative route(s) to the ascorbate-glutathione pathway for keeping the H_2O_2 level within a range compatible with life preservation. GSH could be linked to H_2O_2 and/or organic peroxide reduction by at least two ascorbate-independent routes involving certain types of peroxiredoxin (PRX) and/or glutathione S-transferase (Noctor et al. 2012). In addition, phenolic substrate can be oxidized by H_2O_2 using type III peroxidase in the vacuole (Smirnoff and Arnaud 2019). Moreover, our previous studies based on metabolomics analysis showed that TR9 photobionts have more polyols and phenolic compounds than Csol photobionts, which could also help act as ROS scavengers, avoiding oxidative damage (Centeno et al. 2016).

Despite the advances in the last few years, it has not yet been possible to establish a clear relationship between stress tolerance level and antioxidant mechanisms. To improve our knowledge of the role of antioxidant enzymes in the DT of TR9 and Csol photobionts, a detailed analysis of the transcript levels of all SOD, CAT, APx and GR encoding genes was carried out.

Changes in antioxidant transcript levels induced by desiccation-rehydration cycles

This is the first study to characterize changes in the almost/ nar complete set of the main antioxidant transcripts of lichen microalgae within the context of several daily cycles of D/R. TBLAST analysis revealed the existence of 10 genes encoding antioxidant enzymes in the TR9 microalgae, of which two corresponded to *CAT*, five corresponded to *SOD*, two corresponded to *GR* and one corresponded to gamma-glutamylcysteine ligase (*GCL*) enzyme (**Fig. 4**). In the case of Csol, the transcripts of the antioxidant genes matched as follows: four

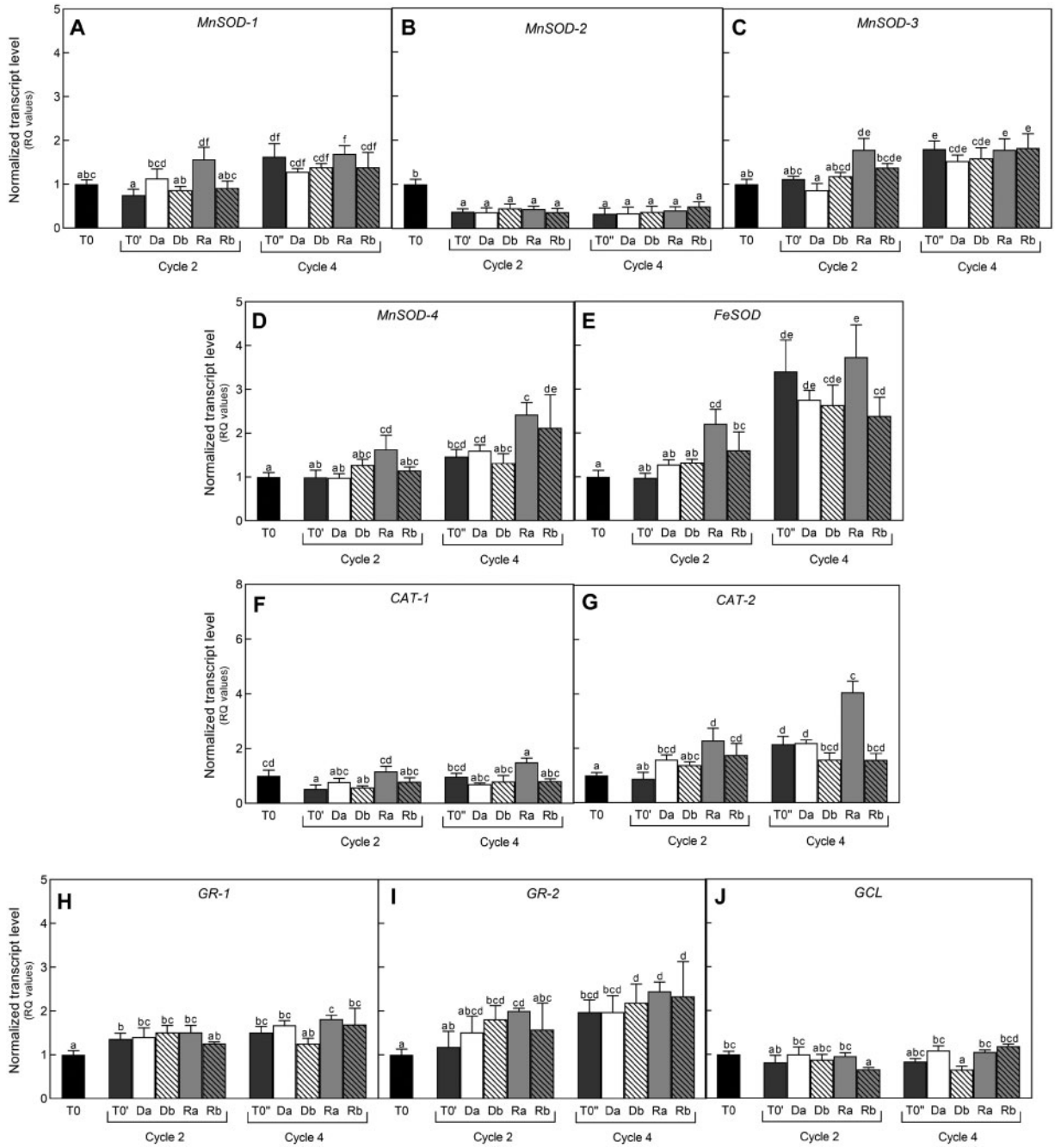

Fig. 4 Changes in the transcript levels of antioxidant encoding genes of TR9 microalgae exposed to cyclic desiccation-rehydration. mRNA levels of genes encoding SOD, *MnSOD-1*, *MnSOD-2*, *MnSOD-3*, *MnSOD-4*, *FeSOD* (A–E, respectively), CAT, *CAT-1 and CAT2* (F, G, respectively), GR, *GR-1*, *GR-2* (H, I, respectively) and *GCL* (J) genes. Values were calculated with $2^{-\Delta\Delta Ct}$ relative quantification for five biological replicates. Error bars show the standard error. Details of color and pattern of bars are given in the legend to **Fig. 2**.

to *CAT*; six to *SOD*; three to *GR*; one to *GCL*; and two to *APx* nonredundant transcripts. From these Csol genes, three *CAT*, one *SOD*, one *GR* and one *APx* were not included in the quantitative expression analysis because their transcripts were barely detectable, indicating that these genes are nonfunctional, at least under the conditions employed in our study. The expressed Csol antioxidant genes are shown in **Fig. 5**.

FeSODs are located in the chloroplast; MnSODs are located in the mitochondrion and peroxisome; and CuZn SODs are located in the chloroplast, cytosol, and possibly in the extracellular space (Alscher et al. 2002). Most eukaryotic algae contain either FeSOD or MnSOD or both (Wang et al. 2011). The results of the TR9 transcript level demonstrated different transcriptional responses during D/R cycles depending on the SOD isozyme-encoding gene (**Fig. 4**). While transcript levels of *MnSOD-2* decreased and those of *MnSOD-1* and *MnSOD-3* slightly increased (**Fig. 4A–C**, respectively), the amount of *MnSOD-4* and *FeSOD* transcripts increased during D/R cycles

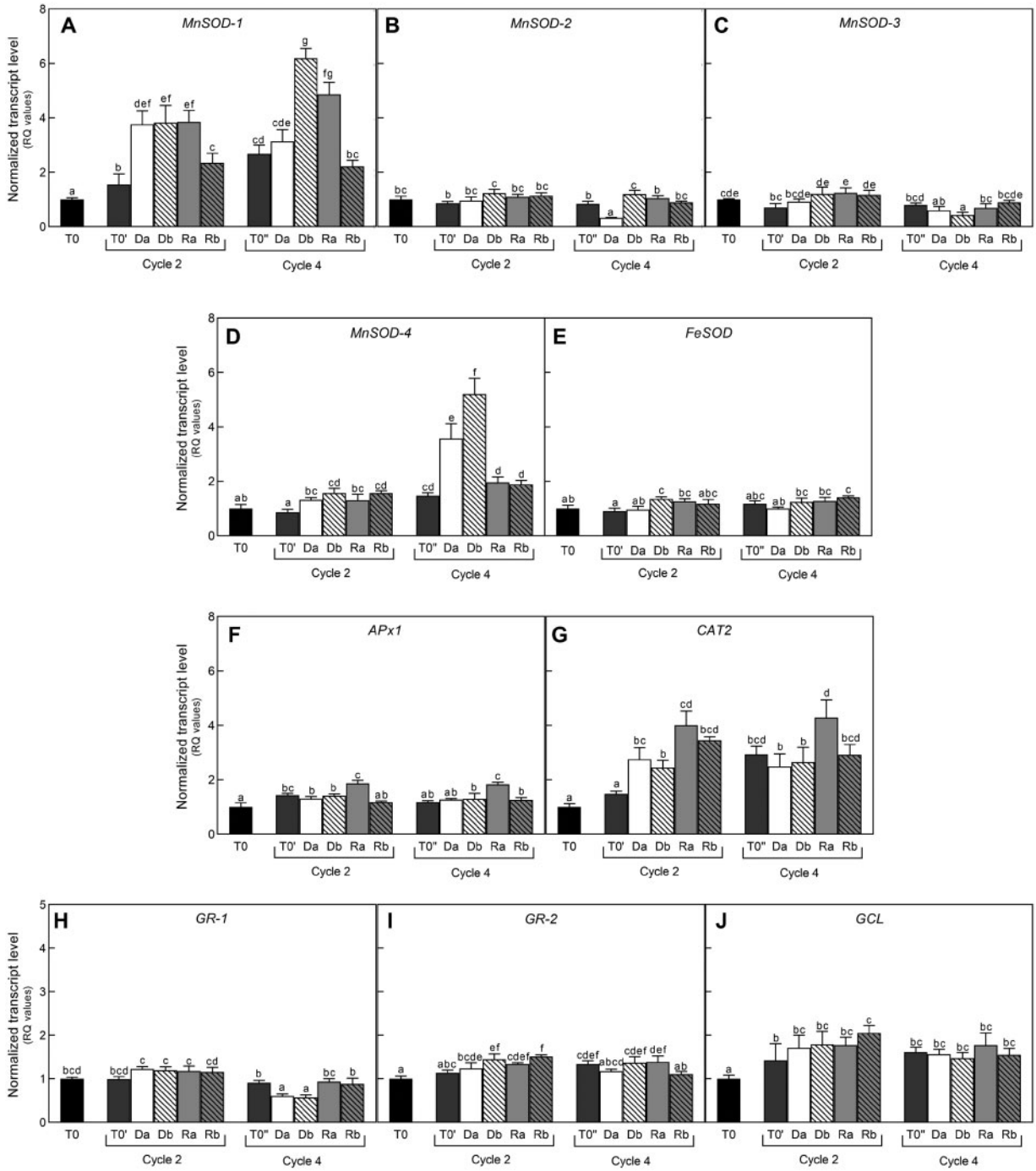

Fig. 5 Changes in the transcript levels of antioxidant encoding genes of CsoI microalgae exposed to cyclic desiccation-rehydration. mRNA levels of genes encoding SOD: *MnSOD-1*, *MnSOD-2*, *MnSOD-3*, *MnSOD-4*, *FeSOD* (A–E, respectively); APx: *APx1* (F); CAT: *CAT* (G); GR: *GR-1*, *GR-2* (H, I, respectively) and *GCL* (J). Values were calculated with $2^{-\Delta\Delta Ct}$ relative quantification for five biological replicates. Details of color and pattern of bars are given in the legend to **Fig. 2**.

(**Fig. 4D and E**, respectively). In CsoI, the *MnSOD-1* and *MnSOD-4* transcripts also increased compared with the initial control during the successive cycles of D/R (**Fig. 5A, D**) and demonstrated a transcriptional increase during desiccation treatments (50D and 100D) at cycle 4. In this species, the expression of the other two *MnSOD* and *FeSOD* genes did not change (**Fig. 5B, C, E**). Studies have shown that SOD transcripts are induced in plant species under different stresses, such as heat, cold, drought, osmotic, salt and oxidative stresses (Wang et al. 2011, Feng et al. 2016, Zhou et al. 2017). In tomato, among nine SOD genes, four (SlSOD2, SlSOD5, SlSOD6 and SlSOD8) were upregulated under drought treatment (Feng et al. 2016). In *T. gelatinosa*, an over-expression of one putatively mitochondrial *MnSOD* gene and enzyme upregulation upon dehydration

was observed, probably as a response to *MnSOD* mRNAs built up in preparation to rehydration (Carniel et al. 2016).

Ascorbate and thiol peroxidases have numerous isoforms and are found in all subcellular compartments (Smirnoff and Arnaud 2019). Some studies have reported an increase in stress resistance as a result of the over-expression of peroxidases, such as APx (Dietz 2016, Maruta et al. 2016). In *Klebsormidium crenulatum*, an alpine aeroterrestrial alga, desiccation induced the transcriptional upregulation of genes, including those involved in the ascorbate-glutathione pathway (Holzinger et al. 2014). As mentioned earlier, *TR9* and *Csol* seem use different metabolic strategies for keeping the H_2O_2 within homeostatic levels. The absence of detectable levels of APx-encoding genes supports the absence of ascorbate in *Trebouxia* phycobionts (Kranner et al. 2005, Gasulla et al. 2009) and with previous results concerning the metabolic profile of *TR9* microalgae (Centeno et al. 2016). On the other hand, ascorbate seems to play an important role in Csol microalgae (Centeno et al. 2016). Ascorbate peroxidase-encoding gene (*APx1*) transcript levels analysis revealed an increase during the first hour of rehydration (**Fig. 5F**) and this gene is probably related to the activation and/or preservation of the antioxidant system to deal with high ROS formation inside cell compartments. The desiccation-induced increase in APx activity observed during the second D/R cycle (**Fig. 3H**) could be partially explained by the transcriptional induction of the *APx1* gene. Besides, the overall trend of APx activity in the second D/R cycle closely resembled the variation for ascorbic acid previously observed during one cycle of D/R in the same microalga (Centeno et al. 2016). This is consistent with strong evidences demonstrating that the stability of APx is highly dependent on the concentration of ascorbic acid (Shigeoka et al. 2002 and references therein).

Corroborating the zymogram analysis, CAT genes were expressed in TR9 and Csol. Both *CAT* isoforms, *CAT1* and *CAT2*, found in TR9 and *CAT2* from Csol presented a similar profile (**Figs. 4F, G, 5G**). The transcript level increased significantly during D/R cycles compared with the initial T0 and rehydration after 1 h of rehydration (1R) (**Figs. 4G, 5G**). CAT is most likely restricted to peroxisomes (Smirnoff and Arnaud 2019). Peroxisomal CAT mutants have been studied in *Arabidopsis* and tobacco and show a key role in H_2O_2 removal (Queval et al. 2007). Gechev et al. (2013) studied the CAT-encoding genes in the resurrection plant *H. rhodopensis*, and their transcript levels were high under desiccated and rehydrated conditions.

Previous studies have shown that over-expression of GR leads to an increase in cellular GSH levels in response to biotic and abiotic stresses (Foyer et al. 2001, Kouřil et al. 2003). The synthesis of GSH is a two-step process catalyzed by GCL and glutathione synthetase. GCL is the rate-limiting enzyme, as it is subject to feedback inhibition by the overproduction of GSH (Foyer et al. 2001). *GR* and *GCL* transcripts were quantified in both species (**Figs. 4, 5**H–J, respectively). In TR9 photobionts, the transcript levels of *GR1* and *GCL*, which are key enzymes for GSH synthesis, remained approximately constant throughout the experiment. However, expression of the gene encoding the *GR2* isoform progressively increased during D/R cycles (**Fig. 4I**), resembling the GR activity profile observed under the same conditions (**Fig. 2I**). These results strongly suggest that the *GR2* gene could be involved in the antioxidant response of TR9 to cyclic D/R. On the other hand, in Csol, the *GR1* (**Fig. 5H**) transcript level decreased at D/R cycle 4, while transcript levels of *GR2* (**Fig. 5I**) and *GCL* (**Fig. 5J**) slightly increased during D/R cycles compared with their initial T0 values. Under oxidative stress conditions, post-translational activation of GCL could contribute to the rapid increase in GSH synthesis in higher plants (Rausch et al. 2007). In *T. gelatinosa*, the upregulation of three microsomal glutathione *S-transferases* occurred during dehydration, suggesting that they are a part of the mechanism to keep the intracellular redox homeostasis (Carniel et al. 2016). Yobi *et al.* (2012) found that the levels of γ-glutamyl amino acids were significantly higher in *Selaginella lepidophylla* (desiccation-tolerant) than in *Selaginella moellendorffii* (desiccation-sensitive) in response to dehydration, which indicates that γ-glutamyl amino acids or glutathione are involved in the acquisition of DT. Therefore, the maintenance of *GCL* levels in TR9 and their increase in Csol could indicate different strategies to maintain glutathione homeostasis during D/R cycles.

A holistic view of transcriptions levels suggests the existence of an acclimation process, from a permanent hydrated state to cyclic desiccation periods. Some genes, such as TR9 *MnSOD-1*, *MnSOD-3*, *MnSOD-4*, *FeSOD*, *GR-2* and Csol *MnSOD-1*, *CAT*, *GR-2* and *GCL*, were likely induced by the increase in ROS formation provoked by cyclic D/R conditions. It should be noted that the induction of such a number of antioxidant genes, along with their enzymatic activities, has not been observed in lichen algae until the present study. This study has been possible by two essential facts: (i) we searched for and studied all the genes encoding the main antioxidant enzymes, and (ii) our study was not limited to one cycle of D/R but to several cycles, allowing us to observe acclimation processes that often occur under natural conditions. It is highly plausible that the failure to find inducible antioxidant mechanisms associated with DT in lichen thalli (obviously collected from its natural habitat) could be because those specimens were already acclimated. On the other hand, the lack of antioxidant response of isolated lichen algae to desiccation (Kranner et al. 2002; Gasulla et al. 2009) could be because cultures were only submitted to a single D/R cycle, which probably was not enough to acclimate. Our results with nonacclimated microalgae clearly indicate that, at least in part, their DT rely on their capacity to induce certain key genes along several D/R cycles.

The physiological process by which plants are able to activate defence responses faster, better or both is called *priming*. This may be initiated in response to an environmental cue and may also persist as a residual effect following an initial exposure to the stress (Filippou et al. 2013). In our results, the induction of antioxidant genes pointed to above could be included as *primed* responses within a specific biological context, such as lichen algae, which are endowed with relatively strong constitutive mechanisms of defence, suggesting a strategy of metabolic economy to cope with D/R stress. In addition, the fine and fast control of ROS levels seems to be crucial if most lichen algae are often subjected to daily variation in water availability. If part

of the enzymatic antioxidant system acts as a prompt and regulated response (according to the current ROS formation rate), it will confer a more efficient strategy against oxidative damage associated with desiccation stress.

Materials and Methods

Microalgae isolation and culture

The *Trebouxia* sp. TR9 was isolated from the lichen *R. farinacea* according to Casano et al. (2011), and *C. simplex* (formerly known as *C. solorinae-saccatae* strain 216-12) was obtained from Sammlung von Algenkulturen at Göttingen University (Germany). Both microalgae were axenically cultured on small nylon square membranes in semi-solid Bold 3N medium (Bold and Packer 1962) in a growth chamber maintained at a continuous temperature of 15°C and with light/dark cycles of 14 h (25 μmol PAR·m^{-2}·s^{-1})/10 h. All experiments were carried out with 21-day-old cultures (~180–200 mg FW).

Desiccation-rehydration treatments

In the first experiments, TR9 and CsoI cultures on the nylon squares were removed from the culture medium and subjected to slow desiccation in a closed container with saturated solutions of either potassium acetate (22–25% RH), $MgCl_2$ (35–37% RH) or $Mg(NO_3)_2$ (53–58% RH) within the growth chamber for up to 90 d. At the indicated times (**Fig. 1**), five cultures of each species were transferred onto water vapor-saturated sealed Petri dishes (Centeno et al. 2016) for up to 24 h under growth chamber conditions. The maximal photochemical PSII efficiency by chlorophyll *a* fluorescence was measured shortly before the end of the dark period in rehydrated samples.

The following experiments were performed in a phytotron (KK 115 Top+, Pol-Eko-Apparatus, Poland) in which, in addition to temperature and light conditions, some air hydric parameters such as RH and the speed of air movement can be controlled. Temperature was set at 15°C and the photoperiod in 14 h of light (25 μmol PAR·m^{-2}·s^{-1}) and 10 h of darkness. Desiccation treatment started with the light phase and rehydration began with 4–6 h under light followed by 10 h of darkness. For rapid desiccation experiments, cultures of each microalgae on their nylon supports were subjected to daily cycles of 8–10 h desiccation at 25–30% RH for TR9 or 55–60% for CsoI, moderate air movement (20% of maximum capacity), followed by 14–16 h rehydration in water vapor-saturated sealed Petri dishes. The slow desiccation experiments were performed under the same conditions except that the lowest air speed was employed. At the indicated intervals, 5–8 samples of TR9 and CsoI were collected and weighed to follow their RWC (**Fig. 1**) as described by Centeno et al. (2016). In other experiments, cultures of each microalgae were subjected up to four cycles of either rapid or slow desiccation. At 0%, 50% and 100% desiccation and after 1 and 14–16 h rehydration, five to eight samples were acclimated to darkness (when necessary), and their remnant photosynthetic capacity was assayed by fluorometry as described below. For the transcript level determination and the assay of antioxidant enzymes, TR9 and CsoI cultures were submitted to up to four daily cycles of slow D/R. At 0%, 50% and 100% desiccation and after 1 and 14–16 h R, five samples of each microalgae were collected. Every sample was fractionated into three aliquots (~40–100 mg each) and immediately frozen in liquid N_2 and maintained at −80°C until use.

Measurements of chlorophyll *a* fluorescence

Chlorophyll *a* fluorescence was measured in dark-acclimated algae using a modulated pulse fluorometer PEA (Plant Efficiency Analyser, Hansatech, UK). The initial, remnant or recovered photosynthetic capacity was assessed through the fluorescence parameter F_v/F_m (variable fluorescence/maximum fluorescence), which estimates the maximum quantum yield of PSII (Baker and Oxborough 2004). The minimum fluorescence (F_o) was obtained after dark adaption for 15 min and the maximum fluorescence (F_m) was determined with a 2.2 s saturating pulse (3,500 μmol photons·m^{-2}·s^{-1}) of red LED's light (peak wavelength 650 nm). Maximal variable fluorescence (F_v) was calculated as $F_m - F_o$.

Protein extraction and antioxidant enzyme activities

Frozen aliquots of TR9 and CsoI were homogenized using a steel microbead homogenizer (Retsch, MM400, Germany) in the presence of 50 mM Tris–Cl (pH 7.5), 2 mM EDTA, 1 mM ascorbic acid, 10% (v/v) glycerol and 1% (w/v) insoluble polyvinyl pyrrolidone. The homogenates were centrifuged at 20,000×*g* for 20 min at 4°C, and the supernatants were used for antioxidant enzyme assays. The total protein concentration in the extracts was determined spectrophotometrically with Coomassie Brilliant Blue according to Bradford (1976), using bovine serum albumin as a standard. The activities of the antioxidant enzymes APx and GR were carried out by spectrophotometric assays as described by Amako et al. (1994) and Schaedle and Bassham (1977), respectively.

In addition, SOD and CAT isoforms were assayed through specific zymograms in which 10 μg of total proteins were usually electrophoresed under native conditions, and the activity band(s) of each enzyme was revealed by specific staining (Woodbury et al. 1971, Álvarez et al. 2012). MnSOD isoforms were distinguished from FeSOD isoforms as described (Álvarez et al. 2012). SOD isoforms were grouped into four groups (**Figs. 2A, 3A**). The intensity (activity) of each SOD isoform group and CAT isoform(s) was estimated using ImageJ software and posteriorly corrected for possible protein loading biases (**Figs. 2B–H, 3B–G**). For this correction, the same extracts were subjected to SDS-PAGE and stained with Coomassie Brilliant Blue (Supplementary Fig. S1). At least two well-defined bands in all lanes were quantified using ImageJ.

Transcript levels of genes codifying antioxidant enzymes

RNA was extracted from half-algal culture (50–100 mg FW) following the protocol of Jones et al. (1985). The quality of isolated RNAs was checked on denaturing agarose gels. RNA was quantified using a NanoDrop ND-1000™ spectrophotometer (Daemyung, Korea). Coextracted DNA contaminants were degraded using the DNAse I RNA-free kit (Invitrogen, California, USA), and the complementary DNA (cDNA) was synthesized with the RevertAid First Strand cDNA Synthesis kit (Thermo-Fisher Scientific, Massachusetts, USA) using the supplied oligo-dT primer following the manufacturer's guidelines.

Sequences encoding enzymes involved in the antioxidant cell system were searched for in the translated TR9 transcriptome database (housed in our computers in the University of Alcalá) employing *Arabidopsis thaliana* cDNA sequences and the TBLASTX tool (https://blast.ncbi.nlm.nih.gov/Blast.cgi). The cDNA sequences of antioxidant genes in the close relative *Coccomyxa subellipsoidea* C-169 (NCBI: txid 574566) were used to design a set of primers to amplify the respective homologous genes in CsoI employing cDNA as a template (Supplementary Table S1). Amplification products were sequenced with an ABI 3130 Genetic analyzer using the ABI BigDye™ Terminator Cycle Sequencing Ready Reaction kit (Applied Biosystems, California, USA).

Specific primers were designed for each antioxidant gene of TR9 (Supplementary Table S2) and CsoI (Supplementary Table S3) for transcript quantification by real-time PCR (qPCR). PCR amplification was carried out in a 10 μl total volume containing 1 μl of 10-fold diluted cDNA, 0.5 μl each primer and 5 μl 2X Fast SYBR-Green Master Mix (Applied Biosystems, CA, USA) using a 7500 Fast Real-Time PCR system (Applied Biosystems) under standard conditions of the apparatus. Five biological replicates and two technical replicates were used in this study. Two negative controls were included for each primer pair, in which cDNA was replaced by water or total RNA. The absence of nonspecific PCR products and primer dimers were verified by dissociation curves and by agarose gel electrophoresis. The amplification efficiency of each set of primers was checked to be higher than 95% following the standard curve method described by da Costa et al. (2015). Transcript quantifications were normalized to three reference genes (Supplementary Fig. S2): *Ap47* (Clathrin adaptor complexes subunit), *Act* (Actin) and *PP2A* (Serine/threonine protein phosphatase) following the strategy proposed by Vandesompele et al. (2002). Reference gene selection was based on studies conducted in other plant species subjected to abiotic stresses, including salinity and drought stress (da Costa et al. 2015 and references therein).

Statistical analysis

The changes in RWC and antioxidant enzyme activities during D/R cycles were repeated twice, starting with new cultures each time. All analyses were conducted with three or five replicates per treatment for each point of the analyses. Data were analyzed using the multiple sample comparison (Statgraphics Centurion XVII, 2016, StatPoint Technologies 2016) Fisher's least significant difference (LSD) test ($P < 0.05$).

Supplementary Data

Supplementary data are available at PCP online.

Funding

This study was supported by the Spanish Ministry of Science, Innovation and Universities [CGL2016-80259-P], the Coordenação de Aperfeiçoamento de Pessoal de Nível Superior-Brazil [CAPES-Code 001 to A.F.H.] and the University of Alcalá (post-doctoral contract to F.G.).

Disclosures

The authors have no conflicts of interest to declare.

References

Alscher, R.G., Erturk, N. and Heath, L.S. (2002) Role of superoxide dismutases (SODs) in controlling oxidative stress in plants. *J. Exp. Biol*. 53: 1331–1341.

Álvarez, R., del Hoyo, A., Díaz-Rodríguez, C., Coello, A.J., del Campo, E.M. and Barreno, E. (2015) Lichen rehydration in heavy metal-polluted environments: Pb modulates the oxidative response of both *Ramalina farinacea* thalli and its isolated microalgae. *Microb. Ecol.* 69: 698–709.

Álvarez, R., del Hoyo, A., García-Breijo, F., Reig-Armiñana, J., del Campo, E.M., Guéra, A., et al. (2012) Different strategies to achieve Pb-tolerance by the two *Trebouxia* algae coexisting in the lichen *Ramalina farinacea*. *J. Plant. Physiol*. 169: 1797–1806.

Amako, K., Chen, G.X. and Asada, K. (1994) Separate assays specific for ascorbate peroxidase and guaiacol peroxidase and for the chloroplastic and cytosolic isozymes of ascorbate peroxidase in plants. *Plant Cell Physiol.* 35: 497–504.

Baker, N.R. and Oxborough, K. (2004) Chlorophyll fluorescence as a probe of photosynthetic productivity. *In* Advances in Photosynthesis and Respiration. Chlorophyll a Fluorescence: A Signature of Photosynthesis. Edited by Papageorgiou, G.C., and Govindjee, G. pp. 65–82. Springer Netherlands, Dordrecht.

Banchi, E., Candotto, C.F., Montagner, A., Petruzzellis, F., Pichler, G., Giarola, V., et al. (2018) Relation between water status and desiccation-affected genes in the lichen photobiont *Trebouxia gelatinosa*. *Plant Physiol. Biochem*. 129: 189–197.

Bold, H.C. and Parker, B.C. (1962) Some supplementary attributes in the classification of chlorococcum species. *Arch. Mikrobiol.* 42: 267–288.

Bradford, M.M. (1976) A rapid and sensitive method for the quantitation of microgram quantities of protein utilizing the principle of protein-dye binding. *Anal. Biochem*. 72: 248–254.

Carniel, F.C., Gerdol, M., Montagner, A., Banchi, E., De Moro, G., Manfrin, C., et al. (2016) New features of desiccation tolerance in the lichen photobiont *Trebouxia gelatinosa* are revealed by a transcriptomic approach. *Plant Mol. Biol.* 91: 319–339.

Casano, L.M., del Campo, E.M., García-Breijo, F.J., Reig-Armiñana, J., Gasulla, F., Del Hoyo, A., et al. (2011) Two *Trebouxia* algae with different physiological performances are ever-present in lichen thalli of *Ramalina farinacea*. Coexistence versus competition? *Environ. Microbiol*. 13: 806–818.

Catalá, M., Gasulla, F., Pradas del Real, A.E., García-Breijo, F., Reig-Armiñana, J. and Barreno, E. (2010) Fungal-associated NO is involved in the regulation of oxidative stress during rehydration in lichen symbiosis. *BMC Microbiol.* 10: 297.

Centeno, D.C., Hell, A.F., Braga, M.R., del Campo, E.M. and Casano, L.M. (2016) Contrasting strategies used by lichen microalgae to cope with desiccation–rehydration stress revealed by metabolite profiling and cell wall analysis. *Environ. Microbiol.* 18: 1546–1560.

Challabathula, D., Zhang, Q. and Bartels, D. (2018) Protection of photosynthesis in desiccation-tolerant resurrection plants. *J. Plant Physiol*. 227: 84–92.

da Costa, M., Duro, N., Batista-Santos, P., Ramalho, J.C. and Ribeiro-Barros, A.I. (2015) Validation of candidate reference genes for qRT-PCR studies in symbiotic and non-symbiotic *Casuarina glauca* Sieb. ex Spreng. under salinity conditions. *Symbiosis* 66: 21–35.

del Hoyo, A., Álvarez, R., del Campo, E.M., Gasulla, F., Barreno, E. and Casano, L.M. (2011) Oxidative stress induces distinct physiological responses in the two *Trebouxia* phycobionts of the lichen *Ramalina farinacea*. *Ann. Bot*. 107: 109–118.

Dietz, K.J. (2016) Thiol-based peroxidases and ascorbate peroxidases: why plants rely on multiple peroxidase systems in the photosynthesizing chloroplast? *Mol. Cells* 39: 20–25.

Dinakar, C. and Bartels, D. (2013) Desiccation tolerance in resurrection plants: new insights from transcriptome, proteome and metabolome analysis. *Front. Plant Sci*. 4: 482.

Farrant, J.M. (2000) A comparison of mechanisms of desiccation tolerance among three angiosperm resurrection plant species. *Plant Ecol*. 151: 29–39.

Farrant, J.M. and Moore, J.P. (2011) Programming desiccation-tolerance: from plants to seeds to resurrection plants. *Curr. Opin. Plant Biol*. 14: 340–345.

Farrant, J.M., Willigen, C.V., Loffell, D.A., Bartsch, S. and Whittaker, A. (2003) An investigation into the role of light during desiccation of three angiosperm resurrection plants. *Plant. Cell Environ.* 26: 1275–1286.

Feng, K., Yu, J., Cheng, Y., Ruan, M., Wang, R., Ye, Q., et al. (2016) The SOD gene family in tomato: identification, phylogenetic relationships, and expression patterns. *Front. Plant Sci*. 7: 1279.

Fernández-Marín, B., Becerril, J.M. and García-Plazaola, J.I. (2010) Unravelling the roles of desiccation-induced xanthophyll cycle activity in darkness: a case study in *Lobaria pulmonaria*. *Planta* 231: 1335–1342.

Filippou, P., Tanou, G., Molassiotis, A. and Fotopoulos, V. (2013) Plant acclimation to environmental stress using priming agents. *In* Plant Acclimation to Environmental Stress. Edited by Tuteja, N. and Gill, S.S. pp. 1–27. Springer New York, New York.

Foyer, C.H., Theodoulou, F.L. and Delrot, S. (2001) The functions of inter- and intracellular glutathione transport systems in plants. *Trends Plant Sci*. 6: 486–492.

Gasulla, F., Barreno, E., Parages, M.L., Cámara, J., Jiménez, C., Dörmann, P., et al. (2016) The role of phospholipase d and MAPK signaling cascades in the adaption of lichen microalgae to desiccation: changes in membrane lipids and phosphoproteome. *Plant Cell Physiol.* 57: 1908–1920.

Gasulla, F., de Nova, P.G., Esteban-Carrasco, A., Zapata, J.M., Barreno, E. and Guéra, A. (2009) Dehydration rate and time of desiccation affect recovery of the lichenic algae *Trebouxia erici*: alternative and classical protective mechanisms. *Planta* 231: 195–208.

Gechev, T.S., Benina, M., Obata, T., Tohge, T., Sujeeth, N., Minkov, I., et al. (2013) Molecular mechanisms of desiccation tolerance in the resurrection glacial relic *Haberlea rhodopensis*. *Cell. Mol. Life Sci.* 70: 689–709.

Georgieva, K., Dagnon, S., Gesheva, E., Bojilov, D., Mihailova, G. and Doncheva, S. (2017) Antioxidant defense during desiccation of the

resurrection plant *Haberlea rhodopensis*. *Plant Physiol. Biochem*. 114: 51–59.

Gill, S.S. and Tuteja, N. (2010) Reactive oxygen species and antioxidant machinery in abiotic stress tolerance in crop plants. *Plant Physiol. Biochem*. 48: 909–930.

Gray, D.W., Lewis, L.A. and Cardon, Z.G. (2007) Photosynthetic recovery following desiccation of desert green algae (Chlorophyta) and their aquatic relatives. *Plant. Cell Environ.* 30: 1240–1255.

Heber, U., Soni, V. and Strasser, R.J. (2011) Photoprotection of reaction centers: thermal dissipation of absorbed light energy vs charge separation in lichens. *Physiol. Plant*. 142: 65–78.

Holzinger, A., Kaplan, F., Blaas, K., Zechmann, B., Komsic-Buchmann, K. and Becker, B. (2014) Transcriptomics of desiccation tolerance in the streptophyte green alga *Klebsormidium* reveal a land plant-like defense reaction. *PLoS One* 9: e110630.

Inupakutika, M.A., Sengupta, S., Devireddy, A.R., Azad, R.K. and Mittler, R. (2016) The evolution of reactive oxygen species metabolism. *J. Exp. Bot.* 67: 5933–5943.

Jones, J.D.G., Dunsmuir, P. and Bedbrook, J. (1985) High level expression of introduced chimaeric genes in regenerated transformed plants. *EMBO J.* 4: 2411–2418.

Komura, M., Yamagishi, A., Shibata, Y., Iwasaki, I. and Itoh, S. (2010) Mechanism of strong quenching of photosystem II chlorophyll fluorescence under drought stress in a lichen, *Physciella melanchla*, studied by subpicosecond fluorescence spectroscopy. *Bioenergetics* 1797: 331–338.

Kouřil, R., Lazár, D., Lee, H., Jo, J. and Nauš, J. (2003) Moderately elevated temperature eliminates resistance of rice plants with enhanced expression of glutathione reductase to intensive photooxidative stress. *Photosynthetica* 41: 571–578.

Kranner, I. (2002) Glutathione status correlates with different degrees of desiccation tolerance in three lichens. *New Phytol.* 154: 451–460.

Kranner, I., Beckett, R., Hochman, A. and Nash, T.H. (2008) Desiccation-tolerance in lichens: a review. *Bryologist* 111: 576–594.

Kranner, I., Beckett, R.P., Wornik, S., Zorn, M. and Pfeifhofer, H.W. (2002) Revival of a resurrection plant correlates with its antioxidant status. *Plant J.* 31: 13–24.

Kranner, I. and Birtić, S. (2005) A modulating role for antioxidants in desiccation tolerance. *Integr. Comp. Biol.* 45: 734–740.

Kranner, I., Cram, W.J., Zorn, M., Wornik, S., Yoshimura, I., Stabentheiner, E., et al. (2005) Antioxidants and photoprotection in a lichen as compared with its isolated symbiotic partners. *Proc. Natl. Acad. Sci. USA* 102: 3141–3146.

Kranner, I., Zorn, M., Turk, B., Wornik, S., Beckett, R.P. and Batič, F. (2003) Biochemical traits of lichens differing in relative desiccation tolerance. *New Phytol*. 160: 167–176.

Krog, H. and Swinscow, T.D.V. (1986) *Solorina Simensis* and *S. Saccata*. *Lichenologist* 18: 57–62.

Maruta, T., Sawa, Y., Shigeoka, S. and Ishikawa, T. (2016) Diversity and evolution of ascorbate peroxidase functions in chloroplasts: more than just a classical antioxidant enzyme? *Plant Cell Physiol*. 57: 1377–1386.

Mayaba, N. and Beckett, R.P. (2001) The effect of desiccation on the activities of antioxidant enzymes in lichens from habitats of contrasting water status. *Symbiosis* 31: 113–121.

Mubarakshina Borisova, M.M., Kozuleva, M.A., Rudenko, N.N., Naydov, I.A., Klenina, I.B. and Ivanov, B.N. (2012) Photosynthetic electron flow to oxygen and diffusion of hydrogen peroxide through the chloroplast envelope via aquaporins. *Biochim. Biophys. Acta* 1817: 1314–1321.

Noctor, G., Mhamdi, A., Chaouch, S., Han, Y., Neukermans, J., Marquez-Garcia, B., et al. (2012) Glutathione in plants: an integrated overview. *Plant. Cell Environ.* 35: 454–484.

Oliver, M.J., O'Mahony, P. and Wood, A.J. (1998) 'To dryness and beyond'—preparation for the dried state and rehydration in vegetative desiccation-tolerant plants. *Plant Growth Regul*. 24: 193–201.

Queval, G., Issakidis, -Bourguet, E., Hoeberichts, F.A., Vandorpe, M., Gakière, B., et al. (2007) Conditional oxidative stress responses in the *Arabidopsis* photorespiratory mutant cat2 demonstrate that redox state is a key modulator of daylength-dependent gene expression: and define photoperiod as a crucial factor in the regulation of H2O2-induced cell death. *Plant J*. 52: 640–657.

Rausch, T., Gromes, R., Liedschulte, V., Müller, I., Bogs, J., Galovic, V., et al. (2007) Novel insight into the regulation of GSH biosynthesis in higher plants. *Plant Biol. (Stuttg)* 9: 565–572.

Roach, T. and Krieger-Liszkay, A. (2014) Regulation of photosynthetic electron transport and photoinhibition. *Curr. Protein Pept. Sci.* 15: 351–362.

Schaedle, M. and Bassham, J.A. (1977) Chloroplast glutathione reductase. *Plant Physiol*. 59: 1011–1012.

Shigeoka, S., Ishikawa, T., Tamoi, M., Miyagawa, Y., Takeda, T., Yabuta, Y., et al. (2002) Regulation and function of ascorbate peroxidase isoenzymes. *J. Exp. Bot.* 53: 1305–1319.

Silberstein, L., Siegel, B.Z., Siegel, S.M., Mukhtar, A. and Galun, M. (1996) Comparative studies on *Xanthoria parietina*., a pollution resistant lichen: and *Ramalina Duriaei*: a sensitive species. II. evaluation of possible air pollution-protection mechanisms. *Lichenologist* 28: 367–383.

Smirnoff, N. and Arnaud, D. (2019) Hydrogen peroxide metabolism and functions in plants. *New Phytol*. 221: 1197–1214.

Statgraphics Centurion XVII, Version 17.2.0. (2016) StatPoint Technologies, Inc., Virgnia, USA.

Vandesompele, J., De Preter, K., Pattyn, F., Poppe, B., Van Roy, N., De Paepe, A., et al. (2002) Accurate normalization of real-time quantitative RT-PCR data by geometric averaging of multiple internal control genes. *Genome Biol*. 3: RESEARCH0034.

Wang, J., Sommerfeld, M. and Hu, Q. (2011) Cloning and expression of isoenzymes of superoxide dismutase in *Haematococcus pluvialis* (Chlorophyceae) under oxidative stress. *J. Appl. Phycol.* 23: 995–1003.

Weissman, L., Garty, J. and Hochman, A. (2005a) Rehydration of the lichen *Ramalina lacera* results in production of reactive oxygen species and nitric oxide and a decrease in antioxidants. *Appl. Environ. Microbiol*. 71: 2121–2129.

Weissman, L., Garty, J. and Hochman, A. (2005b) Characterization of enzymatic antioxidants in the lichen *Ramalina lacera* and their response to rehydration. *Appl. Environ. Microbiol*. 71: 6508–6514.

Woodbury, W., Spencer, A.K. and Stahmann, M.A. (1971) An improved procedure using ferricyanide for detecting catalase isozymes. *Anal. Biochem*. 44: 301–305.

Yobi, A., Wone, B.W.M., Xu, W., Alexander, D.C., Guo, L., Ryals, J.A., et al. (2012) Comparative metabolic profiling between desiccation-sensitive and desiccation-tolerant species of *Selaginella* reveals insights into the resurrection trait. *Plant J*. 72: 983–999.

Zhou, Y., Hu, L., Wu, H., Jiang, L. and Liu, S. (2017) Genome-wide identification and transcriptional expression analysis of cucumber superoxide dismutase (SOD) family in response to various abiotic stresses. *Int. J. Genomics* 2017: 7243973.

J. Phycol. **56,** 170–184 (2020)

DOI: 10.1111/jpy.12928

THE CHLOROPLAST GENOME OF THE LICHEN-SYMBIONT MICROALGA *TREBOUXIA* SP. TR9 (TREBOUXIOPHYCEAE, CHLOROPHYTA) SHOWS SHORT INVERTED REPEATS WITH A SINGLE GENE AND LOSS OF THE *RPS4* GENE, WHICH IS ENCODED BY THE NUCLEUS[1]

Fernando Martínez-Alberola, Eva Barreno

ICBIBE, Botánica, Facultad de Ciencias Biológicas, Universitat de València, Dr. Moliner 50, Burjassot, Valencia 46100, Spain

Leonardo M. Casano, Francisco Gasulla

Department of Life Sciences, University of Alcalá, Alcalá de Henares, Madrid 28805, Spain

Arantzazu Molins, Patricia Moya

ICBIBE, Botánica, Facultad de Ciencias Biológicas, Universitat de València, Dr. Moliner 50, Burjassot, Valencia 46100, Spain

María González-Hourcade, and Eva M. del Campo[2]

Department of Life Sciences, University of Alcalá, Alcalá de Henares, Madrid 28805, Spain

The Trebouxiophyceae is the class of Chlorophyta algae from which the highest number of chloroplast genome (cpDNA) sequences has been obtained. Several species in this class participate in symbioses with fungi to form lichens. However, no cpDNA has been obtained from any *Trebouxia* lichen-symbiont microalgae, which are present in approximately half of all lichens. Here, we report the sequence of the completely assembled cpDNA from *Trebouxia* sp. TR9 and a comparative study with other Trebouxiophyceae. The organization of the chloroplast genome of *Trebouxia* sp. TR9 has certain features that are unusual in the Trebouxiophyceae and other green algae. The most remarkable characteristics are the presence of long intergenic spacers, a quadripartite structure with short inverted repeated sequences (IRs), and the loss of the *rps4* gene. The presence of long intergenic spacers accounts for a larger cpDNA size in comparison to other closely related Trebouxiophyceae. The IRs, which were thought to be lost in the Trebouxiales, are distinct from most of cpDNAs since they lack the rRNA operon and uniquely includes the *rbc*L gene. The functional transfer of the *rps4* gene to the nuclear genome has been confirmed by sequencing and examination of the gene architecture, which includes three spliceosomal introns as well as the verification of the presence of the corresponding transcript. This is the first documented transfer of the *rps4* gene from the chloroplast to the nucleus among Viridiplantae. Additionally, a fairly well-resolved phylogenetic reconstruction, including *Trebouxia* sp. TR9 along with other Trebouxiophyceae, was obtained based on a set of conserved chloroplast genes.

Key index words: **chloroplast; gene transfer; genome; lichen; microalga; *rps4*; symbiont; *Trebouxia***

***Abbreviations*: cpDNA, chloroplast genome; IR, inverted repeat; LSC, large single copy; ML, maximum likelihood; ncORFs, non-conserved ORFs; ORF, open reading frame; SSC, small single copy; tr, tandem repeats**

Microalgae constitute ideal models for experimental evolution studies due to their ability to adapt and/or acclimate to changing environmental conditions and their short generation times (reviewed in Brodie et al. 2017). Algae are widespread organisms, occupying a vast range of habitats (from desert crusts to oceans), and can be either free-living or involved in a variety of associations with diverse organisms (reviewed in Grube et al. 2017). Behind the wide diversity of extant algae lies a complex evolutionary history which involved the acquisition of photosynthetic capacity by groups of taxonomically different organisms through different endosymbiotic events. There is strong evidence that plastids surrounded by two envelope membranes evolved from a single cyanobacterial endosymbiosis which gave rise to the Archaeplastida (reviewed in Archibald 2015). This super-group of organisms includes three different lineages: land plants and green algae (Chloroplastida, Viridiplantae), the red algae (Rhodophyta), and a small group of freshwater microalgae known as Glaucophyta (Adl et al. 2005). The phylum Chlorophyta comprises the majority of described species of green algae and has

[1]Received 28 June 2019. Accepted 15 September 2019. First Published Online 3 October 2019. Published Online 6 November 2019, Wiley Online Library (wileyonlinelibrary.com).
[2]Author for correspondence: e-mail eva.campo@uah.es.
Editorial Responsibility: O. De Clerck (Associate Editor)

traditionally been divided into four distinct classes: the Trebouxiophyceae and Chlorophyceae (freshwater or terrestrial), the Ulvophyceae (coastal), and the Prasinophyceae (predominantly marine planktonic; Leliaert et al. 2012). However, new classes have been recognized within the Chlorophyta phylum (Moestrup 1991, Marin 2012), such as the Chlorodendrophyceae (Massjuk 2006, Massjuk and Lilitska 2011) and Palmophyllophyceae (Leliaert et al. 2016), although their acceptance remains controversial. Members of the Trebouxiophyceae class exhibit noticeable morphological and ecological diversity, with species distributed among numerous lineages (Leliaert et al. 2012, Lemieux et al. 2014a, Turmel et al. 2015, Leliaert and De Clerck 2017, Fang et al. 2018). Some Trebouxiophyceae have the ability to establish diverse symbiotic associations, including with lichens. Of these, the *Trebouxia* genus includes strains that are present in approximately half of all lichens (reviewed in Grube et al. 2017). Consequently, this is one of the best studied genera as regard its diversity in lichens. Most studies have focused on phylogenetic relationships and the diversity of strains involved in lichen symbioses with respect to their ecological responses (Muggia et al. 2017). However, little is known to date about the chloroplast genome from *Trebouxia* algae. Only a few chloroplast-encoded genes have been exploited as molecular markers for phylogenetic reconstructions and photobiont diversity evaluations (e.g., del Campo et al. 2010, Werth and Sork 2010, Casano et al. 2011, Muggia et al. 2011, 2017, Moya et al. 2015, 2018, Catalá et al. 2016, Fang et al. 2018, Škaloud et al. 2018).

The structure of chloroplast genomes (cpDNA) is highly conserved, especially in land plants (reviewed in Daniell et al. 2016). Generally, they comprise a single circular molecule with a quadripartite structure consisting of two copies of an inverted repeat region (IR) that\ separate two single-copy regions: the large single-copy (LSC) and the small single-copy (SSC) sequences. In spite of its conservative nature, the chloroplast genome has undergone substantial changes over evolutionary time. Among Viridiplantae, the green algae are the organisms that exhibit the most marked changes in their architecture compared to land plants, including the possession of a high number of type I introns (e.g., Turmel et al. 2015, 2016, 2017, Daniell et al. 2016, Lemieux et al. 2016, del Hoyo et al. 2018). The lack of complete closed cpDNA genomes from *Trebouxia* algae for use as a reference impedes the study of their general organization in this algal genus. It is not known, for example, whether they have a quadripartite structure, if inverted repeat regions are present, and if they are, their extent and composition. Hence, this study reports the sequence of the chloroplast genome of *Trebouxia* sp. TR9, a phycobiont of the lichen *Ramalina farinacea*, whose completely sequenced mitochondrial genome has been recently published (Martínez-Alberola et al. 2019) and has been extensively studied in recent years in relation to many ecological and physiological traits (Casano et al. 2011, 2015, del Hoyo et al. 2011, Álvarez et al. 2012, del Campo et al. 2013, Centeno et al. 2016, Moya et al. 2017, Hell et al. 2019). This is the first completely assembled chloroplast genome from a lichen-symbiont microalga belonging to the *Trebouxia* genus obtained from high-throughput sequencing. Here, we discuss the structure, organization, gene content, and new features found in comparison with other chloroplast genomes reported for Trebouxiophyceae microalgae. We also provide a fairly resolved phylogenetic reconstruction on the basis of well-conserved chloroplast genes coding for proteins.

MATERIALS AND METHODS

Phycobiont isolation and culture conditions. *Trebouxia* sp. TR9 was isolated from the lichen *Ramalina farinacea* (Gasulla et al. 2010) and cultured in BOLD'S BASAL 3N medium (Bold and Parker 1962) in a growth chamber at 20°C under a 12:12 h light:dark cycle (lighting conditions: 25 μmol photons $\cdot$ $m^{-2} \cdot s^{-1}$).

DNA isolation, high-throughput, and sanger sequencing. Genome assembly and annotation: DNA extraction and purification were performed according to the protocol described by (Ausubel et al. 2003). Purified DNA was sequenced using a combination of high-throughput sequencing technologies including ROCHE 454 GS FLX Titanium (Lifesequencing facilities, Parc Cièntific, University of Valencia, Spain), ROCHE 454 "paired-end" GS JUNIOR (Genomics Unit, SCSIE-University of Valencia). Initially, we obtained a total of 240,256 single-end (SE) reads with an average length of 580 bp and a total length of 13,92 Mb, which were obtained through ROCHE 454 GS FLX Titanium. After filtering, the resulting 140,740 reads were assembled with MIRA v3.2.0. (Chevreux et al. 2004) into 6,757 contigs comprising 4,711,918 nt. This assembly strategy showed a N50 value of 729 considering all contigs (the largest contig included 59,973 nt). Subsequently, we had 154,237 paired-end reads (PE; insert size ~3,000 nt) with an average length of 393 nt and 60,66 Mb, which were obtained through ROCHE 454 GS JUNIOR. A total of 104,113 paired reads were retained for further analyses after the separation of PE reads from each other and from adapters in both forward and reverse directions with an average length of 191 and 175 nt and a total length of 19,95 and 18,22 Mb, respectively. Newbler v2.86 (Roche) was used for assembly paired reads obtained from ROCHE 454 GS JUNIOR by setting the OverlapMinMatchIdentity=90. Filtering of reads was performed with LUCY v1.20p (Chou and Holmes 2001). Contigs/scaffolds corresponding to the chloroplast genome were selected using BLASTn, BLASTx, and tBLASTx (Altschul et al. 1997) against a local database of chloroplast genomes from Viridiplantae built from NCBI nucleotide databases. Afterwards, all the sequences, identified as belonging to the chloroplast genome, were assembled with MIRA v3.2.0. (Chevreux et al. 2004). The final result was a total of 113 contigs which were reduced to 45 after PCR amplifications and Sanger sequencing. With the information of the ROCHE GS JUNIOR "paired-end" readings, the Newbler assembler calculated the distance between the 45 contigs whose junctions were impossible to sequence due, in large part, to the presence of numerous repetitions and homopolymeric regions. After assembling the complete genome (Fig. 1), additional PCR amplifications and

Sanger sequencing were performed to confirm junctions between LSC, IRs, and SSC regions with appropriate primer pairs (Table S1 in the Supporting Information and Fig. 2). PCRs were performed in a 96-well LabCycler (SensoQuest Biomedizinische Elektronik, Goettingen, Germany) using EmeraldAmp GT PCR Master Mix (Takara Bio Inc., Shiga, Japan). PCR products were purified using Illustra GFX PCR DNA (GE Healthcare Life Science, Buckinghamshire, England) and sequenced with an ABI 3100 Genetic Analyzer using an ABI BigDye™ Terminator Cycle Sequencing Ready Reaction Kit (Applied Biosystems, Foster City, CA, USA).

Most of the genes and open reading frames (ORFs) were identified and annotated using the MFannot organelle genome annotator (Lang et al. 2007) and BLAST searches against the NCBI databases. Introns and tRNA genes were identified with RNAweasel.

Sequencing of the rps4 *gene from* Trebouxia *sp. TR9.* The *rps4* mRNA was searched among a collection of transcripts obtained after total cDNA sequencing of *Trebouxia* sp. TR9. The search was performed with tBLASTn using the sequence of the RPS4 protein of *Coccomyxa* sp. C-169 as template (accession YP_004222050). As a result, a transcript was identified as

FIG. 1. Gene map of the complete chloroplast genome of the microalga Trebouxia sp. TR9. Genes shown inside the circle are transcribed clockwise, and genes outside are transcribed counterclockwise. Genes with introns are marked with asterisks. The dark gray in the inner circle corresponds to the GC content and the light gray corresponds to the AT content. The dark and light gray in the outer circle corresponds to the LSC and SSC regions, respectively. The two inverted repeat regions are indicated as IRA andIRB between the LSC and SSC regions. [Color figure can be viewed at wileyonlinelibrary.com]

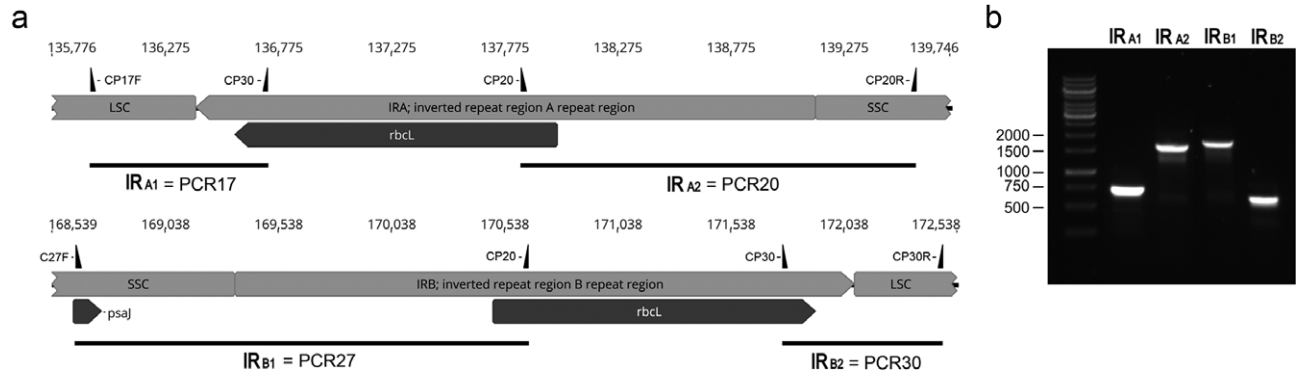

FIG. 2. Analysis of junctions between each IR sequence and SC regions in the *Trebouxia* sp. TR9 chloroplast genome. (a) Genetic maps showing junctions between each IR sequence and SC regions of the cpDNA from *Trebouxia* sp. TR9. Primer locations and polarities are indicated as black triangles on the maps showing the junctions between each IR sequence and SC regions. PCR products resulting from amplifications with each primer pair are indicated below maps. Primers and PCR products correspond to those of Table S1. (b) Agarose gel electrophoresis of PCR amplification products obtained to test junctions between each IR sequence and SC regions.

the product of the expression of the chloroplast *rps4* gene. The gene encoding such transcript was amplified by PCR and sequenced with Sanger method. For this purpose, we used DNA extracted form *Trebouxia* sp. TR9 as template and primers (listed below), which were designed on the basis of the previously identified *rps4* transcript. Exons and introns within the *rps4* gene were predicted with Augustus software (Stanke and Morgenstern 2005). The obtained sequences of the *rps4* transcript and the corresponding gene are available at the NCBI databases with accessions MK630219 and MN083271, respectively.

List of oligonucleotides:

rps4_1F: 5′-ATAGCGCACGTCGTCTAACG-3′
rps4_2R: 5′-AATTGCTGACTGAGAGGACG-3′
rps4_3F: 5′-AATTGTGCGGAGACTTGGAG-3′
rps4_4R: 5′-ATGAGACGCACACCATACTG-3′
rps4_5FB: 5′-TCTTGCACCCACCATGTCAG-3′
rps4_6R: 5′-GTAATATGACCGTGGCAGAC-3′
rps4_7F: 5′-ACTCAAGTAGCCGACCTATG-3′
rps4_intron3F: 5′-CCAGCTTGATTGCTGATAGC-3′
rps4_intron3R: 5′-ATACCAGAGTCCTGATCACC-3′
rps4_7R: 5′-CATAGGTCGGCTACTTGAGT-3′
rps4_8R: 5′-CTGAATTCTGGTGCTTGAGC-3′

Phylogenetic analyses. Phylogenetic reconstructions were performed based on alignment of the concatenated amino acid sequences resulting from the translation of 36 conserved chloroplast genes. The amino acid sequences obtained were aligned with Muscle (Edgar 2004) and trimmed with Gblocks (Castresana 2000) using stringent selection options which do not allow many contiguous non-conserved positions. For maximum-likelihood (ML) analyses, the substitution model used was LG+G+I, which was selected according to the automatic model selection of PhyML (Lefort et al. 2017). The concatenated nucleotide matrix of 27 taxa and 7,206 aa was analyzed with PhyML (Guindon et al. 2010). Bootstrap probabilities (Felsenstein 1985) were calculated to estimate the robustness of the clades from 100 replicates in the data. The consensus tree was drawn with FigTree (Rambaut 2008).

Additional analyses. Repeat sequences were detected with the online version of REPuter (Kurtz et al. 2001). We included direct, reverse, and palindromic repeat sequences with minimum repeat size of 30 bp. To avoid redundancy, one of the two inverted repeat (IR) regions was removed prior to identification of repeat motifs. Gene maps were constructed with Geneious R11 (Kearse et al. 2012). Tandem repeats were found using the Tandem repeats finder program (Benson 1999). Predictions of trans-membrane domains were obtained using Phobius (Kall et al. 2004). Searches for possible transit peptides were performed with TargetP 1.1 (Emanuelsson et al. 2007). Predictions of protein motifs were performed by comparison against the NCBI-CDD motif library (Marchler-Bauer et al. 2013) using *the GenomeNet protein motif search service (*https://www.genome.jp/tools/motif/). Protein structures were computed using phyre2 (Kelley et al. 2015) and graphically visualized with RasMol (Sayle and Milner-White 1995). The alignment of the cpDNAs from *Myrmecia israeliensis* and *Trebouxia* sp. TR9 was carried out using the ProgressiveMauve algorithm of Mauve 2.3.1 (Darling, et al. 2010).

RESULTS

The chloroplast genome of *Trebouxia* sp. TR9: sequencing, assembly, and structural features. The chloroplast genome of *Trebouxia* sp. TR9 (Fig. 1; accession MK643158) is a circular molecule of 303,163 bp with a GC content of 31.9%. The cpDNA from *Trebouxia* sp. TR9 showed a quadripartite structure with a LSC region (267,489 bp), a SSC region (30,194 bp), and a pair of short IR sequences (2,740 bp, each one). The IR sequences in the cpDNA of *Trebouxia* sp. TR9 include the *rbc*L gene but not the rRNA operon. The existence of inverted repeated sequences in the cpDNA forms *Trebouxia* sp. TR9 and junctions with either the SSC or LSC regions were confirmed by a series of PCR reactions with specific primers (Fig. 2) whose products were sequenced to test their specificity.

Analysis of the gene content of the cpDNA from Trebouxia *sp. TR9 reveals the transfer of the* rps4 *gene to the nucleus.* The cpDNA of *Trebouxia* sp. TR9 included a total of 138 genes (Table 1) and a total of nine group I introns interrupting three different genes: a single gene encoded a protein (*psaA*) and two encoded rRNAs (*rrs* and *rrl*). Intron lengths ranged from 1,361 bp to 634 bp for introns 4 and

TABLE 1. List of annotated genes in the *Trebouxia* sp. TR9 chloroplast genome.

Classification of genes	Gene names	Number
RNA genes		
Ribosomal RNAs	*rrnf, rrnl, rrs*	3
Transfer RNAs	*trnA(ugc), trnC(gca), trnD(guc), trnE(uuc), trnF(gaa), trnG(gcc), trnG(ucc), trnH(gug), trnI(cau), trnI(gau), trnK(uuu), trnL(caa), trnL(uaa), trnL(uag), trnMe(cau), trnMf(cau), trnN(guu), trnP(ugg), trnQ(uug), trnR(acg), trnR(ucu), trnS(cgu), trnS(uga), trnT(ggu), trnT(ugu), trnV(uac), trnW(cca), trnY(gua)*	28
Protein genes		
Photosynthesis		
Chlorophyll biosynthesis	*chlB, chlI, chlL, chlN*	4
Photosystem I	*psaA, psaB, psaC, psaI, psaJ, psaM*	6
Photosystem II	*psbA, psbB, psbC, psbD, psbE, psbF, psbH, psbI, psbJ, psbK, psbL, psbM, psbN, psbT, psbZ*	15
Cytochrome b6/f	*petA, petB, petD, petG, petL*	5
ATP synthase	*atpA, atpB, atpE, atpF, atpH, atpI*	6
Rubisco	*rbcL*	2
Ribosomal proteins		20
Large subunit	*rpl2, rpl5, rpl12, rpl14, rpl16, rpl19, rpl20, rpl23, rpl32, rpl36*	10
Small subunit	*rps2, rps3, rps7, rps8, rps9, rps11, rps12, rps14, rps18, rps19*	10
Transcription/translation		
RNA polymerase	*rpoA, rpoB, rpoC1, rpoC2*	4
Translation initiation factor 1	*infA*	1
Translation elongation factor Tu	*tufA*	1
Chloroplast envelope membrane protein	*cemA*	1
Transport proteins	*cysA, cysT*	2
Other proteins	*accD, ccsA, ftsH, minD, tilS*	5
Conserved reading frames	*ycf1, ycf3, ycf4, ycf12, ycf20, ycf47*	6
Intron-encoded homing endonucleases	*orf171 (rrl, intron 2)* *orf93 (rrl, intron 3)* *orf236 (rrl, intron 4)* *orf71 (rrl, intron 5)* *orf300 (psaA)*	5
Non-conserved hypothetical proteins	*orf90* *orf321* *orf429* *orf451*	4
Total		138

5 in the *rrl* gene. Five introns encoded ORFs whose products were identified as homing endonucleases, one within intron of the *psb*A gene and the remaining four within introns 2, 3, 4, and 5 of the *rrl* gene. All the proteins encoded within introns belonged to the LAGLIDADG family, with sizes ranging from 300 aa within the *psb*A gene to 71 aa within the *rrl* gene (intron 5). The protein-coding gene content of the cpDNA from *Trebouxia* sp. TR9 was similar to other Trebouxiophyceae except for the absence of the *rps4* gene as in the case of *Trebouxia aggregata* and *Myrmecia israeliensis* (Fig. 3). Consequently, we wondered whether this gene could have migrated to the nucleus in *Trebouxia* sp. TR9. The presence of a nuclear-encoded *rps4* gene was confirmed by its sequencing with Sanger method. The obtained DNA sequence indicated the existence of a complete *rps4* gene, which included four exons separated by three spliceosomal introns (Fig. 4a). This finding confirmed our initial assumption that this gene was coded in the nuclear genome instead of the plastome in *Trebouxia* sp. TR9. The deduced protein encoded by the *rps4* gene had 251 aa in *Trebouxia* sp. TR9 and was recognized as the ribosomal protein S4 (CHL00113) by comparison against the NCBI-CDD database using *the* GenomeNet protein motif search service (*e-value of 9e-108).* In *Trebouxia* sp. TR9, the RPS4 protein had an extra sequence of 50 aa (Fig. 4b), which was predicted as a transit peptide for targeting the chloroplast with TargetP (Emanuelsson et al. 2007). Interestingly, we also found the complete sequence of the *rps4* gene in *Trebouxia* sp. strain TZW2008 available at the NCBI (GenBank assembly accession: GCA_002118135.1), which is the photosynthetic partner of the lichen *Usnea hakonensis.* The *rps4* gene in this *Trebouxia*

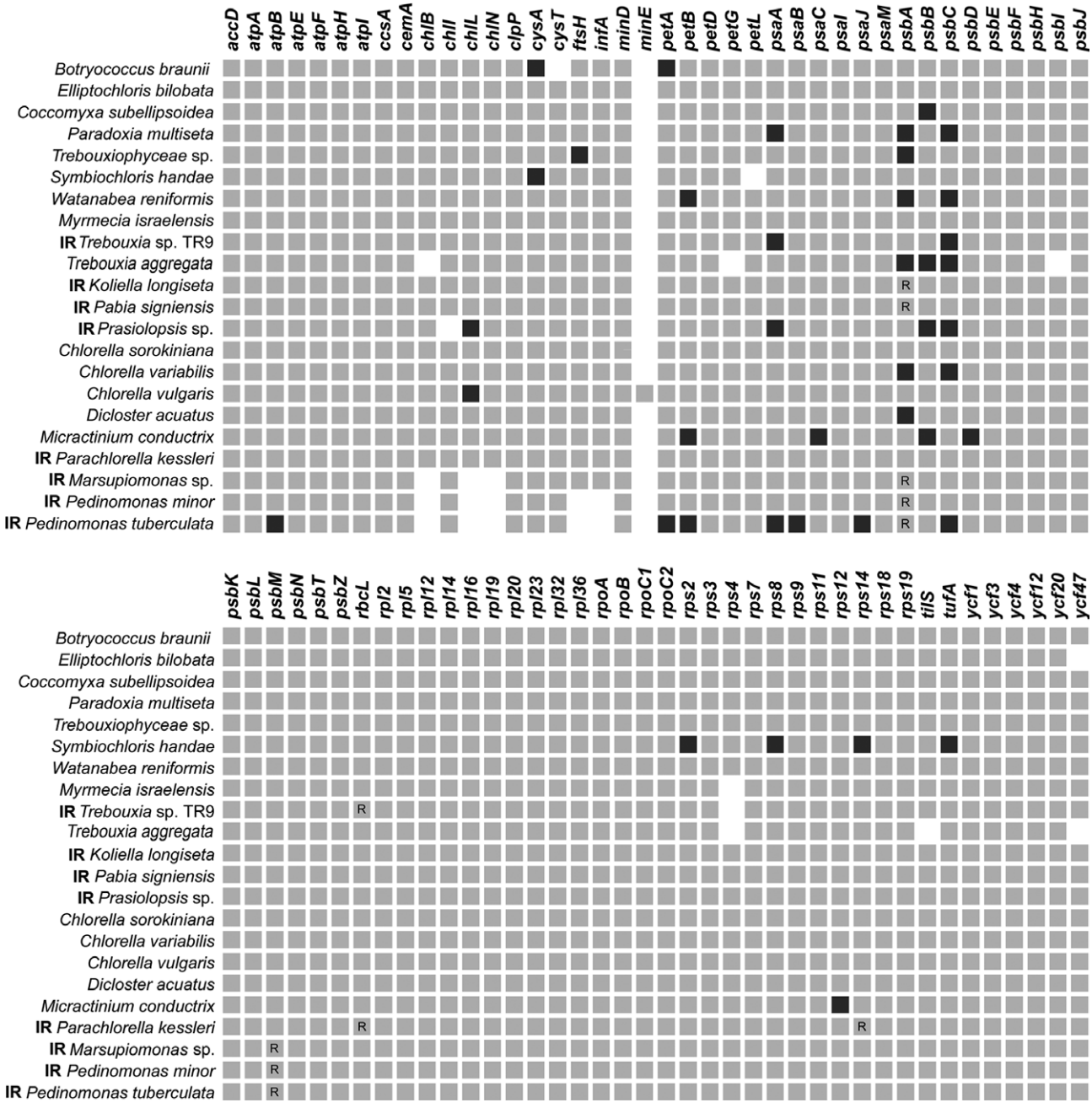

FIG. 3. Gene repertoires coding for proteins of the cpDNAs from the Trebouxiophyceae and Pedinophyceae examined in this study. Light and dark gray squares indicate the presence of the corresponding gene without or with introns, respectively. Empty spaces indicate the absence of the corresponding gene. Repeated genes are indicated with "R".

species had 1,093 bp (positions 232,96 to 234,052 in assembly TrTZW2008_1.0 [contig_122]), which included spliceosomal introns predicted with Augustus (Stanke and Morgenstern 2005). Alignment of the chloroplast RPS4 protein from a number of green algae and two land plants (Fig. 4c) showed high conservation of this protein.

Non-conserved open reading frames (ncORFs) showed no significant similarity to any known proteins. Three non-conserved ORFs (ncORFs) were found in a row within the LSC region between the *psaB* and *cemA* genes (*orf321*, *orf429*, and *orf451* in Fig. 1). Since the translation products of these three ORFs showed no significant similarity to any known proteins, they were defined as hypothetical proteins. Only the predicted protein encoded by *orf451* yielded alignments with four hypothetical proteins encoded by ORFs in the chloroplast genome of other green algae (Fig. 1): the Trebouxiophyceae *Prasiola crispa* (*orf1151*, accession AKZ21081), with

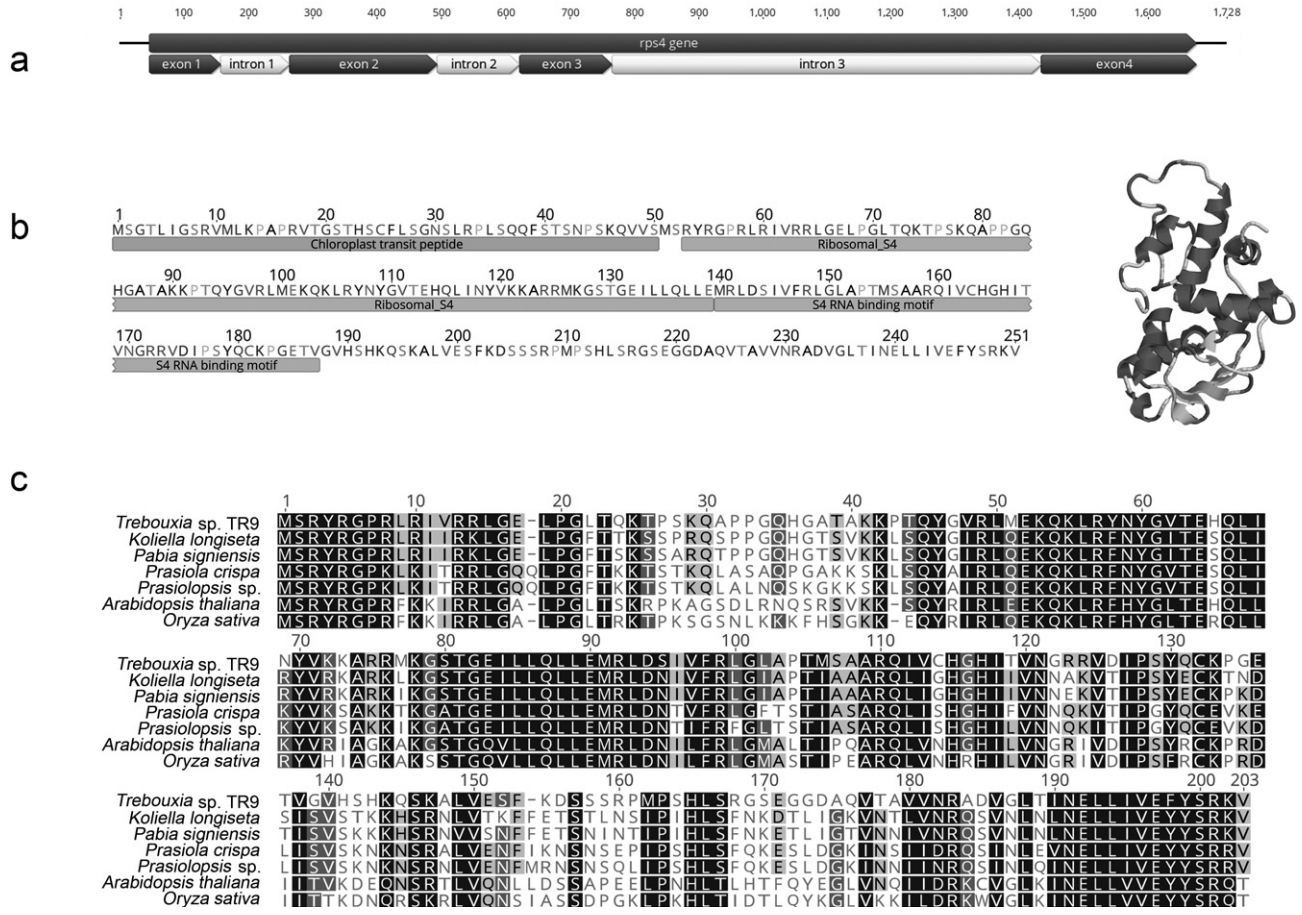

FIG. 4. Structure of the nuclear-encoded *rps4* gene of *Trebouxia* sp. TR9 and alignment of the RPS4 proteins. (a) Genetic map of the *rps4* gene from *Trebouxia* sp. TR9. The complete gene is depicted as a dark gray arrow at the top. Exons and introns are indicated at the bottom as dark and light gray arrows, respectively. (b) Primary and secondary structures of the chloroplast RPS4 protein encoded in the nuclear genome from *Trebouxia* sp. TR9 resulting from translation of the reconstructed mRNA. (c) Alignment of the chloroplast RPS4 protein from several algae and plants. GenBank accessions for *Arabidopsis thaliana*, *Oryza sativa*, and *Prasiola crispa* are NC_000932, NC_031333, and KR017750, respectively. GenBank accessions for the remaining algae are indicated in Figure 7.

71% of query coverage, 23% of identity, and an e-value of 5e-10; the Chlorophyceae *Oedocladium carolinianum* UTEX LB 1686 (*orf354*, accession YP_009310764), with 64% of query coverage, 24% of identity, and an e-value of 5e-14; and the Prasinophyceae *Nephroselmis olivacea* NIES 484 (*orf594*, accession NP_050894), with 66% of query coverage, 25% of identity, and an e-value of 7e-08. The predicted protein encoded by *orf451* also yielded alignments with hypothetical proteins encoded by ORFs in the chloroplast genome of ferns (e.g., the fern *Mankyua chejuensis*, *orf295*, accession YP_005352949), with 54% of query coverage, 23% of identity, and an e-value of 5e-08. The hypothetical protein encoded for *orf1151* from *P. crispa* was predicted as a phage- or plasmid-associated DNA primase by the GenomeNet protein motif search service (e-value of 3e-18). Predictions of trans-membrane domains revealed the presence of five trans-membrane domains in the protein encoded by *orf321* and a single trans-membrane domain in the protein encoded by *orf429*; no trans-membrane domains were predicted for the protein encoded by *orf451*. No functional motifs were found for either *orf321* or *orf451*. An additional ncORF (*orf90*) was found within the LSC region between the *rps12* and *rps7* genes, which was predicted as a YhgA-like putative transposase by the GenomeNet protein motif search service (e-value 6.33e-03).

Comparative analyses of the structure of the cpDNA from Trebouxia *sp. TR9 with other Trebouxiophyceae.* A comparison of the structure of the cpDNAs from different Trebouxiophyceae and Pedinophyceae (Fig. 5) revealed that *Trebouxia* sp. TR9 had one of the largest cpDNAs. This markedly larger size was mainly due to the presence of large intergenic spacers occupying 69.27% of the genome. Similarly, in other large cpDNAs, such as those from *Symbiochloris handae* and *Prasiolopsips* sp., more than 60% was occupied by intergenic spacers (63.91% and 66.69%, respectively). Conversely, in *Chlorella sorokiniana*, which had the shortest cpDNA among

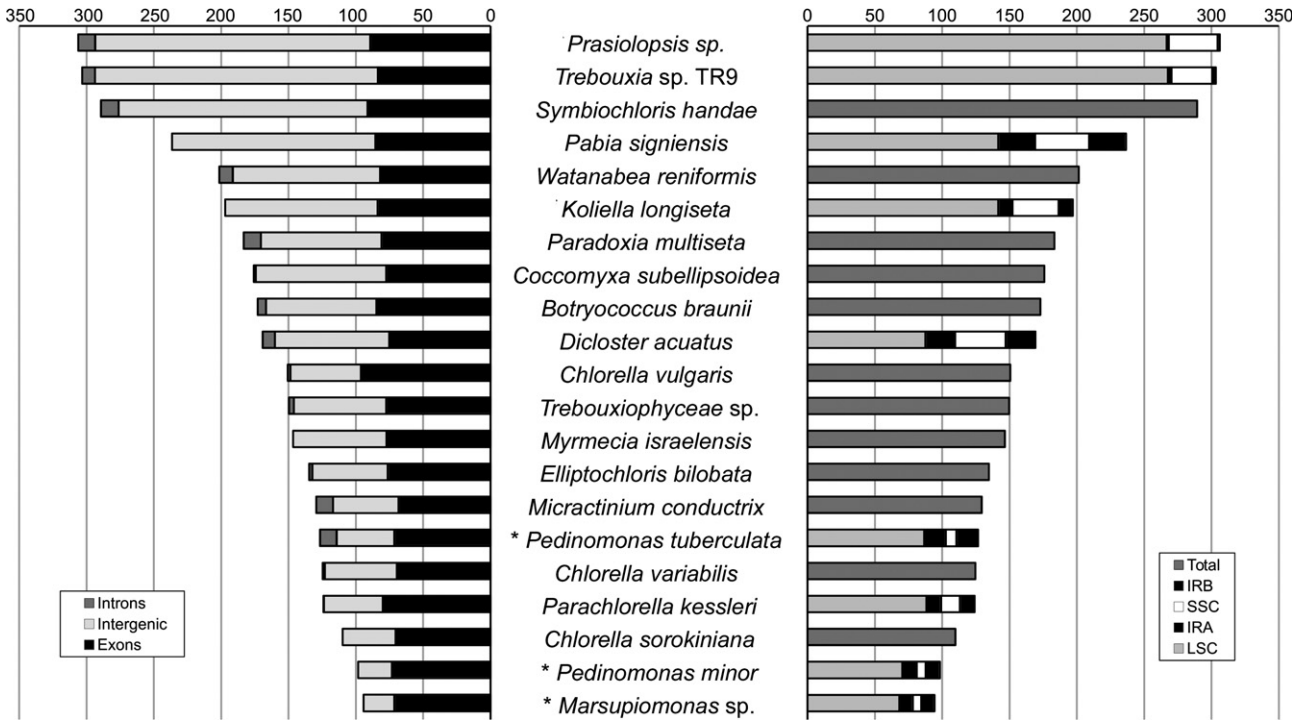

FIG. 5. Total lengths (bp) of different regions of the cpDNAs in Trebouxiophyceae and Pedinophyceae (marked with asterisks). Total lengths (bp) of different regions of the cpDNAs. Exonic, intronic, and intergenic sequences are indicated on the left, whereas IRs, LSC, and SSC regions are indicated on the right.

the Trebouxiophyceae studied, only 35.72% of the genome was occupied by intergenic spacers. The smallest, most compact chloroplast genomes belonged to the Chlorellales and Pedinophyceae. Interestingly, the most expanded cpDNAs belonged to three lichen algae: *Trebouxia* sp. TR9 (303,163 bp), *Symbiochloris handae* (289,394 bp), and *Trebouxia aggregata* (245,794 bp after adding all partial plastid sequences available in GenBank). To determine whether the presence of large intergenic spacers was related to larger cpDNAs, we searched for repetitive sequences in general (*rs*) including direct, reverse, and palindromic repeat sequences with minimum repeat size of 30 bp with REPuter (Kurtz et al. 2001) and tandem repeats (*tr*) in particular, which are a very important subtype of repeats consisting on two (or more) copies of the repeat immediately follow each other in the DNA sequence using the Tandem repeats finder program (Benson 1999). Our results indicated that *Trebouxia* sp. TR9 with the largest cpDNA had also the highest numbers of repeated sequences with a total of 1129 *rs* and 315 *tr* (Fig. 6). The remaining Trebouxiophyceae had a variable number of *tr* ranging from fewer than 8 in *Chlorella sorokiniana*, *Trebouxiophyceae* sp., and *Micractinium conductrix* to more than 100 in *Dicloster acuatus*, *Coccomyxa* sp., and *Trebouxia* sp. TR9. Similarly, they had a variable number of *tr* ranging from fewer than 15 in *Chlorella sorokiniana*, *Parachlorella kessleri*, and *Micractinium conductrix* to more than 1,000 in *Prasiolopsis* sp., *Trebouxia* sp. TR9, and *T. aggregata*. Plastomes with sizes of more than 200 Kbp had the highest number of *rs* more than 900, whereas cpDNAs with sizes less than 125 Kbp had the lowest number of *rs* with less than 30. Chloroplast genomes with a high number of *rs* had not necessarily a high number of *tr*. For instance, *Botryococcus braunii* had 829 *rs* and 20 *tr*, whereas *Dicloster acuatus* had 98 *rs* and 103 *tr*.

The architectures of the chloroplast genomes are diverse among Trebouxiophyceae. To determine the level of gene rearrangements in the Trebouxiales, we compared gene orders in the plastomes of *Trebouxia* sp. TR9 and *Myrmecia israeliensis* by aligning them (Fig. S1 in the Supporting Information). The results revealed low synteny due to extensive rearrangements including 21 reversals and great extensions of intergenic regions between conserved blocks. Only the large stretch including blocks 13, 14, and 15 (Fig. S1) is well conserved in both *M. israeliensis* and *Trebouxia* sp. TR9 except for the reversal of the *rpl16* gene and the lack of *rps36* between *infA* and *rps11* in *Trebouxia* sp. TR9. Another remarkable difference between the plastomes of *Trebouxia* sp. TR9 and *M. israeliensis* is the presence of small IRs in *Trebouxia* sp. TR9 and their absence in *M. israeliensis*. Among the studied Trebouxiophyceae, only cpDNAs from six algal species had recognizable IRs, in Trebouxiales, Prasiolales, and Chlorellales (Fig. 6). Neither the presence/

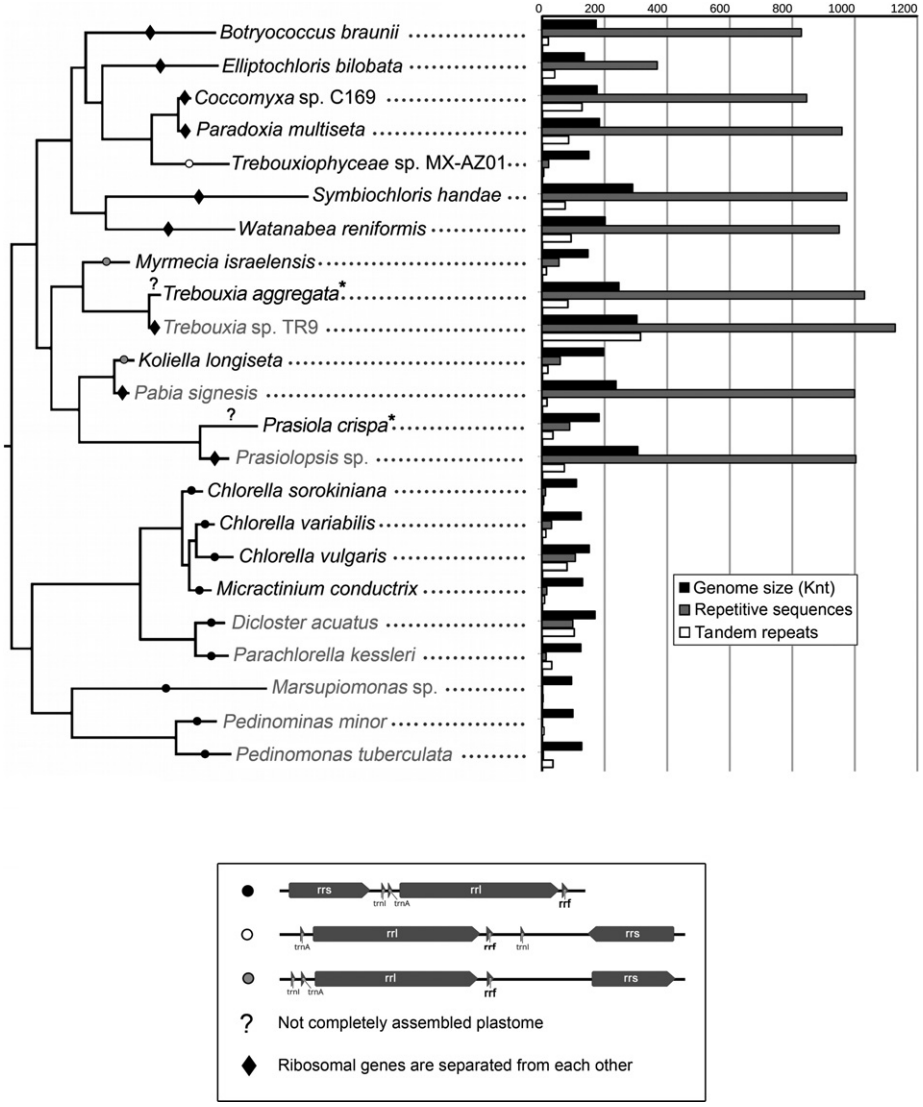

FIG. 6. Content of repeats including repetitive sequences in general ≥ 30 bp and tandem repeats in particular within the chloroplast genomes examined in this study. Genome sizes and number of repeats are indicated in relation to the phylogenetic relationships of algal species. Algae whose cpDNA has IRs are indicated in gray letters. Taxa whose cpDNA has not been completely sequenced/assembled are indicated with asterisks.

absence nor the lengths or gene content of the IR regions were related to the phylogenetic relationships among Chlorophyta algae. All the IRs analyzed contained the rRNA operon except for three Trebouxiophyceae: *Trebouxia* sp. TR9, *Prasiolopsis* sp., and *Stichococcus bacillaris*. In the cpDNAs of green algae, the genes coding rRNAs can appear either within an operon or separated and even scattered along the plastome. All the analyzed algal species belonging to the Chlorellales analyzed in this study had the ribosomal genes within an operon, which included *rrs, rrl*, and *rrf* genes (in this order) as in Pedinophyceae. However, in the remaining algal groups within Trebouxiophyceae, the ribosomal genes were not included in an operon and if so, their arrangement was different from that of Chlorellales and Pedinophyceae (Fig. 6). Interestingly, all of the cpDNAs whose ribosomal genes were not included in operons had a high proportion of ssr. This observation suggested that the presence of abundant ssr may promote intensive gene rearrangements, which can include disruption of conserved operons. The comparative analysis of the IRs from 43 Chlorophyta algae showed a very variable length (Fig. S2 in the Supporting Information), ranging from fewer than 3 Kb in the Trebouxiophyceae *Prasiolopsis* sp. and *Trebouxia* sp. TR9 (1.7 and 2.7 Kb, respectively) to 46,137 bp in the Prasinophyceae *Nephroselmis olivacea*. As far as we know, the chloroplast genome of *Trebouxia* sp. TR9 and *Prasiolopsis* sp. have the shortest IRs from among the Chlorophyta algae whose cpDNA has

been completely sequenced. Overall, the IRs analyzed contained 40 different genes coding for proteins, which appeared with different frequencies. The *psbA* gene was the most frequent (17 out of 43 IRs) followed by *chlN*, *psbM*, and *rbcL* (5 out of 43 IRs). Genes coding tRNAs for 15 different aa were also recurrently present in the IRs, with the tRNAs for alanine and isoleucine being the most frequent (39 and 44 occurrences, respectively).

Phylogenetic relationships between Trebouxia *sp. TR9 and other Trebouxiophyceae.* Here, we present a phylogenetic reconstruction of relationships between *Trebouxia* sp. TR9 and other Trebouxiophyceae (Fig. 7), including two prasinophytes (*Nephroselmis astigmatica* and *N. olivacea*) and two streptophytes (*Chlorokybus atmophyticus* and *Chara vulgaris*) as outgroup. All analyses were based on an alignment of 7,206 aa, including the sequences of 20 proteins related to photosynthesis (encoded by genes *atpA*, *atpB*, *atpE*, *petA*, *petB*, *psaA*, *psaB*, *psbA*, *psbB*, *psbC*, *psbD*, *psbE*, *psbH*, *psbJ*, *psbK*, *psbL*, *psbN*, *psbT*, *psbZ*, and *rbcL*), 14 ribosomal proteins (encoded by genes *rpl2*, *rpl5*, *rpl14*, *rpl16*, *rpl20*, *rpl23*, *rps02*, *rps03*, *rps07*, *rps08*, *rps11*, *rps12*, *rps18*, and *rps19*) and proteins encoded by genes *tufA* and *ycf3*. The phylogram obtained (Fig. 7) shows two major sister clades (clade I and clade II). Clade I includes the Trebouxiales *Myrmecia israeliensis*, *Trebouxia* sp. TR9, and *T. aggregata*, together with the Prasiolales *Koliella longiseta*, *Pabia signiensis*, *Prasiola crispa*, and *Prasiolopsis* sp., and other Trebouxiophyceae of uncertain systematic classification. Clade II includes the Chlorellales *Chlorella sorokiniana*, *C. variabilis*, *C. vulgaris*, *Dicloster acuatus*, *Micractinium conductrix*, and *Parachlorella kessleri*, together with the Pedinophyceae *Marsupiomonas* sp., *Pedinomonas minor*, and *P. tuberculata*. This phylogenetic reconstruction shows that *Trebouxia* sp. TR9 is closely related to *T. aggregata*, another lichen phycobiont whose cpDNA has not been completely sequenced (Turmel et al. 2015). The two lichen microalgae were included within a sub-clade together with *Myrmecia israeliensis* (Trebouxiales).

DISCUSSION

There is a much higher number of sequenced chloroplast genomes in the Trebouxiophyceae than in the other green algal classes (e.g., Lemieux et al. 2014a, Turmel et al. 2015). In this algal class, chloroplast genomes show a 3.3-fold variation in size (Turmel et al. 2015). The chloroplast genome from *Trebouxia* sp. TR9 described here is the first completely assembled chloroplast genome from a *Trebouxia* phycobiont and is the largest one reported in the Trebouxiophyceae apart from *Prasiolopsis* sp. SAG 84.81, whose cpDNA has a similar size of 306,152 bp (Turmel et al. 2015). Size variations in

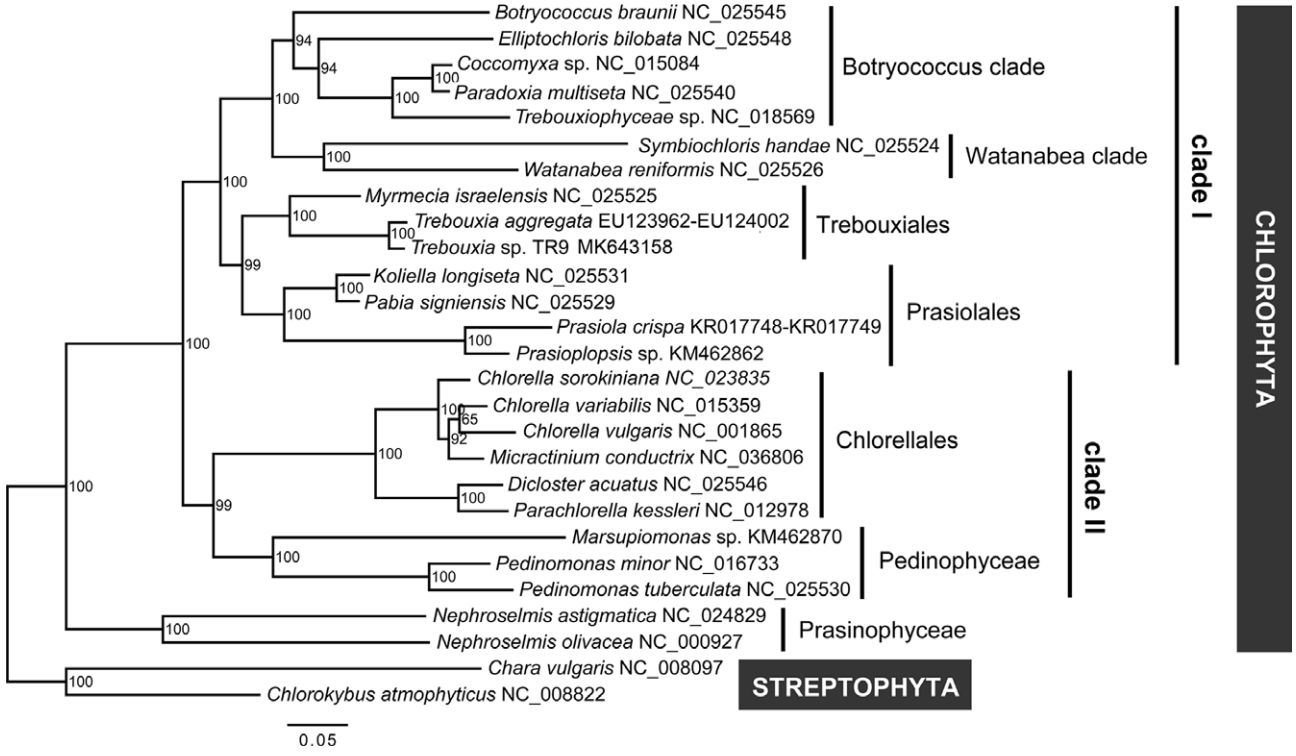

FIG. 7. Phylogram inferred with the maximum-likelihood method and based on alignment of the concatenated amino acid sequences resulting from the translation of 36 selected chloroplast genes coding for proteins from 27 green algal species. Bootstrap values are indicated in the nodes. The scale bar indicates substitutions/site. Current taxonomic classifications are indicated on the right.

chloroplast genomes have mainly been attributed to four factors: (i) differences in length of intergenic spacers, (ii) fluctuations in intron content, (iii) expansion/shrinkage-disappearance of IRs, and (iv) the presence of long non-conserved ORFs (Turmel et al. 2005, 2015, Brouard et al. 2010, Muñoz-Gómez et al. 2017, Cremen et al. 2018). The loosely packed chloroplast genome of *Trebouxia* sp. TR9 may be the consequence of an expansion of intergenic regions, which may have occurred through gain of tandem repeat units. The large sizes of the chloroplast genomes in *Trebouxia* sp. TR9 and *Prasiolopsis* sp. with respect to other Trebouxiophyceae are mainly attributable to the presence of large intergenic spacers. However, explanations of the underlying mechanisms of variations in DNA content, structural arrangement, and gene content of eukaryotic genomes in general are still a matter of debate. *Trebouxia* sp. TR9 and *Prasiolopsis* sp. are considered symbionts of fungi (Muggia et al. 2017) and sloths, respectively (Suutari et al. 2010, Fountain et al. 2017). *Myrmecia israeliensis*, a free-living, symbiotic microalga closely related to *Trebouxia* sp. TR9 and *Prasiolopsis* sp., has a chloroplast genome with a fairly average size (146,596 bp; Fig. 5). Other symbiotic Trebouxiophyceae such as *Chlorella heliozoae*, *C. variabilis*, and *Micractinium conductrix*, which are protist endosymbionts, generally have larger chloroplast genomes than other closely related, free-living algae (Fan et al. 2017). These observations indicate the existence of extensive variations in non-coding regions in the plastomes of closely related species within individual lineages and suggest that the transition to symbiosis might be responsible for enlargement of the chloroplast genomes in some Trebouxiophyceae. Both genome expansion and shrinkage have been proposed as evolutionary strategies to achieve an optimal balance between genome stability and plasticity (Schubert and Vu 2016). We hypothesize that genome plasticity may be more important than stability in symbiotic algae, and is possibly necessary for successful associations in each habitat type. However, it will be necessary to obtain more plastome sequences from symbiotic Trebouxiophyceae to corroborate this hypothesis.

The chloroplast genomes of green algae exhibit greater variability in the presence/absence, size, and gene content of IRs than land plants (e.g., Pombert et al. 2005, 2006, Brouard et al. 2010, Lemieux et al. 2014b, 2016, Sun et al. 2016, Turmel et al. 2017). This renders it difficult to determine how many times this structure has been lost during the evolution of green algae. Generally, chloroplast genomes from green algae and plants have IR sequences that include the rRNA operon but rarely include the *rbc*L gene. Conversely, IR sequences in the cpDNA of *Trebouxia* sp. TR9 include the *rbc*L gene but not the rRNA operon. After analyzing the availability of cpDNAs at the NCBI (accessed on October 31, 2018) from Chlorophyta algae, we found that 42 out 126 cpDNAs had IRs including that of *Trebouxia* sp. TR9. According to Turmel et al. (2015), at least seven independent losses of IRs may have taken place among the Trebouxiophyceae, one of them in a superclade including the Trebouxiales. Thus, the finding of IRs in the chloroplast genome of *Trebouxia* sp. TR9, which belongs to the Trebouxiales, suggests that wider sampling with more representatives of each lineage will be necessary to obtain a clearer picture of IR losses during the evolution of the Trebouxiophyceae and green algae in general. The IRs of the chloroplast genome of *Trebouxia* sp. TR9 exhibit two features that are rather unusual among the Trebouxiophyceae and other green algae: (i) the absence of any rRNA gene and (ii) the presence of the *rbc*L gene. One possible explanation for the absence of rRNA genes within the IRs in *Trebouxia* sp. TR9 and other Trebouxiophyceae (e.g., *Prasiolopsis* sp. and *Stichococcus bacillaris*) may be the occurrence of repeated events of IR contraction, as previously proposed by Turmel et al. (2017). An alternative explanation for both the absence of rRNA genes and the presence of the *rbc*L gene might be the de novo creation of IRs.

Interestingly, the stretch including the *atpA* gene followed by the *atpF*, *atpH*, *atpI*, and *rps2* genes (in this order) is located at one of the two ends of the LSC adjacent to the IRB in *Trebouxia* sp. TR9 as in many other green algae (Turmel et al. 2015). Similarly, the simultaneous presence of the *rbc*L gene and the rRNA operon with various combinations of additional genes has been found in several green algae (e.g., *Nephroselmis olivacea* [Prasinophyceae; Turmel et al. 1999], *Oedogonium cardiacum* and *Oedocladium carolinianun* [Chlorophyceae; Brouard et al. 2008, 2016], *Parachlorella kessleri* [Trebouxiophyceae; Turmel et al. 2009b], and *Entransia fimbriata* [Streptophyta, Turmel et al. 2005]). Considering all these observations and the absence of any gene in the extremely reduced IRs of the cpDNA from *Prasiolopsis* sp., the most plausible explanation for the evolution of the *Trebouxia* sp. TR9 IRs is a progressive migration of genes from the IRs to either the SSC or LCS regions.

The chloroplast genomes from diverse green algae lineages contain genes encoding non-conserved ORFs (e.g., Prasinophyceae [Turmel et al. 1999], Trebouxiophyceae [Turmel et al. 2015], Chlorophyceae [Brouard et al. 2008, McManus et al. 2017], and Ulvophyceae [Cremen et al. 2018]). However, the evolutionary origins of these genes remain unknown. It has been proposed that they may be remnants of the cyanobacterial ancestor of plastids, which were differentially lost in the chloroplast genomes of all other algal lineages (Cremen et al. 2018). However, most of the ncORFs identified do not show close affinities with cyanobacterial genes. An alternative hypothesis supports the notion that ncORFs could be vestiges of viral infections (e.g., in Chlorophyceae [Brouard et al. 2008,

McManus et al. 2017], Prasinophyceae [Lemieux et al. 2014b], Trebouxiophyceae [Turmel et al. 2015], and Zygnematophyceae [Lemieux et al. 2016]) or acquired from mitochondria (Brouard et al. 2016) or bacteria (Leliaert et al. 2016). In the results section, we showed that the predicted protein encoded by *orf451* in the chloroplast genome of *Trebouxia* sp. TR9 yielded alignments with hypothetical proteins encoded by *orf151* in the chloroplast genome of the Trebouxiophyceae *Prasiola crispa*. This hypothetical protein of *P. crispa* was predicted as a phage- or plasmid-associated DNA primase, whose presence has been reported in a variety of green algal lineages (e.g., Prasinophyceae [Turmel et al. 1999, 2009a] and Chlorophyceae [Leliaert and López-Bautista 2015, Brouard et al. 2016, Cremen et al. 2018]). In ferns, some ncORFs named "Mobile Open Reading Frames in Fern Organelles" (MORFFO) are thought to have shaped plastome evolution (Robison et al. 2018). Some of these MORFFO share similarities with conserved domains associated with primase genes found in mobile elements of cyanobacteria similar to the ncORFs found in *P. crispa* (Robison et al. 2018). The presence of similar ncORFs in distant algal lineages, such as the Chlorophyceae (Brouard et al. 2016), Prasinophyceae (Lemieux et al. 2014b), and Trebouxiophyceae (this study, and Turmel et al. 2015), and even in ferns (Robison et al. 2018), supports the hypothesis of the presence of the extant ncORFs in an ancestor of green algae and land plants after being differentially lost in the chloroplast genomes of certain lineages during evolution.

In addition to gene gain, chloroplast genomes have undergone losses of genes whose functions have been assumed by nuclear-encoded genes (e.g., *rpl22* [Gantt et al. 1991, Jansen et al. 2011], *infA* [Millen et al. 2001], *rps16* [Ueda et al. 2008], *accD* [Magee et al. 2010], and *rpl32* [Park et al. 2015]). However, the present study shows the first evidence of the transfer of the *rps4* gene to the nucleus. Chloroplast ribosome SSU contains 16S rRNA and 24 proteins. In all, 12 of these proteins are encoded by the chloroplast genome (uS2c, uS3c, uS4c, uS7c, uS8c, uS11c, uS12c, uS14c, uS15c, bS16c, bS18c, and uS19c) while the remaining 12 proteins (bS1c, uS5c, bS6c, uS9c, uS10c, uS13c, uS17c, bS20c, bS21c, cS22-PSRP2, cS23-PSRP3, and bTHXc-PSRP4) are encoded by the nuclear genome and post-translationally imported into the chloroplast (Tiller and Bock 2014). Six of the ribosomal proteins of the 30S subunit (uS4c, uS7c, uS8c, uS15c, uS17c, and bS20c) are primary binding proteins since they can bind directly to 16S rRNA (Sykes and Williamson 2009). In the chloroplast ribosome, the uS4c protein surrounds the mRNA entry site together with the proteins uS3c and uS5c in an orientation similar to bacteria (Ahmed et al. 2017) and helps to initiate assembly of 16S rRNA, serving to organize and stabilize its tertiary structure through the S4/S9 N-terminal domain (Davies et al. 1998). The essential role of the chloroplast uS4c protein in land plants has been demonstrated in studies on mutants (e.g., Rogalski et al. 2008, Tang et al. 2018). The *rps4* gene is present in the chloroplast genomes of land plants, and even in the highly reduced chloroplast genome of two plant species in the endoparasite genus *Pilostyles* (Apodanthaceae; *P. aethiopica* and *P. hamiltonii*), each retaining just five or six possibly functional genes (Bellot and Renner 2015). Loss of the *rps4* gene in *Trebouxia* sp. TR9 (this study), *Myrmecia israeliensis*, and *Koliella corcontica* (Turmel et al. 2015) suggests that this gene might have been lost several times in different algal lineages within the Trebouxiophyceae. Gene transfer from the chloroplast genome to the nuclear genome is an important process in the evolution of contemporary chloroplasts from free-living cyanobacteria to endosymbionts. However, most studies on the evolution of DNA sequences from chloroplasts found in nuclear genomes have been performed in land plants (reviewed in Xiong et al. 2009). Thus, our finding of an unreported and unusual functional transfer of an essential gene from the chloroplast to the nuclear genome in the unicellular microalga *Trebouxia* sp. TR9 underlines the importance of sequencing more genomes and/or transcriptomes from understudied green algal groups, including symbiotic representatives. This would contribute to knowledge of the evolutionary history and interplay of chloroplast- and nuclear-encoded genes after endosymbiosis and the possible impact of symbiotic interactions with other organisms.

Phylogenetic reconstructions based on chloroplast gene sequences have contributed to resolve deep-level relationships within the Trebouxiophyceae (Lemieux et al. 2014a). However, the monophyly of this group is still a matter of debate. Some studies support the monophyly of Trebouxiophyceae (e.g., Leliaert et al. 2016, Fan et al. 2017, Fang et al. 2018), whereas others place the Chlorellales in a separate clade (e.g., Fučíková et al. 2014, Lemieux et al. 2014a, 2015, Sun et al. 2016). Recent studies evaluate the relevance to phylogenetic inference of the evolution of organellar-encoded proteins (Mekvipad and Satjarak 2019). Our phylogenetic reconstruction is based on set chloroplast-encoded proteins, which were considered suitable to resolve phylogenetic relationships among Chlorophyta algae (Mekvipad and Satjarak 2019). In this study, *Trebouxia* sp. TR9 appears closely related to *Trebouxia aggregata* and *Myrmecia israeliensis*, being consistent with previously published phylogenetic reconstructions (Lemieux et al. 2014a, 2015, Martínez-Alberola et al. 2019).

This study was funded by grants CGL2016-79158-P and CGL2016-80259-P from the Ministry of Economy and Competitiveness (MINECO, Spain) and FEDER and

PROMETEO/2017/039 Excellence in Research (Generalitat Valenciana, Spain).

Adl, S. M., Simpson, A. G. B., Farmer, M. A., Andersen, R. A., Anderson, O. R., Barta, J. R., Bowser, S. S. et al. 2005. The new higher level classification of eukaryotes with emphasis on the taxonomy of protists. *J. Eukaryot. Microbiol.* 52:399–451.

Ahmed, T., Shi, J. & Bhushan, S. 2017. Unique localization of the plastid-specific ribosomal proteins in the chloroplast ribosome small subunit provides mechanistic insights into the chloroplastic translation. *Nucleic Acids Res.* 45:8581–95.

Altschul, S. F., Madden, T. L., Schaffer, A. A., Zhang, J., Zhang, Z., Miller, W. & Lipman, D. J. 1997. Gapped BLAST and PSI-BLAST: a new generation of protein database search programs. *Nucleic Acids Res.* 25:3389–402.

Álvarez, R., del Hoyo, A., García-Breijo, F., Reig-Armiñana, J., del Campo, E. M., Guéra, A., Barreno, E. & Casano, L. M. 2012. Different strategies to achieve Pb-tolerance by the two *Trebouxia* algae coexisting in the lichen *Ramalina farinacea*. *J. Plant Physiol.* 169:1797–806.

Archibald, J. M. 2015. Genomic perspectives on the birth and spread of plastids. *Proc. Natl. Acad. Sci. USA* 112:10147–53.

Ausubel, F. M., Brent, R., Kingston, R. E., Moore, D. D., Seidman, J. G., Smith, J. A. & Struhl, K. 2003. *Current Protocols in Molecular Biology*. John Wiley & Sons Inc, New York, 600 pp.

Bellot, S. & Renner, S. S. 2015. The plastomes of two species in the endoparasite genus *Pilostyles* (Apodanthaceae) each retain just five or six possibly functional genes. *Genome Biol. Evol.* 8:189–201.

Benson, G. 1999. Tandem repeats finder: A program to analyze DNA sequences. *Nucleic Acids Res.* 27:573–80.

Bold, H. C. & Parker, B. C. 1962. Some supplementary attributes in the classification of *Chlorococcum* species. *Arch. Mikrobiol.* 42:267–88.

Brodie, J., Chan, C. X., De Clerck, O., Cock, J. M., Coelho, S. M., Gachon, C., Grossman, A. R. et al. 2017. The algal revolution. *Trends Plant Sci.* 22:726–38.

Brouard, J. S., Otis, C., Lemieux, C. & Turmel, M. 2008. Chloroplast DNA sequence of the green alga *Oedogonium cardiacum* (Chlorophyceae): unique genome architecture, derived characters shared with the Chaetophorales and novel genes acquired through horizontal transfer. *BMC Genom.* 9:290.

Brouard, J. S., Otis, C., Lemieux, C. & Turmel, M. 2010. The exceptionally large chloroplast genome of the green alga *Floydiella terrestris* illuminates the evolutionary history of the Chlorophyceae. *Genome Biol. Evol.* 2:240–56.

Brouard, J. S., Turmel, M., Otis, C. & Lemieux, C. 2016. Proliferation of group II introns in the chloroplast genome of the green alga *Oedocladium carolinianum* (chlorophyceae). *Peer J* 4:e2627.

del Campo, E. M., Casano, L. M., Gasulla, F. & Barreno, E. 2010. Suitability of chloroplast LSU rDNA and ITS diverse group I introns for species recognition and phylogenetic analyses of lichen-forming *Trebouxia* algae. *Mol. Phylogenet. Evol.* 54: 437–44.

del Campo, E. M., Catalá, S., Gimeno, J., del Hoyo, A., Martínez-Alberola, F., Casano, L. M., Grube, M. & Barreno, E. 2013. The genetic structure of the cosmopolitan three-partner lichen *Ramalina farinacea* evidences the concerted diversification of symbionts. *FEMS Microbiol. Ecol.* 83:310–23.

Casano, L. M., Braga, M. R., Álvarez, R., del Campo, E. M. & Barreno, E. 2015. Differences in the cell walls and extracellular polymers of the two *Trebouxia* microalgae coexisting in the lichen *Ramalina farinacea* are consistent with their distinct capacity of immobilizing extracellular Pb. *Plant Sci.* 236:195–204.

Casano, L. M., del Campo, E. M., García-Breijo, F. J., Reig-Armiñana, J., Gasulla, F., del Hoyo, A., Guéra, A. & Barreno, E. 2011. Two *Trebouxia* algae with different physiological performances are ever-present in lichen thalli of *Ramalina farinacea*. Coexistence versus competition? *Environ. Microbiol.* 13:806–18.

Castresana, J. 2000. Selection of conserved blocks from multiple alignments for their use in phylogenetic analysis. *Mol. Biol. Evol.* 17:540–52.

Catalá, S., del Campo, E. M., Barreno, E., García-Breijo, F. J., Reig-Armiñana, J. & Casano, L. M. 2016. Coordinated ultrastructural and phylogenomic analyses shed light on the hidden phycobiont diversity of *Trebouxia* microalgae in *Ramalina fraxinea*. *Mol. Phylogenet. Evol.* 94:765–77.

Centeno, D. C., Hell, A. F., Braga, M. R., del Campo, E. M. & Casano, L. M. 2016. Contrasting strategies used by lichen microalgae to cope with desiccation-rehydration stress revealed by metabolite profiling and cell wall analysis. *Environ. Microbiol.* 18:1546–60.

Chevreux, B., Pfisterer, T., Drescher, B., Driesel, A. J., Muller, W. E., Wetter, T. & Suhai, S. 2004. Using the miraEST assembler for reliable and automated mRNA transcript assembly and SNP detection in sequenced ESTs. *Genome Res.* 14:1147–59.

Chou, H. H. & Holmes, M. H. 2001. DNA sequence quality trimming and vector removal. *Bioinformatics* 17:1093–104.

Cremen, M. C. M., Leliaert, F., Marcelino, V. R. & Verbruggen, H. 2018. Large diversity of nonstandard genes and dynamic evolution of chloroplast genomes in Siphonous green algae (Bryopsidales, Chlorophyta). *Genome Biol. Evol.* 10:1048–61.

Daniell, H., Lin, C. S., Yu, M. & Chang, W. J. 2016. Chloroplast genomes: diversity, evolution, and applications in genetic engineering. *Genome Biol.* 17:134.

Darling, A. E., Mau, B. & Perna, N. T. 2010. progressiveMauve: Multiple Genome Alignment with Gene Gain. *Loss and Rearrangement. PLoS ONE* 5:e11147.

Davies, C., Gerstner, R. B., Draper, D. E., Ramakrishnan, V. & White, S. W. 1998. The crystal structure of ribosomal protein S4 reveals a two-domain molecule with an extensive RNA-binding surface: One domain shows structural homology to the ETS DNA-binding motif. *EMBO J.* 17:4545–58.

Edgar, R. C. 2004. MUSCLE: multiple sequence alignment with high accuracy and high throughput. *Nucleic Acids Res.* 32:1792–7.

Emanuelsson, O., Brunak, S., von Heijne, G. & Nielsen, H. 2007. Locating proteins in the cell using TargetP, SignalP and related tools. *Nat. Protoc.* 2:953–71.

Fan, W., Guo, W., Van Etten, J. L. & Mower, J. P. 2017. Multiple origins of endosymbionts in Chlorellaceae with no reductive effects on the plastid or mitochondrial genomes. *Sci. Rep.* 7:10101.

Fang, L., Leliaert, F., Novis, P. M., Zhang, Z., Zhu, H., Liu, G., Penny, D. & Zhong, B. 2018. Improving phylogenetic inference of core Chlorophyta using chloroplast sequences with strong phylogenetic signals and heterogeneous models. *Mol. Phylogenet. Evol.* 127:248–55.

Felsenstein, J. 1985. Confidence limits on phylogenies: an approach using the bootstrap. *Evolution* 39:783–91.

Fountain, E. D., Pauli, J. N., Mendoza, J. E., Carlson, J. & Peery, M. Z. 2017. Cophylogenetics and biogeography reveal a coevolved relationship between sloths and their symbiont algae. *Mol. Phylogenet. Evol.* 110:73–80.

Fučíková, K., Leliaert, F., Cooper, E. D., Škaloud, P., D'Hondt, S., De Clerck, O., Gurgel, C. F. D. et al. 2014. New phylogenetic hypotheses for the core chlorophyta based on chloroplast sequence data. *Front. Ecol. Evol.* 2:63.

Gantt, J. S., Baldauf, S. L., Calie, P. J., Weeden, N. F. & Palmer, J. D. 1991. Transfer of *rpl22* to the nucleus greatly preceded its loss from the chloroplast and involved the gain of an intron. *EMBO J.* 10:3073–8.

Gasulla, F., Guéra, A. & Barreno, E. 2010. A rapid and effective method for isolating lichen phycobionts into axenic culture. *Symbiosis* 51:175–9.

Grube, M., Seckbach, J. & Muggia, L. 2017. *Algal and Cyanobacteria Symbioses*. World Scientific, New Jersey, 680 pp.

Guindon, S., Dufayard, J. F., Lefort, V., Anisimova, M., Hordijk, W. & Gascuel, O. 2010. New algorithms and methods to estimate maximum-likelihood phylogenies: assessing the performance of PhyML 3.0. *Syst. Biol.* 59:307–21.

Hell, A. F., Gasulla, F., González-Hourcade, M., del Campo, E. M., Centeno, D. C. & Casano, L. M. 2019. The tolerance to cyclic desiccation of lichen microalgae is related with their

habitat preferences and involves specific priming of the antioxidant system. *Plant Cell Physiol.* 60:1880–91.
del Hoyo, A., Álvarez, R., del Campo, E. M., Gasulla, F., Barreno, E. & Casano, L. M. 2011. Oxidative stress induces distinct physiological responses in the two *Trebouxia* phycobionts of the lichen *Ramalina farinacea*. *Ann. Bot.* 107:109–18.
del Hoyo, A., Álvarez, R., Gasulla, F., Casano, L. M. & del Campo, E. M. 2018. Origin and evolution of chloroplast group I introns in lichen algae. *J. Phycol.* 54:66–78.
Jansen, R. K., Saski, C., Lee, S. B., Hansen, A. K. & Daniell, H. 2011. Complete plastid genome sequences of three Rosids (*Castanea*, *Prunus*, *Theobroma*): evidence for at least two independent transfers of *rpl22* to the nucleus. *Mol. Biol. Evol.* 28:835–47.
Kall, L., Krogh, A. & Sonnhammer, E. L. 2004. A combined transmembrane topology and signal peptide prediction method. *J. Mol. Biol.* 338:1027–36.
Kearse, M., Moir, R., Wilson, A., Stones-Havas, S., Cheung, M., Sturrock, S., Buxton, S. et al. 2012. Geneious basic: An integrated and extendable desktop software platform for the organization and analysis of sequence data. *Bioinformatics* 28:1647–9.
Kelley, L. A., Mezulis, S., Yates, C. M., Wass, M. N. & Sternberg, M. J. 2015. The Phyre2 web portal for protein modeling, prediction and analysis. *Nat. Protoc.* 10:845–58.
Kurtz, S., Choudhuri, J. V., Ohlebusch, E., Schleiermacher, C., Stoye, J. & Giegerich, R. 2001. REPuter: The manifold applications of repeat analysis on a genomic scale. *Nucleic Acids Res.* 29:4633–42.
Lang, B. F., Laforest, M. J. & Burger, G. 2007. Mitochondrial introns: a critical view. *Trends Genet.* 23:119–25.
Lefort, V., Longueville, J. E. & Gascuel, O. 2017. SMS: Smart model selection in PhyML. *Mol. Biol. Evol.* 34:2422–4.
Leliaert, F. & De Clerck, O. 2017. Refining species boundaries in algae. *J. Phycol.* 53:12–6.
Leliaert, F. & López-Bautista, J. M. 2015. The chloroplast genomes of *Bryopsis plumosa* and *Tydemania expeditiones* (Bryopsidales, Chlorophyta): Compact genomes and genes of bacterial origin. *BMC Genom.* 16:204.
Leliaert, F., Smith, D. R., Moreau, H., Herron, M. D., Verbruggen, H., Delwiche, C. F. & De Clerck, O. 2012. Phylogeny and molecular evolution of the green algae. *Crit. Rev. Plant Sci.* 31:1–46.
Leliaert, F., Tronholm, A., Lemieux, C., Turmel, M., DePriest, M. S., Bhattacharya, D., Karol, K. G., Fredericq, S., Zechman, F. W. & López-Bautista, J. M. 2016. Chloroplast phylogenomic analyses reveal the deepest-branching lineage of the Chlorophyta, Palmophyllophyceae Class. nov. *Sci. Rep.* 6:25367.
Lemieux, C., Otis, C. & Turmel, M. 2014a. Chloroplast phylogenomic analysis resolves deep-level relationships within the green algal class *Trebouxiophyceae*. *BMC Evol. Biol.* 14:211.
Lemieux, C., Otis, C. & Turmel, M. 2014b. Six newly sequenced chloroplast genomes from Prasinophyte green algae provide insights into the relationships among Prasinophyte lineages and the diversity of streamlined genome architecture in picoplanktonic species. *BMC Genom.* 15:857.
Lemieux, C., Otis, C. & Turmel, M. 2016. Comparative chloroplast genome analyses of Streptophyte green algae uncover major structural alterations in the Klebsormidiophyceae, Coleochaetophyceae and Zygnematophyceae. *Front. Plant. Sci.* 7:697.
Lemieux, C., Vincent, A. T., Labarre, A., Otis, C. & Turmel, M. 2015. Chloroplast phylogenomic analysis of chlorophyte green algae identifies a novel lineage sister to the Sphaeropleales (Chlorophyceae). *BMC Evol. Biol.* 15:264.
Magee, A. M., Aspinall, S., Rice, D. W., Cusack, B. P., Semon, M., Perry, A. S., Stefanović, S. et al. 2010. Localized hypermutation and associated gene losses in legume chloroplast genomes. *Genome Res.* 20:1700–10.
Marchler-Bauer, A., Zheng, C., Chitsaz, F., Derbyshire, M. K., Geer, L. Y., Geer, R. C., Gonzales, N. R. et al. 2013. CDD: conserved domains and protein three-dimensional structure. *Nucleic Acids Res.* 41:D348–52.
Marin, B. 2012. Nested in the Chlorellales or independent class? phylogeny and classification of the Pedinophyceae (Viridiplantae) revealed by molecular phylogenetic analyses of complete nuclear and plastid-encoded rRNA operons. *Protist* 163:778–805.
Martínez-Alberola, F., Barreno, E., Casano, L. M., Gasulla, F., Molins, A. & del Campo, E. M. 2019. Dynamic evolution of mitochondrial genomes in Trebouxiophyceae, including the first completely assembled mtDNA from a lichen-symbiont microalga (*Trebouxia* sp. TR9). *Sci. Rep.* 9:8209.
Massjuk, N. P. 2006. Chlorodendrophyceae class. nov. (Chlorophyta, Viridiplantae) in the Ukrainian flora: I. the volume, phylogenetic relations and taxonomical status. *Ukr. Biokhim. Zh.* 63:601–14.
Massjuk, N. P. & Lilitska, G. G. 2011. Chlorodendrophyceae. *In* Tsarenko, P. M., Wasser, S. P. & Nevo, E. [Eds.] *Algae of Ukraine: Diversity, Nomenclature, Taxonomy, Ecology and Geography*. A.R.A. Gantner Verlag K. G, Ruggell, Liechtenstein, pp. 14–7.
McManus, H. A., Sánchez, D. J. & Karol, K. G. 2017. Plastomes of the green algae hydrodictyon reticulatum and pediastrum duplex (sphaeropleales, chlorophyceae). *Peer J* 5:e3325.
Mekvipad, N. & Satjarak, A. 2019. Evolution of organellar genes of chlorophyte algae: Relevance to phylogenetic inference. *PLoS ONE* 14:e0216608.
Millen, R. S., Olmstead, R. G., Adams, K. L., Palmer, J. D., Lao, N. T., Heggie, L., Kavanagh, T. A. et al. 2001. Many parallel losses of *infA* from chloroplast DNA during angiosperm evolution with multiple independent transfers to the nucleus. *Plant Cell* 13:645–58.
Moestrup, Ø. 1991. Further studies of presumedly primitive green algae, including the description of Pedinophyceae class. nov. and resultor gen. nov. *J. Phycol.* 27:119–33.
Moya, P., Chiva, S., Molins, A., Jadrna, I., Škaloud, P., Peksa, O. & Barreno, E. 2018. *Myrmecia israeliensis* as the primary symbiotic microalga in squamulose lichens growing in European and Canary Island terricolous communities. *Fottea* 18:72–85.
Moya, P., Molins, A., Martinez-Alberola, F., Muggia, L. & Barreno, E. 2017. Unexpected associated microalgal diversity in the lichen *Ramalina farinacea* is uncovered by pyrosequencing analyses. *PLoS ONE* 12:e0175091.
Moya, P., Škaloud, P., Chiva, S., García-Breijo, F. J., Reig-Armiñana, J., Vančurová, L. & Barreno, E. 2015. Molecular phylogeny and ultrastructure of the lichen microalga *Asterochloris mediterranea* sp. nov. from Mediterranean and Canary Islands ecosystems. *Int. J. Syst. Evol. Microbiol.* 65:1838–54.
Muggia, L., Baloch, E., Stabentheiner, E., Grube, M. & Wedin, M. 2011. Photobiont association and genetic diversity of the optionally lichenized fungus *Schizoxylon albescens*. *FEMS Microbiol. Ecol.* 75:255–72.
Muggia, L., Candotto-Carniel, F. & Grube, M. 2017. The lichen photobiont *Trebouxia*: towards an appreciation of species diversity and molecular studies. *In* Grube, M., Seckbach, J. & Muggia, L. [Eds.] *Algal and Cyanobacteria Symbioses*. World Scientific, New Jersey, pp. 111–45.
Muñoz-Gómez, S. A., Mejía-Franco, F. G., Durnin, K., Colp, M., Grisdale, C. J., Archibald, J. M. & Slamovits, C. H. 2017. The new red algal subphylum *Proteorhodophytina* comprises the largest and most divergent plastid genomes known. *Curr. Biol.* 27:1677–84.e4.
Park, S., Jansen, R. K. & Park, S. 2015. Complete plastome sequence of *Thalictrum coreanum* (Ranunculaceae) and transfer of the *rpl32* gene to the nucleus in the ancestor of the subfamily Thalictroideae. *BMC Plant Biol.* 15:40.
Pombert, J. F., Lemieux, C. & Turmel, M. 2006. The complete chloroplast DNA sequence of the green alga *Oltmannsiellopsis viridis* reveals a distinctive quadripartite architecture in the chloroplast genome of early diverging Ulvophytes. *BMC Biol.* 4:3.
Pombert, J. F., Otis, C., Lemieux, C. & Turmel, M. 2005. The chloroplast genome sequence of the green alga *Pseudendoclonium akinetum* (Ulvophyceae) reveals unusual structural features and new insights into the branching order of Chlorophyte lineages. *Mol. Biol. Evol.* 22:1903–18.

Rambaut, A. 2008. FigTree: Tree figure drawing tool. 1.3.1. Institute of Evolutionary Biology, University of Edinburgh.
Robison, T. A., Grusz, A. L., Wolf, P. G., Mower, J. P., Fauskee, B. D., Sosa, K. & Schuettpelz, E. 2018. Mobile elements shape plastome evolution in ferns. *Genome Biol. Evol.* 10:2558–71.
Rogalski, M., Schottler, M. A., Thiele, W., Schulze, W. X. & Bock, R. 2008. Rpl33, a nonessential plastid-encoded ribosomal protein in tobacco, is required under cold stress conditions. *Plant Cell* 20:2221–37.
Sayle, R. A. & Milner-White, E. J. 1995. RASMOL: Biomolecular graphics for all. *Trends Biochem. Sci.* 20:374.
Schubert, I. & Vu, G. T. H. 2016. Genome stability and evolution: attempting a holistic view. *Trends Plant Sci.* 21:749–57.
Škaloud, P., Moya, P., Molins, A., Peksa, O., Santos-Guerra, A. & Barreno, E. 2018. Untangling the hidden intrathalline microalgal diversity in *Parmotrema pseudotinctorum*: *Trebouxia crespoana* sp. nov. *The Lichenologist* 50:357–69.
Stanke, M. & Morgenstern, B. 2005. AUGUSTUS: a web server for gene prediction in eukaryotes that allows user-defined constraints. *Nucleic Acids Res.* 33:W465–7.
Sun, L., Fang, L., Zhang, Z., Chang, X., Penny, D. & Zhong, B. 2016. Chloroplast phylogenomic inference of green algae relationships. *Sci. Rep.* 6:20528.
Suutari, M., Majaneva, M., Fewer, D. P., Voirin, B., Aiello, A., Friedl, T., Chiarello, A. G., Chiarello, A. G. & Blomster, J. 2010. Molecular evidence for a diverse green algal community growing in the hair of sloths and a specific association with *Trichophilus welckeri* (Chlorophyta, Ulvophyceae). *BMC Evol. Biol.* 10:86.
Sykes, M. T. & Williamson, J. R. 2009. A complex assembly landscape for the 30S ribosomal subunit. *Annu. Rev. Biophys.* 38:197–215.
Tang, X., Wang, Y., Zhang, Y., Huang, S., Liu, Z., Fei, D. & Feng, H. 2018. A missense mutation of plastid RPS4 is associated with chlorophyll deficiency in Chinese cabbage (*Brassica campestris* ssp. pekinensis). *BMC Plant Biol.* 18:130.
Tiller, N. & Bock, R. 2014. The translational apparatus of plastids and its role in plant development. *Mol. Plant.* 7:1105–20.
Turmel, M., de Cambiaire, J. C., Otis, C. & Lemieux, C. 2016. Distinctive architecture of the chloroplast genome in the chlorodendrophycean green algae *Scherffelia dubia* and *Tetraselmis* sp. CCMP 881. *PLoS ONE* 11:e0148934.
Turmel, M., Gagnon, M. C., O'Kelly, C. J., Otis, C. & Lemieux, C. 2009a. The chloroplast genomes of the green algae *Pyramimonas*, *Monomastix*, and *Pycnococcus* shed new light on the evolutionary history of prasinophytes and the origin of the secondary chloroplasts of euglenids. *Mol. Biol. Evol.* 26:631–48.
Turmel, M., Otis, C. & Lemieux, C. 1999. The complete chloroplast DNA sequence of the green alga *Nephroselmis olivacea*: Insights into the architecture of ancestral chloroplast genomes. *Proc. Natl. Acad. Sci. USA* 96:10248–53.
Turmel, M., Otis, C. & Lemieux, C. 2005. The complete chloroplast DNA sequences of the charophycean green algae *Staurastrum* and *Zygnema* reveal that the chloroplast genome underwent extensive changes during the evolution of the Zygnematales. *BMC Biol.* 3:22.
Turmel, M., Otis, C. & Lemieux, C. 2009b. The chloroplast genomes of the green algae *Pedinomonas minor*, *Parachlorella kessleri*, and *Oocystis solitaria* reveal a shared ancestry between the Pedinomonadales and Chlorellales. *Mol. Biol. Evol.* 26:2317–31.
Turmel, M., Otis, C. & Lemieux, C. 2015. Dynamic evolution of the chloroplast genome in the green algal classes Pedinophyceae and Trebouxiophyceae. *Genome Biol. Evol.* 7:2062–82.
Turmel, M., Otis, C. & Lemieux, C. 2017. Divergent copies of the large inverted repeat in the chloroplast genomes of Ulvophycean green algae. *Sci. Rep.* 7:994.
Ueda, M., Nishikawa, T., Fujimoto, M., Takanashi, H., Arimura, S., Tsutsumi, N. & Kadowaki, K. 2008. Substitution of the gene for chloroplast RPS16 was assisted by generation of a dual targeting signal. *Mol. Biol. Evol.* 25:1566–75.
Werth, S. & Sork, V. L. 2010. Identity and genetic structure of the photobiont of the epiphytic lichen *Ramalina menziesii* on three oak species in Southern California. *Am. J. Bot.* 97:821–30.
Xiong, A. S., Peng, R. H., Zhuang, J., Gao, F., Zhu, B., Fu, X. Y., Xue, Y., Jin, X. F., Tian, Y. S., Zhao, W. & Yao, Q. H. 2009. Gene duplication, transfer, and evolution in the chloroplast genome. *Biotechnol. Adv.* 27:340–7.

Supporting Information

Additional Supporting Information may be found in the online version of this article at the publisher's web site:

Figure S1. Extent of chloroplast genome rearrangements in the *Trebouxiales*: *Myrmecia israeliensis* and *Trebouxia* sp. TR9. The alignment of the cpDNAs from *M. israeliensis* (a) and *Trebouxia* sp. TR9 (b) was carried out using the ProgressiveMauve algorithm of Mauve 2.3.1, which depicts the order and orientation of each locally collinear block (Darling, et al. 2010). (c) Genetic map of the *Trebouxia* sp. TR9 cpDNA. (d) Arrangement of genes along the plastomes of *M. israeliensis* and *Trebouxia* sp. TR9 at the top and bottom, respectively. Numbers within black rectangles indicate sets of genes, which are conserved in the two algal species and correspond to the numbers within circles of (b). Genes encoding rRNAs are indicated in red. The *rbc*L gene is indicated on a green background. Genes belonging to the SSC in the cpDNA of *Trebouxia* sp. TR9 are indicated on pink background.

Figure S2. Comparison of IR lengths and gene content of the cpDNAs from different Chlorophyta lineages. Total lengths (Kbp) of IRs are indicated at the top. Gene repertoires of IRs are indicated at the bottom. The systematic classification is indicated to the left of each number (C: Chlorophyceae, Cd: Chlorodendrophyceae, P: Prasinophyceae, Pe: Pedinophyceae, T: Trebouxiophyceae, U: Ulvophyceae). GenBank accessions are indicated to the right of each number.

Table S1. List of primers used for amplification and Sanger sequencing of doubtful sections.

Anexo V. Financiación.

Esta tesis doctoral no habría sido posible sin la financiación del Ministerio de España. de Ciencia, Innovación y Universidades (CGL2016-80259-P).